

6th Biennial Workshop on Japan-Kamchatka-Alaska Subduction Processes (JKASP-2009)



Mitigating natural hazards in active arc environments

Linkages among tectonism, earthquakes, magma genesis and eruption in volcanic arcs, with a special focus on hazards posed by arc volcanism and great earthquakes

JUNE 22-26, 2009

SCIENTIFIC PROGRAM & ABSTRACTS

GEOPHYSICAL INSTITUTE
UNIVERSITY OF ALASKA FAIRBANKS
FAIRBANKS, ALASKA



6th Biennial Workshop on Japan-Kamchatka-Alaska Subduction Processes (JKASP-2009)

Mitigating natural hazards in active arc environments

Linkages among tectonism, earthquakes, magma genesis and eruption in volcanic arcs, with a special focus on hazards posed by arc volcanism and great earthquakes

JUNE 22-26, 2009

**GEOPHYSICAL INSTITUTE
UNIVERSITY OF ALASKA FAIRBANKS
FAIRBANKS, ALASKA**



Conference Sponsors

Geophysical Institute / University of Alaska Fairbanks
Volcano Hazards Program, United States Geological Survey
National Science Foundation
Office of the Vice Chancellor for Research, University of Alaska Fairbanks
College of Natural Science and Mathematics, University of Alaska Fairbanks

Local Organizing Committee

Steve McNutt, Geophysical Institute, University of Alaska Fairbanks
Jeff Freymueller, Geophysical Institute, University of Alaska Fairbanks
Pavel Izbekov, Geophysical Institute, University of Alaska Fairbanks
Tina Neal, Alaska Volcano Observatory, USGS, Anchorage

Field Trips, Workshops, and Short Courses

Jim Begét, University of Alaska Fairbanks
Joanne Bourgeois, University of Washington
Brandon Browne, California State University, Fullerton
John Eichelberger, Volcano Hazards Program Coordinator, USGS, Washington, D.C.
Steve Kirby, USGS, Menlo Park, CA
Peter Webley, Geophysical Institute, University of Alaska Fairbanks

Technical Support*

Leslie Almberg (volume of abstracts)

Kristen Buley (logistics)

Tom Burton (IT support)

Joanna Cruzan (invitation letters, visa support)

Deb Chapman (logistics)

Ludmila Eichelberger (volume of abstracts)

Candace O'Connor (editorial work)

Shannon Slater (travel)

Geophysical Institute graduate students

*All at the Geophysical Institute, University of Alaska Fairbanks

General Information

Registration Desk – Geophysical Institute foyer

Monday, June 22

9:00 a.m. – 6:00 p.m.

Conference Fees

Professionals	\$400 (USD)
(includes all group events, transportation, and Fairbanks area field trip)	

Students	\$150 (USD)
(includes all group events, transportation, and Fairbanks area field trip)	

Lunch and Coffee Breaks

Lunch will be provided in the Globe Room at the Geophysical Institute each day of the conference. A bag lunch will be provided for the field trip. Coffee will be available in the morning prior to the technical sessions.

Table of Contents

SCIENTIFIC PROGRAM.....	5
Sunday, June 21.....	7
Monday, June 22	9
Tuesday, June 23	11
Wednesday, June 24.....	17
Thursday, June 25.....	23
Friday, June 26.....	25
ABSTRACTS.....	33
Pre-Meeting Workshops And Short Courses.....	33
State of The Arc: Overview.....	41
Recent Eruptions In The Northern Pacific (Oral).....	49
Recent Eruptions In The Northern Pacific (Poster)	63
Volcanism And Volcanic Processes (Oral)	95
Volcanism And Volcanic Processes (Poster).....	111
Subduction Zone Seismicity And Structure (Oral).....	123
Subduction Zone Seismicity And Structure (Poster)	141
Volcano Geophysics (Oral)	169
Tsunamis And Tsunami Hazards (Oral).....	177
Subduction Zone Tectonic Processes, Volcano Geophysics, Tsunamis And Tsunami Hazards (Poster)	187
Geothermal Power (Oral)	211
Comparative Study of Bezymianny, Shiveluch, And Mount St Helens Volcanoes – Results of PIRE-Kamchatka Project (Oral).....	215
Comparative Study of Bezymianny, Shiveluch, And Mount St Helens Volcanoes – Results of PIRE-Kamchatka Project (Poster)	227
The Kurile Biocomplexity Project (Oral)	253
Hazards, Monitoring And Risk Reduction (Oral)	263
The Kurile Biocomplexity Project, Hazards, Monitoring And Risk Reduction, Interdisciplinary Studies (Poster)	271
Author index.....	305

SCIENTIFIC PROGRAM

Sunday, June 21

PRE-MEETING WORKSHOPS AND SHORT COURSES

Aleutians Geohazards Discussion and Planning Meeting I GI Auditorium, 8:30 – 17:30

Convener: Steve Kirby (USGS)

Although low in population density, Alaska is an important provider of natural resources to the Nation, such as fishing, oil and gas, ore deposits, and tourism. Geohazards potentially threaten the infrastructure that provides these resources. Tsunamis created in the Aleutians threaten regional and distant shorelines. The overall seismicity rate for shallow Aleutian earthquakes of all types is among the highest in the world. Since 1900 the Alaska/Aleutian subduction system has produced nine great ($M > 8$) subduction earthquakes, including four of the ten largest subduction earthquakes on record. Three of these giant shocks spawned destructive ocean-crossing tsunami waves. Likewise, the Aleutian volcanic arc is among the most active in the world, including the 1912 Novarupta explosive eruption, the largest in the 20th century. Dozens of calderas and gravitational collapse structures in this island chain are testimony to giant explosive eruptions, flank collapses, and possible volcano-induced tsunamis in the recent geologic past. The purposes of this workshop is to provide a forum for scientists from diverse backgrounds to meet and discuss opportunities for improving appraisals of Aleutian geohazards through integrated on-shore and marine investigations, to identify common informational needs (e.g., satellite, LIDAR, aeromagnetic and multibeam sonar surveys), and to provide opportunities for these scientists to plan initiatives to support such investigations. The workshop will also give planners and decision makers a chance to find out about the high level of enthusiasm and research potential for making advances in appraisals of geohazards in the Aleutian subduction system.

8:30 Welcome: Brian Rogers, UAF Chancellor

8:35 Introduction and announcements: John Eichelberger

Overview presentations

8:45 History and pre-history of native peoples in the Aleutians: Debbie Corbett

9:10 Geological setting, history, and forearc structure of the Alaska/Aleutian subduction system: What we know and possible pathways toward a systems-level understanding: Dave Scholl and Holly Ryan

9:30 Plate motions: Present understanding and future directions: Jeff Freymueller

10:00 The pre-digital seismic record of the great subduction earthquakes in the Aleutians: State of knowledge and future needs: Emile Okal

10:30 Break, 30 minutes

11:00 Tsunami monitoring, modeling, and forecasting in the Aleutians: Vasily Titov

11:25 Near-shore record of tsunamis in the north Pacific: Discoveries and lessons learned from the Kuril island arc and Kamchatka: Joanne Bourgeois

- 11:50 The Aleutian arc: eruptive history and prehistory: [John Eichelberger](#)
12:05 Volcanic sources for Aleutian tsunamis: [Chris Waythomas](#)
12:30 Catered Lunch

Topical Presentations

- 13:30 Shallow earthquake mechanisms and block rotations in the Aleutians: [Natalia Ruppert](#)
13:50 Inundation modeling for near-field tsunami sources with applications to the Aleutians: [Elena Suleimani](#)
14:10 The Quaternary geologic record of great earthquakes and tsunamis: current knowledge and prospects: [Gary Carver and George Plafker](#)
14:30 Prospects of using prehistoric land-level data to assess earthquake magnitudes and recurrence in the Aleutians: [Rich Briggs](#)
14:50 Along-strike variability of subduction: the Amlia Fracture Zone Corredor: [Katie Keranen](#)
15:10 Breaks
15:40 Discussion
17:00 Adjourn for the day

Discussion: How are geohazards connected at the systems and practical level?

19:00-22:00 Group Dinner at the Roundup Steakhouse and Bar

Remote Sensing Short Course

WRRB 004, 9:00 – 17:00

Instructor: Peter Webley, Geophysical Institute, UAF

- 9:00 – 17:00 This course will provide attendees with first hand experience of analyzing remote sensing datasets for monitoring volcanoes across the North Pacific. The short course will include some basics and principles of remote sensing, understanding of thermal monitoring using satellite data, the detection of volcanic ash and SO₂ clouds and also the use of dispersion modeling for predicting and tracking of volcanic clouds. The remote sensing data that will be analyzed during the course includes AVHRR, GOES, MODIS, OMI, AIRS and ASTER. In addition, instruction will be provided on how to use the AVO Remote Sensing tools. A detailed program of the short course and all course materials will be provided to all participants upon arrival to Fairbanks.

Monday, June 22

The PIRE-Kamchatka Project workshop

Globe Room, GI, 9:00 – 17:00

Conveners: Pavel Izbekov and Michael West (Geophysical Institute, UAF)

9:00 – 9:15 Introduction and welcome note by Pavel Izbekov (Geophysical Institute, UAF) and John Eichelberger (USGS)

9:15 – 10:15 Invited talks

Pavel Izbekov OVERVIEW OF THE CURRENT PROGRESS OF THE PROJECT

Jeff Freymueller DEFORMATION

Mike West SEISMICITY

Pavel Plechov PETROLOGICAL ASPECTS

Oleg Melnik MODELING PERSPECTIVES

10:15 – 10:30 Coffee break

10:30 – 12:00 Reports on individual projects

12:00 – 13:00 WORKING LUNCH

13:00 – 15:15 Reports on individual projects

15:15 – 15:30 Coffee break

15:30 – 17:00 Future plans and directions

Volcano Monitoring in the North Pacific: Improving collaborations and exchange

GI Auditorium, 13:00 – 17:00

Convener: Christina Neal (USGS)

13:00 – 17:00 This meeting offers a unique opportunity to gather volcano scientists from AVO, KVERT, SVERT, Japanese monitoring and research institutions, and others involved in volcano monitoring and warning operations in the North Pacific. The purpose of this workshop is to review the operational status of relevant institutions, examine existing collaborations, and share ideas for new initiatives that will improve both our science and our warnings. We will hear from representatives of SVERT, KVERT, AVO, and others who will describe the state of operations at each facility. Then, we will discuss the priorities for sharing technology, people, and information, as well as look for ways to streamline communications and augment organizational support. At the conclusion of this workshop, we will discuss updating our operational agreements and try to establish tangible objectives for the coming years.

Aleutians Geohazards Discussion and Planning Meeting II

IARC 401, 8:30 – 12:00

Moderator: Steve Kirby (USGS)

- Short information presentations on the geospatial, marine geophysical, and logistical resources in the Aleutians. NOAA, UAF, State of AK, and USGS
- Discussion Topic 1: What are the key scientific questions that need to be answered to advance Aleutian geohazard appraisals?
- Discussion Topic 2: How can integrated marine and onshore investigations improve assessments of multiple hazards?
- Discussion Topic 3: What are the common informational needs for remote surveys of the Aleutian arc (multibeam sonar, LIDAR, ground-penetrating radar, aeromag, ...), crustal deformation (GPS), and earthquake and volcano eruptive history?
- Discussion Topic 4: Given the high cost of working in the Aleutians, what are the highest-priority island targets or segments of the archipelago that have the highest prospects for providing fundamental information relevant to the geohazards of the arc?
- Discussion Topic 5: What would be the most effective way to structure a persuasive document that articulates the reasons for initiating new integrated hazards work in the Aleutians? Do existing written sources provide valuable guidance?

RECEPTION

IARC lobby, 19:00 – 21:00

TRANSPORTATION WILL BE PROVIDED

Tuesday, June 23

PLENARY SESSION

08:00 Coffee will be available at GI

State of the arc: Overview

GI Auditorium, 8:20 – 10:00

Chair: Steve McNutt

- | | |
|-------|--|
| 08:20 | Introduction: Steve McNutt (GI, UAF) |
| 08:25 | Welcome: Chancellor Brian Rogers (Chancellor of UAF) |
| 08:35 | Welcome: Roger Smith (Director of the Geophysical Institute, UAF) |
| 08:40 | Welcoming remarks from John Eichelberger (USGS), Evgenii Gordeev (Institute of Volcanology and Seismology), and a senior representative of Hokkaido University |
| 09:00 | Scientific and Societal Importance of the North Pacific: Keynote speaker, Dave Scholl (University of Alaska Fairbanks) |
| 09:15 | Tectonic setting and activity of the North Pacific, Jeff Freymueller (University of Alaska Fairbanks) |
| 09:30 | Links between quaternary volcanism, neotectonism and upper-plate structural style in the Aleutian arc: New perspectives, Chris Nye (Alaska Division of Geological and Geophysical Surveys) |
| 09:45 | International cooperation in monitoring volcanic hazards in the North Pacific, Tina Neal (USGS) |
| 10:00 | BREAK, 15 minutes |

TECHNICAL SESSIONS

Recent Eruptions in the Northern Pacific

GI Auditorium, 10:15 – 12:00

Presiding: Jessica Faust Larsen (UAF)

10:15 – 10:30 Jessica F. Larsen, Christina A. Neal, Janet R. Schaefer and the staff of the Alaska Volcano Observatory THE JULY-AUGUST 2008 ERUPTION OF OKMOK VOLCANO, ALASKA: PRELIMINARY GEOLOGY, PETROLOGY AND GEOCHEMISTRY

10:30 – 10:45 Natalia A. Ruppert, Roger A. Hansen, and Stephanie Prejean SEISMIC SWARM

ASSOCIATED WITH THE 2008 ERUPTION OF KASATOCHI VOLCANO,
ALASKA

10:45 – 11:00 Kate Bull and AVO staff CHRONOLOGY OF THE 2009 ERUPTION OF
REDOUBT VOLCANO

11:00 – 11:15 Ken Dean, Jon Dehn, Peter Webley, and John Bailey SATELLITE
OBSERVATIONS OF VOLCANIC CLOUDS FROM THE ERUPTION OF
REDOUBT VOLCANO, ALASKA, 2009

11:15 – 11:30 O.A. Girina, A.G. Manevich, S.V. Ushakov, A.A. Nuzhdaev, D.V. Melnikov,
N.A. Malik, Yu.V. Demyanchuk KVERT PROJECT: DANGER FOR
AVIATION DURING ERUPTIONS OF KAMCHATKAN AND NORTHERN
KURILES VOLCANOES IN 2006-2008

11:30 – 11:45 Ramsey, M.S., Carter, A., Wessels, R., Dehn, J., Duda, K., and Muder, M. THE
ASTER URGENT REQUEST PROGRAM: A COLLABORATIVE MULTI-
AGENCY, MULTI-YEAR EFFORT TO MONITOR THE NORTH PACIFIC
VOLCANOES FROM SPACE

11:45 – 12:00 Arron Steiner and Brandon Browne CHANGES IN MAFIC- FELSIC MAGMA
MIXING STYLES AT AUGUSTINE VOLCANO OVER THE PAST 2,200
YEARS

12:00 – 13:00 LUNCH (IN UAF GLOBE ROOM)

Volcanism and Volcanic Processes

GI Auditorium, 13:00 – 14:45

Presiding: John Eichelberger (USGS) and Pavel Izbekov (UAF)

13:00 – 13:15 John C. Eichelberger, David W Scholl, and Evgeny I Gordeev ALEUTIAN
SUBDUCTION: A SCIENTIFIC OPPORTUNITY WHOSE TIME HAS
RETURNED

13:15 – 13:30 Philip R. Kyle, Vera V. Ponomareva, Rachelle C. Rourke GEOCHEMICAL
FINGERPRINTING OF TEPHRA FROM MAJOR HOLOCENE ERUPTIONS
IN KAMCHATKA

13:30 – 13:45 Belousov Alexander, Belousova Marina, Chang-Hwa Chen ERUPTIONS IN THE
RECENT HISTORY OF THE TATUN VOLCANIC GROUP, NORTHERN
TAIWAN

- 13:45 – 14:00 Pavel Plechov, Maria Shur, Alexander Perepelov, Michail Puzankov, Oleg Dirksen, Lilia Bazanova NON-SUBDUCTION-RELATED ISLAND ARC VOLCANISM: SEDANKINSKY DOL, KAMCHATKA
- 14:00 – 14:15 Takeshi Hasegawa and Mitsuhiro Nakagawa FORMATION AND EVOLUTION OF SILICIC MAGMAS DURING CALDERA-FORMING ERUPTIONS OF AKAN VOLCANO, EASTERN HOKKAIDO, JAPAN: COMPARING THE LARGEST ERUPTION (AK2) WITH THE OTHER ERUPTIONS
- 14:15 – 14:30 Brian R. Jicha and Brad S. Singer AN “INACTIVE” STRATOVOLCANO THAT ERUPTED ~ 3000 YEARS AGO: KONIJI ISLAND, ALEUTIANS
- 14:30 – 14:45 Theresa M. Kayzar, Bruce K. Nelson, Pavel E. Izbekov, Marina Belousova, Alexander Belousov VOLATILES IN THE KAMCHATKA VOLCANIC ARC AT FOUR VOLCANIC CENTERS (BEZYMIANNY, KLYUCHEVSKOY, KARYMSKY, AND SHIVELUCH): APPLICATIONS FOR URANIUM-SERIES ISOTOPIC DATA
- 14:45 – 15:00 BREAK, 15 minutes

**Recent Eruptions in the North Pacific
Volcanism and Volcanic Processes**

GI Globe Room, 15:00 – 16:00

- POSTER SESSION
- Presiding: Jessica Faust Larsen (UAF) and Pavel Izbekov (UAF)
- 15:00 – 16:00 Belousova Marina, Belousov Alexander, Chang-Hwa Chen LARGE-SCALE EDIFICE FAILURES IN THE RECENT HISTORY OF TATUN VOLCANIC GROUP, NORTHERN TAIWAN
- 15:00 – 16:00 Yu.I. Blokh, V.I. Bondarenko, V.A. Rashidov, A.A. Trusov SURVEY OF THE BERG SUBMARINE VOLCANO: THE KURIL ISLAND ARC
- 15:00 – 16:00 K. Bull, C. Bacon, A. Calvert, J. Beget, C. Coombs and K. Wallace REDOUBT VOLCANO GEOLOGIC MAPPING AND HAZARD ASSESSMENT; A PROGRESS REPORT
- 15:00 – 16:00 Helena Buurman and Michael West INVESTIGATING PRE-ERUPTIVE PROCESSES AT AUGUSTINE VOLCANO USING REPEATING EARTHQUAKES

- 15:00 – 16:00 Cheryl Cameron, Chris Nye, and Christina Neal QUATERNARY VENT INVENTORY OF ALASKA
- 15:00 – 16:00 Dirksen O., Danhara T., Diekmann B. TEPHROCHRONOLOGICAL INVESTIGATION AT THE TWO-YURTS LAKE AREA, SREDINNY RANGE, KAMCHATKA AND HISTORY OF LANDSCAPE EVOLUTION DURING THE HOLOCENE
- 15:00 – 16:00 Dirksen Oleg V., Bazanova Lilia I. LATE QUATERNARY VOLCANIC ACTIVITY IN THE SEDANKA LAVA FIELD, NORTHERN PART OF THE SREDINNY RANGE, (KAMCHATKA)
- 15:00 – 16:00 Sergei Fedotov, Nikolay Zharinov, Larissa Gontovaya, Alex Sobissevitch GIANT BASALTIC KLYUCHEVSKOY VOLCANO: ERUPTIONS, THE MAGMA FEEDING SYSTEM, AND SEISMOTOMOGRAPHY
- 15:00 – 16:00 Gavrilenko M.G., Ozerov A.Yu. HIGH-MAGNESIA BASALTS - SOURCE OF CALC-ALKALINE SERIES OF GORELY VOLCANO (KAMCHATKA).
- 15:00 – 16:00 Olga A. Girina and Adam J. Carter 2006-2008 ERUPTIONS OF BEZMIANNY VOLCANO
- 15:00 – 16:00 Boris Gordyechik, Tatiana Churikova, Gerhard Wörner, Anna Volynets, Paul Layer GEODYNAMICAL CONDITIONS AT THE NORTH OF THE KAMCHATKA SUBDUCTION ZONE: GEOCHEMICAL EVIDENCE
- 15:00 – 16:00 Khleborodova, O. A. A HYPOTHESIS ON STRUCTURAL EQUILIBRIUM IN NATURAL MELTS AND THE MECHANISM OF WATER SOLUTION AT LOW AND HIGH PRESSURE
- 15:00 – 16:00 Krasheninnikov S.P., Portnyagin M.V., Ponomareva V.V., Kuvikas O.V., Mironov N.L. PERIODIC VOLCANIC ACTIVITY OF KLYUCHEVSKOY AND USHKOVSKY VOLCANOES DURING THE EARLY HOLOCENE INFERRRED FROM TEPHRA STUDY
- 15:00 – 16:00 Jumpei Nishimoto, Mitsuhiro Nakagawa, Tsuyoshi Miyamoto, Mitsuhiro Taniguchi MAGMA SYSTEM OF THE 10th CENTURY ERUPTION OF BAITUSHAN VOLCANO, CHINA-NORTH KOREA BORDER, AS INFERRRED FROM GEOCHEMICAL CHARACTERISTICS
- 15:00 – 16:00 Storcheus A.V. DECOMPRESSION MODEL OF VOLCANIC EXPLOSIONS - ADVANTAGES AND DISADVANTAGES

- 15:00 – 16:00 Wendy K. Stovall, Bruce F. Houghton, Sarah A. Fagents, Don A. Swanson
ERUPTION DYNAMICS OF HAWAIIAN-STYLE LAVA FOUNTAINS: THE
CASE STUDY OF THE OPENING AND CLOSING EPISODES OF THE 1959
KĪLAUEA IKI ERUPTION
- 15:00 – 16:00 Anna Volynets, Tatiana Churikova, and Gerhard Wörner GEOCHEMICAL
MODELING OF THE COMPOSITION AND AMOUNT OF SLAB FLUID FOR
KAMCHATKA SREDINNY RANGE VOLCANIC ROCKS
- 15:00 – 16:00 Robert B. Watts FIELD OBSERVATIONS ACROSS AN EXHUMED SUPRA-
SUBDUCTION ZONE ON THE ISLE OF CULEBRA, PUERTO RICO
- 15:00 – 16:00 Shimpei Uesawa and Mitsuhiro Nakagawa TEPHROSTRATIGRAPHY OF
YOTEI VOLCANO, SOUTHWEST HOKKAIDO, JAPAN

Volcanism and Volcanic Processes

GI Auditorium, 16:00 – 17:45

Presiding: Pavel Izbekov (UAF) and John Eichelberger (USGS)

- 16:00 – 16:15 Mitsuhiro Yoshimoto BASALTIC-ANDESITIC PYROCLASTIC FLOW
DEPOSIT OF THE 3.3Ka ERUPTION AT TOKACHIDAKE VOLCANO,
NORTHERN JAPAN
- 16:15 – 16:30 Richard W. Sanderson and Michael West EXPLOSIVE SEISMIC SIGNALS AT
KARYMSKY VOLCANO 2008
- 16:45 – 17:00 Allison L Payne and John C Eichelberger TI-IN-QUARTZ
GEOTHERMOMETRY OF MAGMAS FROM KATMAI, ALASKA: A
COMBINED CATHODOLUMINESCENCE/ELECTRON MICROPROBE
STUDY
- 17:00 – 17:15 Erika L. Rader and Jessica Larsen WATER UNDER-SATURATED PHASE
EQUILIBRIA OF BASALTIC ANDESITES FROM WESTDAHL VOLCANO,
ALASKA
- 17:15 – 17:30 Tatiana Churikova, Boris Gordeychik, Gerhard Wörner, Boris Ivanov, Alexander
Maximov MINERALOGY AND PETROLOGY OF KAMEN VOLCANO
ROCKS, KAMCHATKA
- 17:30 – 17:45 E. Duarte, E. Fernández VOLCANIC ACTIVITY AND EARTHQUAKES IN
CENTRAL AMERICA: SOME GENERALITIES

Recent Eruptions in the North Pacific

GI Globe Room, 17:45 – 18:45

Volcanism and Volcanic Processes

POSTER SESSION

Presiding: Jessica Faust Larsen (UAF) and Pavel Izbekov (UAF)

Additional poster viewing time or informal discussions.

Wednesday, June 24

08:00 Coffee will be available at GI

Subduction Zone Seismicity and Structure

GI Auditorium, 8:30 – 10:00

Presiding: Michael West and Steve McNutt (GI, UAF)

- 8:30 – 8:45 Geoffrey A. Abers, Douglas Christensen, Joshua Calkins IMAGING AND EARTHQUAKES ALONG 600 KM TRANSECT OF SUBDUCTION IN CENTRAL ALASKA: BEAAR TO MOOS
- 8:45 – 9:00 Funiaki Kimata, Takeo Ito, Endra Gunawan, Agustan, Takao Tabei, Iruwan Meilano, Didik Sugiyanto, Irwandy GREAT EARTHQUAKES ALONG THE TRENCHES AND HUGE ACTIVE FAULTS TRAVERSING THE BACK ARC ISLANDS : 2004 SUMATRA-ANDERMAN EARTHQUAKE AND SUMATRAN FAULT
- 9:00 – 9:15 Takahido Maeda and Tsutomu Sasatani LONG-PERIOD GROUND MOTIONS FROM LARGE INTERPLATE EARTHQUAKES; THE 2003 TOKACHI-OKI EARTHQUAKE
- 9:15 – 9:30 Sergei A. Fedotov, Alexey V. Solomatin, Sergey D. Chernyshev LONG-TERM EARTHQUAKE FORECAST FOR THE KURIL-KAMCHATKA ARC FOR 2009-2014
- 9:30 – 9:45 Matthew M. Haney, Stephanie G. Prejean, Rachel Murphy, and Cliff Thurber SEISMIC VELOCITY STRUCTURE AT THE VOLCANOES OF KATMAI, ALASKA, FROM LOCAL EARTHQUAKES AND AMBIENT NOISE
- 9:45 – 10:00 Anna Konovalova and V. A. Saltykov ABOUT THE NECESSITY OF REMOVING GROUPED EARTHQUAKES FROM THE CATALOGUE OF KAMCHATKAN EARTHQUAKES IN ORDER TO ESTIMATE SEISMICITY PARAMETERS

Subduction Zone Seismicity and Structure

GI Globe Room, 10:00 – 11:00

POSTER SESSION

Presiding: Michael West and Steve McNutt (GI, UAF)

- 10:00 – 11:00 Anna Bellesiles, Christensen, D., Abers, G., Song, X. MANTLE ANISOSTROPY IN ALASKA FROM SHEAR WAVE SPLITTING OBSERVATIONS

- 10:00 – 11:00 Branden Christensen, Stephen R. McNutt, Leah Burris SWARMS VERSUS MAINSHOCK-AFTERSHOCK SEQUENCES: A SYSTEMATIC STUDY IN TERMS OF ENERGY
- 10:00 – 11:00 Chubarova O.S., Gusev, A.A., Chebrov V.N. PROPERTIES OF STRONG GROUND MOTIONS OF OLYUTORSKY EARTHQUAKE IN APRIL 20, 2006 AND ITS AFTERSHOCKS FROM DIGITAL RECORDS.
- 10:00 – 11:00 Matt Gardine and Michael West INVESTIGATING THE DEEP CRUSTAL SEISMIC STRUCTURE OF COLIMA VOLCANO, MEXICO
- 10:00 – 11:00 Ophelia George, Michael West ANALYSIS OF DEEP SEISMICITY AT MOUNT SPURR, COOK INLET, ALASKA
- 10:00 – 11:00 Anna Konovalova and Vadim Saltykov LOCATION OF B-VALUE ANOMALIES: PROCEDURE AND RESULTS
- 10:00 – 11:00 Kozhevnikova T.Yu. and Senyukov S.L. EXPERIENCE WITH REMOTE DETERMINATION OF ASH PLUME INITIATION AND HEIGHT USING LOCAL SEISMICITY AT SHEVELUCH AND KARYMSKY VOLCANOES, KAMCHATKA
- 10:00 – 11:00 Yulia Kugaenko, Irina Nuzhdina, and Victor Chebrov MUTNOVSKY VOLCANO SEISMICITY STUDIED USING DATA FROM THE “MUTNOVSKY” SEISMIC STATION (KAMCHATKA, RUSSIA)
- 10:00 – 11:00 Nuzhdina I.N. and Senyukov S.L. SEISMICITY OF KLUCHEVSKOY VOLCANO (KAMCHATKA, RUSSIA) BETWEEN 1999-2008: SPATIO-TEMPORAL ANALYSIS OF THE EARTHQUAKES
- 10:00 – 11:00 V.M. Pavlov and I.R. Abubakirov A MOMENT TENSOR ESTIMATION ALGORITHM BASED ON A NEW METHOD OF SYNTHETIC SEISMOGRAM CALCULATION
- 10:00 – 11:00 Saltykov V. A., Kugaenko Yu. A. , Kravchenko N. M. PRECURSORY ANOMALIES IN PARAMETERS OF MULTI-SCALE SEISMICITY BEFORE LARGE CRUST EARTHQUAKE MW=6.8 AND KARYMSKY SEISMO-VOLCANIC CRISIS ON JANUARY 1-2, 1996 IN KAMCHATKA, RUSSIA
- 10:00 – 11:00 Vadim Saltykov and Andrey Patonin STAGES OF ACOUSTIC RESPONSE IN LABORATORY MODELING OF TIDAL INFLUENCE UPON SEISMICITY

- 10:00 – 11:00 Samoylenko S.B., Gordeev E.I., Melnik O.E. MODELING OF SEISMIC WAVE PROPAGATION IN AN INHOMOGENEOUS THREE-PHASE MAGMA
- 10:00 – 11:00 Ashley Shuler, Göran Ekström, Michael West, Sergey Senyukov MEASURING TEMPORAL CHANGES IN SEISMIC VELOCITY AT BEZYMIANNY VOLCANO USING AMBIENT NOISE CROSS-CORRELATION
- 10:00 – 11:00 Alexander Storcheus ON THE PROBLEM OF CALCULATING SEISMIC WAVE ENERGY
- 10:00 – 11:00 Hiroaki Takahashi, Takahiro Maeda, Minoru Kasahara FOCAL REGIONS OF GREAT EARTHQUAKES AND A SEISMIC GAP IN THE CENTRAL KURIL ISLANDS FROM HISTORICAL GEOPHYSICAL DATA
- 10:00 – 11:00 Teruhiro Yamaguchi, Minoru Kasahara, Hiroaki Takahashi, Muneo Okayama, Masamitsu Takada, Masayoshi Ichiyanagi DEVELOPMENT OF CRUSTAL DEFORMATION DATABASE
- 10:00 – 11:00 Yusuke Yamashita, Hiroshi Shimizu, Kazuhiko Goto REPEATING EARTHQUAKES ACTIVITY IN THE HYUGA-NADA REGION, SOUTHWEST JAPAN, HIGH ANGLE SUBDUCTION ZONE

Subduction Zone Seismicity and Structure (continued)

GI Auditorium, 11:00 – 12:00

Presiding: Michael West and Steve McNutt (GI, UAF)

- 11:00 – 11:15 David W. Scholl, Holly Ryan, Katie M. Keranen, Ray E. Wells, and Stephen H. Kirby RAPID FOREARC SUBSIDENCE AND BASIN FORMATION IDENTIFIES SOURCE AREAS OF GREAT EARTHQUAKES AND TRANSOCEANIC TSUNAMIS—EXAMPLE OF THE ANDREANOF FOREARC, ALEUTIAN ISLANDS
- 11:15 – 11:30 Natalia A. Ruppert, Natalia P. Kozyreva, and Roger A. Hansen STRONG CRUSTAL EARTHQUAKES IN CENTRAL ALEUTIAN ISLANDS IN 2006-2008: IMPLICATIONS FOR THE BLOCK ROTATION MODEL
- 11:30 – 11:45 Hiroaki Takahashi and Jun'ichi Miyamura VOLCANIC AND NON-VOLCANIC DEEP LOW-FREQUENCY EARTHQUAKES OCCURRING IN JAPANESE ISLANDS
- 11:45 – 13:00 LUNCH (IN UAF GLOBE ROOM)

Volcano Geophysics

GI Auditorium, 13:00 – 14:00

Presiding: Jeff Freymueller (GI, UAF)

13:00 – 13:15 Michael E. West REAL TIME EARTHQUAKE PROCESSING AT VOLCANOES: WHAT IS AND ISN'T FEASIBLE

13:15 – 13:30 J.A. Power, Z. Lu, S.G. Prejean, C. Wicks, D. Dzurisin A CONCEPTUAL MODEL OF AKUTAN VOLCANO, ALASKA, INFERRED FROM OBSERVATIONS OF SEISMICITY AND GROUND DEFORMATION: 1996 - 2009

13:30 – 13:45 Yuhki Kohno, Satoshi Matsumoto, Takeshi Matsushima, Kenji Uehira, Kodo Umakoshi, Hiroshi Shimizu MAGMA CHAMBER MODEL BENEATH UNZEN VOLCANO INFERRED FROM GEODETIC AND SEISMIC DATA

13:45 – 14:00 Takeshi Matsushima, Takao Tabei, Tsuyoshi Watanabe, Setsuya Nakada, Yuichi Morita, Fukashi Maeno, Atsushi Watanabe, Jun Oikawa, Teruyuki Kato GEODETIC OBSERVATIONS AT ANATAHAN VOLCANO, NORTHERN MARIANA ISLANDS

Subduction Zone Tectonic Processes, Volcano Geophysics, Tsunamis and Tsunami Hazards

GI Globe Room, 14:00 – 15:30

POSTER SESSION

Presiding: Jeff Freymueller (GI, UAF) and Jody Bourgeois (U Washington)

14:00 – 15:30 Vilory Bakhtiarov CHARACTERISTIC PROPERTIES OF TIME SERIES OF CONTINUOUS GPS POINTS ON KAMCHATKA (2000-2008)

14:00 – 15:30 Jeff Benowitz, Paul Layer, Stephanie Perry, Paul Fitzgerald OVERVIEW OF GEODYNAMIC MODELS FOR NEogene ALASKA OROGENESIS

14:00 – 15:30 Chebrov V., Droznin D., Gusev A., Mishatkin V., Sergeev V., Shevchenko Y., Chebrov D. SEISMIC NETWORK DEVELOPMENT FOR THE RUSSIAN FAR EAST: VIEW OF A TSUNAMI WARNING SYSTEM

14:00 – 15:30 Julie Elliott, Jeff Freymueller, and Chris Larsen ACCRETIONARY TECTONICS OF SOUTHERN ALASKA CONSTRAINED BY GPS

- 14:00 – 15:30 Ronni Grapenthin, Jeffrey T. Freymueller, Vilory Bakhtiarov, Sergey Serovetnikov A POINT IN A VOLCANIAN ERUPTION: DECOMPOSING THE CONTINUOUS GPS RECORD OF THE 2008 KARYMSKY ERUPTION USING WAVELETS
- 14:00 – 15:30 Ryo Honda, Minoru Kasahara and Toru Mogi GRAVITY ANOMALY OVER THE NORTHERN HOKKAIDO REGION, NORTHERN JAPAN
- 14:00 – 15:30 Nikolay Shestakov, Vilory Bakhtiarov, Vasily Levin, Nikolay Titkov, Sergey Serovetnikov, Nikolay Vasilenko, Alexander Prytkov, Dmitry Frolov INVESTIGATION OF PRE-, CO- AND EARLY POSTSEISMIC CRUSTAL DEFORMATIONS CAUSED BY OLUTORSKOE (20.04.2006, Mw=7.6) AND GREAT KURIL (15.11.2006, Mw=8.3; 13.01.2007, Mw=8.1) EARTHQUAKES FROM KINEMATIC ANALYSIS OF 30-SEC GPS DATA
- 14:00 – 15:30 Tatiana Pinegina and Joanne Bourgeois STRONG SUBDUCTION-ZONE EARTHQUAKES AND TSUNAMIS ALONG SOUTHERN KAMCHATKA AND THE NORTH KURIL ISLANDS DURING THE LATE HOLOCENE
- 14:00 – 15:30 Breany MacInnes, Robert Weiss, Joanne Bourgeois TSUNAMI DEPOSITS CAN DISTINGUISH THE DISTRIBUTION OF SLIP DURING THE 1952 KAMCHATKA EARTHQUAKE
- 14:00 – 15:30 Dmitry Nicolsky, Roger Hansen, Elena Suleimani, David West TSUNAMI MODELING AND INUNDATION MAPPING IN ALASKA: CURRENT STATUS OF THE PROJECT
- 14:00 – 15:30 Droznin D., Chebrov D. ALGORITHMS AND SOFTWARE FOR REAL-TIME PROCESSING OF SEISMIC SIGNALS FOR A TSUNAMI WARNING SYSTEM
- 14:00 – 15:30 Sang-Ho Yun, Scott Hensley, Paul Rosen, Paul Lundgren IMPROVEMENT IN DETECTING VOLCANIC EVENTS WITH DESDynI MISSION

Tsunamis and Tsunami Hazards

GI Auditorium, 15:30 – 17:15

Presiding: James Beget (GI, UAF)

- 15:30 – 15:45 James Beget and Jason Addison TSUNAMI AND PALEO-EARTHQUAKE HISTORY OF THE SOUTH-CENTRAL ALASKAN SEGMENT OF THE ALEUTIAN SUBDUCTION ZONE DETERMINED AT VALDEZ, ALASKA

- 15:45 – 16:00 Ryan, H. F., Lee, H. J., Haeussler, P. J., Alexander, C. R., and Kayen, R. E.
MULTIPLE PALEO-SUBMARINE LANDSLIDE DEPOSITS TRIGGERED BY
EARTHQUAKES ON THE ALASKAN MEGATHRUST AT PORT VALDEZ,
ALASKA
- 16:00 – 16:15 Sterling, Kara, William Knight, Paul Whitmore GENERATING TSUNAMI
SOURCES FOR THE JAPAN-KURIL-KAMCHATKA AND ALEUTIAN-
ALASKAN SUBDUCTION ZONES, AND FORECASTING THE THREAT
FOR THE WEST COAST AND ALASKA TSUNAMI WARNING CENTER'S
AREA OF RESPONSIBILITY
- 16:15 – 16:30 Elena Suleimani, Dmitry Nicolsky, Roger Hansen NEAR-FIELD MODELING
OF THE 1964 ALASKA TSUNAMI: A SOURCE FUNCTION STUDY
- 16:45 – 17:00 Steblov, Grigory M., Mikhail G. Kogan, Boris V. Levin, Nikolai F. Vasilenko,
Alexander S. Prytkov, and Dmitry I. Frolov SIZES AND SLIP DISTRIBUTIONS
OF THE 2006–2007 GREAT KURIL EARTHQUAKES FROM GPS
COSEISMIC OFFSETS

Thursday, June 25

08:00 Coffee will be available at GI

Geothermal Power – Field trip to Chena Hot Springs

GI Auditorium, 8:30 – 9:00

Chena Hot Springs, 9:00 – 22:00

8:30 – 9:00 Lucien Y. Bronicki and Brigitte A. Martini TAPPING GEOTHERMAL ENERGY IN ACTIVE VOLCANIC ENVIRONMENTS: LESSONS FROM WORLDWIDE PRODUCTION AND PLANS FOR MT. SPURR GEOTHERMAL DEVELOPMENT

9:00 – 16:00 Local field trip, Hot springs, metamorphism and geothermal power

16:00-20:00 Dinner and back-arc soak at Chena Hot Springs Resort

20:00-21:00 Open Discussion, Chena Hot Springs Resort

21:00 Return to Fairbanks

Friday, June 26

08:00 Coffee will be available at GI

Comparative study of Bezymianny, Shiveluch, and Mount St Helens Volcanoes – Results of PIRE-Kamchatka project

GI Auditorium, 8:30 – 10:00

Presiding: Pavel Izbekov and Michael West (GI, UAF)

8:30 – 8:45 Izbekov, Pavel COMPOSITIONAL TRENDS AT BEZYMIANNY VOLCANO

8:45 – 9:00 Oleg Melnik, Alexei Barmin, Stephen Sparks MODELLING OF THE ERUPTION DYNAMICS OF A SILICIC VOLCANO

9:00 – 9:15 Pavel Plechov, Vasily Shcherbakov, Alexandra Tzay, Madeleine Humphreys TIME CONSTRAINTS FOR MAGMA SUPPLY IN BEZYMYANNY AND SHIVELUCH VOLCANIC SYSTEMS

9:15 – 9:30 Theresa M. Kayzar, Bruce K. Nelson, Pavel E. Izbekov, Marina Belousova, Alexander Belousov, and PIRE Research Team GEOCHEMICAL TRACING OF VOLCANIC GASES AT BEZYMIANNY AND SHIVELUCH VOLCANO: IMPLICATIONS FOR MAGMATIC PLUMBING SOURCES

9:30 – 9:45 Alexander Belousov, Marina Belousova, Amanda B. Clarke, Barry Voight, Kim Genereau EVOLUTION OF DEPOSIT CHARACTERISTICS OF BLAST-GENERATED PYROCLASTIC DENSITY CURRENT WITH DISTANCE FROM VOLCANO: KEY TO TRANSPORTATION/DEPOSITION MECHANISMS OF THE BEZYMIANNY, 1956 AND MOUNT ST. HELENS, 1980 EVENTS

9:45 – 10:00 Senyukov S.L. EXPERIENCE OF PREDICTING EXPLOSIVE ERUPTIONS AT BEZYMIANNY VOLCANO, KAMCHATKA

Comparative study of Bezymianny, Shiveluch, and Mount St Helens Volcanoes – Results of PIRE-Kamchatka project

GI Globe Room, 10:00 – 11:00

POSTER SESSION

Presiding: Michael West and Jeff Freymueller (GI, UAF)

10:00 – 11:00 Leslie D. Almberg, John C. Eichelberger, Jessica F. Larsen, Florian Fusseis
THREE-DIMENSIONAL DEGASSING STRUCTURES IN THE UPPER CONDUIT OF ANDESITE-DACITE VOLCANIC SYSTEMS – BEZYMIANNY, RUSSIA, UNZEN, JAPAN, OBSIDIAN DOME AND MOUNT ST. HELENS, USA

10:00 – 11:00 Natalia Gorbach, Maxim Portnyagin and Vera Ponomareva VOLCANIC AND CHEMICAL GEOLOGY OF SHIVELUCH VOLCANO: THREE PHASES OF EVOLUTION

10:00 – 11:00 Krivomazova O.V. LITHOLOGICAL CHARACTERISTICS OF PYROCLASTIC DENSITY CURRENTS OF BEZYMIANNY VOLCANO IN 2005-2008 YEARS.

10:00 – 11:00 Olga Kuvikas, Maxim Portnyagin, Vera Ponomareva MAJOR AND VOLATILE ELEMENTS IN GLASSES FROM LARGE EXPLOSIVE KAMCHATKA ERUPTIONS CORRELATE WITH DEPTH TO SUBDUCTING PLATE

10:00 – 11:00 T. Lopez, S. Ushakov, T. Clark and P. Izbekov A COMPARISON OF VOLCANIC SO₂ EMISSION RATES FROM BEZYMIANNY, SHIVELUCH, AND MOUNT ST. HELENS VOLCANOES

10:00 – 11:00 Owen K. Neill, Julia E. Hammer, Pavel E. Izbekov, Marina G. Belousova, Alexander B. Belousov, Amanda B. Clarke, Barry Voight EDIFICE PRESSURE PRIOR TO THE 30 MARCH, 1956 ERUPTION OF BEZYMIANNY VOLCANO, KAMCHATKA, RUSSIA

10:00 – 11:00 Senyukov S.L. and Droznina S.Ya. PRELIMINARY 1-D VELOCITY MODEL OF BEZYMIANNY VOLCANO (KAMCHATKA, RUSSIA), USA-RUSSIA PIRE PROJECT

10:00 – 11:00 Sergey Serovetnikov, Vilory Bahtiarov, Nikolay Titkov GPS MONITORING OF BEZIMIANY VOLCANO, KAMCHATKA IN 2006-2009

10:00 – 11:00 Violetta Shanina PETROPHYSICAL PROPERTIES OF VOLCANIC ROCKS OF BEZYMIANNY VOLCANO, KAMCHATKA, FAR EASTERN RUSSIA

10:00 – 11:00 Vasily Shcherbakov, Pavel Plechov, Pavel Izbekov PLAGIOCLASE ZONING AS AN INDICATOR OF PROCESSES IN MAGMA SYSTEM BENEATH BEZYMYANNY VOLCANO, KAMCHATKA

10:00 – 11:00 Jill Shipman, Pavel Izbekov, and John Eichelberger PETROLOGIC INSIGHT INTO THE MAGMATIC SYSTEMS AT BEZYMIANNY AND SHIVELUCH VOLCANOES, KAMCHATKA, RUSSIA

10:00 – 11:00 Wendy K. Stovall, Bruce F. Houghton, PIRE Team (2006) INVESTIGATING THE PLINIAN PHASE OF THE 1956 BEZYMIANNY ERUPTION USING MICROTTEXTURAL ANALYSIS OF PYROCLASTIC FLOW DEPOSITS

10:00 – 11:00 Weston A. Thelen, Michael West, Stephen D. Malone PRACTICAL APPLICATIONS OF MULTIPLET BEHAVIOR AT MOUNT ST. HELENS, WASHINGTON AND BEZYMIANNY VOLCANO, RUSSIA

10:00 – 11:00 Yulia Tsvetkova and Oleg Melnik INFLUENCE OF MAGMA-WALLROCK HEAT TRANSFER ON ERUPTION DYNAMICS

10:00 – 11:00 S. M. van Manen and J. Dehn FIFTEEN YEARS OF SPACEBORNE THERMAL OBSERVATIONS AT BEZYMIANNY: DOME GROWTH, PRECURSORS AND EXPLOSIVE ERUPTIONS

The Kurile Biocomplexity Project

GI Auditorium, 11:00 – 12:00

Presiding: Joanne Bourgeois (University of Washington)

11:00 – 11:15 Ben Fitzhugh, Joanne Bourgeois, Mike Etnier, Erik Gjesfield and KBP teams SOME MULTI-DISCIPLINARY RESULTS FROM THE 2006, 2007 AND 2008 EXPEDITIONS OF THE KURIL BIOCOMPLEXITY PROJECT

11:15 – 11:30 Mitsuhiko Nakagawa, Akira Baba, Yoshihiro Ishizuka, Takeshi Hasegawa, Ayumi Kosugi TEPHROSTRATIGRAPHY OF KURIL ISLANDS: EVALUATION OF HOLOCENE ERUPTIVE ACTIVITY OF KURIL ARC

11:30 – 11:45 Breany MacInnes and Joanne Bourgeois DIRECT MEASUREMENTS OF TSUNAMI EROSION BY THE KURIL BIOCOMPLEXITY PROJECT: THE 2006 AND 2007 KURIL ISLAND EVENTS

11:45 – 12:00 Joanne Bourgeois, Tatiana Pinegina, Breany MacInnes, M. Elizabeth Martin, Ekaterina Kravchunovskaya, Nadezhda Razzhegaeva, Vera Ponomareva & KBP teams PALEOTSUNAMI STUDIES IN THE CENTRAL KURIL ISLANDS—PRELIMINARY REPORT BASED ON THREE KURIL-BIOMPLEXITY-PROJECT FIELD SEASONS

12:00 – 13:00 LUNCH (IN UAF GLOBE ROOM)

Hazards, Monitoring and Risk Reduction

GI Auditorium, 13:00 – 14:30

Presiding: Christina Neal (USGS)

13:00 – 13:15 Christina Neal, Kristi Wallace, Chris Waythomas, Cheryl Cameron, Matt Glazewski IMPACTS ON MARINE OPERATIONS DURING 2008 ALEUTIAN ERUPTIONS: TOWARDS IMPROVING WARNING MESSAGES FOR VESSELS AT SEA

13:15 – 13:30 Peter Webley and Ken Dean PREDICTING VOLCANIC ASH CLOUD MOVEMENT ACROSS THE NORTH PACIFIC USING THE PUFF DISPERSION MODEL

13:30 – 13:45 Zhong Lu, Dan Dzurisin, Chuck Wicks, and John Power USING INSAR TO MAP AND STUDY DEFORMATION OF ALEUTIAN VOLCANOES

13:45 – 14:00 O.A. Girina and C.A. Neal KAMCHATKAN VOLCANIC ERUPTION RESPONSE TEAM (KVERT) PROJECT IN 2006-2009

14:00 – 14:15 Paul Lundgren, Zhong Lu, Charles Wicks, Scott Hensley APPLICATION OF UAVSAR TO ACTIVE U.S. VOLCANOES

14:15 – 14:30 R. Greg Vaughan, Laszlo P. Keszthelyi, Ashley Gerard Davies, Henry Heasler, Cheryl Jaworowski, David J. Schneider, Jacob B. Lowenstern REMOTE SENSING OF VOLCANIC THERMAL FEATURES: EXPLORING THE LIMITS OF SUB-PIXEL THERMAL FEATURE MEASUREMENT USING ASTER TIR DATA

**The Kurile Biocomplexity Project
Hazards, Monitoring and Risk Reduction
Interdisciplinary Studies**

GI Globe Room, 14:30 – 16:00

POSTER SESSION

Presiding: Jody Bourgeois (U Washington) and Christina Neal (USGS)

- 14:00 – 15:30 Alexander Belousov and Marina Belousova LARGE SCALE FAILURES AND DEBRIS AVALANCHE DEPOSITS OF VOLCANOES OF KURILE ISLANDS
- 14:00 – 15:30 Kei Ioki and Yuichiro Tanioka TSUNAMI SOURCE OF THE 1963 KURILE EARTHQUAKE
- 14:00 – 15:30 D.N. Kozlov and R.V. Zharkov CURRENT DATA DESCRIBING THE CONDITION OF THE INTRACALDERA LAKE BIRYUZOVOE (KURIL ISLANDS)
- 14:00 – 15:30 Colby S. Phillips INITIAL SOURCE EVALUATION OF ARCHAEOLOGICAL OBSIDIAN FROM THE KURIL ISLANDS, FAR EASTERN RUSSIA, USING PORTABLE XRF
- 14:00 – 15:30 N.G. Razzhigaeva, L.A. Ganzev, T.A. Grebennikova, E.D. Ivanova, V.M. Kaistrenko, A.A. Kharlamov GRAIN SIZE COMPOSITION AND MICROFISSILS FROM DEPOSITS OF THE 15 NOVEMBER 2006 TSUNAMI IN THE CENTRAL KURILE ISLANDS
- 14:00 – 15:30 Rybin A.V., Zharkov R.V., Kozlov D.N., Chibisova M.V., Degterev A.V. PRELIMINARY RESULTS FROM A STUDY OF ACTIVE CENTRAL KURIL ISLANDS VOLCANOES UNDER THE AUSPICES OF THE "KBP 2006-2008" PROJECT
- 14:00 – 15:30 Yuichiro Tanioka and Ioki, Kei GREAT INTERPLATE EARTHQUAKES ALONG THE CENTRAL KURILE SUBDUCTION ZONE
- 14:00 – 15:30 James W. Taylor OKHOTSK MIGRATION AND ANIMAL PROCUREMENT IN NORTHERN JAPAN AND THE RUSSIAN FAR EAST: ISOTOPIC ANALYSIS OF HUMANS, PIGS, DOGS, AND BEARS
- 14:00 – 15:30 Chibisova M. V. and Rybin A.V., MONITORING VOLCANIC ACTIVITY IN THE KURIL ISLANDS

- 14:00 – 15:30 E. Duarte, E. Fernández OVSICORI-UNA: 25 YEARS OF VOLCANO AND SEISMIC MONITORING IN COSTA RICA
- 14:00 – 15:30 Dmitry Melnikov ALOS PALSAR INTERFEROMETRY OF THE KLYUCHEVSKAYA GROUP OF VOLCANOES, KAMCHATKA
- 14:00 – 15:30 A.A. Nuzhdaev and O.A. Girina THE KVERT PROJECT: ASH DANGER FOR AVIATION IN KAMCHATKA AND NORTHERN KURILES IN 2005-2008
- 14:00 – 15:30 Peter Rinkleff and Catherine Cahill MICROMETER-SCALE VOLCANIC ASH COLLECTION AND CHARACTERIZATION STUDIES IN ALASKA AND KAMCHATKA
- 14:00 – 15:30 Sally Kuhn Sennert, Edward Venzke, Lee Siebert, Paul Kimberly NEW ADVANCES IN THE COLLABORATIVE USGS/SMITHSONIAN WEEKLY VOLCANIC ACTIVITY REPORTS: DOCUMENTING CURRENT ACTIVITY FOR SCIENTISTS AND NON-SCIENTISTS
- 14:00 – 15:30 Sobolevskaya O.V., Senyukov S.L. THE THERMAL ANOMALIES TEMPERATURES RESEARCH ON KAMCHATKAN ACTIVE VOLCANOES WITH THE PURPOSE OF DETERMINATION OF THEIR SHORT-TERM ERUPTIONS PRECURSORS
- 14:00 – 15:30 Anna Bulochnikova PROCESSES OF RELIEF FORMATION IN THE CONTINENT-OCEAN BORDER ZONE (COMMANDOR ISLANDS)
- 14:00 – 15:30 Firstov, P.P. and Tristanov, A.B. WAVE DISTURBANCES IN THE ATMOSPHERE CAUSED BY STRONG EXPLOSIVE ACTIVITY AND FORMATION OF PYROCLASTIC FLOWS FROM BEZYMIANNY VOLCANO (KAMCHATKA)
- 14:00 – 15:30 Yuri Manstein ELECTROMAGNETIC SOUNDING AND 2D DC TOMOGRAPHY OF THE SHALLOW STRUCTURES OF KAMCHATKA VOLCANOES, FAR-EASTERN RUSSIA
- 14:00 – 15:30 Renat Shakirov and Anatoly Obzhirov METHANE ESCAPE, GAS HYDRATES, AND MUD VOLCANOES IN THE SEA OF OKHOTSK AND ON SAKHALIN ISLAND
- 14:00 – 15:30 R. Zharkov and D. Kozlov THE MODERN SOLFATARIC-HYDROTHERMAL ACTIVITY OF THE VOLCANOES OF THE CENTRAL AND NORTHERN KURILS

Discussion, Concluding Remarks, and Wrap up

GI Auditorium, 16:00 – 18:00

Presiding: Steve McNutt (GI, UAF)

18:30 Depart GI for Farewell Banquet. Transportation will be provided.

Saturday, June 27

Participants depart for home or prepare for post-workshop excursions.

Notes

ABSTRACTS

PRE-MEETING WORKSHOPS AND SHORT COURSES

WHAT CAN PREHISTORIC LAND-LEVEL CHANGES TELL US ABOUT FOREARC GEODYNAMICS IN THE CENTRAL AND WESTERN ALEUTIANS?

Rich Briggs, Alan Nelson

Geologic Hazards Team, US Geological Survey, Golden, CO, USA.

Details of the history of land-level change (inferred from local relative sea-level changes) in the Aleutian forearc underpin our knowledge of paleoearthquake, paleotsunami, and eustatic sea-level history, and, therefore, our geodynamic understanding of the forearc. Along the eastern Aleutian-Alaskan subduction zone, forearc islands above the 1964 rupture area - such as Middleton, Montague, and Kodiak - display complex vertical deformation histories that integrate the effects of megathrust rupture, upper plate deformation, and the interplay between glacio-isostatic and eustatic influences on relative sea-level change. Great megathrust earthquakes in Japan, Indonesia, Chile, and elsewhere have not left a simple, cumulative record of coastal uplift or subsidence above and around their rupture areas. Complex vertical forearc deformation is especially well-demonstrated by the outer arc islands off Sumatra where the elastic behavior of the forearc wedge dominates the Holocene deformation pattern and net deformation is only a small fraction of overall plate convergence. While it will be challenging to reconstruct megathrust rupture histories from forearc island uplift in the Aleutians, application of new, more precise techniques for measuring subsidence, and possibly uplift, at suitable coastal sites can provide rates of upper-plate deformation that could contribute substantially to understanding subduction geodynamics.

Despite a flurry of great megathrust ruptures in the mid-20th century, late Quaternary uplift in the central and western Aleutian islands has been little studied. The geomorphic reconnaissance of Morris and Bucknam found evidence for relative vertical stability of the arc during the past 5000 years. Black, and more recently Jordan, documented mid-Holocene beach berms and marine terraces that record several to tens of meters of glacio-isostatic relative sea level change, implying relatively low rates of vertical tectonic deformation. Local volcanic effects on land-level change aside, rates of tectonic uplift in most of the Aleutian arc appear to be low (<1-2 mm/yr).

Because Aleutian islands nearest the trench potentially overlie areas of megathrust rupture, they are particularly important targets for study. At most subduction zones, rupture areas lie beneath the ocean floor where surface deformation cannot be measured. In the Aleutians, the outer Shumagin, Sanak, and Delarof islands extend from the arc to within ~110 km of the trench. Of these, only the outer Shumagin islands have been the focus of detailed land-level change studies. Winslow and Johnson used ¹⁴C dates from peat overlying inferred marine surfaces to derive average Holocene uplift rates of 3 ± 1 mm/yr, with local rates as high as 12 mm/yr, which they attributed to differential deformation on upper-plate structures. Key underlying assumptions of this early work were that the Shumagins were cumulatively uplifted during sequential paleoearthquakes, and that sea level had risen asymptotically to its present level after the last glacial maximum. In contrast, early field observations by Black and more recent models of global glacial isostatic adjustment suggest a mid-Holocene relative sea-level high of several meters in the Aleutians due to glacio-eustatic effects. Furthermore, the geomorphology of many of the outer Shumagin islands - in particular drowned coastlines and the lack of old, raised marine terraces - suggests sustained late-Quaternary subsidence in many places.

The need for a re-evaluation of Holocene uplift rates in the Shumagins and a reconstruction of the history of late-Quaternary land-level change suggests several intriguing questions. Recent geodetic data suggest that the Shumagin section of the subduction zone is freely slipping or only weakly coupled. If this is the case, what stresses drive the ongoing internal deformation of the upper plate here, as evidenced by the presence of the islands? In Sumatra, outer arc islands probably correspond to regions where the plate boundary is highly coupled—why is this not the case in the Shumagins? Does the late Quaternary subsidence in the outer Shumagins that we infer from imagery reflect only the influence of upper-plate structures? Perhaps most importantly from a hazards perspective, do outer Shumagin coasts show evidence for episodic strain accumulation and release on the underlying megathrust? Detailed mapping and dating of key coastal sites may answer these questions.

ONSHORE STUDIES IN A REMOTE ISLAND CHAIN – LESSONS LEARNED IN THE KURIL BIOCOMPLEXITY FIELD CAMPAIGN, SUMMERS 2006 – 2008

Joanne Bourgeois

Earth & Space Sciences, Univ. of Washington, Seattle, WA, USA.

The Kuril Biocomplexity Project (KBP) (<http://depts.washington.edu/ikip/index.shtml>) is an NSF-funded, multi-disciplinary research project led by the University of Washington and being conducted by a team of American, Japanese and Russian scholars and students, examining a 5000-year history of human-environmental interactions along the Kuril Island chain (see Fitzhugh et al., JKASP abstract). KBP had its start in surveys carried out by the International Kuril Island Project, IKIP (<http://artedi.fish.washington.edu/okhotskia/ikip/index.htm>). The focus of that project was a biological survey. Finding some archaeological sites, IKIP leaders invited Ben Fitzhugh (with a supplement from NSF) to join the summer 2000 campaign for a preliminary archaeological survey. It then took us four tries to get substantial funding for KBP from NSF. We held workshops of investigators, invited experts, and students at UW each year to refine the proposal. Fitzhugh is PI; I am a co-PI & lead geological investigator on the project..

After the three unsuccessful submissions to NSF Biocomplexity, but with encouragement, we submitted a 4th time and were funded beginning September 2005 for a total of 5 years. Now we have completed three major field expeditions (summers 2006, 2007, 2008, each 4-6 weeks long; supplemented by a Russian IVGG cruise in 2007) and are focusing on analyzing those data

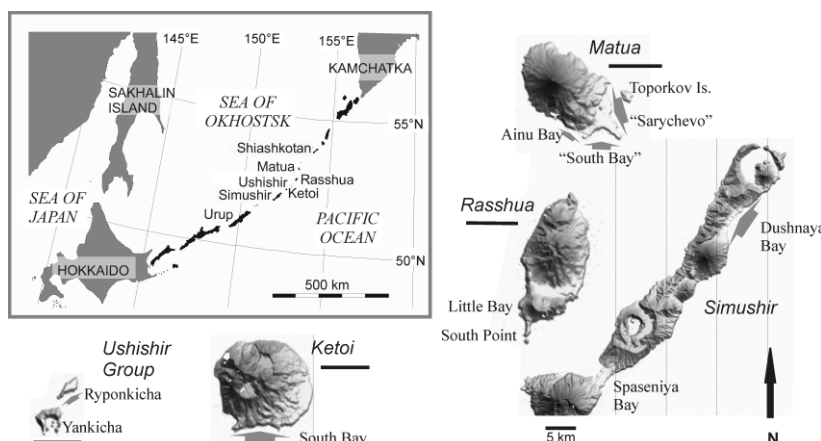
and then modeling island paleobio-geography including people.

Like the Aleutians, the Kurils are remote, isolated and subject to heavy weather; we received NSF logistical support via Polar Programs. We used chartered (private) Russian vessels, out of Yuzhno-Sakhalinsk, that could sleep about 30 scientific crew.

The central Kurils are

especially remote, so we focused our efforts there to maximize use of the ship and other logistical costs. Northern and southern islands can be visited by more regular transport. Field studies focused on archaeology, zooarchaeology, volcanology, geomorphology and paleoseismology/tsunami studies, with samples also collected for paleoenvironmental and paleoclimate analysis, and geodesy. We also took a school teacher via the ARCUS program.

Our first field season was primarily in reconnaissance mode, although teams were put ashore for stays of a few days to a week or more near a known archaeological site; where lake cores were to be taken (for paleoecology); and where a focused team could be left while other tasks were accomplished, with an easy return to the same place. The Russian GPS team visited stations already operating (or set new ones in operation where someone could maintain them), worked in campaign style at remote sites (two days minimum) and installed new remote, battery-powered instruments on Kharimkotan, Matua and Keto (several days minimum).



The second season, shortened by a budget cutback, focused primarily on detailed studies in selected sites; teams would be put ashore for camps of several days to two weeks or so. The third season was in this mode as well, but also included “clean up” – visiting key localities missed in prior years, revisiting sites for additional information. Shore access was by zodiac (put on the water by a small crane), critical to our success; we had only two in the first year, but had four in subsequent years—the boats were racked on the ship unless with a shore camp. The ship would sometimes have to move to a place protected from the weather, and it was not uncommon for some of us to be “stranded” on ship (office work possible, no lab) or left longer than planned on shore. Teams ashore had to be prepared for such possibilities. Satellite phones, ship-to-shore radios, and walkie-talkies were a must.

I will describe basically how our “geo” team(s) tended to operate, particularly the paleoseismologists/tsunami-ologists (as we were called) (see Bourgeois abstract). Also, our first two field seasons were punctuated by the 15 Nov 2008 Mw subduction-zone earthquakes and consequent tsunami, so we added a post-tsunami survey to our tasks (see MacInnes et al. JKASP abstract). Our teams used techniques developed on Kamchatka (see Pinegina JKASP abstract) and benefiting from the many ash layers present in the Kurils, though these tephra are much less studied than on Kamchatka. For that reason two volcanological teams, typically working in tandem, excavated peats and examined cleaned outcrops to develop a Holocene tephra stratigraphy for the central Kurils (see Nakagawa JKASP abstract).

Meanwhile, paleoseismologists measured coastal topographic profiles and made excavations along those profiles to determine tsunami and paleotsunami history. To measure one profile and to make several excavations on that profile, required a team of 3-5, including at least one expert to examine, describe & sample excavations. Teams of six or more (with at least two experts) could do two profiles at once, or split to different sites. If no other KBP team was involved, we also had to find, dig and sample a reference tephra excavation, preferably in peat. With sufficient team size, surveying and digging could be done in tandem, and depending on profile length and excavation depth, more than one profile with excavations measured. The keys were to choose good locations (e.g. from Google Earth or if Russians had air photos or detailed maps) and good excavation spots, not too far from good anchorage, though we sometimes crossed islands in cases where nearby anchorage or landing was bad. Easy sometimes, others not.

With many teams working in time and space, record keeping is critical. I developed a spreadsheet to list all activities on any given date, sortable by various descriptors (island, activity, samples, lat/long,...). On board we organized and entered all data on paper and into laptops. When onshore for an extended time, we took a generator and a large tent to do office work. We drew all our sections as soon as possible, marked all samples on sections and in field notes, as well as on the spreadsheet, and attempted correlations based on field data. By the third year, we had a scanner on board to scan in as much data as possible before even returning to Sakhalin.

Of course there is much work to do with all these data! And many people working on them.

Participation in the Kuril Biocomplexity Project was made possible in part by US NSF grant ARC-0508109; Ben Fitzhugh, PI, and various logistical and financial support from: Univ. of Washington; Hokkaido University Museum; Historical Museum of Hokkaido; Sakhalin Regional Museum; and the Far East Branch of the Russian Academy of Sciences (IMGG: Yuzhno-Sakhalinsk, IVGG: Petropavlovsk-Kamchatsky, NEISRI:Magadan).

A more complete list of participants can be found at: <http://depts.washington.edu/ikip/KBPpublic/KBPpeople/People.shtml>

DISTRIBUTION OF SEISMICITY AND SEISMIC COUPLING NEAR THE AMLIA FRACTURE ZONE IN THE CENTRAL ALEUTIANS

Katie Keranen¹, Gavin Hayes², Dave Scholl³, Holly Ryan⁴, Steve Kirby⁵

¹USGS WEHZ, Seattle, WA, USA.

²USGS NEIC, Golden, CO, USA.

³USGS CMG-Emeritus, Menlo Park, CA, USA.

⁴USGS CMG, Menlo Park, CA, USA.

⁵USGS WEHZ, Menlo Park, CA, USA.

The Aleutian subduction zone is the source region for many great tsunamigenic earthquakes. Earthquakes are not distributed evenly along the Aleutian margin but rather cluster into particular segments. One fundamental segment boundary occurs at the Amlia Fracture Zone (AFZ), a major north-striking fault on the oceanic slab now being subducted at the Aleutian trench. Across the AFZ a change in dip of the subducting plate, seismicity, age of the plate, extensional vs. compressional characteristics of the upper plate, and roughness of the seafloor entering the trench demonstrate a clear change in the structure of the subduction zone between adjacent segments. These changes are also apparent in satellite free-air gravity anomalies and in the height of the outer rise. To the east of the AFZ, the plate dips more steeply than to the west, the upper plate shows extensive extension in the fore-arc, and back-arc extension occurs in the Amlia-Amukta Basin. Virtually no seismicity is recorded in the ~100 km to the east of the AFZ. To the west, the plate dips less steeply and the upper plate shows compressional characteristics in the fore-arc. The western Amlia segment has background seismicity and has produced three recent large earthquakes (1957, 1986, and 1996) that generated local and/or transoceanic tsunamis. In the eastern Amlia segment, no large earthquakes have been recorded, and the best known rupture areas of the three largest earthquakes either terminate near the AFZ or show little to no slip in the eastern Amlia section (Cross and Freymuller, 2007). These observations demonstrate a strong linkage between observable geologic characteristics and the occurrence of great earthquakes along the Aleutian margin. To assess the degree of coupling (and variations in coupling) along the strike of the subduction zone near the AFZ, we systematically compare the moment released by earthquakes within the seismogenic zone to the potential moment accumulated by steady plate motions over the same time period. By removing the largest events (which dominate the moment release signal, but repeat over longer intervals), we analyze the background spatial and temporal variability of moment release, which suffers less from artifacts arising from the analysis of an incomplete catalog. These comparisons identify areas of sustained moment deficit, others of variable seismicity rates (e.g. leading up to great earthquakes), and still other areas of sustained moment release, which we in turn attempt to relate to plate boundary structure and the underlying causes for coupling along the subduction interface. By systematically studying the geologic setting and seismic coupling along global subduction margins, we aim to understand the controlling factors of great earthquakes and better estimate the seismic and tsunami risk for individual margin segments.

STATE OF THE ARC: OVERVIEW

TECTONIC SETTING AND ACTIVITY OF THE NORTH PACIFIC

Jeff Freymueller

Geophysical Institute, University of Alaska Fairbanks, Fairbanks, AK, USA.

When topography and bathymetry are viewed together, the connected subduction systems of the Japan, Kuril-Kamchatka, and Aleutian arcs represent one of the longest and most spectacular systems on the planet. Subduction in all of these arcs is driven by the motion of the Pacific plate, which moves northwestward to westward at a rapid rate. Subduction of the Pacific plate drives great earthquakes along these arcs, and a nearly continuous line of arc volcanoes. The North Pacific is the greatest natural laboratory for subduction processes on the planet.

Early views of plate tectonics held that the North American plate was the overriding plate in all of these arcs, but the more detailed understanding we have after two decades of GPS measurements shows that most, if not all of the overriding crust belongs to one of a series of microplates or smaller blocks that move independently from both North America and Eurasia as part of a large, diffuse deforming belt. The northeastern part of Eurasia and the northwestern part of North America are made up of a collage of tectonic blocks of various sizes; the details of block motions and boundaries, not to mention the existence (or not) of particular blocks, remain the focus of vigorous research and debate. Independently moving blocks or microplates that have been proposed for this general region include the South and North China blocks, Amurian plate, Northeast and Southwest Japan blocks, Okhotsk plate, Bering plate, the Southern Alaska or Wrangell block, and the Yakutat block. New evidence from Alaska suggests the existence of a Kenai-Kodiak forearc block, which may extend well to the southwest and include part of what has been recently described as the Bering plate.

In this talk, I will provide a brief overview of the evidence for pervasive motion and deformation of the overriding plate around the North Pacific, along with discussion and speculation about the forces that are driving the deformation of the region in the broad. In the south, deformation of the overriding plate is driven mainly by the India-Eurasia collision, which has caused large pieces formerly part the Eurasian plate to move in response to the impact of India. Farther north, deformation may be driven by the convergence between the Eurasian and North American plates. In Alaska, the collision of the Yakutat block in southeast Alaska may be the most significant driver of deformation. Lateral escape of blocks from continent-continent collision zones explains most of the present deformation.

IMPACTS ON MARINE OPERATIONS DURING 2008 ALEUTIAN ERUPTIONS: TOWARDS IMPROVING WARNING MESSAGES FOR VESSELS AT SEA

Christina Neal¹, Kristi Wallace¹, Chris Waythomas¹, Cheryl Cameron², Matt Glazewski³

¹*Alaska Volcano Observatory, Alaska Science Center, U.S. Geological Survey, 4210 University Drive, Anchorage, AK USA.*

²*Alaska Volcano Observatory, Division of Geological and Geophysical Surveys, 3354 College Road, Fairbanks AK USA.*

³*National Weather Service, Ocean Prediction Center, 5200 Auth Road, Room 405, Camp Springs, MD, USA.*

The impacts of explosive volcanic eruptions on marine operations are poorly documented in the scientific literature and, as a consequence, warning protocols and general awareness of the hazard among mariners are lacking. The purpose of this presentation is to collate information about the effects of recent Aleutian Island volcanic activity on marine vessels and apply lessons learned during these events to improve maritime warning procedures. The worldwide risk to ocean-going vessel traffic due to volcanic activity is not well quantified, and certainly less than the daily risk to aviation and people on the ground. However, in Alaska alone, more than 300 large ships travel Great Circle routes through and near the Aleutian chain every month. Thus, the potential for volcanic impacts is not negligible.

Two major and one minor eruption in the Aleutians during the summer of 2008 produced trace to heavy tephra fall upon at least several marine vessels operating in the vicinity of each eruption. Thanks to modern methods of communications while at sea, reports and photographs from mariners experiencing ash fall and observing eruptions in progress are now received at AVO via our web site or interagency partners such as the National Weather Service or U.S. Coast Guard.

Okmok Volcano. From July 12 through mid-August, 2008, Okmok Volcano on Umnak Island (~120 km southwest of Unalaska/Dutch Harbor) produced nearly continuous ash clouds that rained varying amounts of ash onto the surrounding sea on numerous occasions. The most voluminous and significant ash fall occurred during the opening phase on July 12. On that day, boats in the general vicinity of Umnak Pass, including the fishing vessel that rescued a family fleeing the eruption, experienced ash fall of up to several millimeters over the course of several hours. The only report of damage was a collapsed air filter on a small fishing boat. Other vessel owners indicated hours of clean-up were required to remove the ash. The U.S. Coast Guard responded to the July 12 eruption by temporarily closing Umnak Pass to all vessel traffic. Accumulation of lahar deposits at the mouth of multiple drainages on Umnak Island led to submarine debris flows which in turn altered the seafloor topography up to several miles off shore. Although pumice fragments several centimeters in diameter washed up on beaches of Unalaska within several weeks of the July 12 eruption, AVO received no reports of damage or disruption to vessels from encounters with floating pumice at sea.

Cleveland Volcano. In late July, Cleveland Volcano on Chuginadak Island, 75 km west of the community of Nikolski, produced a series of ash clouds reaching as high as 20,000 ft above sea level. Lava accumulating on the upper flanks also generated hot, rubbly flows down the steep flanks of the volcano which entered the sea, forming boulder deltas at the shoreline. Several fishing vessels reported ash fall but no damage. Cleveland Volcano is frequently active and minor ash falls have occurred repeatedly since its last major series of eruptions in 2001.

Kasatochi Volcano. After several weeks of increasing seismic unrest, the 3-km-wide island volcano Kasatochi, located 80 km east of Adak, exploded in three violent pulses on August 7. Ash and gas clouds from these events reached in excess of 45,000 ft above sea level. The most ash-rich of these dropped up to several inches (more than 7 cm) of ash on islands to the south of Kasatochi. One fishing boat that was about 13 km from the volcano reported 4-5 inches (10-13 cm) of ash; photos suggest perhaps 1-2 inches (2.5 – 5 cm) of coarse ash and lapilli fallout (Figure 1.) Small tsunamis likely produced by the entry of pyroclastic flows into the sea were recorded at tide gauges on Amchitka, Adak, and Atka Islands, but no damage was reported.



Figure 1. Deck of the F/V Larissa M, covered in more than 3 cm (1.2 inches) of ash and lapilli fallout from the August 7, 2008 eruption of Kasatochi Volcano. Photo by Marge Tillion, used with permission.

In the wake of these events, AVO, USGS, NOAA, and others are reviewing protocols and mechanisms in place to issue timely guidance to the maritime community concerning volcanic activity. These groups are also working to develop standard marine warning messages and to conduct outreach to the maritime community on the nature of volcanic hazards at sea. The primary concern is ash fall, which can diminish visibility, interfere with onboard electronics, radios, and possibly navigation equipment, as well as foul air and water intakes and cargo holds. Ash is heavy, especially when wet, and in extreme events could pose a loading hazard. Fine ash is also an eye and respiratory irritant for the crew. Other volcanic phenomena such as volcanic gas clouds, floating rafts of pumice, and tsunami generated by a variety of flowage processes into the sea are also of potential concern for boats very near the site of eruption. Even more dangerous are pyroclastic flows and surges that can be devastating to boats caught in their path, or a sudden submarine eruption directly beneath a ship. These dramatic events, while extremely rare, have occurred historically. Further documentation of eruption impacts on marine vessel traffic in the North Pacific will improve our understanding of volcano hazards at sea.

LINKS BETWEEN QUATERNARY VOLCANISM, NEOTECTONISM AND UPPER-PLATE STRUCTURAL STYLE IN THE ALEUTIAN ARC: NEW PERSPECTIVES

Christopher Nye^{1,2}, Katie Keranen³, Paul Decker⁴, Jeff Freymueller^{1,5}

¹*Alaska Volcano Observatory, a cooperative program of the US Geological Survey, UAF Geophysical Institute, and Alaska Division of Geological & Geophysical Surveys.*

²*Alaska Division of Geological & Geophysical Surveys, Fairbanks, AK, USA.*

³*US Geological Survey, Seattle, WA, USA.*

⁴*Alaska Division of Oil and Gas, Anchorage, AK, USA.*

⁵*Geophysical Institute, University of Alaska Fairbanks, Fairbanks, AK, USA.*

The Aleutian arc extends about 3,000 km westward from central Alaska, and has often been described as being structurally simple, with downdip subduction velocity nearly constant over the majority of its length; a reasonably homogeneous subducted plate; and no complications from intra-arc or back arc rifting or spreading. Enough new data from diverse subdisciplines have accumulated to warrant reevaluation of our previous view and a new look at links between geology, geophysics and volcanology.

The classic view that the arc is structurally simple first started to change in the 1980's, with the demonstration that the western arc was broken up into a series of blocks which rotate clockwise and translate westward as convergence becomes more oblique and transpressional forces became more important (*cf. Geist et al. 1988, Tectonics 7:327-341*). New information about ongoing deformation via GPS (*Freymueller et al. 2009, AGU Monograph 179:1-42*) and integrated over geologic time (*cf. Redfield et al., 2007, Geology 35:1039-1042*) shows that the entire arc is undergoing arc-parallel deformation related to westward extrusion caused by the accretion of the Yakutat Block at the eastern end of the arc.

The classic view was also that the presence of an upper plate which is continental in the east and oceanic in the west presents a good opportunity to investigate the influence of the upper plate on volcanism because so many of the variables are controlled. However, an along-arc seismic profile across this junction shows that the Moho is at essentially the same depth in the oceanic and continental arcs (*cf. Fliedner and Klemperer 1999, JGR 104:10,667-10,694*), calling into question the role of "thickened continental crust". Additionally abundant new geochemical data have not found a geochemical offset associated with the transition from oceanic to continental crust.

Figure 1a shows major tectonic elements of the arc as they are currently understood. Figure 1b is at the same scale and projection and shows only known volcanic vents. The removal of all other information from Figure 1b facilitates the identification of major disjoints in the volcanic chain (smaller-scale segmentation of the arc has been addressed by others).

The disruption of the volcanic chain at 173.3W longitude (I in Figure 1b) coincides with a change in structural style in the forearc (seen in seismic reflection data) from compressional to the west to extensional to the east. An abrupt change in the number of earthquakes at this transition suggests that the forearc is more strongly coupled to the subducting Pacific plate to the west. A mirror disruption of the volcanic chain occurs at 156.5W longitude (II in Figure 1b). To the east the Bruin Bay Fault is a thrust, marking compression near the arc crest. To the west crestal arc-parallel faulting changes to normal. This also marks the eastward limit of the North Aleutian basin, a kilometers-thick Tertiary-Quaternary(?) extensional sedimentary basin immediately north of the arc crest.

The two disruptions in the volcanic front at I and II (Figure 1b) divide the arc into three first-order segments. The outer two typically have small-volume, crystal-rich calcalkaline magmas which are andesite to dacite in whole-rock composition with dacite to rhyolite groundmass glass. The central region contains those volcanoes which are larger, basaltic-andesite to andesite, tholeiitic, have dramatically lower crystal contents and more mafic groundmass glass. The central segment also has small crystal-rich calcalkaline andesite volcanoes – it's the presence of the large mafic tholeiitic volcanoes, rather than the absence of smaller crystal-rich andesite volcanoes which is important.

I and II also mark major topographic irregularities on the subducting Pacific Plate – the Amelia Fracture Zone at I and the chain of seamounts derived from the Cobb hotspot at II. Because these are oblique with respect to plate motion their intersection with the trench migrates, the former to the west, and the latter to the east. They may be acting to decouple the subducted plate from the overriding plate as they migrate outward, causing the transition from a forearc and

arc that is compressional to one that is extensional. This change may in turn allow easier passage of magmas to the surface in the central arc. Thus the stress regime in the upper plate may be an essential factor in modification of parental magmas and in the origin of calcalkaline vs. tholeiitic magmas. An extreme case of compression limiting volcanism is seen at III (Figure 1b), where there is a 330-km long gap in volcanism spati-ally associated with the uplift of the Alaska Range – geophysical evidence suggests that this is only a volcanic gap, not a magmatic gap.

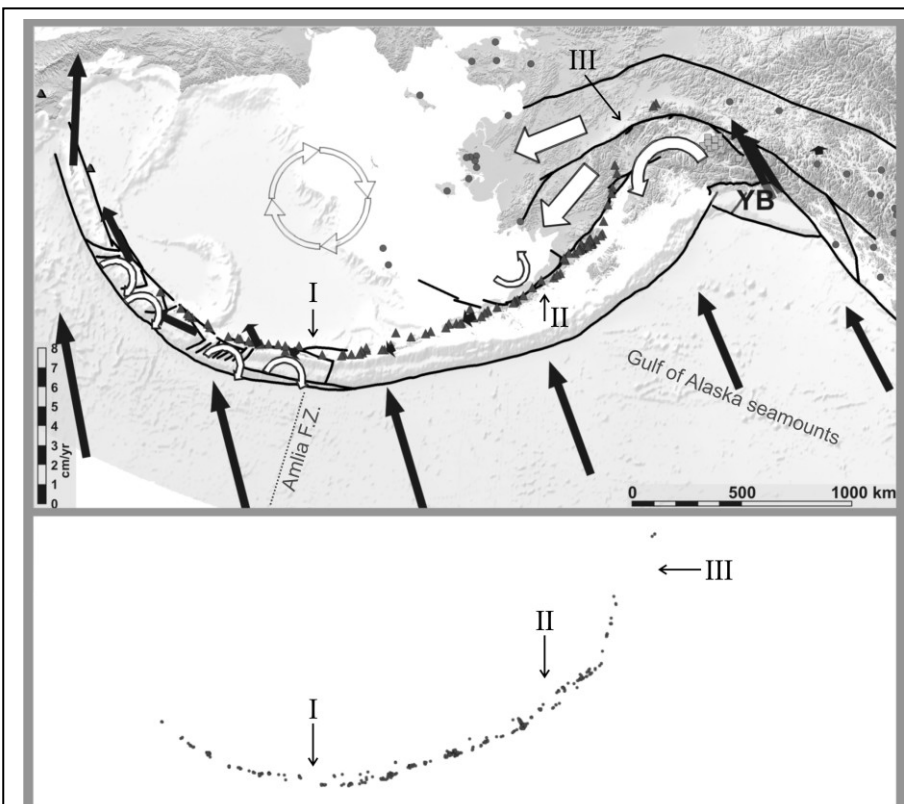


Figure 1a (top panel). Major tectonic and structural features of the Aleutian arc. Black arrows are current day plate motions relative to North American, with lengths proportional to velocities given by the scale in the lower left-hand corner. White arrows indicate geologically constrained movement and are not proportional to rate. Other symbols are black lines, major faults; YB, Yakutat Block; triangles, major Quaternary arc volcanic centers; circles, non-arc Quaternary volcanic centers; squares, Wrangell volcanoes (arc volcanoes displaced from the Aleutian arc).

Figure 1b (bottom panel) shows Aleutian arc volcanic vents at the same scale, projection, and orientation as the top panel. I, II, and III are first order spatial dislocations discussed in the text.

RECENT ERUPTIONS IN THE NORTHERN PACIFIC

ORAL PRESENTATIONS

CHRONOLOGY OF THE 2009 ERUPTION OF REDOUBT VOLCANO

Katharine F. Bull¹, Alaska Volcano Observatory staff^{1,2,3}, colleagues from the Cascade Volcano Observatory⁴ and USGS Menlo Park⁵

¹AVO-DGGS, 3354 College Rd, Fairbanks, AK 99709.

²AVO-USGS, 4210 University Dr., Anchorage, AK 99508.

³AVO-UAF, 903 Koyukuk Drive, Univ. of Alaska, Fairbanks, AK 99775-7320.

⁴USGS-CVO, 1300 SE Cardinal Court, Bldg 10, Suite 100, Vancouver, WA 98683-9589.

⁵USGS, 345 Middlefield Road, Menlo Park, CA 94025.

Redoubt Volcano is a 10,200-ft (3110-m) stratovolcano located 170 km (106 mi) southwest of Anchorage, Alaska, on the west side of Cook Inlet. Recent unrest began in the summer of 2008 when increased H₂S odor was detected during geological field work. In late September, the Alaska Volcano Observatory (AVO)'s seismic network recorded periods of volcanic tremor. Throughout the fall, AVO noted increased fumarolic emissions and accompanying ice- and snow-melt on the 1990 dome and in the upper Drift Glacier area. Gas measurements also showed elevated H₂S and CO₂ emissions. On November 5th, the AVO raised the aviation color code to Yellow and alert level to Advisory. Starting at 19:11 AKST, January 23, 2009, 48 hours of intermittent tremor and discrete, low-frequency to hybrid events began, and on January 25, AVO raised the color code to Orange and the alert level to Watch. Over the next 6 weeks, seismicity waxed and waned, an estimated 5-6 million m³ of ice on the Drift Glacier were lost due to melting, and volcanic gas emissions increased. Debris flows sourced from ice-holes near the 1990 dome and at lower-elevations overran the surface and margins of the Drift Glacier. Out-flow water draining the Drift Glacier was sampled multiple times over 10 days. The results from each sample yielded similar chemistry, suggesting the water represented a perched, shallow groundwater system large enough to maintain a nearly fixed composition for period of at least 10 days, and not purely glacial meltwater. On March 10, alert levels were lowered to Yellow/Advisory.

At 13:05 AKST, March 15, during a gas and observation overflight, a vigorous steam plume containing minor ash was emitted from a new vent in the summit ice cap just behind the position of the 1990 dome, and rose to ~15,000 ft. asl. The plume was accompanied by weak seismicity. Based on these events, the alert levels were raised again to Orange/Watch, although within 48 hours the seismicity decreased, no further ash emissions occurred, and levels were lowered again to Yellow/Advisory. The March 15 explosion deposited ash on and south of the summit, over a ~2.8 million m² area, and consisted of broken crystal fragments, dense lithic fragments and no juvenile ash—likely the result of a phreatic explosion. Following the phreatic event, satellite images revealed a small dome growing within the March 15 vent.

The first magmatic explosion occurred on March 22. Over the next two weeks, 20 explosions produced ash plumes that reached at least 20,000 ft, and up to 60,000 ft asl, based on radar, satellite, and pilot reports. Ash fall was deposited to the N, S, E and W of the volcano, including on the city of Anchorage and communities on the Kenai Peninsula, and also reached as far as Fairbanks, ~500 miles to the N. Several lahars were produced during the 2009 eruption, but none were as large in volume or extent as the two following explosions on March 23rd and April 4th that inundated the Drift River valley to the coast, 27 mi from the vent. Time-lapse cameras captured pyroclastic flows down the north side of the volcano during several of the explosions, and ballistics and pyroclastic flow deposits were observed on the south flank's Crescent glacier.

Approximately 2 days prior to the 4/4 explosion, a swarm of repeating LP earthquakes began, coincident with ongoing extrusion. LP swarms were also detected in late April. The rate of repeating earthquakes declined markedly during the ~12 hours prior to the explosion.

Preliminary petrologic studies indicate the pre-April 4 dome was more silicic (61.1 wt% SiO₂), than products erupted during the March explosive events (57.3-59.1 wt% SiO₂). The silicic composition is similar to the composition of magma erupted at the end of 1989-90 eruption. On April 4, juvenile clasts in tephra fall deposits contained dark (mafic) and light (silicic) pumice varieties, as well as banded pumices, indicating that both silicic and mafic magmas erupted together.

After April 4th the volcano moved into a period of dome-building, and no explosions occurred. Seismicity and volcanic gas emissions remained high. Continued lava extrusion and growth of the dome were tracked by Forward-looking Infra-red (FLIR) photography, photogrammetry from webcam images and overflight photography, as well as seismicity due to rockfalls off the dome surface. Late on April 4th, the new dome was seen in satellite images to be round in shape and measured 270 m in diameter. By May 14th the dome was 435 m diameter at its widest point, and the dome, plus a northern lava-flow extension, reached 1225 m in total length. The volume change over this same time period ranged from close to 1M m³ to well over 30M m³ (and possibly to 60M m³).

This presentation will provide an overview of Redoubt's activity from the precursory phase through the eruption to the time of the meeting. We will also include information on the multiple data streams available to AVO, and descriptions of the geological observations made to date.

SATELLITE OBSERVATIONS OF VOLCANIC CLOUDS FROM THE ERUPTION OF REDOUBT VOLCANO, ALASKA, 2009

Ken Dean, Jon Dehn, Peter Webley, and John Bailey

Geophysical Institute, University of Alaska Fairbanks.

Redoubt Volcano began erupting on 23 March 2009 (UTC) and was followed by 17 additional events over a nine day period as of 31 March 2009. The volcano is located on the Alaska Peninsula, 175 km southwest of Anchorage, Alaska. The last eruption was in 1989/1990 and seriously disrupted air traffic in the region, including the near catastrophic engine failure of a passenger jet. Plumes and ash clouds from the recent eruption were observed on AVHRR, MODIS and GOES data. Sulfur dioxide clouds were observed on OMI, AIRS and Calipso data. The eruption produced volcanic clouds up to 18 km which are some of the highest detected in recent times in the North Pacific region. Volcanic cloud heights were measured using ground-based radar, plume temperature and wind shear methods. Even though radar showed the greatest heights, satellite data and wind shears suggest that the largest concentrations of ash may be at lower altitudes. Light ash fall occurred in the Cook Inlet basin and northward into Alaska's interior. Sulfur dioxide clouds were detected thousands of kilometers to the east as they drifted across North America.

KVERT PROJECT: DANGER FOR AVIATION DURING ERUPTIONS OF KAMCHATKAN AND NORTHERN KURILES VOLCANOES IN 2006-2008

Olga Girina, Sergey Ushakov, Alexander Manevich, Anton Nuzhdaev, Dmitry Melnikov, Natalie Malik

Institute of Volcanology and Seismology FED RAS, 683006, Petropavlovsk-Kamchatsky, Russia.

The Kamchatkan Volcanic Eruption Response Team (KVERT) is a collaborative project of scientists from the Institute of Volcanology and Seismology, the Kamchatka Branch of Geophysical Surveys, and the Alaska Volcano Observatory. The purpose of KVERT is to reduce the risk of costly, damaging, and possibly deadly encounters of aircraft with volcanic ash clouds. To reduce this risk KVERT collects all possible volcanic information and issues eruption alerts to aviation and other emergency officials.

Thirty active volcanoes are located on Kamchatka and six are found on two Northern Kurile Islands. In this region several eruptions each year produce ash clouds that threaten the safety of air travel across the North Pacific. During 2006-2008, seven volcanoes in Kamchatka and the Northern Kuriles erupted; four of these volcanoes produced ten strong explosive events.

Sheveluch: The Level of Concern Color Code for Aviation (LCCCA) was Yellow from January until December 03, 2006, and Orange from December 04, 2006 till December 31, 2008. The LCCCA was declared Red on December 19, 2007 and December 25-26, 2006, because on these days explosions produced ashes up to 10 km above sea level (ASL). The ash column rose to 15 km ASL on March 29, 2007. Ash plumes rising to 5-6 km ASL from hot avalanches were frequently registered from December 2006 to December 31, 2008. Klyuchevskoy: The LCCCA was Green from January 01 until December 17, 2006 and from August 17, 2007 until August 07, 2008; Yellow from December 18, 2006 until February 14, 2007, from July 27, 2007 until August 16, 2008, and from August 08, 2008 until October 15, 2008; and mainly Orange from February 15 until July 26, 2007, and from October 11 until December 31, 2008. The LCCA was Red for short periods of time: May 16-30, 2007, June 19-24, 2007, and December 09-10, 2008. A large explosive-effusive eruption occurred in 2007: ash plumes rose to 10-12 km ASL and extended > 5500 km in different directions from the volcano. A strong explosive-effusive eruption occurred in 2008: ash columns rose to 8.0 km ASL, and ash plumes extended > 700 km from the volcano.

Bezymianny: The LCCCA was mainly Yellow, but it was set to Orange due to strong explosive events on May 06-07 and 10, 2006, December 25-27, 2006, May 11-15, 2007, October 16-19, 2007, November 09-21, 2007, July 11-23, 2008, and August 11-20, 2008, and to Red on May 09, 2006, December 24, 2006, and October 15, 2007. For example, on May 9 and December 24, 2006, eruptive columns rose to 13-15 km ASL. On May 12 and October 14-15, 2007, and on August 19, 2008, ash columns rose to 9-10 km ASL, while ash plumes extended > 1300 km in different directions from the volcano.

Karymsky: The LCCCA was mainly Orange owing to moderate and strong explosive activity of this volcano. Conditions on the volcano were relatively tranquil and the LCCA was Yellow on September 08-19, 2006; from December 06, 2007 until March 12, 2008, and from June 16 until July 23, 2008. Very strong explosive events were registered at the volcano on May 13-14, 2006, and ash columns rose to 8 km ASL.

Chikurachki: The LCCCA was mainly Green but was set to Orange for explosive eruptions that occurred from March 04 until April 26 and from August 19 till November 14, 2007, and from August 01-29, 2008. Ash plumes rose to 4.8-6.1 km ASL and extended > 260 km from the volcano.

THE JULY-AUGUST 2008 ERUPTION OF OKMOK VOLCANO, ALASKA: PRELIMINARY GEOLOGY, PETROLOGY AND GEOCHEMISTRY

Jessica F. Larsen¹, Christina A. Neal², Janet R. Schaefer³ and the staff of the Alaska Volcano Observatory

¹*Geophysical Institute, University of Alaska, Fairbanks, AK, USA.*

²*U.S. Geological Survey, Alaska Science Center, Anchorage, Alaska, USA.*

³*Alaska State Division of Geological and Geophysical Surveys, Fairbanks, Alaska, USA.*

Okmok Volcano, on Umnak Island in the eastern Aleutian arc, erupted suddenly and violently at 19:43 UTC on July 12, 2008. The eruption began with a blast producing ash, lapilli, and gas, followed within an hour by a more water-rich tephra column, reaching ~16 km above sea level. The 2008 eruption was the first predominantly phreatomagmatic event in the United States since Ukinrek Maars in 1977. It lasted approximately 5-weeks and was preceded by less than 5 hours of precursory seismicity, with no notable short-term geodetic precursors.

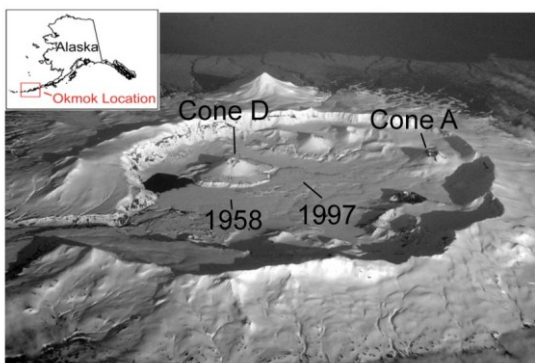


Figure 1. Inset: Location of Okmok Volcano, Aleutian Islands, Alaska. The photograph shows the physiography of Okmok Caldera, including the locations of Cones A and D, and the 1997 and 1958 lava flows.

producing pulsating columns of ash and large amounts of steam. The eruption produced a new cluster of explosion craters, forming during the first two weeks of the eruption and extending about 2 km across the northwest flank of Cone D and adjacent caldera floor. One crater formed next to, and eventually captured and drained, a pre-existing lake northeast of Cone D. A tephra ring grew atop the longest-lived 2008 vent, creating a 250-300 m high tuff cone. By August 13, only the tuff cone was active. The new explosion craters had filled with water and formed a new lake 0.6 km² in area west of Cone D. The pre-eruption lake northeast of Cone D re-filled, and now has a significantly modified shoreline.

Early during the 2008 eruption, lahars were generated by rainwater falling on newly emplaced tephra on the flanks of the volcano. The lahars impacted major drainages on the northeastern to southeastern flanks of the volcano, creating large new deltas offshore.

Post-July 12 tephra is planar-bedded, fine-grained fall and surge deposits with abundant accretionary lapilli. Individual ash beds are porous, reflecting post-emplacement de-watering. Combining estimated volume from stratigraphy and isopach mapping with the 16 km initial

plume height suggests a preliminary Volcanic Explosivity Index (VEI) of 4, making this the largest and most explosive eruption from Okmok within the last century.

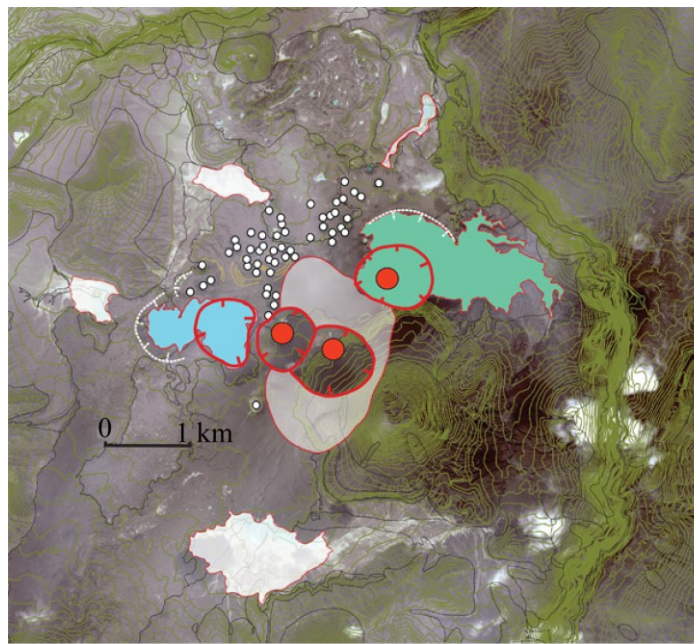


Figure 2. Map of 2008 explosion craters and the new tuff cone overlain onto a Quickbird satellite image. Image processed at the USGS-AVO by Rick Wessels. Image data courtesy of NASA/GSFC/METI/ERSDAC/JAROS, and U.S./Japan ASTER Science Team. QuickBird data copyright Digital Globe Corp.

preliminary model suggests that the 2008 eruption tapped older margins of the subsurface plumbing system at Okmok, flushing out slightly more evolved magmas than those erupted from Cone A.

References

- Begét, J.E., J.F. Larsen, C.A. Neal, C.J. Nye, and J.R. Schaefer, (2005), Preliminary volcano-hazard assessment for Okmok Volcano, Umnak Island, Alaska, *Alaska Division of Geological & Geophysical Surveys Report of Investigation 2004-3*, 32 p., 1 sheet, scale 1:150,000.

Preliminary observations by scanning electron microscopy and electron microprobe analyses indicate a diverse population of tephra grains in ash collected on Umnak Island. Blocky, poorly vesicular grains coexist with higher vesicularity grains. Plagioclase and olivine microlites vary in concentration within the tephra grains. Broken phenocrysts identified in ash collected July 12 are olivine, plagioclase, and clinopyroxene. Groundmass glass analyses from glass-rich lapilli grains are 50-54 wt. % SiO₂. Whole rock analyses of juvenile scoria cluster around 55 wt. % SiO₂, and extend possibly as high as 57.5 wt. % SiO₂. The petrological characteristics and juvenile chemistries are notably different between the 2008 products and those from other historic eruptions from Cone A. One

THE ASTER URGENT REQUEST PROGRAM: A COLLABORATIVE MULTI-AGENCY, MULTI-YEAR EFFORT TO MONITOR THE NORTH PACIFIC VOLCANOES FROM SPACE

Michael Ramsey¹, Adam Carter¹, Rick Wessels², Jonathan Dehn³, Kenneth Duda⁴, Michael Muder¹

¹*Department of Geology and Planetary Science, Univ. of Pittsburgh, Pittsburgh, PA, USA.*

²*Alaska Volcano Observatory, USGS Alaska Science Center, Anchorage, AK, USA.*

³*Geophysical Institute/Alaska Volcano Observatory, Univ. of Alaska, Fairbanks, AK, USA.*

⁴*EROS Data Center, Sioux Falls, SD, USA.*

The Advanced Spaceborne Thermal Emission and Reflection Radiometer (ASTER) instrument is a Japanese-built imaging sensor on the NASA Terra satellite. It has been acquiring data of volcanic eruptions from soon after its launch in December 1999. One of the first examples was the observations of the large pyroclastic flow deposit emplaced at Bezymianny volcano (Kamchatka, Russia). The first images in March of 2000, just weeks after the eruption, revealed the extent, composition, and cooling history of this large deposit and of the active lava dome. Similar studies have been carried out at Kluichevskoi and Sheveluch volcanoes over the past nine years. These early datasets spurred interest in volcano monitoring in the north Pacific using ASTER and gave rise to a five year old program of rapid response scheduling and imaging of volcanic activity throughout the Aleutian, Kamchatka and Kurile arcs. This program was designed to automate the ASTER sensor's ability for targeted observational scheduling using multiple satellites and an expedited system of processing. This urgent request protocol (URP) is one of the unique characteristics of ASTER, providing a limited number of emergency observations, typically at a much-improved temporal resolution and quicker turn around bypassing processing in Japan, which can add several days to a week to the process. The ongoing research/operational program is a collaboration between NASA, the USGS, AVO, IVS/KVERT, the University of Pittsburgh (UP) and the University of Alaska – Fairbanks (UAF) and has proven to be highly successful.

Due to the coarse spatial resolution of AVHRR data, the automated near-real time satellite monitoring at times can fail to capture the non-eruptive character or small-scale activity at many of these remote volcanoes. However, these data can be used to trigger ASTER into a “rapid response” mode. Specifically for Kamchatka, several beneficial factors have combined resulting in nearly 1400 ASTER images of the five most thermally-active Kamchatka volcanoes (Bezymianny, Karimsky, Kluichevskoi, Sheveluch and Tolbachik). These factors include the orbital alignment of Terra, the high latitude of the peninsula, and the persistent activity in Kamchatka. From the inception of the automated rapid response program in 2003, an additional 350 scenes have been acquired over these volcanoes, many soon after larger eruptions. These data have produced valuable quantitative information on the small-scale activity and larger eruptions. The core of the triggering mechanism for ASTER data is based on the *Okmok II* algorithm used to automatically scan AVHRR data for thermal anomalies. Numerous improvements have been implemented to *Okmok II* since the ASTER URP program came online and include: a series of tests to decrease the number of false alarms, and a web-based visualization tool/database. This tool allows for quick communication with the EROS Data Center (SD) and the Jet Propulsion Laboratory (CA) for ASTER tasking.

Numerous eruptions have been observed in Kamchatka, which have displayed varying volcanic styles including basaltic lava flow emplacement, silicic lava dome growth, pyroclastic flow emplacement, volcanic ash plume production, fumarolic activity, and geothermal emission. The high spatial/moderate spectral resolution ASTER data is ideal for deriving the energy flux from both high and low temperature systems, mapping chemical and textural changes of the volcanic products, and for imaging and understanding recent volcanic deposits (Figure 1).

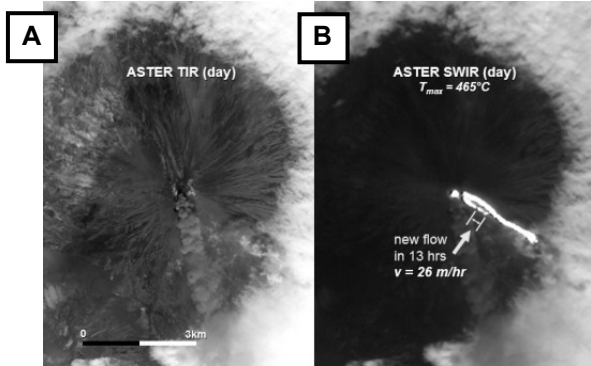


Figure 1. ASTER TIR (A) and SWIR (B) data collected as part of the ASTER URP project during the 2007 eruption of Kliuchevskoi volcano, Russia. These data were acquired ~13 hours after the night time data on 7 June 2007 and show the continued effusion of a basaltic lava flow to the southeast. Using the ASTER-derived DEM from this scene and the infrared data, the length and velocity of the flow was calculated. Such an approach and would not have been possible without the URP data and can be used to validate effusion rate/subpixel temperature models based on lower resolution data (e.g., AVHRR).

The entire ASTER archive has been queried, and the portion of images collected as emergency requests (ASTER-URP) were extracted. Sheveluch volcano has had persistently-elevated activity levels during most of the lifetime of ASTER. Activity has varied from exogenous dome growth to explosive ash-producing eruptions to the emplacement of significant pyroclastic flow deposits. The *Okmok II* algorithm has generated a number of AVHRR hotspots that have been used to trigger an ASTER data request (Figure 2). Peaks in ASTER image collection were observed in 2002, 2005, and 2007, which correlated with increased dome activity. Subsequent acquisition of higher spatial resolution ASTER images have captured a wide array of activity at this volcano and documented changed in temperature, texture, and emplacement conditions of the lava dome. Similarly, eruptions at Kliuchevskoi volcano have been well-documented and lava flow emplacement/effusion rates have been calculated using the high temporal resolution ASTER data ($\Delta t = 13$ hours) as well as the DEM capability (Figure 1).

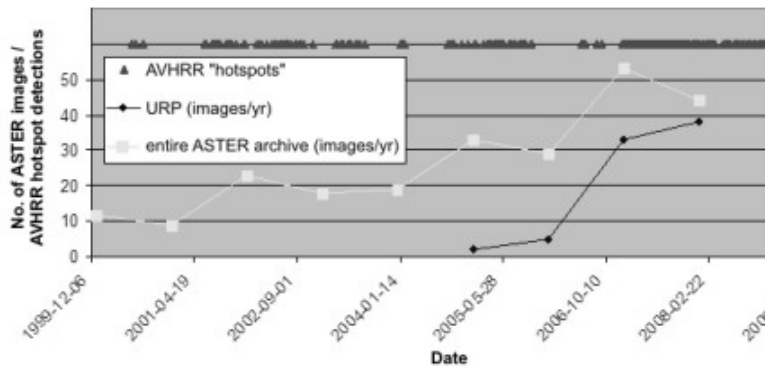


Figure 2. ASTER image archive (2000 to 2008) over the very active Sheveluch volcano, Kamchatka, Russia (light grey line). The dark grey triangles indicate confirmed AVHRR hotspot detections (their placement on the y-axis is arbitrary). The ASTER instrument collected an average of 16 images/year prior to the start of the URP/AEICS program. That has increased to an average of 40 image/year following its start in 2005 (black line).

In summary, the current ASTER rapid response program in Kamchatka and Alaska has resulted in many hundreds of new ASTER scenes, only a small fraction of which have been analyzed to date. The focus of this research will be on specific eruptions of the Kamchatka volcanoes, the science results stemming from those data, and the future expansion plans for global ASTER URP data in the next two years.

SEISMIC SWARM ASSOCIATED WITH THE 2008 ERUPTION OF KASATOCHI VOLCANO, ALASKA

Natalia A. Ruppert¹, Roger A. Hansen¹, and Stephanie Prejean²

¹*Alaska Earthquake Information Center, Univ. of Alaska Fairbanks, Fairbanks, Alaska, USA.*

²*Alaska Volcano Observatory/USGS, Anchorage, Alaska, USA.*

On August 6, 2008, a vigorous seismic swarm was detected by the automatic earthquake processing system at the Alaska Earthquake Information Center in close proximity to the little known Kasatochi Volcano in the central Aleutian arc. Starting at 15:00 UTC on August 6, the intensity and frequency of the earthquakes rapidly increased resulting in ~1,100 events located over the course of 48 hours. The largest earthquake, magnitude 5.8, occurred about 27 hours into the sequence and about 3.5 hours before the first explosion. This discharge was followed by more explosions, with declining frequency and intensity through ~22:00 UTC on August 8. The seismic swarm intensity started to decline at ~18:00 UTC on August 8. Overall, there was a strong causative relation between behavior of the seismic swarm and the eruption episodes.

Due to seismic network limitations in the region, determining accurate locations of the Kasatochi seismicity became a challenge. The volcano is located ~40 km NE of the nearest seismic network, and to the east of the volcano, only a single station was operating at ~80 km distant. We used waveform cross-correlation and double difference relocation method to refine locations of the earthquakes. The resulting locations form a NNE-trending linear feature that extends for ~12 km from volcano to the south. A smaller linear trend of earthquakes started after the M5.8 earthquake and parallels the main trend about 5 km to the east. Some earthquakes are located beneath the volcano.

Moment tensor inversions of the 12 largest events resulted in solutions with large non-double-couple components. The rupture time history of the M5.8 earthquake, as determined from P-wave analysis, suggests that the non-double-couple component of the moment tensor does not reflect fluid flow directly. Rather, it may result from the movement of gas or a phase change as fluids exsolve from ascending magma.

While there were very few detected earthquakes prior to August 6, the biologists working on the Kasatochi island at the time reported hundreds of felt earthquakes as early as August 2. Magnitude of completeness of the recorded catalog is estimated at ~1.6, and possibly as low as 1.4. It means that the earthquakes felt by biologists on the island were generally smaller than M1.5.

Several explanations can be proposed for occurrence of the Kasatochi seismic swarm:

1. Detected earthquake on a linear trend south of the island are mislocated and all seismicity is located beneath the island and related to the magma passing through the conduit to the surface. Cons: Tests with earthquake relocations indicate that the linear trend is real.

2. Linear earthquake trend indicates intrusion of a dike system that allowed for magma passage from the storage chamber to the volcano crater. Cons: This would imply too high a rate of magma movement. The estimated maximum compressive stress axis is about 50° to the earthquake trend, more typical for a tectonic fault, not a dike.

3. Two earthquake sources were active at the same time, one beneath the volcano associated with the magma passage from the deeper storage to the surface and another, indicated by the linear trend to the south, was triggered seismicity on a preexisting crustal fracture.

We'll explore these hypothesis in detail in our presentation in light of the swarm observations.

CHANGES IN MAFIC- FELSIC MAGMA MIXING STYLES AT AUGUSTINE VOLCANO OVER THE PAST 2,200 YEARS

Arron Steiner, Brandon Browne

Department of Geological Sciences, California State University, Fullerton.

This study describes findings from field measurements and geochemical analysis of host and enclave lava samples found in up to 3-m-diameter lava blocks contained in debris avalanche deposits from Augustine Island ranging in age from 125 to 2,200 years old. Changes in the abundance and composition of quenched mafic enclaves in host andesitic dome material are observed, suggesting that the mafic – felsic mixing dynamics in the Augustine magma reservoir has changed over time. Mafic enclaves are characterized by a spherical morphology with crenulate margins, widespread vesicles and an acicular groundmass; indicating that they formed as a result of rapid cooling of hot mafic magma when intruded into a cooler silicic magma host. Field measurements show a decline in the diameter and abundance of mafic enclaves in dome material through time, where enclaves range from 1 to 36 cm in diameter and account for up to 15 vol% of host dome material from 2,200 year old debris avalanche deposits located on the Southeast Point compared to 1 to 12 cm diameters and 3-5 vol% of host dome material contained in the 5 debris avalanche deposits emplaced between 1,700 and 125 years ago. Enclaves are virtually absent from dome material contained in pyroclastic flow and debris avalanche deposits emplaced during historic eruptions of 1883, 1935, 1964, 1976, 1986, and 2006, where enclaves typically range from 1 to 5 cm in diameter (or were not observed at all) and account for less than 1 vol% of the host dome material. Enclave phenocryst mineralogy is dominated by plagioclase and hornblende with lesser clinopyroxene, orthopyroxene and Fe-Ti oxides that commonly display exsolution texture. Olivine and quartz (invariably embayed and surrounded by plagioclase + CPX reaction halos) are extremely rare but do occur. Microlites are mostly plagioclase and hornblende with rare apatite and Fe-Ti oxides. Enclaves from Augustine can be classified as high-aluminum (17.4-19.6 wt% Al_2O_3) basalts and basaltic andesites (51.4 – 57.3 wt% SiO_2) that exhibit calc-alkaline differentiation trends and belong to the medium-K series (0.37-0.80 wt% K_2O) compared to host lavas, which are typically andesites (59.4 – 62.6 wt% SiO_2). Enclaves generally contain more MgO , MnO , CaO , FeO , Ni , Cr , Sc and V than host lavas and less Na_2O , K_2O , Ba , Rb , Zr and Nb than host lavas. Enclave and host andesite material are similar in terms of P_2O_5 , Sr and Y concentrations. The compositional variation of enclaves does not change systematically through time, as the most primitive enclaves are from both the oldest (~2,200 years old) and the youngest (2006 eruption) deposits examined. Enclaves and host lavas through time likely share a common source region as evidenced by their similar trace and rare earth element concentrations when normalized to primitive mantle, which indicates generation through mixing of a rising lithospheric mantle melt (N-MORB) and partial melting of a mafic-lower-crustal source. Thus, the change in enclave abundance over time does not appear to be a result of changing magma compositions, but rather likely represents a change in either (1) the manner in which compositional end-members mingle in the magma reservoir prior to eruption and/or (2) the volume of intruding basaltic magma material during mixing events.

RECENT ERUPTIONS IN THE NORTHERN PACIFIC

POSTER PRESENTATIONS

INVESTIGATING PRE-ERUPTIVE PROCESSES AT AUGUSTINE VOLCANO USING REPEATING EARTHQUAKES

Helena Buurman and Michael West

Geophysical Institute, University of Alaska Fairbanks, Alaska Volcano Observatory.

Augustine volcano, located in south central Alaska, was well instrumented when it erupted in early 2006. The seismological record of the eruption is rich and varied, containing a precursory earthquake swarm, explosive eruptive activity and subsequent dome growth on both short period and broad-band instruments. We focus on a cluster of highly similar earthquakes which occurred between the initial phreatic explosions on January 11 and the onset of the magmatic explosions on January 12. We propose that small but systematic changes in the otherwise highly repetitive waveforms result from changes in the edifice linked with the final ascent of magma prior to eruption. Waveform evolution can result from a small change in source mechanism, changes in source location or changes in the velocity structure along the raypath. We use a combination of techniques including double difference hypocentre relocation, coda wave interferometry and relative travel time residuals to assess the most likely cause of the waveform evolution. We further consider the volcanological processes that are capable of producing this type of seismicity. While the dataset we use is unique in its station coverage and data quality, we present techniques for assessing volcanic processes through seismicity that could be applied to eruptive sequences at other volcanoes.

QUATERNARY VENT INVENTORY OF ALASKA

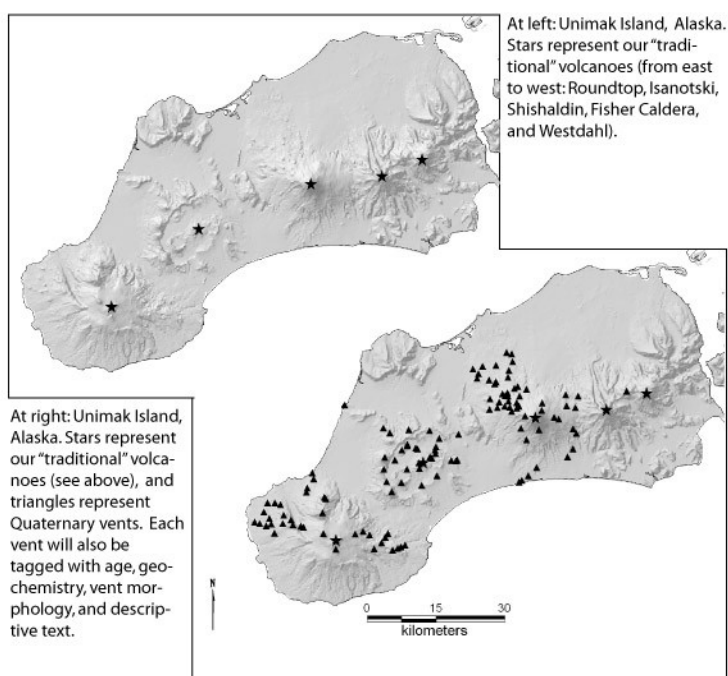
Cheryl Cameron¹, Chris Nye¹, and Christina Neal²

¹Alaska Division of Geological and Geophysical Surveys, Fairbanks, AK.

²Alaska Science Center, US Geological Survey, Anchorage, AK.

How many “volcanoes” are in Alaska? What exactly counts as a “volcano”? The most defensible list of “volcanoes” in Alaska is a list of vents, instead of our current list of major edifices and selected smaller vents. In the interest of enlarging our knowledge about Alaskan volcanism, and toward creating criteria and rules for a hierarchical classification of Alaskan volcanoes, we have begun re-compiling Quaternary vent information (Luedke and Smith completed a late Cenozoic, 1:2,000,000 scale compilation in 1986). So far, we have more than 1,200 identified vents (in contrast to the traditionally listed ~140 centers and ~250 subfeatures previously included in the Geologic Database of Information on Volcanoes in Alaska [GeoDIVA]). We recognize that some areas have more detailed knowledge than others, and anticipate that this list will grow and change as our mapping improves and expands. We plan to have the initial, basic information entered and available by the end of 2009.

We are categorizing vents using as much data as is available, including: text description, geochemistry, most recent period of activity, morphology, and data quality, as well as keeping track of where each piece of information came from.



vents. If you have experience creating or using volcano classification schemes for other geographical areas, we would appreciate discussion about what you found to be helpful.

Once all known vent information has been identified and compiled, we will establish explicit criteria to create hierarchical categorizations of vents and groups of vents. Using these rules with impartially applied qualifiers describing age and type of volcanic activity, our resulting list will aid investigations into spatial-temporal variations which may have genetic implications as well as provide a firm basis for authoritative enumeration of volcanoes.

Please contact us if you have information to share about Alaskan Quaternary

TEPHROCHRONOLOGICAL INVESTIGATION AT THE TWO-YURTS LAKE AREA, SREDINNY RANGE, KAMCHATKA, AND HISTORY OF LANDSCAPE EVOLUTION DURING THE HOLOCENE

Dirksen, O.¹, Danhara, T.², Diekmann, B.³

¹*Institute of Volcanology and Seismology, Petropavlovsk-Kamchatsky, Russia.*

²*Kyoto Fission Track Co. Ltd., Kyoto, Japan.*

³*Alfred-Wegener-Institute für Polar- und Meeresforschung (AWI), Potsdam, Germany.*

Tephrochronological investigations have covered most of southern and eastern Kamchatka, while Sredinny Ridge, especially its central and northern parts, is still unstudied in terms of distal tephra stratigraphy. We present herein the preliminary results of distal tephra identification in lacustrine cores and subaerial sections obtained at and around Two-Yurts Lake, Sredinny Range – the area of paleoenvironmental research in the framework of the German-Russian KALMAR project.

All the cores are characterized by the presence of numerous distal ash layers, which could be used as stratigraphical markers. Tephrochronological investigations were based on complex analyses of ash layers, which included careful description during the field work and lab processing, detailed mineralogical examination of the ash fraction 0,125-0,25 mm, and chemical analyses of volcanic glass shards. As a reference we used the results of our investigations of tephra layers within central Kamchatka as well as the characteristics of several ash horizons at the foot of Shiveluch Volcano. Tephra study allowed two main groups of ash to be distinguished: (1) ash from Shiveluch Volcano and (2) ash originating from other Kamchatka volcanoes. Characteristic features of the first group are large amounts of hornblende crystals (GHb>>BHb), prevalence of OPx over CPx, elevated MgO, and medium K₂O content. Being hardly distinguished by mineralogy and glass chemistry from each other, these ashes were further identified on the basis of their stratigraphic position and correlation with sections at the W and NW feet of Shiveluch Volcano (Ponomareva et al., 1998, 2007) as well as by a few radiocarbon dates obtained. In the cores and sections we recognized with high confidence the 950 (SH₂), 1700, 1750 (SH₃^a), 2800, and 4800 ¹⁴C yrs BP ashes. Tephras formed ca 1100, 1600, 2900, 3200, and 3500 ¹⁴C yrs BP were identified less reliably. From the second group we found KS₁ and, possibly, KS₂ ash from Ksudach Volcano with ages 1800 and 6000 ¹⁴C yrs BP, respectively. Four ash samples from this group are still unrecognized. Identified ash samples can be used to form a rather detailed tephrochronological scheme used to reconstruct the landscape evolution of this area during the Late Quaternary.

The lake occupies a wide U-shaped river valley which has been excavated by repeated glacial advances during the Late Pleistocene. A moraine ridge and a voluminous landslide ca 10-15 kyr BP created a dam which led to the lake formation. Since the beginning of the Holocene the gradual evolution of the lake ecosystem was interrupted several times by volcanic ash falls. The most considerable event occurred here about 3.0- 2.8 kyr BP. An avalanche of the lava plateau surrounding the SE sector of the lake depression, probably triggered by a powerful earthquake, formed a huge landslide which entered the lake and caused a “lake tsunami”, with a surge as much as 10 meters high as far as 3 km from the lake. This event was followed by a series of smaller landslides, the youngest of which occurred ca. 2 kyr BP. Strong tectonic activity ca. 3.0-2.8 kyr BP also happened at other regions of Kamchatka as evidenced by a series of river terraces. This period of reinforced tectonic dislocations correlates in time very well with an

abrupt onset of monogenetic volcanic activity within many areas of Kamchatka (the Tolmachev, Tolbachik, and Sedanka lava fields, and the Bakening and Vilyuchik volcanic areas), even far from the assumed edge of the subducted Pacific plate. A similar pattern of tectonic-magmatic process interactions also occurred in the Early Holocene. The reasons for increased magma production are unknown, but the tectonic movements for which we have discovered evidence probably created additional displacements in the upper crust which significantly facilitated the uplift of fresh magma.

1. Ponomareva V.V., Pevzner M.M., Melekestsev I.V. (1998) Large debris avalanches and associated eruptions in the Holocene eruptive history of Shiveluch Volcano, Kamchatka, Russia. Bull Volcanol 59/7: 490-505
2. Ponomareva V.V., Kyle P.R., Pevzner M.M., Sulerzhitsky L.D., Hartman M. (2007) Holocene eruptive history of Shiveluch Volcano, Kamchatka Peninsula. In: "Volcanism and Subduction: The Kamchatka Region", American Geophysical Union Geophysical Monograph Series, Volume 172: 263-282

LATE QUATERNARY VOLCANIC ACTIVITY IN THE SEDANKA LAVA FIELD, NORTHERN PART OF THE SREDINNY RANGE, KAMCHATKA

Oleg Dirksen, Lilia Bazanova

Institute of Volcanology and Seismology, Piipa blvd., 9, Petropavlovsk-Kamchatsky, 683006, Russia.

Kamchatka's Sredinny Range extends as far as 800 km from the SW to the NE, mostly parallel to the Kuril-Kamchatka trench, and represents the westernmost volcanic zone in Kamchatka. The quaternary volcanic centers of the Sredinny Range are concentrated at the axial and western part of the Range within an echeloned graben-like structure. The Sedanka lava field is situated in the central part of the Range, 100 km NW from Shiveluch, the northernmost active volcano in Kamchatka (fig. 1), and comprises several small shield- and stratovolcanoes and more than 250 monogenetic scoria and lava cones of different ages.

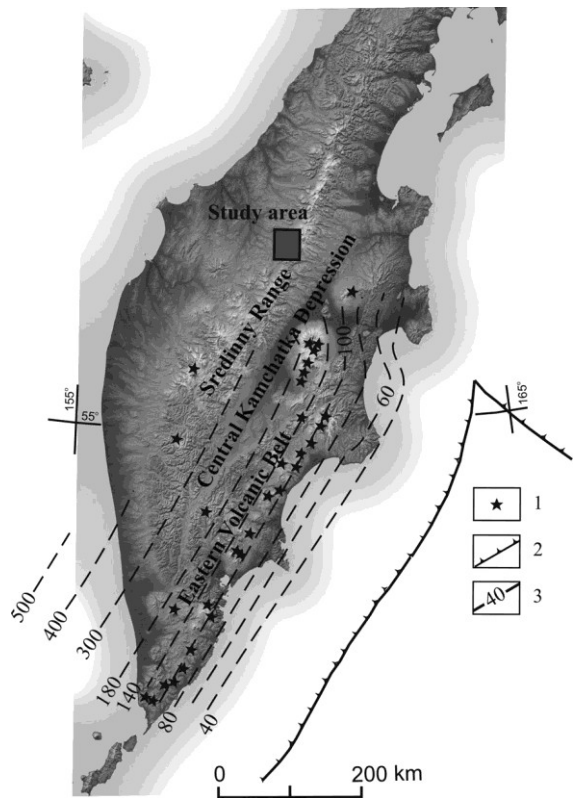


Fig. 1. Schematic map of Kamchatka. 1-Holocene volcanoes; 2- Kuril-Kamchatka and Aleutian trenches; 3- depth to slab surface, km [after Gorbatov et al., 1997].

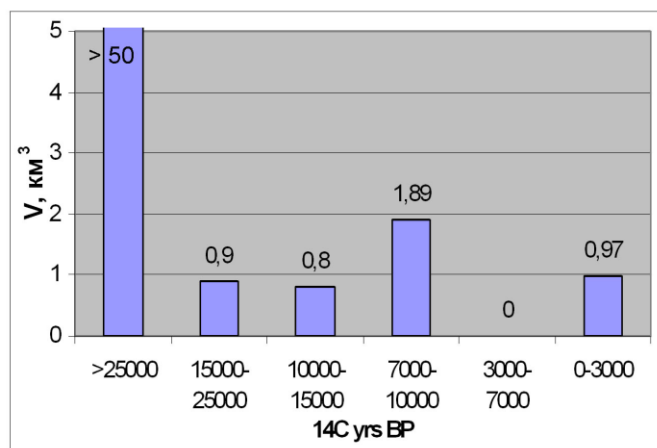


Fig. 2. Volumes of erupted products during revealed intervals at the Sedanka lava field.

Dating the eruptive centers rests on three cornerstones: geological mapping, tephrochronological studies, and radiocarbon dating. This region was an area of extensive glaciation during the Last Glacial Maxima (LGM) and different glacial landforms and deposits provide reliable proxies to distinguish Late Pleistocene eruptive centers. Age determination within the Holocene was accomplished using tephrochronological studies of soil-pyroclastic sections in which several marker ash layers were identified; seven layers originated from Shiveluch Volcano and three are from Opala, Ksudach, and Khangar volcanoes. These marker ash layers constitute a detailed chronological record for dating the eruptive centers within the Sedanka lava field. Our geological and tephrochronological studies revealed three main stages of

volcanic activity in this area: (1) Late Pleistocene, (2) Early Holocene, and (3) Late Holocene (fig. 2).

Most shield- and stratovolcanoes were formed before the LGM (i.e. 50000- 25000 ^{14}C yrs BP). Their edifices as well as more than 200 cinder cones of the same age have been glacially eroded or covered with glacial deposits. The total volume of the erupted products is more than 50 km 3 , giving an average discharge rate of $20*10^5 \text{ m}^3/\text{yr}$. The LGM and post-LGM periods (25000-10000 ^{14}C yrs BP) were characterized by a weakening of eruptive activity. Forty-four centers which appeared at that time erupted about 0.7 km 3 of material (an average discharge rate of $1*10^5 \text{ m}^3/\text{yr}$)

Volcanic centers (14 centers) from the Early Holocene were formed after the complete retreat of LGM glaciers (ca 10000 ^{14}C yrs BP) but before the deposition of KHG ash, i.e. earlier than 7000 ^{14}C yrs BP. The total volume of erupted products during this stage is estimated to be 1.9 km 3 (an average discharge rate of $6*10^5 \text{ m}^3/\text{yr}$).

The Early Holocene stage was followed by 4000 ^{14}C yrs of repose period. Then, ca 3000 ^{14}C BP, volcanic activity resumed. The Late Holocene stage is marked by the appearance of 7 scoria cones and voluminous eruptions of Titila Volcano, which is probably the only known potentially active Icelandic-type shield volcano in Kamchatka. Their tephras are sandwiched between two Shiveluch ash layers with ages of about 2550 and 2800 ^{14}C BP. The total volume of erupted products has been roughly estimated to be 1.0 km 3 and the average discharge rate was about $3*10^5 \text{ m}^3/\text{yr}$.

Quaternary volcanic activity in this area is still not explained by modern geodynamic models. The subducted Pacific plate has been detected below the southern part of the Range only, where volcanic rocks clearly demonstrate the leading role of subduction fluids in magma generation. But in the northern Sredinny Range the erupted rocks demonstrate OIB features (high Nb and Ti) combined with an IAB signature (enrichment in volatile-mobile elements) [Ponomareva et al., 2007]. Therefore, to explain the volcanic activity further north of the triple junction of the Kuril-Kamchatka and Aleutian arcs, more complex models must be invoked. However the stages of volcanism revealed at the Sedanka lava field correlate very well in time with epochs of high monogenetic volcanic activity in Southern Kamchatka and the Central Kamchatka Depression (the Tolmachev and Tolbachik lava fields and the Bakening and Vilyuchik volcanic areas) where volcanism is obviously induced by subduction of the Pacific plate. The close temporal relationship of volcanic unrest in Northern and Southern Kamchatka probably testifies to common causes of volcanic activity (i.e. enhanced magma generation or increased crustal permeability) in these areas that are located in different Kamchatka geodynamic regimes.

Gorbatov A., Kostoglodov V., Suarez G., Gordeev E. 1997, Seismicity and structure of the Kamchatka subduction zone. J. Geophys. Res., 102, 17883-17898.

Ponomareva V.V., Churikova T.G., Melekestsev I.V., Braitseva O.A., Pevzner M.M., Sulerzhitsky L.D. (2007) Late Pleistocene- Holocene volcanism on the Kamchatka Peninsula, Northwest Pacific region. In: Volcanism and Subduction: The Kamchatka Region, American Geophysical Union Geophysical Monograph Series, Volume 172: 165-198.

GIANT BASALTIC KLYUCHEVSKOY VOLCANO: ERUPTIONS, THE MAGMA FEEDING SYSTEM, AND SEISMOTOMOGRAPHY

Sergei Fedotov^{1,2}, Nikolay Zharinov¹, Larissa Gontovaya¹, Alex Sobissevitch²

¹ Institute of Volcanology and Seismology, Far East Branch Russian Academy of Sciences, Petropavlovsk-Kamchatsky 683006, Russia.

² Schmidt Institute of Physics of the Earth, Russian Academy of Sciences, Moscow 123995, Russia.

The giant Klyuchevskoy Volcano is one of the most powerful and active basaltic volcanoes on our planet. It is located in the area where the Kuril-Kamchatka Volcanic Arc and the Aleutian Volcanic Arc intersect. Klyuchevskoy is a stratovolcano with more than 6000 years of eruptive history and it is still in the beginning of its lifecycle. Its height is ~4750 m and the summit crater diameter is ~700 m; numerous flank vents and cinder cones are located on the volcanic flanks and edifice. The present volume of the volcano is ~250 km³. Average production of basalts per year is as much as 60×10^6 t, equal to half the annual production of juvenile material and one-quarter the total annual production of all 70 Kuril-Kamchatka Volcanic Arc active volcanoes. The Klyuchevskoy volcano has demonstrated *13 explosive-effusive summit eruptions and more than 17 flank lava eruptions since 1932*. The total volumes of erupted materials have been estimated to be 2×10^9 t and 2.3×10^9 t respectively. High-alumina basalts are common for both flank and summit volcanic products, while eruptive activity located close to the basement of the volcanic cone is represented by magnesian basalts. More than 90% of the pyroclastics and volcanic gases are erupted from the summit crater. The volcanic explosivity index is more than 21% for summit eruptions and less than 5% for flank eruptions, on average [1, 2, 4].

Continuous study of Klyuchevskoy Volcano started in 1935 at the Kamchatka Volcanological Station, Academy of Sciences of the USSR. Studies carried out since then include, but are not limited to: volcanic eruptions and volcanic products, petrology, seismicity, ground deformations, deep structure, prediction of volcanic eruptions, and estimation of environmental impact. One of the most important research areas has been the study of the magma feeding system and mechanisms of volcanic activity based on observations of volcanic eruptions, seismicity, and ground deformations, as well as on numerical modeling, seismotomography, and petrology [1-5]. The results obtained to date indicate that the magma feeding system of Klyuchevskoy Volcano originates at a depth of about 160 km and may be divided into five parts.

Part 1: about 160 km under Klyuchevskoy Volcano. The deep source of energy, fluids, and melts is located near the upper boundary of the subducting Pacific plate. Heat produced in this seismogenic zone due to major seismic and aseismic deformations could be sufficient to initiate partial melting.

Part 2: the asthenosphere, 160 – 40 km deep. Partial melts in the asthenosphere, formation of picrite magmas, gravity-driven convection, and the rise of diapirs and magmatic columns originate here. Magmatic conduits responsible for feeding eruptions may extend from depths of 50-60 km to the summit crater.

Part 3: the crustal-mantle layers at depths of 40 – 25 km. Here the overpressure of magmas squeezed out of the mantle should reach its maximum value. Near to the lower boundary of the lithosphere, intruding magma migrates upward and accumulates in deep intermediate magmatic chambers. Magma intrusion differentiation and formation of magnesian basalts are accompanied by swarms of minor long-period seismic events.

Part 4: depths of 25 – 5 km. Crystalline crust, magma rise in conduits, and magma differentiation originate here. Prior to major summit eruptions, an upward displacement of both the center of magma overpressure and hypocenters of volcanic earthquakes have been observed.

Part 5: depths of 5 – 0 km, the upper part of the crust and the volcanic edifice. Accumulation and degassing of high-alumina basalts, production of magmas for summit and flank eruptions, intrusion of radial dikes and sills, hypocenters of volcano-tectonic and volcanic earthquakes, and sources of volcanic tremor are here. Magma overpressure may be up to 500 bars. Formation and development of peripheral magmatic chambers is possible under such conditions. Concentration of water in melt may exceed 2.9%. Major summit eruptions may be followed by 500 m sinking of the crater bottom. At the same time, the pressure in the upper part of the magmatic feeding system may drop by 100 Bars or more.

During the most powerful summit and flank eruptions from 1935 – 2008 the amount of erupted lavas reached 0.3 km³. The corresponding volume of the magmatic feeding system is estimated to be 160 km³ if the pressure decrease was 150 Bars. Hundreds of vertical dikes from the central magmatic column may fill only 1/3 of the volume at distances up to 4 km. The total volume of dikes at depths of about 10 km is estimated to be 150 km³ [1, 2].

The structure and properties of the crust and upper mantle beneath the volcano has been studied by means of various geophysical methods, including seismotomography. Low seismic velocity anomalies at depths of 36 – 28 and 5 – 0 km have been observed under Klyuchevskoy Volcano [3, 5]. These anomalies coincide with locations of the maximum number of seismic events and outline where magma accumulates in intermediate and shallow chambers.

Comparative studies of magmatic feeding systems of the great basaltic volcanoes of the world (Klyuchevskoy, Etna, Piton de la Fournaise, Kilauea, etc.) may help us to improve our understanding of the mechanism of volcanic activity.

References

1. Fedotov S.A. Magmatic Feeding Systems and Mechanism of Volcanic Eruptions. 2006. Moscow: "Nauka", 455 p. (In Russian, translated Abstracts and Conclusion.)
2. Fedotov S.A., Zharinov N.A. Eruptions, Deformation, and Seismicity of Klyuchevskoy Volcano, Kamchatka in 1986-2005 and Mechanism of Its Activity. 2007. Journal of Volcanology and Seismology. 1(2): 71–97.
3. Fedotov S.A., Zharinov N.A., Gontovaya L.I., Sobissevitch A.L. The Klyuchevskoy Volcano (Kamchatka): Eruptive Activity, the Magma Feeding System, Seismotomography. Changes of Natural Environments and Climate: Natural and Possible Consequent Human-Induced Catastrophes. Vol. 2. Recent Volcanism of Northern Eurasia. Moscow: IGEM RAS, 2008. Ch. 11, pp. 273–294. (In Russian.)
4. Khrenov A.P., Dvigalo V.N., Kirsanov I.T., Fedotov S.A., Gorel'chik V.I., Zharinov N.A. Klyuchevskoy Volcano. Active Volcanoes of Kamchatka. Fedotov S.A., Masurenkov Yu.P. (Eds). Moscow: "Nauka", 1991. Vol. 1. Ch. 6, pp. 106-155. (In Russian and English.)
5. Khubunaya S.A., Gontovaya L.I., Sobolev A.V., Nizkous I.V. Magma Chambers beneath the Klyuchevskoy Volcanic Group. 2007. Journal of Volcanology and Seismology. 1(2): 98-118.

HIGH-MAGNESIA BASALTS – SOURCE OF CALC-ALKALINE SERIES OF GORELY VOLCANO (KAMCHATKA)

Maxim Gavrilenko¹, Alexey Ozerov¹

¹Institute of Volcanology & Seismology, Petropavlovsk-Kamchatskiy, Russia.

Gorely Volcano is a large, long-lived shield-type volcano in South Kamchatka that is currently in an eruptive phase (prior eruptions occurred in 1980-81 and 1984-86). The volcano has a complicated structure; it has a number of complexes, but in general Gorely consists of two edifices - ancient and modern. The ancient edifice (Old Gorely) has a shield-shaped form with a central caldera (13x12 km). The modern edifice (Young Gorely) occupies the central part of the caldera; it is represented by three fused cones, which form a ridge that stretches out in the northwest direction. The absolute height of the central cone is 1829 m. At the top there are 11 craters superimposed on each other, and on the slopes there are about 40 cinder cones with lava flows of varying lengths.

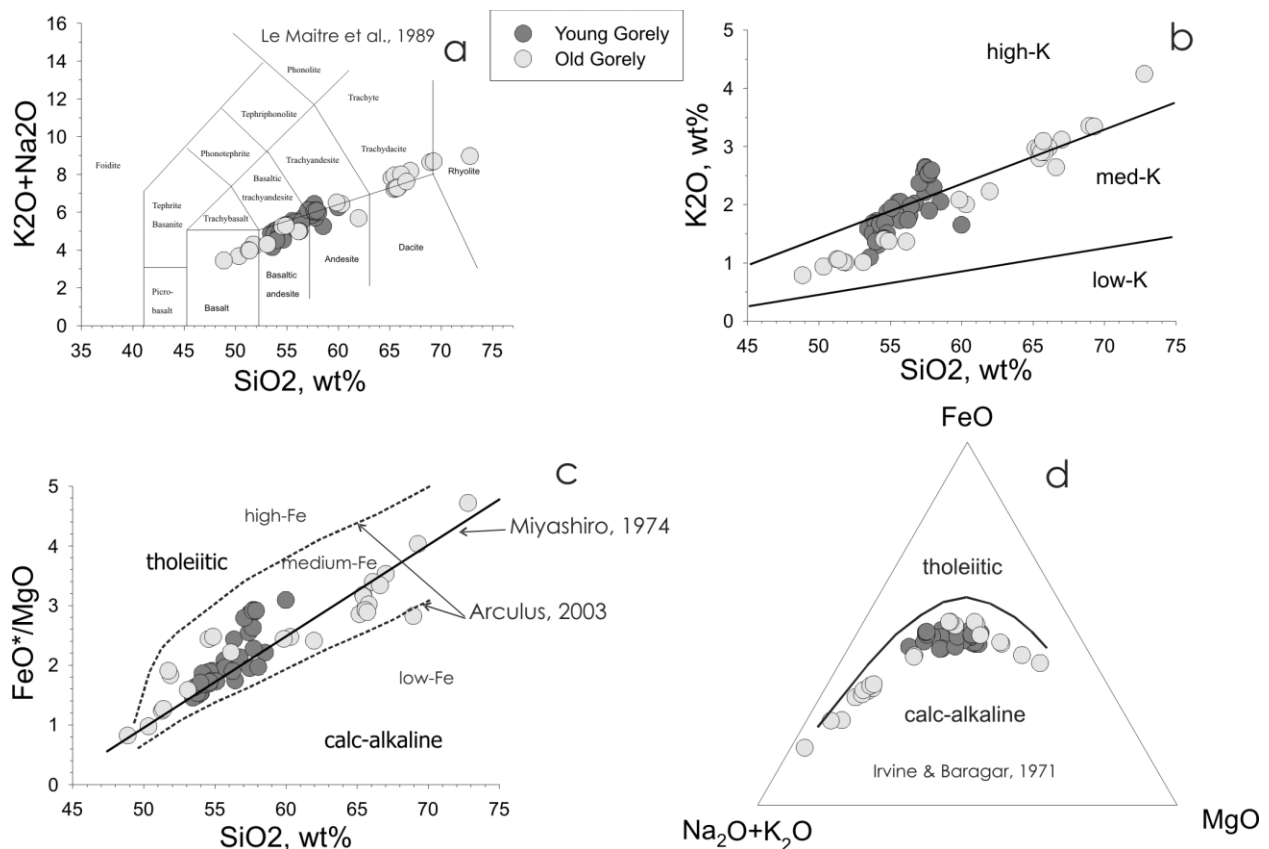


Figure 1. Classification diagrams of Gorely Volcano rocks: (a) $\text{Na}_2\text{O} + \text{K}_2\text{O}$ – SiO_2 (TAS-diagram [Le Maitre et al., 1989]); (b) K_2O - SiO_2 diagram; (c) FeO^*/MgO - SiO_2 diagram [Miyashiro, 1974; Arculus, 2003]; (d) AFM diagram [Irvine and Baragar, 1971].

After geochemical analysis two evolution series were found. First, Old Gorely Volcano is represented by a suite of compositions ranging from basalt to rhyolite; within this series, high-Mg basalts (MgO , 11 wt %) were discovered. Second, Young Gorely's edifice is composed of basalt,

andesite and dacite only. The reconstruction of chemical evolutionary trends shows that both volcanic series of Gorely Volcano share the same genetic history with similar evolutionary stages. We suggest fractionation of an upper mantle peridotite as a common means to produce both volcanic series; this process generated all the rocks (from basic to acidic) that have been found. It is necessary to add that the discovery of high-Mg basalts at Gorely Volcano demonstrates that Southern Kamchatka eruptive centers, like those of Central Kamchatka, are being fed by a mantle source.

The two magmatic series of Old Gorely and Young Gorely volcanoes were formed under different geodynamic conditions. Between these two series was a powerful stage of caldera formation, during which 100 km^3 of ignimbrites were emplaced. The 12-km-diameter caldera's collapse was the catalyst for a large-scale reorganization of the volcanic feeding system. Following caldera collapse, Young Gorely Volcano was formed by activity inside the caldera and shows very similar evolutionary trends to those of Old Gorely volcano. Therefore, it can be confidently stated that crustal components are practically absent in the evolution of the series, and the compositional range is attributed directly to the evolution of the magmatic melts of Gorely Volcano.

Microprobe analyses conducted on olivine and pyroxene phenocrysts from Gorely Volcano lavas show that there were at least two stages of crystallization during the evolution of magmatic melt. The first stage corresponds to crystallization of high-Mg and middle-Mg olivines, Mg# 88-77. The second crystallization stage is characterized by pyroxene phenocrysts with core compositions of Mg# 73-67.

The two-stage character of initial magmatic melt evolution is confirmed by results of the computer simulation (COMAGMAT; Ariskin et al., 1993). The first stage is characterized by comparatively high pressures (6-8 kbar), corresponding to formation at depth, and low oxygen fugacity (1% Fe^{3+} in total Fe). In contrast, the magmatic evolution of the second stage occurred in near-surface conditions (1-1.5 kbar) with high oxygen fugacity (Ni-NiO buffer). The existence of this stage of crystallization suggests the presence of a shallow magma chamber which is responsible for generating the caldera and thick ignimbrite complex.

References

- Arculus, R.J. (2003) Use and abuse of the terms calc-alkaline and calcalkalic, *Journal of Petrology*, 44 (5): 929-935.
- Ariskin, A.A., Barmina, G.S., Frenkel, M.Ya., Nielsen, R.L. (1993) COMAGMAT: a Fortran program to model magma differentiation processes, *Computers and Geosciences*, 19: 1155-1170.
- Irvine, T.N., Baragar, W.R. (1971) A guide to the chemical classification of the common igneous rocks, *Canadian Journal of Earth Sciences*, 8:523-548.
- Miyashiro, A. (1974) Volcanic rock series in island arcs and active continental margins, *American Journal of Science*, 274: 321-355.
- Selyangin, O.B., Ponomareva, V.V. (1999) Gorelovsky volcanic center, Southern Kamchatka: Structure and evolution, *Volcanology and Seismology*, 2:3-23.
- Kirisanov, I.T., Melekescev, I.V. (1991) Gorely Volcano, In: *Active Volcanoes of Kamchatka*, 2:294-317.

2006-2008 ERUPTIONS OF BEZYMIANNY VOLCANO

Olga A. Girina¹ and Adam J. Carter²

¹*Institute of Volcanology and Seismology FED RAS, Petropavlovsk-Kamchatsky, Russia.*

²*Department of Geology and Planetary Science, University of Pittsburgh, Pittsburgh, USA.*

Bezymianny volcano is one of the most active volcanoes of Kamchatka, Russia. Growth of the Novy lava dome in the explosive crater has continued from 1956 until present.

Six strong explosive eruptions of this volcano occurred in 2006-2008. Ash plumes rose up to 15 km (49,200 ft.) ASL and ash plumes drifted mainly to the east. As a result of these eruptions pyroclastic deposits were formed, including ash fall, pyroclastic flows, and surges. Flow deposits accumulated in the valley on the southeastern flank of the volcano. The run-out of the flow deposits varied from 4-5 to 8-9 km.

Thanks to satellite monitoring of the volcano, volcanologists were able to trace the development of volcanic activity changes before and after every eruption. Satellite monitoring is the only method for predicting a Bezymianny explosive eruption when seismic activity of neighboring Klyuchevskoy volcano is very high.

GEODYNAMICAL CONDITIONS AT THE NORTH OF THE KAMCHATKA SUBDUCTION ZONE: GEOCHEMICAL EVIDENCE

Boris Gordeychik¹, Tatiana Churikova¹, Gerhard Wörner², Anna Volynets¹, Paul Layer³

¹*Institute of Volcanology and Seismology FED RAS, Petropavlovsk-Kamchatski, Russia.*

²*GZG Abteilung Geochemie, Universität Göttingen, Germany.*

³*University of Alaska Fairbanks, Department of Geology and Geophysics, Fairbanks, USA.*

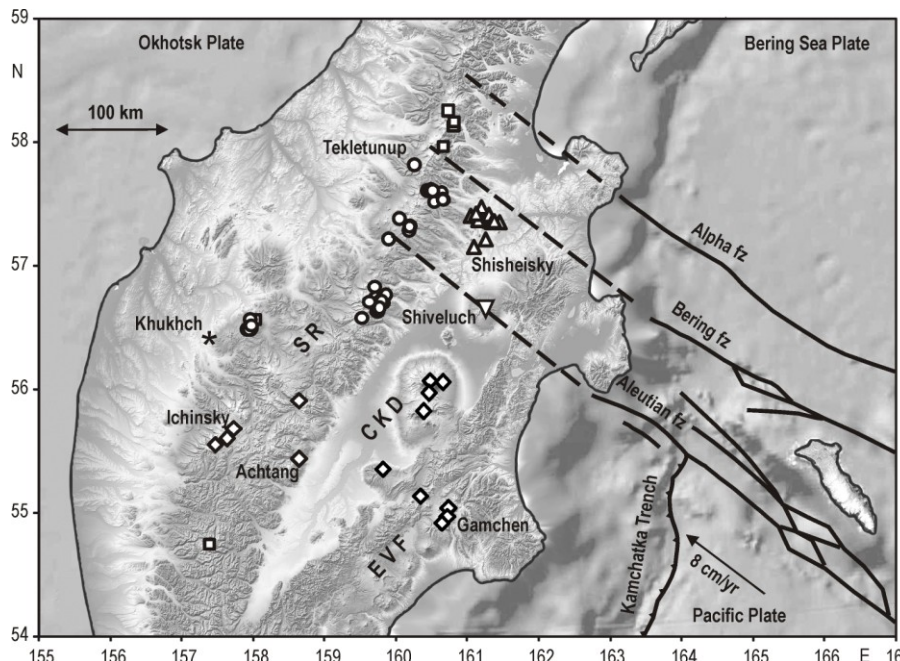
The results of this report are based on two transects which were carried out through Kamchatka peninsula during the last decade: (1) a SE-NW cross-arc transect and (2) a SW-NE Sredinny Range (SR) along-arc transect. These data together with the first Ar-Ar dating offer an opportunity to study the geochemical feature distribution of the volcanic rocks in space and time.

The cross-arc transect (Fig. 1, Churikova et al., 2001, 2007), extending from the Gamchen Volcano in the Eastern Volcanic Front (EVF) through the Central Kamchatka Depression (CKD) to Ichinsky Volcano in the SR, is based only on Quaternary rocks; it showed a continuous geochemical zonation from the arc front to the back arc of the present subduction zone, including strong and gradual increases in LILE, LREE, and HFSE in whole rocks. The transect along the SR back arc (Volynets et al., this meeting) from the Achtang lava field to Tekletunup Volcano (Fig. 1) comprises two age groups, each uniform in geochemical features. Late Miocene-Pliocene rocks (3.05-6.19 Ma) represent voluminous plateau lavas of depleted basalts with low HFSE and HREE. Fluid-mobile elements are enriched; enrichment patterns are in fact similar to typical arc front lavas. The younger group of Quaternary rocks (<1 Ma) is represented by monogenetic cones and stratovolcanoes that combine the typical LILE/HFSE-enrichment of a subduction setting with enrichment in all incompatible elements.

Geological and geophysical studies (Legler, 1977; Avdeiko et al., 2007) suggest that in Eocene-Miocene time the present back arc represented the active volcanic front of the Proto-Kamchatka subduction zone. Later, the Kamchatka arc system was modified by a step-by-step accretion of the Kronotsky terranes from south to north. The time of that accretion and the outward southeast 200 km shift of the subduction zone to the presently active EVF is estimated to have occurred from 40 to 2 Ma (Alexeiev et al., 2006; Lander & Shapiro, 2007).

Our data can help to better constrain the timing of this event. We argue that the systematic change in SR rock geochemistry with time is the result of this arc shift, and has been facilitated by a massive slab roll-back event. In this scenario, the SR plateau lavas represent the volcanic front until as recently as 3 Ma; the area west of the Miocene Sredinny arc front constituted the back arc region at that time. Volcanic rocks of that region (Mt. Khukhch: 3.78 Ma, Fig. 1) are indeed characterized by the absence of an arc signature; some even exhibit true within-plate trace element patterns (Perepelov et al. 2006). The younger Quaternary rocks at SR are the present back arc lavas of the recent subduction zone. Both the systematic across-arc geochemical zonation from the contemporary arc front to the back arc and the uniform geochemistry of young volcanic rocks along the SR show that the volcanism of the whole region is explained by only one mechanism – subduction of the Pacific Plate below Kamchatka. A trend is documented from fluid-dominated melting in the EVF, through the upwelling of a strongly fluid-fluxed mantle below the CKD (Dendorf et al. 2000), to melting of a fluid-enriched mantle aided by strong upwelling and decompression in the SR back arc region.

SR magmatism has continued to be active up to the Holocene, even though seismic data today do not signal a downgoing plate below this region. Geophysical studies have shown that the



edge of the Pacific Plate is traced below Shiveluch Volcano while Portnyagin et al. (2005) show that the slab edge may be traced somewhat further north at the Shisheisky complex (Fig. 1). We argue that the northern edge of the Pacific Plate is represented by a wide (150 km) boundary as a set of transform faults that can be projected on Kamchatka's surface from the morphology of the downgoing oceanic plate (Fig. 1). At the depth where fluid release is possible, this edge is marked by the termination of Holocene volcanoes on the surface. The absence of young volcanism to the north of the on-land projection of the Alpha fault, then, marks the plate boundary at depth (Fig. 1). The movements of the melts across the vector of subduction and small scale convection motions could be strong at the slab edge (Davaille and Lees, 2004) and thus magmatism will show a diffuse image of the slab edge. However, this slab edge is weak at best at the volcanic front, probably due to the fact that the slab edge has not been sufficiently heated at this position (Davaille & Lees, 2004).

Fig. 1. Tectonic sketch map of the region, where three plates are joined based on Seliverstov (1998). Relative motion of the Pacific and Bering Sea plates produces the system of transform fault zones Aleutian, Bering, and Alpha. Dashed lines show the extension of these transform zones under the Okhotsk Plate. Data sources for Quaternary volcanism: upturned triangle – Shiveluch (Yogodzinski et al, 2001), triangles – Shisheisky complex (Portnyagin et al., 2005), squares – data from Pevzner & Volynets (2006), rhombs – cross-arc transect from Churikova et al. (2001), circles – SR long-arc transect from Volynets et al. (this meeting), star – from Perekopov et al. (2006).

REFERENCES: Alexeiev et al., 2006: *Int J Earth Sci (Geol Rundsch)*, **95**, 977-993; Avdeiko et al., 2007: *Geophysical Monograph Series*, **172**, 37-55; Churikova et al., 2001: *J Petrol*, **42** (8), 1567-1593; Churikova et al., 2007: *Contrib Mineral Petr*, **154** (2), 217-239; Davaille & Lees, 2004: *Earth Planet Sci Lett*, **226**, 293-304; Dorendorf et al., 2000: *Earth Planet Sci Lett*, **175**, 69-86; Kirby et al., 1996: *Rev Geophys*, **34**, 261-306; Lander & Shapiro, 2007: *Geophysical Monograph Series*, **172**, 57-64; Legler, 1977: Moscow, Oceanology Institute AS USSR, 137-169; Perekopov et al., 2006: *Doklady Earth Sciences, Geochemistry*, **409** (5), 765-768; Portnyagin et al., 2005: *Geology*, **33** (1), 25-28; Seliverstov, 1998: Moscow, Nauchnij mir, 164 p.; Yogodzinski et al., 2001: *Nature*, **409**, 500-504.

depth of Kamchatka seismicity decreases from south to north. Kirby et al. (1996) showed that the absence of seismicity does not mean the absence of a plate, because at temperatures higher than 600-700°C seismicity is lost. Davaille & Lees (2004) argued that the seismicity of the subducted Pacific slab is gradually decreasing to the north as result of its heating.

Yogodzinski et al. (2001) argued that the

A HYPOTHESIS ON STRUCTURAL EQUILIBRIUM IN NATURAL MELTS AND THE MECHANISM OF WATER SOLUTION AT LOW AND HIGH PRESSURE

Olga A. Khleborodova

Institute of Volcanology & Seismology, Petropavlovsk-Kamchatskiy, Russia.

The magmatic differentiation process is complicated. It is known that both high total pressure P and fluid pressure P_f have a significant effect on crystallization. Despite considerable research, many details of this effect are not understood. This phenomenon is certainly related to changes in melt structure with increasing pressure. Conceptual models of the atomic structure of silicate melts are based on laboratory studies using nuclear magnetic resonance, vibrational spectroscopy, and Raman scattering spectroscopy. It has been found that the short-range order in a silicate melt is roughly similar to that in the crystalline state, but long-range order (on the scale of more than a few atomic bond lengths), as would be evident in a symmetrical crystal lattice, is absent. The net structure of a silicate melt consists of structural units resembling the main silicate minerals $Q^4 - \text{SiO}_2$, "plagioclase", $Q^3 - \text{Na}_2\text{SiO}_5$, $Q^2 - \text{CaSiO}_3$ "pyroxene" and $Q^0 - \text{"olivine"}$ (the index represents the number of bridging oxygens in the unit). These structural units have a short lifetime, and they always exchange bridging and non-bridging oxygens with each other. It is supposed that such permanent reconstruction of melt structure is the main mechanism of a viscous melt flow [Liu et al., 1988]. The structural equilibria in simple silicate systems such as glasses have been described by many researchers [e.g., McMillan, 1982; Mysen et al, 1990]. Unfortunately, direct determination of structural complexes in heterogeneous systems is technically difficult. The simulation of structural equilibria in heterogeneous systems is, however, possible if it starts with the concept that increasing a structural unit promotes the crystallization of the corresponding crystalline phase. This assumption is based upon the fact that identical structure of melt unit and solid phase reduces the activation energy barrier needed for crystal nucleation. Modeling the structural equilibria helps us to understand water behaviour at different pressures.

Some structural equilibria which may exist in natural melts are proposed. The influence of total pressure on these equilibria is based on calculations using molten mineral molar volume values. This conforms to the results of experiments on melting in the haplobasaltic systems An-Ol-SiO₂ and An-Ol-Di at different pressures [Dixon et al, 1978; Sen, Presnall, 1984; Liu, Presnall, 1990].

Spectral characterizations of simple silicate melts (glasses) have demonstrated that the water solution mechanism greatly depends on the melt composition (structure) [Xue et al., 2004] Because natural melts are compound systems the shift of structural equilibria back and forth could noticeably impact the water solution mechanism.

The simulated structural equilibria are examined in both diagram of crystal-melt equilibria in tholeiitic basalt in water-saturated systems [Green, 1982] and results of numerical crystallization experiments with the MELTS program on clinopyroxene and plagioclase crystallization depending on pressure and water content [Bindeman et al., 1999]. As a result, a hypothesis to explain various mechanisms of water dissolution and differing crystallization character at low ($\sim 2-4$ kbar) and high ($\sim 2-4$ kbar) pressure in natural magmas is advanced. An explanation of how the differing characteristics of water solutions may influence crystalline phase assemblages and the distribution of the components in melt fluid is offered as well.

It is common that P_f in a magma system is greater than the confining P plus the value of roof rock strength: $P_f > P + \text{roof rock strength}$. Temporal changes in both the building volcanic mass and the strength of the roof rocks can result in changes of pressure in a magma system. Hence, the chemical and mineral composition of later magmas may differ from the composition of previous magmas.

References

- Bindeman I.N., Bailey J.C. Trace elements in anorthite megacrysts from the Kurile Island Arc: A window to across-arc geochemical variations in magma compositions // Earth and Planetary Science Letters, 1999, 169, pp. 209-226.
- Dixon, T.H. O'Donnell, N.L. Brenner, R.L. Schrock, and D.W. Dycus. Liquidus phase relations on the join diopside-forsterite-anorthite from 1 atm to 20 kbar: Their bearing on the generation and crystallization of basaltic magma //Contrib. Mineral. Petrol., 1978, 66, pp. 203-220.
- Green T.H. Anatexis of mafic crust and high pressure crystallization of andesite. In: Thorpe RS, ed. Andesites. New York, John Wiley: 1982, pp. 465-487.
- Liu S.B., Stebbins J.F., Schneider E., Pines A. Diffusive motion in alkali silicate melts: an NMR study at high temperature //Geochim. et cosmochim. Acta., 1988, 52, pp. 527-538.
- Liu T-C., Presnall D.C. Liquidus phase relationships on the join anorthite-forsterite-quartz at 20 kbar with applications to basalt petrogenesis and igneous sapphirine //Contrib. Mineral. Petrol., 1990, 104, pp. 735-742.
- McMillan P., Piriou B., Navrotsky A. A Raman spectroscopic study of glasses along the joins silica-calcium aluminate, silica-sodium aluminate and silica-potassium aluminate //Geochim. et cosmochim. Acta, 1982, 46(11), pp. 2021-2037.
- Mysen B.O. Effect of pressure, temperature, and bulk composition on the structure and species distribution in depolymerized alkali aluminosilicate melts and quenched melts //J. Geophys. Res., 1990, 95, pp. 15733-15744.
- Sen G., Presnall D.C. Liquidus phase relationships on the join anorthite-forsterite-quartz at 10 kbar with applications to basalt petrogenesis //Contrib. Mineral. Petrol., 1984, 85, pp. 404-408.
- Xue X., Kanzaki M. Dissolution mechanisms of water in depolymerized silicate melts: Constraints from ^1H and ^{29}Si NMR spectroscopy and ab initio calculations //Geochimica et Cosmochimica Acta, 2004, 68(24), pp. 5027-5057.

PERIODIC VOLCANIC ACTIVITY OF KLYUCHEVSKOY AND USHKOVSKY VOLCANOES DURING THE EARLY HOLOCENE INFERRED FROM TEPHRA STUDY

Krasheninnikov S.P.^{1,2}, Portnyagin M.V.^{2,3}, Ponomareva V.V.⁴, Kuvikas O.V.⁴, Mironov N.L.²

¹*Geology Department of Moscow State University, Moscow, Russia.*

²*Vernadsky Institute RAS, Moscow, Russia.*

³*IFM-GEOMAR, Kiel, Germany.*

⁴*Institute of Volcanology and Seismology FEB RAS, Petropavlovsk-Kamchatsky, Russia.*

E-mail: spkrasheninnikov@mail.ru

The Klyuchevskoy Group is the largest cluster of active volcanoes in Kamchatka. The history of volcanism in the Klyuchevskoy Group of volcanoes is, however, not well known. The goal of this study was to identify the Klyuchevskoy Group volcanoes which were active during the Early Holocene, and to determine the petrologic character of their pyroclastic rocks.

The rocks studied here were collected from a 12-meter-thick tephra sequence on the northeastern foot of Klyuchevskoy Volcano during the 2007 and 2008 KALMAR field expeditions in Kamchatka. The section comprises a large number of variably grained cinder layers, which span a wide range of composition and were deposited during the entire Holocene. We investigated tephra samples collected from the lower 5 meters of this section, below a thick (0.5 m) layer of Klyuchevskoy cinders (so called “Upper cinders”) dated to around 6 ky ^{14}C and related to the beginning of intensive construction of the Klyuchevskoy volcanic cone [1]. Dating of rocks in the section was performed by interpolating age data between recognized regional marker cinder layers of known age [1,2]. The age of mafic layers was estimated to be between 6.8 and ~11.3 ky cal. BP. The accuracy of the age estimates is about ± 150 cal. years.

On the basis of the age, petrographic, mineralogical, and geochemical data, three rock groups were identified, which were erupted during 6.8 - 9.9, 9.9 - 10.5, and 10.5 -11.3 ky cal. BP, respectively (Fig. 1).

The rocks of the 1st and 3rd groups (6.8 - 9.9 and 10.5 -11.3 ky cal. BP) have porphyric textures, microlithic, highly vesicular groundmass, *Ol*, *Cpx*, *Pig* and *Pl*, and rare *Mgt*, present as phenocrysts and microliths. The samples referred to in this geochemical group have compositions corresponding to middle-K high-alumina basalts and andesites [3] (Table 1). On the petrochemical diagram proposed by M. Peacock [4] these rocks fall at the boundary between calcic and calc-alkali series ($\text{SiO}_2=61$ wt %) [5]. Typical values of $\text{K}_2\text{O}/\text{TiO}_2$ in matrix glasses and melt inclusions are in the range 0.5-1.26. The compositions of these rocks closely resemble those of Klyuchevskoy and Kamen’ volcanic rocks.

Table 1. Average major element compositions of groundmass glasses (wt %).

Rock group	SiO_2	TiO_2	Al_2O_3	FeO	MnO	MgO	CaO	Na_2O	K_2O	P_2O_5
1	58.0 ± 1.7	1.8 ± 0.2	14.2 ± 0.4	9.7 ± 0.9	0.2 ± 0.03	3.4 ± 0.7	6.6 ± 0.8	3.6 ± 0.3	1.7 ± 0.4	0.29 ± 0.07
2	60.1 ± 1.1	1.5 ± 0.1	15.1 ± 0.6	7.5 ± 0.3	0.1 ± 0.02	2.2 ± 0.3	5.0 ± 0.5	3.7 ± 0.2	3.1 ± 0.3	0.69 ± 0.09
3	57.5 ± 1.2	1.9 ± 0.3	13.9 ± 0.4	10.1 ± 0.7	0.2 ± 0.02	3.4 ± 0.6	6.5 ± 0.7	3.7 ± 0.3	1.7 ± 0.3	0.28 ± 0.06

The rocks of the 2nd group (9.9 - 10.5 ky cal. BP) are distinguished by highly porphyric texture and glassy matrix. Rock fragments are often tubular and elongated. Phenocrysts of *Pl* and *Px* are rare. *Pl* crystals are typically tabular and significantly larger (up to 1 sm) than crystals in

the rocks of the first group. The rocks of this group have a high-K trachyandesitic composition (Table 1). According to the Peacock index ($\text{SiO}_2=58.5$ wt %), the rocks belong to the calc-alkaline series [5]. They have concentrations of K_2O and P_2O_5 that are approximately two times higher (Fig. 1), and content of the major elements that is similar to that of the younger group's rocks. The $\text{K}_2\text{O}/\text{TiO}_2$ ratio in matrix glasses and melt inclusions is typically in the range of 1.26-3.52. Close analogs of these rocks are high-K andesites and basaltic andesites of Ushkovsky Volcano [6].

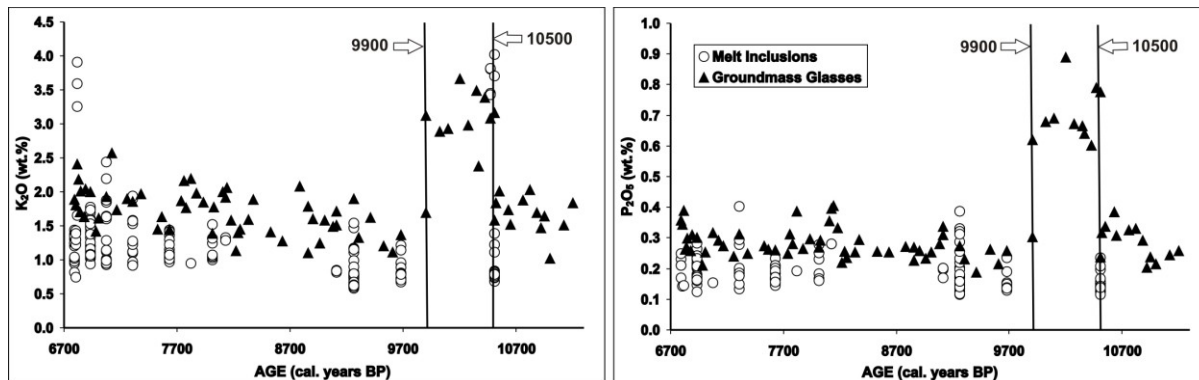


Figure 1. Diagrams of Age – K_2O (left) and Age – P_2O_5 (right) illustrating compositional difference between two groups of studied tephra and evolution of compositions of pyroclastic rocks in the investigated region during 6790 – 11290 cal. BP.

As the result of this study of Early Holocene pyroclastic deposits at the foot of Klyuchevskoy Volcano, we identified two major types of rocks. Middle-K tephra that erupted 6.8 - 9.9 and 10.5 - 11.3 ky cal. BP are compositionally similar to the rocks of Klyuchevskoy Volcano. High-K tephra formed 9.9-10.5 ky cal. BP are likely eruptive products of Ushkovsky Volcano. Our new data suggest that activity of Klyuchevskoy Volcano could have begun up to 5 ky years earlier than was supposed in previous works.

The research was supported by the Russian-German “KALMAR” project and grant from the RFBF № 07-05-00807.

References

1. Braitseva O.A. *et al.* (1995) Ages of calderas, large explosive craters and active volcanoes in the Kuril-Kamchatka region, Russia. *Bull. Volcanol.*, 57: 383-402
2. Ponomareva V.V. *et al.* (2007) Holocene eruptive history of Shiveluch volcano, Kamchatka Peninsula, Russia. In Eichelberger J. *et al.* (eds) Volcanism and Subduction: The Kamchatka Region, *Geophysical Monograph*, 172, AGU, Washington D.C., pp. 263-282
3. Gill J.B. (1981) Orogenic Andesites and Plate Tectonics. Berlin: Springer, 390 pp.
4. Peacock, M.A. (1931) Classification of igneous rock series. *Journal of Geology*, 39: 54-67.
5. Arculus R.J. (2003) Use and abuse of the terms Calcalkaline and Calcalkalic. *J. Petrology*, 44: 929-935
6. Portnyagin M., *et al.* (2007) Geochemistry of primitive lavas of the Central Kamchatka Depression: Magma generation at the edge of the Pacific plate. In: Eichelberger J, *et al.* (eds) Volcanism and Subduction: The Kamchatka Region, *Geophysical Monograph*, 172, AGU, Washington D.C., pp. 203-244

MAGMA SYSTEM OF THE 10th CENTURY ERUPTION OF BAITOUSHAN VOLCANO, CHINA-NORTH KOREA BORDER, AS INFERRED FROM GEOCHEMICAL CHARACTERISTICS

Jumpei Nishimoto¹, Mitsuhiro Nakagawa¹, Tsuyoshi Miyamoto², Mitsuhiro Taniguchi²

¹*Natural History Sci., Hokkaido Univ., Sapporo, Hokkaido, Japan.*

²*CNEAS, Tohoku Univ., Sendai, Miyagi-ken, Japan.*

Baitoushan (Changbaishan) Volcano, located at the border of China and North Korea, sustained a huge eruption in the 10th century. This eruption was the largest Indonesian eruption in the past 2000 years; it was nearly as large as the 1815 eruption of Tambora Volcano (Machida, 1992). Based on stratigraphy, the eruption was divided into two phases: Phase 1, alkali rhyolitic activity; Phase 2, trachytic activity. The quiescence time interval between these two phases was estimated as approximately one year from co-ignimbrite B-Tm ash (Baitoushan-Tomakomai ash) and non-glacial varves found in northeast Japan (Fukusawa et al., 1998; Miyamoto et al., 2004). Based on varved chronology and ¹⁴C wiggle-matching of a charred wood trunk, we believe this eruption occurred around AD938 (Fukusawa et al., 1998; Ishizuka et al., 2003). We examine the magma system of the 10th century eruption using petrography, whole-rock chemistry for major and trace elements, mineral chemistry, and the Sr and Nd isotope ratios.

The essential materials of Phase 1 are white and banded pumices, and of Phase 2, gray pumice and scoria. The groundmass is glassy to hyalo-ophitic in pumices, hyalopilitic in scoria. These ejecta contain alkali feldspar, olivine, clinopyroxene, magnetite, and ilmenite. In addition, plagioclase is also included in scoria and some banded pumices, and minor quartz is included in white pumice. The phenocryst contents are 1-20 wt%, mostly alkali feldspar.

Based on whole-rock chemistry, the juvenile materials are defined as alkali rhyolite (comendite), trachyte, and trachyandesite ($\text{SiO}_2=53\text{-}76 \text{ wt\%}$, $\text{Na}_2\text{O} + \text{K}_2\text{O}=6\text{-}13 \text{ wt\%}$). Most Phase 1 ejecta are alkali rhyolite exhibiting two different liner trends, from alkali rhyolitic ($\text{SiO}_2=73\text{wt\%}$, $\text{Na}_2\text{O}+\text{K}_2\text{O}=10\text{wt\%}$), to trachyandesitic ($\text{SiO}_2=60\text{wt\%}$, $\text{Na}_2\text{O}+\text{K}_2\text{O}=10.5\text{wt\%}$), to trachytic ($\text{SiO}_2=65\text{wt\%}$, $\text{Na}_2\text{O} + \text{K}_2\text{O}=12\text{wt\%}$) on several Harker diagrams. In Phase 2, most ejecta are trachyte. On Harker diagrams, the Phase 2 ejecta show two different liner trends; one trend is of combined trachytic and trachyandesitic; the other, trachytic to high-silica trachytic ($\text{SiO}_2=67.5\text{wt\%}$, $\text{Na}_2\text{O}+\text{K}_2\text{O}=11.5\text{wt\%}$). The latter trend is consistent with the Phase 1 alkali rhyolitic-to-trachytic trend in almost all Harker diagrams except La and Ce. In REE chondrite-normalized patterns, trachyandesite does not exhibit an Eu anomaly. As SiO_2 increases to trachyte, Eu became strongly anomalous. LREE/HREE decreases from trachyte ($\text{La/Yb}=22\text{-}30$) to alkali rhyolite ($\text{La/Yb}=13$). The $^{87}\text{Sr}/^{86}\text{Sr}$ ratios of the 10th century eruptions vary ($^{87}\text{Sr}/^{86}\text{Sr}=0.7048\text{-}0.7060$), correlated with LOI content resulting from weathering. The $^{143}\text{Nd}/^{144}\text{Nd}$ ratios of these vary ($^{143}\text{Nd}/^{144}\text{Nd}=0.51256\text{-}0.51262$) and exhibit no distinct correlation with any chemical content.

Considering the whole-rock chemistry and core compositions of phenocrystic minerals (olivine, clinopyroxene, feldspar), juvenile materials are divided into three types; type I ($\text{Fo}=0\text{-}2$, $\text{Mg\#}=2\text{-}10$, $\text{Or}=35\text{-}40$ An0) from alkali rhyolitic magma, type II ($\text{Fo}=10\text{-}20$, $\text{Mg\#}=20\text{-}40$, $\text{Or}=40\text{-}45$ An5) from trachytic magma, and type III ($\text{Fo}=80$, no Cpx, $\text{Or}=0$ An60) from trachyandesitic magma. The composition variations of phenocryst minerals in several ejecta exhibit a clear trimodal distribution in Phase 1, indicating mixing among these three magmas. In Phase 2,

several ejecta exhibit a clear bimodal distribution and type I phenocryst minerals are not present, indicating mixing of trachytic and trachyandesitic magmas.

Results of fractional crystallization calculations for major elements show that alkali rhyolitic magma can be generated from trachytic magma by 79 % fractionation of mainly alkali feldspar. However, this disagrees with the results of Rayleigh fractionation calculations for trace elements. Light to heavy rare earth element ratios, e.g. La/Yb show that alkali rhyolitic magma cannot be generated by trachytic magma, because these ratios do not decrease with alkali feldspar fractionation. Furthermore, the AFC model calculations cannot reproduce the observed REE ratios even assuming assimilation of basement granodioritic rocks. Therefore, trachytic magma cannot be parental for alkali rhyolitic magma; the presence of these two magmas indicates independent magma chambers.

According to variations in whole-rock and mineral chemistry, we assume the magma system of the 10th century Biatoushan eruption as follows. In Phase 1, the main alkali rhyolitic magma mixed with trachyandesitic and trachytic magmas, and almost all alkali rhyolitic magma was erupted. In Phase 2, the main trachytic magma mixed with trachyandesite magma.

DECOMPRESSION MODEL OF VOLCANIC EXPLOSIONS - ADVANTAGES AND DISADVANTAGES

Alexander Storcheus

Institute of Volcanology & Seismology, Petropavlovsk-Kamchatskiy, Russia.

E-mail: sav@kscnet.ru

Among the basic questions explored by research into the mechanism of volcanic explosions (VEs), from the physical point of view, one of the most interesting is the reasons for the rapid increase of overpressure of volcanic gases in magma under a volcano crater. During the first explosive VE stage, a large overpressure rapidly develops in the VE center. Subsequently, the stage of pyroclastic material outflow and volcanic gas emissions from the volcano crater usually occurs. The overpressure in the VE center increases up to 1000 bars. Verhoogen's [1] hypothesis explaining the mechanism of ash formation forms the basis of the most well-known physical models explaining the reasons of the rapid increase of magma pressure. One substantive provision of this hypothesis is that volcanic ash particles result from coalescing gas vesicles contained in magma. Thus, the size of ash particles depends on the size of gas vesicles. Overpressure of vesicle gas should ensure that lava bombs and blocks are thrown from a cone volcano to a distance of some kilometers.

Pressure of the gas P_g in a growing bubble is defined using the formula [2]:

$$P_g = P_m + 2\sigma / R + \rho_m(\dot{R}\ddot{R} + \frac{3}{2}\dot{R}^2) + \mu \dot{v}/R, \text{ where: } P_m = \text{magma pressure}, \rho_m = \text{magma density},$$

σ = surface tension in a bubble with radius R , μ = dynamic viscosity of magma, \dot{R} and \ddot{R} = speed and acceleration of bubble growth. From formula analysis it is obvious that gas overpressure in a bubble $\Delta P = P_g - P_m$ depends upon 3 factors: 1: force of surface tension, 2: force of inertia of magma, and 3: force of viscous resistance of magma to bubble growth. For viscous liquids, the

inertial member $P_\rho = \rho_m(\dot{R}\ddot{R} + \frac{3}{2}\dot{R}^2)$ will matter only at an initial stage of bubble growth, when acceleration and growth rate of a bubble are great enough. Further, when the growth of a bubble is limited by gas diffusion, the inertial member can be neglected in an estimation of ΔP .

In decompression models, the dominant role in creating overpressure in gas bubbles belongs to the force of viscous resistance of gas bubble expansion because of magma ascent or decompression during a rapid decrease of external pressure. However, the viscous member in the equation implicitly contains time as the important parameter influencing the speed of bubble expansion and, hence, the overpressure in a bubble. The faster a bubble expands, the more gas overpressure is created in it and vice versa. Therefore, non-equilibrium process degassing was accepted as the basic condition for creation of VE models. It is necessary to note that in decompression models, overpressure in an expanding gas bubble cannot exceed the value of the decreasing external pressure and the effect of overpressure could be reduced by slow rates of gas diffusion into a growing bubble. A delay of bubble growth should occur before coalescence owing to: 1) reduction of bubble volumes, and 2) decrease in concentration of volatiles in bubble walls and lower concentration gradient of volatiles in the surrounding melt.

Within the framework of the decompression model one can explain the types of volcanic activity seen at Plinian, or single strong explosions of the Bezymianny type. Models usually explain the decompression by the collapse of a cone volcano or opening of a volcanic crater, but

such phenomena are not always observed, especially for the Volcanian type of VE. Volcanian type explosions usually occur without any preliminary decompression, but overpressure during this type of explosion can reach 20 MPa and more.

Experiments and numerical calculations of decompression models of VE show that even at considerable supersaturation of magma by volatiles and a high decompression level (up to 100 MPa) the quantity of nuclei N in a unit of magma volume does not exceed 10^{15} in 1 m^3 . Therefore, the minimum size of ash particles that form as the result of gas bubble coalescence should exceed 1 micron. But during the strong eruption of Mount St. Helens Volcano in 1980, a minimum fine volcanic ash particle size of $\sim n \cdot 10^{-8}\text{ m}$ was observed in the volcanic cloud [3]. The same particle size was measured after the eruption of Alaid Volcano in 1980. It is necessary to note especially that the spherical form of the fine particles testifies to their formation from liquid magma rather than as a result of large ash particles being crushed as they collide. Formation of such small ash particles is probable only when the quantity of bubbles $N = 10^{21} - 10^{24}/\text{m}^3$. In addition, it is necessary to mention that until now explosions of magma samples during decompression in experiments with magma melts could not be reproduced [4]. Thus, it is possible to assert that the decompression model is not able to provide a sufficiently large overpressure during the first phase of VE, or to explain the observed variety of eruption types and their accompanying phenomena. The imperfection of this model is plain, and it is necessary to search for other mechanisms to play a leading role in explaining VE. It may be that decompression can serve as a promoting factor for VE, but not as the basic causal mechanism.

The analytical solution for a homogeneous nucleation of bubbles in supersaturated magma has been proposed in [5]. It appears that a quasi-equilibrium process of degassing better models the real conditions within a volcanic system at a preparatory VE stage than does the decompression model. The pressure P_g in a bubble in a quasi-equilibrium process of degassing is defined by the force of surface tension σ : $P_g = P_m + 2\sigma/R$. As one of the consequences [5], the critical size of gas nuclei were estimated as $R_0 \sim 10^{-9}\text{ m}$ and the quantity of bubbles in a unit volume of magma $N \approx (1-2) \cdot 10^{23}$ per 1 m^3 .

The development of a model explaining a spectrum of explosive eruptions on the basis of uniform physical processes that provides for spasmodic growth of volcanic gas pressure under a volcano crater during VE is offered. This model is a good fit with experimental data about the physical properties of melts and with natural observations. Thus, the possibility is presented of a physical VE model in which the dominant role in creating high overpressures belongs to the forces of surface tension, in opposition to the VE model based on viscous properties of magmas.

Cited literature:

1. Verhoogen J. (1951) Mechanics of ash formation. Am. J. Sci. 249:729-739.
2. Sparks R.S.J. (1978) The dynamics of bubble formation and growth in magmas: A review and analysis. Journal of Volcanology and Geothermal Research 3:1-37.
3. Hobbs P.V., Radke L.F., Eltgroth M.W., Hegg D.A. (1981) Airborne studies of the emissions from the volcanic eruptions of Mount St. Helens. Science 211:816-818
4. Lensky N.G., Navon O., Lyakhovsky V. (2004) Bubble growth during decompression of magma: Experimental and theoretical investigation. Journal of Volcanology and Geothermal Research 129:7-22.
5. Storcheus A.V. (1983) On the problem of the nature of volcanic explosions. Volcanology and Seismology. № 4.:72-78.

ERUPTION DYNAMICS OF HAWAIIAN-STYLE LAVA FOUNTAINS: THE CASE STUDY OF THE OPENING AND CLOSING EPISODES OF THE 1959 KĪLAUEA IKI ERUPTION

Wendy K. Stovall¹, Bruce F. Houghton¹, Sarah A. Fagents², Don A. Swanson³

¹*University of Hawai‘i at Mānoa, Geology and Geophysics Department, Honolulu, HI USA.*

²*University of Hawai‘i at Mānoa, Hawai‘i Institute of Geophysics and Planetology, Honolulu, HI USA.*

³*U.S. Geological Survey, Hawaiian Volcano Observatory, Hawai‘i National Park, HI USA.*

Hawaiian eruptions are characterized by fountains of gas and ejecta, sustained for hours to days that reach 10s to 100s of meters in height. Kīlauea volcano is the type locality for this eruptive style. Quantitative analysis of the pyroclastic products from the 1959 eruption of Kīlauea Iki, Kīlauea volcano Hawai‘i provide insights into the processes occurring during typical Hawaiian-fountaining activity. This short-lived but powerful eruption contained 17 fountaining episodes and produced a cone and tephra blanket as well as a lava lake that interacted with the vent and fountain during all but the first episode of the eruption.

Microtextural analysis of Hawaiian fountaining products from the opening and closing episodes of the Kīlauea Iki eruption are used to infer vesiculation processes within the fountain and shallow conduit. Vesicle number densities for all clasts are high (10^6 – 10^7 cm $^{-3}$) and scale with increasing fountain height. Post-fragmentation expansion of bubbles within the thermally-insulated fountain overprints the pre-fragmentation bubble populations, leading to a reduction in bubble number density and increase in mean bubble size. However, early quenched rims of some clasts have vesicle-number densities approaching 10^7 cm $^{-3}$, probably a valid approximation to magma conditions near fragmentation. The extent of evolution of clasts from low vesicle-to-melt ratio and corresponding high vesicle-number density to higher vesicle-to-melt ratio and lower vesicle-number density corresponds to the length of residence time within the fountain.

TEPHROSTRATIGRAPHY OF YOTEI VOLCANO, SOUTHWEST HOKKAIDO, JAPAN

Shimpei Uesawa and Mitsuhiro Nakagawa

Department of Natural History Sci., Graduate School of Sci., Hokkaido Univ., Japan.

Yotei Volcano (1898m), located at central southwest Hokkaido, is a stratovolcano which has been built up by many lava flows and tephra falls. The eruptive activity started at least 50,000 years ago. Egusa et al. (2003) show that the volcanic edifice consists of Older and Younger Yotei volcanoes, based on whole-rock chemistry of rocks in debris avalanche deposits and lava flows, and the estimated magma production rate of effusive eruptions during 50,000 years. On the other hand, stratigraphy and distribution of tephra layers from Yotei Volcano are poorly understood because of the difficulty of identifying each tephra on the basis of field occurrences only. Although Kashiwabara et al. (1976) recognized three tephra layers (Yo.Ps-1~3) from Yotei Volcano, Uno (1989) suggests that more than three tephra layers from Yotei Volcano may exist. We carried out a geological survey and petrological analysis of tephras around Yotei Volcano in order to establish the tephrostratigraphy. We determined phenocryst assemblages and chemical compositions of juvenile materials for tephra correlation.

Tephra layers distributed on the eastern foot of Yotei Volcano can be divided into 4 widespread tephras and at least 37 pyroclastic fall units, composed of Plinian eruptions (P1~P19: $>0.1\text{km}^3$) and sub-Plinian eruptions (S1~S18: $<0.1\text{km}^3$) from Yotei Volcano. Tephra layers from Yotei show different trends on SiO_2 - P_2O_5 and TiO_2 - K_2O variation diagrams of glass composition, and can be correlated between each outcrop by combining geological data. Three widespread tephras can be correlated to Kt-2(41~49ka), Spfa-1(40ka), and Ko-i(33.6ka); another is from an unknown source tephra called Shiogama-jyo pumice (Hoshizumi, 1996) which is a crystal-rich pumiceous ash layer. On the basis of their petrological features and long dormancy (more than 7 ka), these tephras can be divided into two main groups: Older Yotei tephras (P14~P19) deposited below the Spfa-1 layer, and Younger Yotei tephras (P1~S14) which cover the Ko-i layer. Older Yotei tephras consist of porphyritic (phenocryst content: 6~37wt%) pumices which contain quartz and hornblende and show a clearly different chemical trend from that of Younger Yotei tephras in the total alkali and Miyashiro diagrams. Based on calculations using loess-chronometry, which measures dormancy of more than 1800 years, the explosive volcanic activity of Younger Yotei Volcano can be divided into four main stages. Phenocrystic mineral components of quartz and hornblende in the Older Yotei tephras decrease from older (Qz:13vol%, Hb:18vol%) to younger (Qz:0.4vol%, Hb:0.7vol%). Younger Yotei tephras are composed of major aphyric pumice (phenocryst content: 2~5wt%), scoria (0.2~0.3wt%) and minor porphyritic scoria (8~15wt%). Bulk density of Younger Yotei pumices slightly decrease from older (500kg/m^3) to younger (300kg/m^3). In the early periods of Stage 1 and Stage 3 of Younger Yotei, the eruption volumes gradually increased. Then, after the largest eruption, eruption volumes abruptly decreased in each successive Stage. We also described the Kuchan Lake Deposit (KLD) distributed on the northwestern to southwestern foot of Yotei Volcano. KLD consists of reworked pumice of the Shikotsu pyroclastic flow deposit (Spfl) and was covered or bulldozed by a Yotei debris avalanche deposit (Yo-da) from Older Yotei Volcano; Yo-da is not covered by Ko-i. The field occurrences and glass composition of KLD imply that the Older Yotei collapse, which generated the Yotei debris avalanche, might have occurred when Younger Yotei volcanic activity began shortly after the fallout of Ko-i.

The latest eruption might have erupted from the Fujimi pyroclastic cone as a flank eruption of Yotei Volcano according to the isopach map (0.37 km^3 , 0.15 DRE km^3). The Younger Yotei Volcano erupted constantly without long quiet intervals such as the interval between the Older Yotei and Younger Yotei volcanic eruptions, and might have exhibited cyclic eruptive activity between explosive and effusive eruptions together with changing glass compositions. The total volume of Yotei tephra accumulated during 50,000 years calculated from isopach maps is approximately 5.3 km^3 (2.12 DRE km^3).

GEOCHEMICAL MODELING OF THE COMPOSITION AND AMOUNT OF SLAB FLUID FOR KAMCHATKA SREDINNY RANGE VOLCANIC ROCKS

A.O.Volynets^{1,2}, T.G.Churikova¹, G.Wörner²

¹*Institute of Volcanology and Seismology FED RAS, Petropavlovsk-Kamchatski, Russia.*

²*GZG Abteilung Geochemie, Universität Göttingen, Deutschland.*

Quaternary volcanism in central Kamchatka develops in three zones, parallel to the trench: the Eastern Volcanic Front, the Central Kamchatka Depression, and the Sredinny Range (back-arc). The Sredinny Range (SR) is located 400 km behind the trench. An active Benioff zone in SR, however, is observed only up to the latitude of the Holocene Ichinsky Volcano, where it is located nearly 350 km above the slab (Gorbatov et al. 1997). In contrast to the southern part of Kamchatka (south of the latitude of Shiveluch Volcano), where the Pacific Plate presently subducts below the Okhotsk Plate at a rate of ~8 cm/a (Scholl 2007), the Bering part of the North American Plate (to the north of Shiveluch Volcano) is assumed to have been stable relative to Kamchatka since Miocene times (Baranov et al. 1991; Trubitsin et al. 1998). North of Shiveluch there is no active volcanic front, and thus there appears to have been no active subduction in the Holocene according to the existing geological and geophysical data (Baranov et al. 1991; Trubitsin et al. 1998; Park et al. 2001; Avdeiko et al. 2002; Davaille and Lees 2004). A lack of active subduction in this region is also confirmed by the absence of plate motions in recent seismic data (Park et al. 2001). Therefore, one would not expect to find young volcanism in the back-arc of this region. However, voluminous Holocene volcanic activity in the SR back-arc was recently confirmed for several stratovolcanoes and numerous monogenetic centers by tephrochronological and radiocarbon methods. Trace element distribution and isotope composition of SR volcanic rocks allows the identification of three components that participate in magma generation in the SR of Kamchatka: (1) variably to strongly depleted N-MORB-type mantle, as demonstrated by low Nb/HREE ratios; (2) enriched OIB-type mantle with higher Ta, Nb concentrations and higher HFSE/HREE ratios; and (3) the trace elements distribution patterns for all studied rocks exhibit clear arc signatures with high fluid-mobile element abundances and high fluid-mobile/immobile element ratios, demonstrating the strong influence of slab fluids even in the absence of evidence for the slab itself. While the Late Miocene - Pliocene plateaus which underlie the Holocene-Late-Pleistocene edifices were produced by high-percentage (20%) melting of a fluid-fluxed but extremely depleted NMORB mantle wedge, the Late Pleistocene - Holocene volcanic rocks were formed by lower degrees of melting (8-10%) from the enriched mantle source (an average of 70 % variably-depleted MORB + 30 % OIB) and a smaller contribution from a slab fluid (Volynets et al., submitted). To estimate the fluid composition and distinguish the relative contribution of each element by mantle source and subduction component we carried out geochemical modeling.

In general, modeled SR fluids demonstrate not only internal conformity, but a great similarity to fluids which were calculated with the same approach for EVF and CKD lavas by Churikova et al. (2001). Substantial differences are observed mainly for the most fluid-mobile, volatile, and chalcophilic element concentrations and their ratios – K/La, Cs/Rb, Ba/Th, U/Th, B/La, Li/B, F/Cl (Wörner et al., 2001; Churikova et al., 2007). All these elements in EVF rocks are present to a much greater extent due to their particularly high mobility in fluid and the proximity of the EVF to the recent trench. Late Miocene - Pliocene plateau lavas of SR are enriched in all these ratios and depleted in Ce/Pb compared to SR Late Pleistocene - Holocene

monogenetic lavas, and conform to the characteristics of EVF rocks. Immobile element contents show that all Late Miocene - Pliocene plateau lavas were formed from the same mantle source of depleted N-MORB mantle, but based on data on chalcophile and siderophile elements we identify fluids of slightly different composition within the group of rocks of this age. Altogether, slab fluids in all Late Pleistocene – Holocene volcanic rocks are slightly more enriched in HFSE and LREE, but depleted in LILE compared to the fluids in Late Miocene - Pliocene plateau lavas. The amount of fluid and OIB components in the source correlates to the age of the rocks. Late Pleistocene - Holocene volcanic rocks have significant amounts (14-55%) of enriched mantle component in their source; they also have a lower amount of involved fluid (0.4-2.5%; in most samples about 1%). Late Miocene - Pliocene lava flows and plateau basalts do not have an OIB-type component in their source and have a higher amount of fluid (1.5 - 4 %; on average more than 2%). These rocks are also produced by higher degrees of partial melting (up to 20 % in comparison with 8 % for Late Pleistocene - Holocene rocks). In addition, they have different mantle source mineralogy (harzburgite for Late Miocene - Pliocene plateau basalts instead of lherzolite for the majority of SR rocks). Results of modeling the slab fluid amount and composition suggest that the fluids were probably all segregated from the same Pacific plate, but were formed under different conditions – the arc front in Late Miocene-Pliocene times, and the back-arc in the Late Pleistocene-Holocene.

References

- Avdeiko et al., 2002: *Geotectonic* **4**: 64-80.
Baranov et al. 1991: *Tectonophysics* **199 (2-4)**: 237-245.
Churikova et al., 2001: *Journal of Petrology*, **42 (8)**: 1567-1593.
Churikova et al., 2007: *Contributions to Mineralogy and Petrology*, **154(2)**: 217-239.
Davaille, Lees, 2004: *Earth and Planetary Science Letters*, **266**: 293-304.
Gorbatov et al., 1997: *Journal of Geophysical Research*, **102(B8)**:17883 – 17898.
Park et al. 2001: *AGU Fall Meeting, EOS* **82 (47)**: F1156.
Scholl 2007: In: Eichelberger J, Gordeev E, Kasahara M, Izbekov P, Lees J (eds) *Volcanism and tectonics of the Kamchatka peninsula and adjacent arcs. Geophysical Monograph Series* 172: 3-35.
Trubitsin et al., 1998: *Physics of Earth* **4**: 10-19.
Volynets et al., submitted to *Contributions to Mineralogy and Petrology*.
Wörner, G. et al., 2001: *Margins Meeting, Schriftenreihe D. Geol. Ges.* **14**: 236-237.

FIELD OBSERVATIONS ACROSS AN EXHUMED SUPRA-SUBDUCTION ZONE ON THE ISLE OF CULEBRA, PUERTO RICO

Robert B. Watts

Department of Geology, University of Puerto Rico-Mayagüez, PO Box 9017, Puerto Rico.

Recent fieldwork has revealed a remarkable sequence of lavas on the western coastline of the isle of Culebra, 18 miles east of Puerto Rico. At the Punta de Molinos (to the north) and the Punta del Soldado (to the south) are exposures of predominantly plagioclase-phyric basaltic lavas that outcrop in various styles of emplacement that are repeated across the entire peninsula. As a consequence of this variation the area has since been eroded to form a hummocky topography. Each hummock is generally a 40 to 50 meter wide zone composed of meter-size pillows and tubes in the way-up position. At one end of a pillow sequence, the pillows are in contact with a 4 to 5 meter zone of near-vertical thin basaltic dykes whilst at the other end the pillows are in direct contact with near-horizontal massive basaltic sheet-flows between 100 to 150 m long and 1 to 5 m thick. These observed structural differences are believed to highlight fluctuations in the eruption rate of the magmas as they were emplaced onto the seafloor. As the rocks of Culebra are believed to be Cretaceous in age (through correlation with the rocks of eastern Puerto Rico) and due to the tectonic location of this isle it is proposed that these sequences represent fragments of the ocean floor originally formed in the supra-subduction zone tectonic setting. As such, the rocks of western Culebra provide a unique insight into the submarine architecture of the ocean floor in a back-arc basin environment.

MAGMA GENESIS IN THE ALEUTIAN ARC WITH EMPHASIS ON LINKAGES BETWEEN HIGH-SR AND LOW-SR PRIMITIVE LAVAS FROM THE WESTERN ALEUTIANS

G. Yogodzinski¹, J. Turka¹, P. Kelemen², K. Sims³, I. Bindeman⁴

¹*University of South Carolina, Department of Geological Sciences, Columbia, SC 29209, United States; gyogodzin@geol.sc.edu; jturka@geol.sc.edu*

²*Lamont-Doherty Earth Observatory, Columbia University, Palisades, NY 10964, United States; E-mail: peterk@ldeo.columbia.edu*

³*Department of Geology and Geophysics, Woods Hole Oceanographic Institution, Woods Hole, MA 02543; E-mail: ksims@whoi.edu*

⁴*University of Oregon, Department of Geological Sciences, Eugene, OR 97403, United States; E-mail: bindeman@uoregon.edu*

Mapping and dredging of seafloor volcanic structures has provided an extensive geochemical data set, which enhances our ability to evaluate the nature of magma genesis in the Aleutians on an arc-wide basis. Along-arc patterns in major elements for high-Mg# lavas ($Mg/Mg+Fe>0.60$) support the findings of Kelemen et al. (2003 AGU Monograph) which indicate that subduction rate and related effects of mantle wedge and subducting plate thermal structure, exert a controlling influence over the nature of Aleutian magmatism. Specifically, our dredge samples, which fill the broad data gap that previously existed in the western Aleutians (Adak-to-Attu), indicate that high Mg# andesite-controlled magmatism at Piip Volcano, and basalt-dominated magmatism like that at Korovin or other eastern Aleutian centers (e.g., Makushin, Akutan, Okmok) evolve along end-member geochemical pathways that are tied to distinctive primitive/primary magma types produced in the subduction zone. Buldir and Little Sitkin volcanoes, which lie at and near the western terminus of emergent Aleutian magmatism, clearly show geochemical patterns that are characteristic of both basalt and high Mg# andesite geochemical styles.

High-Sr, primitive andesite lavas, which have been identified in dredge samples as far to the east as the Islands of Four Mountains ($SiO_2>54\%$, $Sr>700$ ppm, $Y<12$ ppm), are most strongly expressed in the Ingenstrem Depression - a rectangular basin (60X15-20 km), which lies on the Aleutian Ridge crest, immediately west of Buldir island, the western-most emergent Aleutian volcano. There are over 120 volcanic cones within and around this feature, which are each small, but have a combined volume similar that of individual, emergent calc-alkaline volcanoes in the Aleutians (~10 km³; White et al., Fall 2007 AGU).

A striking feature of Ingenstrem lavas is the unusually large proportion of primitive samples ($Mg\#>0.60$), which vary widely in SiO_2 (47-67%). Basalts and basaltic andesites have moderately enriched trace element patterns (e.g., La/Yb 4-8, $Sr/Y<30$) and relatively radiogenic Sr ($87/86=0.7031-0.7033$), typical of Aleutian and other island arc lavas. In contrast, primitive andesites and dacites, which are plagioclase, hornblende and pyroxene-phyric, have high Sr (700-2300 ppm) and fractionated trace element patterns ($Sr/Y>50$), with low Y (<12 ppm) and HREE. Andesites and dacites with high Sr/Y also have systematically higher SiO_2 , Mg#, Cr and Ni compared to low-Sr lavas with similar SiO_2 . Strontium isotopes for Ingenstrem lavas of all compositions are inversely correlated with Sr/Y and SiO_2 , so the most silica-rich samples (66-67% SiO_2) have the most fractionated trace element patterns ($Sr/Y>120$) and the least radiogenic Sr ($87/86<0.7029$). Pb isotopes indicate that the source of Ingenstrem lavas contains little

subducted sediment ($206/204 = 18.41 - 18.56$). The narrow range in Nd isotopes (8.5-9.5eps-Nd) compared to Sr (0.7027-0.7033) suggests that there may be an important source component for these rocks in seawater-altered subducted oceanic crust. However, oxygen isotope measurements on olivine and amphibole separates indicate that all samples are similar to MORB ($\delta^{18}\text{O} = 5.1 - 5.7$, olivine-equivalent). These data indicate that despite the wide variation in major elements, Sr/Y and Sr and Pb isotopes, all samples are relatively well equilibrated with olivine of the depleted upper mantle.

VOLCANISM AND VOLCANIC PROCESSES

ORAL PRESENTATIONS

ERUPTIONS IN THE RECENT HISTORY OF THE TATUN VOLCANIC GROUP, NORTHERN TAIWAN

Alexander Belousov¹, Marina Belousova^{1,2}, Chang-Hwa Chen¹

¹*Institute of Earth Sciences, Academia Sinica, Taipei, Taiwan.*

²*Institute of Volcanology and Seismology, Petropavlovsk, Russia.*

The quaternary dominantly andesitic Tatun Volcanic Group (TVG) occupies 400 km² at the northernmost tip of Taiwan Island, where the Ryukyu and Luzon volcanic arcs merge and collide with Eurasia. The group is considered as potentially active because it has more than 20 well-preserved volcanic edifices, multiple hot springs and fumaroles as hot as 120°C with magmatic isotopic signatures, as well as shallow volcano-tectonic earthquakes registered by the local seismic network. Layers of volcanic ash discovered in the sediments of Taipei basin indicated the possibility of Holocene eruptions of the TVG. The TVG is surrounded by densely populated areas, the largest of which is Taipei City (7 million people), as well as by multiple industrial factories and two nuclear power plants; therefore, the question about timing and styles of the most recent TVG eruptions is not only of academic interest.

We report the first results of our investigations of TVG physical volcanology, with focus on pyroclastic stratigraphy and eruption dynamics. We have found that for the most recent TVG eruptions were common long-term extrusions of crystal-rich, viscous lava. The eruptions formed dominantly monogenetic plug domes, coulees, and lava flows. The domes have heights of 150-350 m, base diameters of 0.5-1.5 km, and volumes of 0.05-0.3 km³. The nine best-preserved TVG lava flows have thicknesses of 80-150 m, lengths of 1-7.5 km, and volumes of 0.07-0.6 km³. For the largest lava flow we estimated an effusion rate of 6.5 m³/s, eruption duration of 1100 days, lava front speed of 3-5 m/hour (method, e.g. Stevenson et al. 1994). Only one pyroclastic edifice was found, represented by a tuff ring ~ 500 m in diameter and 30 m high formed by plinian eruption. Apart from that, few non-reworked pyroclastic deposits are currently preserved at TVG. The available data have shown that the explosive activity of TVG was weak-to-mild, but rather diverse with deposition of fallout tephra, base surges, and pyroclastic flows. Fallout deposits are represented mostly by well-sorted, crystal-rich ash layers ($Md=1.6-3.4$ phi, sorting = 0.9-1.3 phi) left by Vulcanian- and/or Pelean-type activity. Deposits of pumice fallout ($Md = -4-0$ phi, sorting = 1.2-2.4 phi) from Plinian eruptions are less common. Many of the eruptions show evidence of water/magma interaction: poor sorting, wide span of vesicularity of juvenile material, abundant xenoliths of country rocks, associated base surges, as well as ballistics of bread-crust and cauliflower type. Deposits of block-and-ash pyroclastic flows are lithic-rich and probably were formed mostly by collapses of growing domes and advancing lava flows (Merapi type).

Radiocarbon dating of paleolake sediments (near Shamao lava dome) intercalated with four thick (5-20 cm), medium-grained ash layers gave C¹⁴ ages of 13,610 +/- 70 BP for the middle part of the section, and 11,600 +/- 60 BP for the upper part of the section. The paleolake deposits were covered by a lahar deposit formed as a result of reworking of recent block-and-ash pyroclastic flow originated at Cising volcano. Dating of a wood fragment from the lahar deposit gave a C¹⁴ age of 11,620 +/- 60 BP. This indicates that Cising was the source of the latest pyroclastic material deposited in the paleolake. The summit of Cising volcano is covered by a lava coulee 150 m thick and 2 km long, which extruded after the explosive phase. We calculated the

parameters of this eruption: average effusion rate of 1.4 m³/s, eruption duration of 1600 days, and lava front speed of 0.3 m/hour. Our data allow us to conclude that TVG volcanoes erupted multiple times at the Pleistocene – Holocene boundary and possibly more recently. The results obtained form the basis for reassessment of this area's volcanic hazards.

Reference

Stevenson, R.J., Hodder, A.P.W., Briggs, R.M. (1994) Reological estimated of rhyolite lava flows from the Okataina Volcanic Centre, New Zealand. *New Zealand Journal of Geology and Geophysics*, v.37: 211-221

ALEUTIAN SUBDUCTION: A SCIENTIFIC OPPORTUNITY WHOSE TIME HAS RETURNED

John C Eichelberger¹, David W Scholl², and Evgeny I Gordeev³

¹*U.S. Geological Survey, Reston, VA.*

²*U.S. Geological Survey, Menlo Park, CA.*

³*Institute of Volcanology and Seismology, Petropavlovsk-Kamchatsky, Russia.*

Among the most beautifully geometric features of Planet Earth is the string of volcanoes and parallel subduction furrow draped between the facing nations of Russia and the United States. This beauty, carpeted in emerald-green tundra, is both mysterious and dangerous: the Aleutian arc is among the most seismically and volcanically active but poorly understood regions of the two countries. The Aleutians were, in fact, a birthplace of the subduction paradigm (*Coats, 1962; Plafker, 1965; Stauder, 1968*), and it is time to bring subduction science back to this fertile ground.

Some history

In 1971, as the plate tectonic paradigm was being tested, the first drill cores documenting rates of trench fill sedimentation were recovered from the Aleutian Trench axis off Kodiak (DSDP Leg 18). They confirmed rates of axial sedimentation consistent with plate convergence rather than the much slower rates from sparse conventional sampling. Seismic images showed the subduction of lower trench sediment and accretion of upper turbidite layers.

In response to oil shortages of the 1970s, the USGS conducted extensive offshore investigations of the Aleutian SZ (*Scholl et al., 1987*). With 1983 declaration of the U.S. Exclusive Economic Zone, much of the area of the Aleutian-Alaska offshore was imaged by GLORIA sidescan technology. Later, the one-line TACT and EDGE deep seismic studies of the Alaska forearc significantly advanced knowledge of the evolution of this sector, revealing rapid expulsion of pore fluids from the frontal accretionary prism (*Moore et al., 1991; Fuis et al., 2007*). In the west, Russia's R/V Volcanolog and other research vessels plied Aleutian waters during many expeditions, discovering the submerged and active backarc Piip Volcano and conducting bathymetric and seismic surveys and dredging (e.g., *Gainanov et al., 1970; Ustinov and Volk, 1985*).

The end of the Cold War opened scientific opportunities, but did not mitigate the logistical challenges of scientific research in the Aleutian environment. Some important discoveries were made, nonetheless; for example the 1995 findings of ODP Leg 145 correlating a late Cenozoic episode of vigorous Kamchatka and Aleutian volcanism with Northern Hemisphere glaciation (*Rea et al., 1995*). Among explorations of arc structure and history by occasional NSF-, GEOMAR-, and NOAA-sponsored cruises was discovery of a plethora of adakitic submarine vents in pull-apart basins west of the most western of Aleutian subaerial edifices. The advent of GPS instrumentation revealed the complexity of the deformation field, including verification that the Commander Islands sector of the Aleutian Ridge is moving with the Pacific plate, placing the present plate boundary on the Bering-Kresta shear zone.

With parallel growth of volcano and earthquake monitoring and research developments in the Russian Far East and Japan, the Japan-Kamchatka-Alaska Subduction Processes (JKASP) consortium formed to advance scientific collaboration in the region. Multi-disciplinary workshops have been held approximately biennially in Sapporo, Petropavlovsk-Kamchatsky, and Fairbanks since 1998, yielding collaborative efforts including a volume focusing on Kamchatka subduction and its Aleutian junction (*Eichelberger et al, 2007*).

Subduction and life

The contiguous Aleutian and Alaska sectors of the Aleutian SZ represent, in combination, one of the most geohazardous segments of the Pacific Rim. This is true with respect to explosive arc volcanism with by far the largest eruption of the 20th century, repeated nucleation of giant-magnitude earthquakes (24 since 1899), and the consequent launching of destructive local and trans-oceanic tsunamis (5 since 1899).

Much larger eruptions of the geologically recent past, such as the two Okmoks, Fisher, and Aniakchak calderas were global in impact, with devastating local effects to critical ecosystems. The ~1645 BC Aniakchak eruption may have created a trans- Alaska Peninsula dead zone, for a time separating animal and human populations. On a smaller scale, the unexpected and catastrophic eruption of Kasatochi volcano on August 7, 2008 obliterated an island ecosystem that had been carefully monitored by the US Fish and Wildlife Service for decades.

The long-term effect of Aleutian subduction on circulation in the ocean and atmosphere has been profound. The Aleutian Ridge restricted flow of warm Pacific waters into the Bering Sea and onward to the Arctic Ocean and the rise of the Alaska and St. Elias Ranges blocked the flow of warm, moist Pacific air into the interior of Alaska and North America respectively. Thus has Aleutian subduction contributed to the thermal isolation of the Arctic and changed the climate of North America.

Subduction science

Among the scientific lures of Aleutian subduction are prominent lateral changes in a number of forcing factors and boundary conditions. Along its 4000 km reach are 90° rotation of the angle of convergence, changes of sediment input type and thickness, crossing of Pacific Fracture Zones, breakout of backarc volcanism, changes in position of the arc magmatic front, and the transition between ocean-continent and intra-oceanic convergence. These changes provide valuable tests of how subduction parameters affect melt generation and other subduction products. In addition, the spectacular fault scarps offshore of the Commander Islands provide an excellent place to explore arc crust. Finally, there are the “end effects”, with an exposed slab at the Russian western end and jammed subduction at Alaska eastern end.

Subduction and nations

The Aleutian Islands are of considerable importance to both Russia and the United States, and for similar reasons. As in early Holocene time, they are an important transportation corridor. With future opening of the Arctic Ocean, ship traffic will flow between north and south as well as east and west. The Aleutian-Bering Sea region remains one of the few healthy fisheries on Earth, supplying a considerable portion of needs of Russians and Americans and beyond. As such,

sustainability and resilience of the region's communities and their environment are significant issues.

A binational enterprise (with other countries most welcome) would remind Russians and Americans that we are neighbors, despite both having national capitals a third of the world away from the Aleutian arc and a third of a world away from each other.

Acknowledgements

The authors' brief synopsis contains important contributions from S. Kirby (USGS), R. von Huene (USGS), J. Freymueller (University of Alaska Fairbanks), and others.

References cited

- Coats, R. R., Magma type and crustal structure in the Aleutian Arc, in *Crust of the Pacific Basin*, G. A. McDonald and H. Kuno, eds., *Amer. Geophys. Union Monogr.* 6, 1962.
- Eichelberger, J., E. Gordeev, M. Kasahara, P. Izbekov, and J. Lees, eds., Volcanism and subduction: The Kamchatka region, *Amer. Geophys. Union Monogr.* 172, 369p., 2007.
- Fuis G. S., T. E. Moore, G. Plafker, T. M. Brocher, M. A. Fisher, W. D. Mooney, W. J. Nokleberg, R. A. Page, B. C. Beaudoin, N. I. Christensen, A. R. Levander, W. J. Lutter, R. W. Saltus, and N. A. Ruppert, 2007, The Trans-Alaska Crustal Transect and Continental Evolution, *Geology* 36, 267-270, 2007.
- Gainanov A.G., E.N. Isaev, P.A. Stroev, and S.A.Ushakov, Isostasy and the structure of the lithosphere of the Bering Sea and Aleutian arc: Ocean gravimetric investigations. *Moscow State University Issue* 5, 32-40, 1970.
- Moore, J. C., J. Diebold, M. A. Fisher, J. Sample, T. Brocher, M. Talwani, J. Ewing, R. von Huene, C. Rowe, D. Stone, C. Stevens, and D. Sawyer, EDGE deep seismic reflection transect of the eastern Aleutian arc-trench layered lower crust reveals underplating and continental growth, *Geology* 19, p. 420-424, 1991.
- Plafker, G., Tectonic deformation associated with the 1964 Alaska earthquake, *Science* 25, 1675-1687, 1965.
- Scholl, D. W., A. Grantz, J.G. Vedder, eds., Geology and resource potential of the continental margin of western North America and adjacent ocean basins--Beaufort Sea to Baja California: Circum-Pacific Council for Energy and Mineral Resources, *Earth Science Series* 6, 799 p, Houston, Texas, 1987.
- Stauder,W.J., Mechanism of the Rat Island earthquake sequence of February 4, 1965, with relation to island arcs and sea-floor spreading, *J. Geophys. Res.* 73, 3847-3858, 1968.
- Ustinov N.V. and V. Volk, Deep structure of the western part of the Bering Sea, in Geological-Geophysical Investigations in the pacific Ocean, 92-101, St. Petersburg State Organization for Northern Marine Geology, 1985.

FORMATION AND EVOLUTION OF SILICIC MAGMAS DURING CALDERA-FORMING ERUPTIONS OF AKAN VOLCANO, EASTERN HOKKAIDO, JAPAN: COMPARING THE LARGEST ERUPTION (AK2) WITH THE OTHER ERUPTIONS

Takeshi Hasegawa¹, Mitsuhiro Nakagawa¹

¹*Department of Natural History Sci., Graduate School of Sci., Hokkaido Univ., Sapporo, Japan.*

Three caldera volcanoes, Akan, Kutcharo, and Mashu, are clustered on the eastern side of Hokkaido, Japan. Akan caldera has been formed by related pyroclastic flows and plinian eruptions during 1.7 ~ 0.2 Ma. On the basis of intervening paleosols these pyroclastic deposits can be attributed to 40 eruptions, which can also be grouped into 17 eruptive groups (Ak1-Ak17 in stratigraphic ascending order) by significant time intervals represented by 30 cm thick paleosols and unconformity. Ak2 is the largest eruptive group (more than 50 km³DRE), whereas estimated volumes of most of the other groups are less than 10 km³DRE. In this study, we investigated magma processes of Ak1-Ak9, which are well-preserved and provide detailed geological and petrological information.

Juvenile materials of Ak1-Ak9 are composed of dominant white or gray pumice and minor amounts of scoria and banded pumice. Crystal contents (wt%) of Ak2 and Ak1 are 8-17%, whereas those of other eruptive groups are less than 8%. Common phenocryst minerals are plagioclase, augite, hypersthene, and Fe-Ti oxides. In whole-rock compositions of SiO₂ (wt%), Ak2 shows a wider range (60-73%) than that of the other groups. On a K₂O Harker diagram, each group shows a nearly parallel and different trend; Ak2 is characterized by the largest value of K₂O at a given SiO₂ content (SiO₂=70%: K₂O =2.4%). In MgO, Zr, and Ba Harker diagrams, Ak2 shows various compositions of these elements on the silicic side. These characteristics are common to glass compositions. We also determined mineral, REE, and isotope compositions of the most silicic Ak1-Ak9 samples. Or contents (mol%) of Ak2 plagioclase cores are more than 1.2, whereas those of the other groups are less than 1.0. Mg# of Ak2 pyroxene cores (Opx=45-59, Cpx=49-60) are smaller and broader than those of the other groups. LogfO₂ of Ak2 and the other groups plot under and over the QFM buffer line, respectively. Ak2 shows the steepest LREE-enriched pattern. Moreover, Ak2 composition is relatively enriched in 87/86Sr (0.7033-0.7035) and 143/144Nd (0.51294-0.51297) when compared with that of other groups.

Different parallel trends of each group on the K₂O Harker diagram suggest that distinct magma systems were active among the eruptive groups. Compositional variations of SiO₂-MgO, -Zr, and Ba of Ak2 match the variations of all other groups. Furthermore, compositional ranges of Mg# from Ak2 rhyolite pyroxene cores are comparable to ranges found in all other groups. These suggest that several distinct silicic magmas, which could have been responsible for the chemical variations of several eruptive groups, were ejected at the same time in the Ak2 eruption event. This suggestion is consistent with the largest volume of Ak2 and the longest dormancy before Ak2 (more than 200 ky). In Akan caldera, different magmas were repeatedly renewed from group to group. However, there existed a particularly long preparation period before the Ak2 eruption, and several distinct magmas could have stagnated together at that time. At the same time, crystallization could have occurred, resulting in the high crystal contents of Ak2. The other petrological characteristics of Ak2 can be interpreted as the result of remelting or assimilation of relatively enriched crust materials during the long preparation period. At the same time adjacent Kutcharo volcano started its caldera-forming activity; this might have been associated with the anomalous Ak2 event.

AN “INACTIVE” STRATOVOLCANO THAT ERUPTED ~3000 YEARS AGO: KONIJI ISLAND, ALEUTIANS

Brian R. Jicha¹, Brad S. Singer¹

¹*Dept. of Geoscience, University of Wisconsin. Madison, WI, USA.*

More than fifty active volcanoes exist in the Aleutian arc. Eruptions from Aleutian volcanoes pose major hazards to passenger and freight aircraft flying pan-Pacific air routes that follow great circles over the Aleutians. Thus far, less than half of the active Aleutian arc volcanoes have been studied in any detail to evaluate their volcanic hazards and geologic histories. Numerous central and western Aleutian volcanoes were mapped by U.S. Geological Survey scientists for the Alaska Volcano Project, which commenced in the 1940s and continued through the 1960s. Recent investigations led by the Alaska Volcano Observatory have focused on the short-term (i.e., Holocene) eruptive histories by documenting stratigraphic relationships of volcaniclastic deposits and radiocarbon dating of associated buried soils and peat (e.g., Waythomas et al., 1998). The long-term eruptive histories of frontal arc volcanoes are often characterized using a combination of radioisotopic ($K-Ar$, $^{40}Ar/^{39}Ar$, ^{14}C) dating with field mapping and stratigraphy to interrogate the episodic nature of eruptions, complex compositional variability through time, and significant changes in eruption rates and styles. Most of these investigations have been carried out at stratovolcanoes or volcanic fields whose eruptive histories span hundreds of kyr and include tens of km³ of erupted magma. Very few Aleutian arc volcanoes have been studied in this manner (e.g. Katmai, Seguam, Fisher, Westdahl).

Obtaining precise $^{40}Ar/^{39}Ar$ ages from latest Pleistocene to Holocene island arc lavas is difficult due to the extremely low radiogenic ^{40}Ar yields in the presence of large amounts of atmospheric ^{40}Ar . Most of the published Holocene $^{40}Ar/^{39}Ar$ ages have been obtained on sanidine phenocrysts from tephras or K-rich groundmass. Sanidine and K-rich lavas are absent in most island arcs, but recent technical advances allow $^{40}Ar/^{39}Ar$ dating of medium-K (1.0-1.5 wt.% K₂O) lavas. New $^{40}Ar/^{39}Ar$ dating, field observations, and geochemical and isotopic analyses of lava flows establish an eruptive chronology for Koniiji Island in the central Aleutian island arc. Koniiji is a tiny 0.95 km² island that rises only 896 feet above the Bering Sea. Previous accounts describe Koniiji as a mostly submerged, deeply eroded, dormant stratovolcano. However, new $^{40}Ar/^{39}Ar$ ages constrain the duration of subaerial eruptive activity from 15.2 to 3.1 ka. Furnace incremental heating experiments on replicate groundmass separates from two samples of a 30-50 m thick basaltic andesite flow at the southernmost point of the island gave a weighted mean $^{40}Ar/^{39}Ar$ age of 15.2 ± 5.0 (2 σ). The next phase of eruptive activity includes a series of 5.8-4.6 ka basaltic andesitic to andesitic lava flows preserved along the western shoreline. The basal lavas contain numerous mafic enclaves and dioritic cumulates suggesting a major disturbance in the plumbing system during the initial stages of emplacement. The 5.8-4.6 ka lavas are truncated by an andesitic dome complex that includes hornblende-bearing domes, flows and pyroclastics which extruded into the center of the island and comprise the majority of the subaerial eruptive volume. An angular block from within the dome complex yielded $^{40}Ar/^{39}Ar$ age of 3.1 ± 1.9 ka, thereby making it one of the youngest island arc volcanics to be dated using the $^{40}Ar/^{39}Ar$ method. Overall, the $^{40}Ar/^{39}Ar$ data indicate that Koniiji is a nascent stratovolcano that has only recently emerged above sea level, not a glacially-eroded, long-lived volcanic complex like those found on many other central Aleutian Islands.

VOLATILES IN THE KAMCHATKA VOLCANIC ARC AT FOUR VOLCANIC CENTERS (BEZYMIANNY, KLYUCHEVSKOY, KARYMSKY, AND SHIVELUCH): APPLICATIONS FOR URANIUM-SERIES ISOTOPIC DATA

Theresa Kayzar¹, Bruce Nelson¹, Pavel Izbekov², Marina Belousova^{3,4}, Alexander Belousov³

¹*Department of Earth and Space Sciences, University of Washington, Seattle WA, USA.*

²*Geophysical Institute, University of Alaska, Fairbanks AK, USA.*

³*Institute of Earth Sciences, Academia Sinica, Taipei, Taiwan.*

⁴*Institute of Volcanology and Seismology, Petropavlovsk-Kamchatsky, Russia.*

The Kamchatka volcanic arc hosts a diverse suite of active volcanism. Ranging from basaltic to rhyolitic compositions and exhibiting vulcanian to plinian eruptive styles, the active systems in the Kamchatka arc provide a unique setting for comparing and contrasting magma system behavior hypotheses. The complexity of the Kamchatka arc has resulted in a wealth of scientific data that suggests multiple plausible volcanic regimes.

Numerous studies of volcanism in Kamchatka have focused on the mechanisms that drive melting and the sources of voluminous melt in the arc. Klyuchevskoy volcano is the most voluminous active volcano in the world (Popolitov and Volynets 1982, Turner et al. 2007). One hypothesis is that the subduction zone beneath the arc is unusually volatile rich and fluxes the mantle wedge causing abundant melting (Dorendorf et al. 2000, Dossetto et al. 2003). This is especially true in the Klyuchevskoy Group of volcanoes where there may be evidence for seamount subduction (Churikova et al. 2001). However, recent work also suggests that tectonics may drive increased arc activity where breakage of the subducted Pacific Plate leads to increased mantle upwelling (Auer et al. 2009) or, alternatively, rifting in areas such as the Central Kamchatka Depression induce crustal thinning and mantle upwelling (Turner et al. 2007).

Our work uses radiogenic uranium-series (U-series) isotopes to investigate volatile fluxing and the role, if any, it has on eruptive timescales and styles. U-series nuclides in the context of volcanic arc settings are extremely useful for two reasons: 1) the decay timescales of individual nuclides in the U-series decay-chain are on the order of timescales of subduction zone processes as well as shallow magma chamber processes, and 2) U and Ra are both fluid mobile elements that are strongly fractionated from Th during fluid fluxing. Fluid fluxed melting, therefore, produces melts with U and Ra excess relative to Th, or activity ratios of $(^{238}\text{U})/(^{230}\text{Th})$ and $(^{226}\text{Ra})/(^{230}\text{Th})$ greater than 1. U-series systematics coupled with detailed trace element analyses can, therefore, provide constraints on melting due to volatile fluxing, melting due to upwelling, and crustal melting. Published U-series data suggest that the Kamchatka arc shows variable behavior. Turner et al. 2007 report evidence for U excesses from fluid addition to the melting source in the Klyuchevskoy Group, while Dossetto et al. 2003 document U deficits in the Klyuchevskoy Group. All $(^{226}\text{Ra})/(^{230}\text{Th})$ are greater than one; however, the data have been interpreted as resulting from both fluid addition (Dossetto et al. 2003) and decompression melting (Turner et al. 2007).

In our study, we compare two Klyuchevskoy Group volcanoes (Klyuchevskoy and Bezymianny) to Karymsky volcano in the Eastern Volcanic Front and Shiveluch volcano in the northern Central Kamchatka Depression. These four systems have multiple historic eruptions as well as thorough published petrologic and geochemical datasets to supplement interpretations from U-series analyses. We summarize previous data on Kamchatkan volcanism and present new U-Th-Ra and trace element data from time-series samples from these systems with preliminary interpretations for volatile behavior in the Kamchatka volcanic arc.

GEOCHEMICAL FINGERPRINTING OF TEPHRA FROM MAJOR HOLOCENE ERUPTIONS IN KAMCHATKA

Philip R. Kyle¹, Vera V. Ponomareva², Rachelle C. Rourke¹

¹*Earth and Environmental Science, NM Tech, Socorro NM 87801 USA.*

²*Institute of Volcanology and Seismology, Petropavlovsk-Kamchatsky, 683006 Russia.*

The Kamchatka Peninsula is one of the most active volcanic regions in the world. At present there are 29 currently active subduction related volcanoes. Large explosive eruptions were frequent during the Holocene and resulted in widespread dispersal of tephra fall deposits. The largest tephra have been mapped in detail and dated by the ¹⁴C method and provide valuable stratigraphic markers which are useful for constraining the age of geological events such as the timing of paleotsunamis, faulting and to provide a knowledge of the eruption behavior of the volcanoes.

We have analyzed the glass from 89 tephra samples by electron microprobe to provide geochemical characteristics useful for correlating the tephra in Kamchatka and surrounding areas. The samples represent 27 key-marker tephra layers and 11 eruptive centers. The glass is rhyolite in 21 of the tephra samples, dacite in 2 and 2 samples are multimodal and 2 show mixed compositions ranging from andesite/dacite to rhyolite. There is a spread in the chemical compositions of the glass and each eruptive center has a unique chemical signature which allows each to be identified. The glasses are best characterized by their K₂O, CaO and FeO contents. Ten tephra erupted from Shiveluch volcano had similar major element compositions so it is not possible to chemically identify the individual eruptions.

We also analyzed the trace element compositions of 64 bulk tephra samples by instrumental neutron activation analysis to further refine the geochemical characteristics of the tephra. The samples were from 10 different eruptive centers. We found that the tephra could be characterized on the basis of Cr and Th contents and La/Yb ratios. For example all the tephra from Shiveluch are Cr-rich and very distinctive from other Kamchatka tephra.

To test the applicability of the geochemical signatures we analyzed 20 unknown tephra collected at Karaginsky(3), Bering (11), and Attu(5) Islands and Uka Bay(1) and used their chemical compositions to make correlations to known eruptions. Glass compositions and trace element data from bulk tephra samples show the Karaginsky Island and Uka Bay tephra were all erupted from Shiveluch volcano. The 11 Bering Island tephra are correlated to Kamchatka eruptions using their stratigraphic position, age, and glass and bulk chemical analysis. On Bering Island we identified the tephra from the Kurile Lake caldera eruption which was the largest Holocene eruption in Kamchatka. The occurrence of this tephra on Bering Island shows it was more widespread than currently mapped and should be a more valuable marker tephra layer for tephrochronological applications. Five tephra from Attu Island in the Aleutians are tentatively correlated with eruptions from Avachinsky and Shiveluch volcanoes in Kamchatka.

NON-SUBDUCTION-RELATED ISLAND ARC VOLCANISM: SEDANKINSKY DOL, KAMCHATKA.

Pavel Plechov¹, Maria Shur¹, Alexander Perepelov², Michail Puzankov³, Oleg Dirksen³, Lilia Bazanova³

¹*Geological Department, Moscow State University, Moscow, Russia.*

²*Vinogradov Geochemistry Institute, Siberian branch of Russian Academy of Sci., Irkutsk, Russia.*

³*Institute of Volcanology and Seismology, Petropavlovsk-Kamchatsky, Russia.*

Kamchatka is a mature island arc system; it includes numerous volcanic arcs of different ages that are joined together. The recent volcanic arc is related to subduction of the Pacific Plate (rate ~ 9.5 cm/y). The northern corner of the plate is restricted by its junction with the Aleutian trench and Commander Islands. The northern border line of the subducted plate is usually drawn along a large-scale fracture zone, which is marked by the Kamchatka River valley. Fifteen mln. y.a. the Kamchatka-Aleutian junction was 400 km south (near Shipunskiy Peninsula) of its modern position according to the most recent tectonic reconstructions (Park et al., 2002; Avdeyko et al., 2006). Transition of the junction to the north was a main reason for propagation of the Eastern Volcanic Front of Kamchatka.

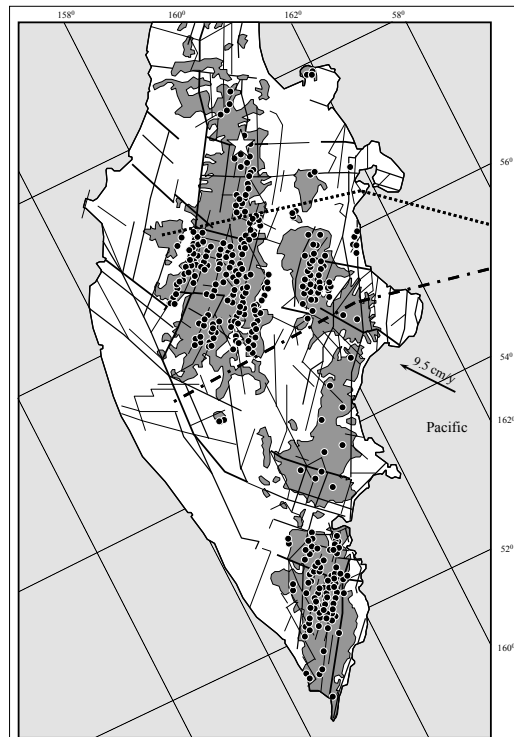


Fig. 1 Schematic map of Holocene-Pleistocene areal volcanoes in Kamchatka. The filled areas represent the areas of quaternary volcanism. The filled dots are areal eruptive centers. The star shows Sedankinsky Dol. Bold dashed lines correspond to the northern edge of the subducted Pacific Plate.

Fig. 1 shows quaternary volcanic areas and hypothetical boundaries of the subducted plate. It is possible that the Holocene-Pleistocene Sredinny Ridge volcanic zone is not related to the modern subduction zone. Meanwhile, more than 120 polygenetic and more than 1000 monogenetic eruptive centers of Holocene-Pleistocene age lie within a 450-km-long longitudinally trending zone with a width of 30-100 km. The scale of Sredinny Ridge basaltic volcanism during the last 40-50 ky significantly exceeds that of other Kamchatka volcanic zones [Bazanova, Pevzner, 2001; Dirksen et al., 2004; Pevzner 2004, 2006].

The Sedankinsky Dol volcanic areal zone is situated far north of any possible boundary of the subducted Pacific plate. Intensive basaltic volcanism appeared here during the late Pleistocene. Two Holocene eruption pulses (9 and 2.5 ky ago) was proved recently [Shur et al., 2009]. All these basalts are enriched in K, Ti, Nd, and LREE compared to "typical island arc" basalts. Basalts often contain skeletal forms of liquidus minerals (olivine up to Fo₈₄₋₈₆) and lack evidence of differentiation. Note the absence of high-Mg olivines, which reflects an equilibrium with mantle substrate. We estimated melt composition, H₂O content (~ 0.3 wt%), temperature (~ 1210 °C), and pressure (~ 1.5 kbar) of crystallization of experimentally reheated melt inclusions in most Fo-

rich olivine phenocrysts. Oxygen fugacity was estimated as NNO from Ol-Sp equilibria [Ballhaus et al., 1991].

We hypothesize that an explanation of the specific features of these basalts is the contribution of the non-mantle substrate to the source of melting. A favorable substrate is amphibole-rich pyroxenite. Such pyroxenites are described in the lowest part of the island arc crust of many palaeo-arcs [Kelemen et al., 2003]. Pyroxenites are known as xenoliths in the high-Ti basalts of Sredinny Ridge. These rocks could be involved in magma generation due to delamination or erosion of the lowest parts of the island arc crust by mantle in mature arcs.

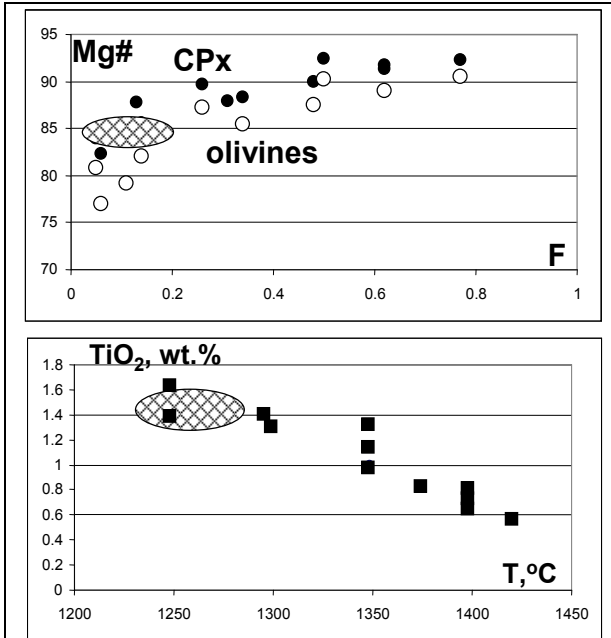


Fig.2 Comparison between Sedankinsky Dol parental melts and experimental data in plots of: a) Mg# vs. melted percentage (F); b) TiO₂ vs temperature (T, °C). Circles reflect experimental data of pyroxenite melting in dry conditions and 8-16 kbar [Kogiso,Hirshmann, 2001]. Empty circles: olivine; filled circles: clinopyroxene; squares: melts. Shaded area shows estimations for parental melts of Sedankinsky Dol basalts.

[Kogiso&Hirshmann, 2001] showed that pyroxenites could be partially melted at 1250°C and 8-16 kbar (similar to crust-mantle boundary conditions) even in dry conditions. Corrected to 8-16 kbar, temperatures for Sedankinsky Dol parental basalt melts are in the range of 1240-1280°C.

We compared compositions of Sedankinsky Dol basalt melt, olivine, and clinopyroxene with the pyroxenite melting experiments of Kogiso and Hirshmann (2001; Fig.2). Experimental data are in good agreement with natural samples with 5-20% melted at 1230-1280°C.

Tabl.1 Estimated parental melt compositions for Sedankinsky Dol basalts.

Sample	PK-02-32	PK-02-21	PK-02-26	PK-02-20	PK-02-27
SiO ₂	48.5 6	46.8 9	48.4 6	47.4 3	47.7 9
TiO ₂	1.60	1.72	1.65	1.62	1.65
Al ₂ O ₃	18.6 4	18.2 8	17.2 7	19.4 5	17.2 6
FeO*	9.94	9.95	9.93	9.95	9.92
MnO	0.32	0.18	0.24	0.17	0.21
MgO	5.54	7.45	7.20	7.40	7.63
CaO	8.60	10.7 7	10.1 3	9.68	10.5 2
Na ₂ O	4.55	3.51	3.64	4.21	3.39
K ₂ O	1.21	0.84	0.82	0.93	0.94
P ₂ O ₅	0.77	0.42	0.39	0.18	0.51
Cr ₂ O ₃	0.03	0.03	0.07	0.07	0.06
Fo, %	79.7	84.1	83.3	83.7	83.7
H ₂ O		0.18	0.29	0.09	
T, °C	1162	1194	1193	1208	1205

Notes: Each column is averaged composition values of glasses from experimentally quenched melt inclusions with correction to olivine-melt equilibrium. Fo: averaged forsterite number for each sample; T: temperature of olivine-melt equilibrium (Ford et al., 1983); Samples PK-02-20, PK-02-21, PK-02-26 from Terpu lava flows, PK-02-32 from Domashniy-2 cone lava flow, PK-02-27 from Kibeney shield volcano.

We can suppose that parental magmas of Sedankinsky Dol (and other Sredinny Ridge magmas of the high-Ti series) could be produced outside of modern supra-subduction zones due to melting of delaminated pyroxenites at a temperature of 1230-1280°C and a pressure of 8-16 kbar, with 5-20% melted. The island arc signature could be partially inherited from pyroxenites, which originated in supra-subduction settings. Elevated concentrations of K, Ti, Nb, and LREE could be explained by low degrees of melting and the hypothetical presence of amphibole in the melt substrate.

VOLCANISM AND VOLCANIC PROCESSES

POSTER PRESENTATIONS

LARGE-SCALE EDIFICE FAILURES IN THE RECENT HISTORY OF TATUN VOLCANIC GROUP, NORTHERN TAIWAN

Marina Belousova^{1,2}, Alexander Belousov¹, Chang-Hwa Chen¹

¹*Institute of Earth Sciences, Academia Sinica, Taipei, Taiwan.*

²*Institute of Volcanology and Seismology, Petropavlovsk, Russia.*

The dominantly andesitic Tatun Volcanic Group of Northern Taiwan was formed mainly during the Pleistocene, and several eruptions occurred in the Early Holocene. The group includes two principal volcanic ridges, SW-NE and W-E; each is approximately 15 km long. The SW-NE ridge is composed of the oldest, deeply eroded volcanoes with no primary volcanic landforms preserved, and not considered here. Our study focused on the W-E ridge, which is composed of 20 closely-spaced, relatively young, well-preserved volcanic edifices superimposed on an older volcanic foundation. Most of the edifices are represented by lava domes of moderate sizes: heights up to 350 m, base diameters up to 1.5 km, and volumes up to 0.3 km³, although due to superposition on the older foundation, absolute altitudes of many of the edifices reach heights of 800 – 1120 m a.s.l. Slopes of the volcanoes are weakly incised by erosion, but many of them have broadly opened, shallow, incised horseshoe-shaped depressions 0.5-1.5 km across. Morphology of these depressions is similar to that of scars formed by large-scale gravitational collapses. Field examination revealed deposits of collapses connected to formation of the horseshoe-shaped scars of volcanoes Datun, Cising, Siaoguanyin, Cigu, and Dajianhou.

The largest of the collapses with a volume ~ 0.1 km³ occurred at Mt. Datun (all indicated volumes and other geometrical characteristics have been calculated approximately due to scarce outcrops and heavy vegetation in the area). The collapse formed a typical debris avalanche deposit composed mainly of block facies: large (meters) domains of strongly shattered, deformed, but not completely intermixed material of the former volcanic edifice. The avalanche traveled a distance L ~ 5 km, dropped a height H ~ 0.8 km, and was moderately mobile H/L ~ 0.16. The age of the collapse is > 20,000 yrs because the related debris avalanche deposit is covered by a younger debris avalanche deposit of Siaoguanyin volcano containing charcoal dated to 19,520 +/- 120 BP.

The Siaoguanyin debris avalanche was very unusual: it was hot during deposition (contains carbonized wood), and had no well-developed block facies. Instead, the deposit is composed of massive, very coarse-grained, fines-poor, gravelly material represented predominantly by very dense, dark grey andesite. Characteristics of the deposit allow us to suggest that in the collapse hot, poorly vesiculated material of a dome or lava flow was involved; this material had no time to cool down completely after extrusion. Despite its much smaller volume (~ 0.02 km³), Siaoguanyin's debris avalanche was more mobile (L ~ 6.5 km; H ~ 0.9 km; H/L ~ 0.14) than the avalanche of Datun. We estimated its speed as 40 m/s at a distance 5 km from the source, based on 80 m of the avalanche run-up height.

The latest large-scale collapse occurred at Mt. Cising. Its C¹⁴ age is 5400 +/- 50 BP determined by dating of vegetation entrained into "bulldozer facies" of the resulting debris avalanche. The collapse with volume ~0.05 km³ occurred in the form of numerous retrogressive landslide blocks, which for unknown reason did not transform into a long runout debris

avalanche. The leading snout of the landslide traveled only 2.2 km, while rear slide blocks traveled only several hundred meters and stopped near the landslide source. Thus its maximum dropped height is only 0.5 km, and $H/L \sim 0.23$. A former lava coulee, which was involved in the collapse, underwent only weak disintegration: collapse material is represented by big boulders with few fine grained matrix.

Collapses of Cigu and Dajianhou volcanoes had the smallest volumes, $\sim 0.01 \text{ km}^3$, and their character is transitional to large rockfalls. The studied collapses occurred after the volcanoes had stopped erupting, and thus were not directly associated with volcanic activity (one possible exception is the Siaoguanyin collapse). Hydrothermally altered rocks do not compose significant parts of the studied debris avalanches, although hydrothermal fields are common in the scars of the collapses. Probably weakening of mechanical properties of the volcanic edifices due to hydrothermal alteration did not play a key role in the studied collapses, but elevated fluid pressure and hydrothermal alteration in the foundations of the volcanoes might have had some role. Scars of the collapses are located on intersections of tectonic faults. Thus, the collapsed parts of the volcanic edifices were detached by tectonic motions, and the collapses were possibly triggered by seismic activity. Our data show that large-scale collapses were common in the history of Tatun Volcanic Group. Future collapses represent a major hazard for the area, which is becoming ever more highly populated.

SURVEY OF THE BERG SUBMARINE VOLCANO: THE KURIL ISLAND ARC

Yu.I. Blokh¹, V.I. Bondarenko², V.A. Rashidov³, A.A. Trusov⁴

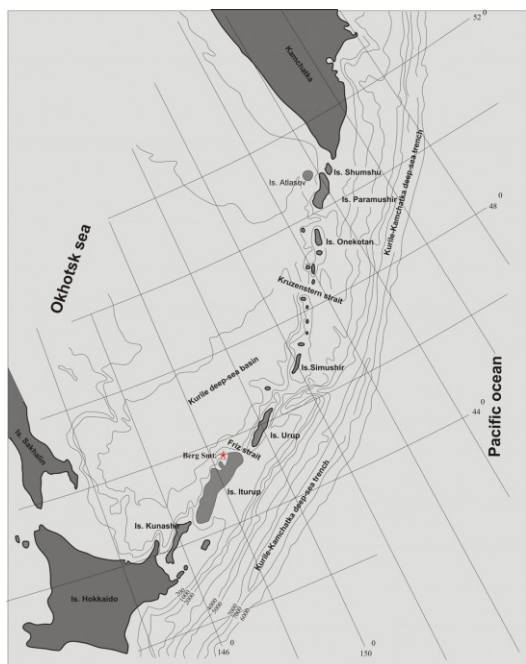
¹Russian State Geological Prospecting University, Moscow, 117873, Russia.

²Kostroma State University, Kostroma, 156000, Russia.

³Institute of Volcanology and Seismology, Far East Division. Russian Academy of Sciences, Petropavlovsk-Kamchatsky, 683006, Russia.

⁴ZAO «GNPP Aerogeofizika», Moscow, 107140, Russia.

The authors have studied the flat-topped Berg submarine volcano (Fig. 1). The volcano is located in the Kurile arc, 16 km north of the northern part of Iturup Island (Bezrukov et al., 1958; Ostapenko, 1978; Gnibidenko and Svarichevsky, 1984; Submarine..., 1992; Blokh et al., 2008).



depth is 480 m (Blokh et al., 2008).

The volcano's edifice is composed of dense rocks with prevailing andesibasalts and basalts, and by altered volcanic rock formations (Ostapenko, 1978; Submarine..., 1992). The basement of the edifice is covered with 600 m thick sediments. The edifice causes a magnetic field anomaly ΔT_a with amplitude exceeding 1200 nT (Fig. 2b).

We used the REIST program to model the edifice. This program is a part of the SIGMA-3D software package for the structural interpretation of gravity and magnetic anomalies (Babayants et al., 2005). An iterative process supported by REIST allowed us to approximate an anomalous field with a mean square error equal to 33 nT using 113 iteration procedures (Blokh et al., 2008).

We found that the most magnetized lava flows effused on the western slope near the summit (Fig. 2c, 2d). The effective magnetization intensity value, which exceeded 9 A/m, and dredge sampling show that these lava flows are likely composed of basalts and are the youngest

At one time it is likely that this volcano rose above sea level, but subsequent attrition has left it submerged 500-700 m beneath the surface of the sea. Loss of material from the flat summit likely occurred in the early Pleistocene or in the Pliocene. The northern flank of the Berg submarine volcano rises 2200-2300 m from the ocean floor, whereas its eastern and southern flanks rise about 1000 m above the floor at the junction with Iturup Island (Fig. 2a).

The volcano's relative elevation is 1800 m, but with bottom sediments covering its basement the elevation comprises 2400 m. The volcano covers an 11x15 km area, with a volume of 105 km³. Volcano slope inclinations vary from 15° near its basement to 25-30° near the summit. The summit is flat and declines northward to Friz strait. The summit measures 5x6.5 km and is located at a depth of 500-700 m (Fig. 2a).

The Fig. 1. Location of Berg submarine minimum volcano.

minimum

volcano.

within the edifice. These lava flows possibly effused about 700,000 years ago after the volcano had already submerged.

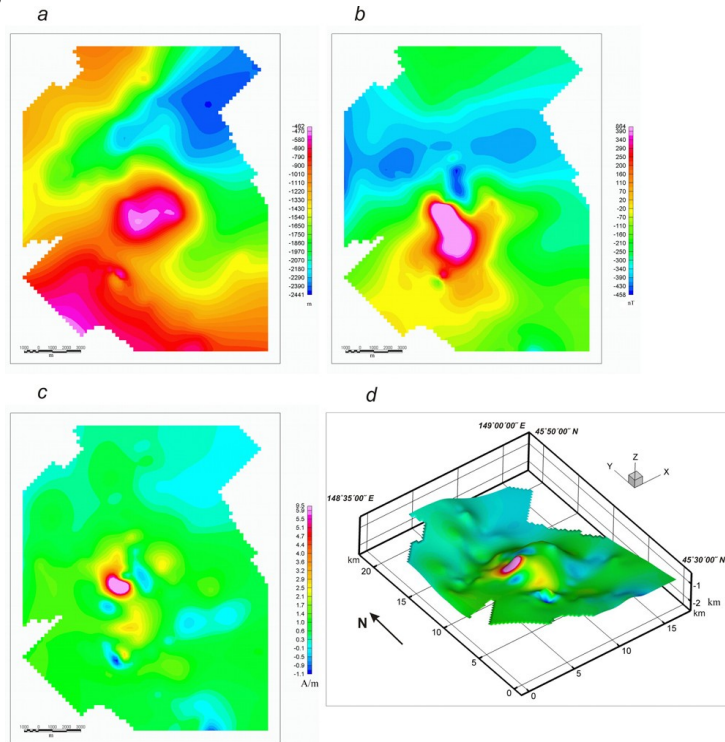


Fig. 2. Berg submarine volcano: *a* - bathymetry; *b* – anomalous magnetic field ΔT_a ; *c* – distribution of the volcano's effective magnetization intensity; *d* – effective magnetization intensity distribution, shown on the volcano's surface.

References

- Babayants P.S., Blokh Y.I., Bondarenko V.I., Rashidov V.A., Trusov A.A. Application of the SIGMA-3D software package for structural interpretation submarine volcanoes of the Kurile island arc // Bulletin of Kamchatka regional association «Educational-scientific center». Earth sciences. 2005. № 2 (6). pp. 67-76 (in Russian).
- Bezrukov P.L., Zenkevich N.L., Kanaev V.F., Uditsev G.B. Submarine volcanoes and mountains of the Kurile arc // Trudy laboratori vulkanologii. 1958. Vyp. 13: Molodoy vulkanizm. pp. 71-88 (in Russian).
- Blokh Yu.I., Bondarenko V.I., Rashidov V.A., Trusov A.A. The Berg submarine volcano: the Kuril Island Arc // Bulletin of Kamchatka regional association «Educational-scientific center». Earth sciences. 2008. № 2 (12). pp. 70-75 (in Russian).
- Gnibidenko G.S., Svarichevsky A.S. Tectonics of the South Okhotsk Deep-Sea Basin // Tectonophysiks. 1984. V. 102. pp. 225-244.
- Ostapenko V.F. Underwater volcanoes of the near-Kuril part of the Sea of Okhotsk and significance to understanding of the latest history of the region // Dokl. Sov. Akad. Nauk 1978. V. 242. № 1. pp. 168-171 (in Russian).
- Submarine Volcanism and Zonation of Kuril Island Arc / Ed. Yu. M. Pusharovskiy. Moscow: Nauka, 1992. 528 p. (in Russian).

This work is sponsored by the Far East Branch of the Russian Academy of Sciences (grant 09-III-A-08-427).

MINERALOGY AND PETROLOGY OF KAMEN VOLCANO ROCKS, KAMCHATKA

Tatiana Churikova¹, Boris Gordyechik¹, Gerhard Wörner², Boris Ivanov¹, Alexander Maximov¹

¹*Institute of Volcanology and Seismology FED RAS, Petropavlovsk-Kamchatski, Russia.*

²*GZG Abteilung Geochemie, Universität Göttingen, Germany.*

Studies of the Klyuchevskaya Group of volcanoes, which have the highest magma production rate across the Kamchatka arc and, in fact, for any arc worldwide, have been published in numerous papers during recent decades [e.g. Kersting & Arculus, 1995; Pineau et al., 1999; Dorendorf et al., 2000; Ozerov, 2000; Churikova et al., 2001; Mironov et al., 2001; Portnyagin et al., 2007; Turner et al., 2007]. However, modern geochemical studies of Kamen volcano, which is located between Klyuchevskoy, Bezymianny, and Ploskie Sopky volcanoes, have not been carried out and Kamen's role in petrogenesis of the Klyuchevskaya Group of volcanoes is unknown. To date only a few papers on this volcano have been published, mostly focusing on a large landslide [Ermakov, 1977; Melekestsev & Braitseva, 1988; Ponomareva et al., 2006]. Space-time proximity of volcanoes in the Klyuchevskaya Group and a common zone of abnormal seismicity below them [Tokarev & Zobin, 1970] suggest their genetic relationship. However, the lavas of neighboring volcanoes are rather different from Kamen lavas: high-Mg and high-Al basalts occur at Klyuchevskoy volcano, Hb-bearing andesites and dacites dominate at Bezymianny, and medium-to-high-K subalkaline rocks at Ploskie Sopky. In this report we present geological, petrographical, mineralogical, and petrochemical data on the rocks of Kamen volcano.

Three consecutive periods of activity are recognized in the geological history of this volcano: stratovolcano formation, development of a dike complex, and formation of numerous cinder and cinder-lava monogenetic cones. The stratovolcano stage is characterized by rather uniform magma evolution: the earliest lavas are essentially olivine-bearing, while higher up in the geological section olivine-pyroxene-bearing rocks are developed with mafic minerals decreasing from base to top. The younger stages of the volcano are characterized by olivine-free and hornblende-bearing lavas. The rocks of the dike complex are olivine-bearing (up to 25% olivine) and hornblende-bearing basalts. Monogenetic cinder and cinder-lava cones are olivine-clinopyroxene basalts and basaltic andesites. Mantle xenoliths are represented by harzburgites and pyroxenites.

The rock series of Kamen volcano is divided into four groups, which combine seven rock types: olivine-bearing (Ol-2Px and Ol-Cpx), olivine-free (2Px-Pl, Cpx-Pl, and abundant Pl), Hb-bearing, and subaphyric rocks. While olivine-bearing rocks are observed in all volcanic stages, olivine-free lavas are present only in the stratovolcano edifice. Lavas of the monogenetic cones are represented by olivine-bearing and subaphyric rocks. Dikes are composed of olivine-bearing and hornblende-bearing rocks.

Kamen volcano olivines vary from Fo₆₀ to Fo₈₃. Their unimodal distribution shows a maximum at Fo₇₉. NiO, Cr₂O₃, and CaO in olivines vary significantly: 0,009% - 0,124%, 0,007% - 0,06% and 0,1% - 0,378%, respectively. NiO/Cr₂O₃ and NiO/CaO ratios are rather low: 3,5 and 0,38, respectively. Due to low Mg# and NiO, olivines of Kamen volcano do not fall into the mantle array of primary magmas after Ozawa [1984].

Clinopyroxenes are augites in composition with magnesian number similar to magnesian number of olivines. Plagioclases have a bimodal distribution with maximum modes at An₅₀ and An₈₆. Oxides are represented by high-Al spinel, magnetite, and titaniferous magnetite. Similar

magnesian numbers of olivine and clinopyroxene argue for equilibrium of these minerals in the melt. Low magnesian numbers of mafic minerals and their low Ni and Cr concentrations testify to significant fractional crystallization of the melt from which the rocks crystallized.

All rocks of the volcano belong to a medium-K calc-alkaline basalt-basaltic-andesitic series. The rocks of the stratovolcano are high-Al and low-Mg ($MgO < 6\%$) and form stable trends on all petrological diagrams, with increasing K_2O and decreasing Al_2O_3 , TiO_2 , CaO , FeO , and MgO from basalts to andesites. The dike complex melts are likely the least fractionated members from the same mantle source. Lavas of the monogenetic cones are high-Mg basalts ($MgO > 6\%$, $SiO_2 = 50.5 - 52.5\%$). They systematically differ from the stratovolcano samples by higher MgO and CaO and low FeO , TiO_2 , Al_2O_3 , and P_2O_5 at similar SiO_2 content (Fig. 1).

The rocks of Ploskie Sopky volcano are systematically enriched in K_2O and P_2O_5 and depleted in Al_2O_3 and MnO compared to rocks from the Kamen stratovolcano at given silica content, and thus could not have originated from the same mantle source by fractional crystallization. In contrast, Kamen and Bezymianny stratovolcanoes form a narrow single trend on all diagrams, where Bezymianny data points comprise a more silica-rich part of the overall trend. High-Al rocks of Klyuchevskoy are close to the Kamen stratovolcano samples, but high-Mg Klyuchevskoy samples show more similarity to cinder cones from Kamen.

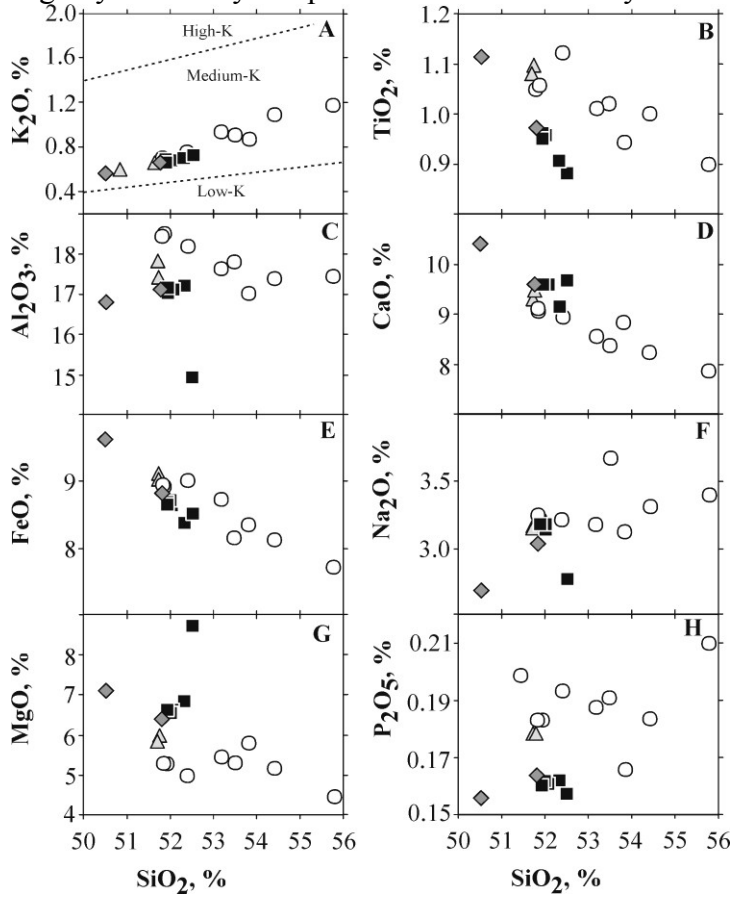


Fig. 1. Harker diagram for Kamen volcano rocks. Circles: stratovolcano rocks; triangles: dike complex basalts; squares: monogenetic cones; diamonds: earlier studied samples from Churikova et al. [2001].

REFERENCES: Churikova et al., 2001: *Journal of Petrology*, **42** (8): 1567-1593; Dorendorf et al., 2000: *Earth Planet. Sci. Lett.*, **175**: 69-86; Ermakov, 1977: Formation dismemberment of the Quaternary volcanic rocks, Moscow, Nedra: 223 p. (in Russian); Kersting & Arculus, 1995: *Earth Planet. Sci. Lett.*, **136**: 133-148; Melekestsev & Braitseva, 1988: *Volcanol. Seismol.*, **6**: 495-508; Mironov et al., 2001: *Petrology*, **9** (1): 46-62; Ozawa, 1984: *Geochimica et Cosmochimica Acta*, **48**: 2597-2611; Ozerov, 2000: *Journal of Volcanology and Geothermal Research*, **95**: 65-79; Pineau et al., 1999: *Chemical Geology*, **135**: 93-124; Ponomareva et al., 2006: *Journal of Volcanology and Geothermal Research*, **158**: 117-138; Portnyagin et

al., 2007: *Geophysical Monograph Series*, **172**: 199-239; Tokarev & Zobin, 1970: *Bulletin of the volcanological station*, **4**: 17-23 (in Russian); Turner et al., 2007: *Geochimica et Cosmochimica Acta*, **71**: 4771-4785.

VOLCANIC ACTIVITY AND EARTHQUAKES IN CENTRAL AMERICA: SOME GENERALITIES

E. Duarte, E. Fernández

Volcanological and Seismological Observatory of Costa Rica (OVSICORI), Universidad Nacional, P.O. Box 2346-3000, Heredia, Costa Rica. Email: eduarte@una.ac.cr, fax (506)2610303

Central America is a highly volcanic and seismic region. Currently about 26 active volcanoes show some kind of activity threatening important populated areas around or near them. On the other hand; at least 51 upper-crustal destructive earthquakes have been compiled since 1900 in the same region. Most of such events caused deaths or heavy damage of Modified Mercalli (MM) intensity larger than VII (White and Harlow 1993). Despite that these large earthquakes were located along the Central American volcanic range no geographical or genetic correlation has been suggested.

Secondary hazards –some seismically triggered- are associated to the general risk in the entire region. Landslides, lahars have taken thousands of lives in recent decades. Volcanic ash, on the other hand, pose an overall risk to regional aerial navigation.

Due to the proximity of important clusters of communities to active volcanoes more regional efforts are required in order to evaluate, study and sustain volcano and seismic monitoring. Specific seismic and volcanic mitigation measures will need more attention in the near future to ensure safety to millions of inhabitants in this less developed region.

Governmental policies –as a regional effort- have to be undertaken in order to include topics like: seismic and volcanic microzonation, building codes, preparedness and education. Equally important, is the planning process to reduce economic and human losses of those less benefited by centralized economies that keep forgetting those living at risk in remote areas.

Summarizing, in terms of geological setting and natural processes, Central America may be similar to the Kamchatsky-Kuril region. In terms of hazards, location of inhabitants and socio-economical conditions there are few similarities. Hence, special attention will be needed in the Central American region departing from politicians, policymakers and researchers, to bring understanding and safety to this needy region.

TI-IN-QUARTZ GEOTHERMOMETRY OF MAGMAS FROM KATMAI, ALASKA: A COMBINED CATHODOLUMINESCENCE/ELECTRON MICROPROBE STUDY

Allison L Payne¹, John C Eichelberger²

¹*Alaska Volcano Observatory, Geophysical Institute, University of Alaska Fairbanks, Fairbanks, AK 99775.*

²*Volcano Hazards Program, US Geological Survey, MS-904, Reston, VA 20192.*

Cathodoluminescence (CL) imagery can reveal subtle chemical zonation in quartz which is not visible by other means (Edwards et al., 2007). Ti⁴⁺ which substitutes for Si⁴⁺ in the quartz lattice at elevated temperatures is believed to be one of the main activators of high-intensity CL emissions in quartz (Landtwing and Pettke, 2005; Wark et al., 2007). The temperature-dependent substitution of Ti⁴⁺ in quartz has been calibrated in the new Ti-in-quartz geothermometer, TitaniQ (Wark and Watson, 2006).

This study uses CL imagery as a map for microprobe analysis of Ti-in-quartz, and applies the TitaniQ geothermometer to reveal the thermal history of quartz crystallization in three suites of magmatic rocks from the Katmai region of the Alaska Peninsula: (1) the 1912 Novarupta high-silica rhyolite lava dome; (2) a nearby sill of hydrothermally altered high-silica rhyolite; and (3) a granodiorite stock which appears to have a transitional, mingled contact with the sill. EPMA detection limits were minimized for trace Ti by the simultaneous detection of Ti on 3 spectrometers, and by using a high beam current of 100nA and extended count times of 200s on peak and background.

Quartz phenocrysts in the Novarupta rhyolite show subtle CL oscillatory zoning, and reveal crystallization temperatures of ~750-820°C across the grains, consistent with previous Fe-Ti oxide temperatures (Hildreth, 1983; Coombs and Gardner, 2001). Quartz from the rhyolite sill shows high CL intensity cores and significant normal Ti zoning, with core to rim temperatures of ~900-650°C, respectively. Dark CL overgrowths and veins throughout the altered rhyolite represent low-T secondary quartz growth, with Ti concentrations approaching 0 ppm. Quartz grains from the granodiorite show complex CL intensity zoning which correlates well with Ti concentrations. Most grains have high-intensity cores with Ti concentrations of 150-180 ppm, corresponding to formation temperatures of ~800-820°C, and lower intensity rims with 130-140 ppm Ti, corresponding to temperatures of ~780-790°C.

Several grains in each of the three sample suits show thin (5-10 µ), high-intensity CL rims, which likely represent Ti enrichment, and may be common in magmatic quartz (Götze et al., 2001). Such rims may be due to the increased incorporation of Ti in quartz during rapid disequilibrium growth from the cooling, degassing, depressurization of the host magma, or heating just prior to eruption, for example, by a basalt trigger. The narrowness of the rims and their proximity to Ti-rich groundmass glass, however, make EPMA analysis difficult.

The simple Ti distribution of quartz in the 1912 rhyolite, together with the multiply-saturated character of the melt (Coombs and Gardner, 2001), is consistent with a very short time span between extraction from a granodiorite mush and eruption (Eichelberger et al., 2006). The higher temperature cores of quartz in the sill are surprising and perhaps explicable by lower magmatic water content than the 1912 magma, with the lower temperature rims attributable to uninterrupted crystallization to solidus. Complexity of zoning in quartz of the granodiorite may be attributed to multi-stage mixing, as evidenced by mafic enclaves, complexly zoned plagioclase, and apparent mingling with the quartz-saturated sill, as well as uninterrupted crystallization to solidus.

WATER UNDER-SATURATED PHASE EQUILIBRIA OF BASALTIC ANDESITES FROM WESTDAHL VOLCANO, ALASKA

Erika L. Rader¹, Jessica Larsen¹

¹*University of Alaska, Fairbanks, Alaska, USA.*

The two most abundant gases released from magmatic systems are typically H₂O and CO₂. However, most phase equilibria studies examining crystallization applied to natural magmatic systems over the past 200 years have relied on H₂O-saturated conditions. The two most abundant gases released from magmatic systems are typically H₂O and CO₂, however, most phase equilibria studies examining crystallization applied to natural magmatic systems over the past 200 years have relied on H₂O-saturated conditions. The experiments were conducted on lava from Westdahl volcano at total pressures (PTotal) of 0–200 MPa and 900–1050 °C, had fO₂ set to the Ni–NiO buffer, and contained either 100% H₂O or 7:3 H₂O to CO₂. A ~25 to 50 °C shift in temperature, at similar pressures is observed in the plagioclase and pyroxene stability curves when CO₂ is added. Microprobe analyses of identified mineral phases, including plagioclase, clinopyroxene, Fe-Ti oxides, and minor orthopyroxene, show a relationship between water content and Al₂O₃ wt %. The shift in the phase curve of plagioclase results in a depletion of Al₂O₃ relative to SiO₂ at higher temperatures. Thus, our experiments indicate a significant effect of CO₂ on the crystallization of mafic magmas at crustal pressures in volcanic arcs and can affect the evolutionary path a magma might take.

EXPLOSIVE SEISMIC SIGNALS AT KARYMSKY VOLCANO 2008

Richard W. Sanderson¹, Michael West²

¹*Dept. Earth & Env. Sci., New Mexico Tech., Socorro, New Mexico, USA.*

²*AVO, Geophysical Institute, Univ. Alaska, Fairbanks, Alaska, USA.*

Detailed interpretation of explosions at volcanoes becomes easier with the integration of contrasting geophysical data sets. At Karymsky volcano, Kamchatka a resurgence of explosive behaviour in July 2008 was recorded simultaneously by seismic, video and thermal devices. Preliminary seismic analysis of 8 explosions shows that signals can be split into components associated with the ejection of material (0.5 – 3.0 Hz) and with debris avalanches (3.0 – 10.0 Hz). Video data was used to confirm 4 explosions, while the 4 others were identified based on waveform similarity. Explosions occurred with repose times anywhere between 0.5 hours and 26 hours, while seismic amplitudes varied by a factor of 10. Observed plumes had differing heights, ash content and debris avalanche volumes. The seismic nature of the semi-permanent passive degassing may also contain important information about the evolving state of the eruptive system. The aim of this work is to confirm that differences in seismic waveform can be well correlated with observable eruptive details.

BASALTIC-ANDESITIC PYROCLASTIC FLOW DEPOSIT OF THE 3.3Ka ERUPTION AT TOKACHIDAKE VOLCANO, NORTHERN JAPAN

Mitsuhiro Yoshimoto

*Department of Natural History Sciences, Faculty of Science, Hokkaido University
N10 W8, Kita-ku, Sapporo, 060-0810 Japan*

A basaltic-andesitic pyroclastic flow deposit associated with a 3.3ka eruption is preserved at the western foot of Tokachidake Volcano, Northern Japan. The deposit can be divided into two units, based on the variation in and content of juvenile materials. The lower unit consists of several flow units that are yellowish-brown in color and contain a large amount of altered or oxidized lithic fragments and a minor amount of juvenile materials composed of pumice, scoria, and cauliflower-shaped bombs. The upper unit consists of several flow units that are dark brown to black in color and mainly contain scoria and cauliflower-shaped bombs as juvenile materials. Although both units are matrix supported and poorly sorted, they lack fine-grained particles (less than 1/16 mm) in the matrix and are more sorted than dacitic and andesitic pyroclastic flow deposits. The lower and upper units are mainly distributed in small valleys and cover areas of 3 km² and 3.6 km², respectively. The ratios of the height and the runout distance are estimated at 0.21-0.32 and 0.15-0.21 for the lower and upper units, respectively, which are similar to pyroclastic flow deposits of Unzen Volcano (dacite) and Fuji Volcano (basalt). The presence and content of juvenile materials in the lower unit suggest that the pyroclastic flow was generated by the collapse of a pyroclastic cone with a volcanic edifice. For the upper unit, it could have been generated by a collapse of the crater wall with lava pool, similar to the volcanic bomb-rich pyroclastic flow deposits reported at Arenal Volcano and Aso Volcano.

SUBDUCTION ZONE SEISMICITY AND STRUCTURE

ORAL PRESENTATIONS

IMAGING AND EARTHQUAKES ALONG 600 KM TRANSECT OF SUBDUCTION IN CENTRAL ALASKA: BEAAR TO MOOS

Geoffrey A. Abers¹, Douglas Christensen², Joshua Calkins¹

¹Lamont-Doherty Earth Observatory of Columbia University, Palisades NY, USA.

² Geophysical Institute, University of Alaska Fairbanks, Fairbanks AK, USA.

Two dense broadband arrays give us new, high-resolution sampling of the subducting plate, mantle wedge, and earthquakes in the Wadati-Benioff zone beneath central Alaska. The arrays sample seismic wavefields at 5-15 km station spacing from the southern Kenai Peninsula to near Fairbanks, with 69 broadband sites including cross lines, resulting in nearly 600 km of continuous wavefield imaging. The northern array, BEAAR, sampled the Alaska Range region from 1999 to 2001, while the southern MOOS array has been sampling structure and earthquakes beneath the Kenai and greater Anchorage area 2007-2009 (due for August demobilization). These arrays provide a remarkable image of the subducting crust to 130 km depth and show that it is 15-20 km thick, probably the Yakutat terrane descending from the coastline to beneath the Alaska Range. It is a distinct low-velocity layer, indicating that it has not metamorphosed to eclogite until 130 km depth. The clearest image comes from migration of scattered waves in teleseismic P-wave coda, essentially receiver function migration, allowing resolution of layers a few km thick. The buoyancy of the subducting plate is greatly enhanced by the thick crust, and may explain the shallow dip of the megathrust beneath Alaska (site of the great 1964 earthquake), as well as the onset of mountain building in the last 5-10 Ma. By virtue of their dense station spacing and recording of S waves through 3-component sampling, the arrays also improve significantly the locations of earthquakes within and above the subducting plate. At depths where the subducting crust underlies mantle, all intraslab earthquakes lie within subducted crust, consistent with models of earthquake generation in which dehydration embrittlement provides a critical trigger. Preliminary results show abundant seismicity within the thrust zone at shallower depths, providing some insight into its geometry and the relative importance of thrust faulting above or below the subducting Yakutat crust. These integrated images are in their early stages, as MOOS data are still being collected, but when complete (and merged with offshore active-source observations) will provide one of the longest dense seismic transects of a subduction zone anywhere.

LONG-TERM EARTHQUAKE FORECAST FOR THE KURIL-KAMCHATKA ARC FOR 2009-2014

Sergei A. Fedotov, Alexey V. Solomatin, Sergey D. Chernyshev

Institute of Volcanology and Seismology, Petropavlovsk-Kamchatskiy, Russia.

A method of long-term earthquake prediction based on discovered regularities of large earthquake locations (seismic gaps) and their seismic cycles was initially proposed by S.A. Fedotov in 1965-1967 for the Kuril-Kamchatka arc and Northeastern Japan [1].

The seismogenic zone of the Kuril-Kamchatka arc occurs at depths of 0-80 km, and is 2100 km long and 100 km wide; the most active part is divided into 17-21 areas. For these areas the stages of seismic cycle are forecasted, the locations of seismic gaps are indicated, and the relative danger of seismic gaps is determined. In addition, the seismic activity A_{10} (the number of small earthquakes per year of the energy class $K_s=10$ or $M=3.6$ over an area 1000 km^2 in size), magnitude M of moderate earthquakes, which are expected with probabilities 0.8, 0.5, and 0.15, the maximum magnitudes of earthquakes, and the probability of the strongest earthquakes with $M \geq 7.7$ are predicted [1-4].

The quantity A_{10} is the leading parameter that allows an estimation of the probability that phase III (the terminal phase) of the seismic cycle has arrived. The activity of moderate and large earthquakes is evaluated using a parameter D (relative seismic energy): $D = E_2/E_1$, where $E_1 \text{ J/yr } 10^3 \text{ km}^2$ is the average normalized seismic energy released per year in the entire Kuril-Kamchatka earthquake-generating zone, and $E_2(t) \text{ J/yr } 10^3 \text{ km}^2$ is the normalized seismic energy released in a segment of interest during one year. Another parameter, A_{11} , is used to represent the activity of medium-sized earthquakes; A_{11} is based on the number of earthquakes of the energy class $K_s=11$ or $M=4.3$ and bigger per year over an area 1000 km^2 in size [1-4].

Three well-defined phases of the seismic cycle can be defined: aftershocks (phase I), a long period of stress buildup and potential seismic energy accumulation (phase II), and increasing seismic activity before the next $M \geq 7.7$ earthquake (phase III). The seismic processes during phase III, the terminal phase of the seismic cycle, can be complex. This phase may contain seismically quiet periods, subsequent foreshock increases, and other phenomena. However, when data were obtained for a large space-time volume (rupture zones or segments of the earthquake-generating zone 100-200 km long or longer and time intervals of 5 or 10 years) the values of A_{10} (phase III) during the last 10 years of the seismic cycle were greater than the mean A_{10} during phase II in 16 cases out of 17. The mean A_{10} (phase III) during the last 5 years of the cycle exceeds the level of A_{10} during phase II by 2σ . These data show that the seismic activity, A_{10} , and the rate of small earthquakes typically increase by factors of 2-2.5 during the last 5-10 years of a seismic cycle for $M \geq 7.7$ earthquakes. In addition, parameters D and A_{11} show a tendency to increase at the end of phase III compared with phase II [3, 4].

The relative hazard for a seismic gap is estimated by the quantity $1-B=1-P(A_{10})P(D)P(A_{11})$, where $P(A_{10})$, $P(D)$, and $P(A_{11})$ are the probabilities that the values of A_{10} , D , and A_{11} during phase II will accidentally exceed their values during the last 5-10 years.

Predictions are renewed twice a year or more often if strong earthquakes occur and the parameters of seismicity in the foregoing 5 years substantially change.

A known seismological method developed in 1965-2008 was used systematically in the Kuril-Kamchatka region [1-4]. The $M \geq 7.7$ earthquakes which occurred in Japan in 1968, in the Kuril Islands in 1969, 1973, and 1978, and in Kamchatka in 1971 occurred in the locations

predicted most likely to experience earthquakes of this size (seismic gaps). The previous Shikotan earthquake, 4.10.1994, $M=8.1$, the Middle Kuril (Simushir) earthquake, 15.11.2006, $M=8.2$ in the Kuril Islands, and the Kronotsky earthquake, 5.12.1997, $M=7.8$ in Kamchatka were also successfully predicted. Successful forecasts of seismicity parameters in segments of the Kuril-Kamchatka earthquake-generating zone were developed for five-year intervals during 1965-2005. Over a 40-year period of applying this method the predictions of the strongest earthquakes were justified with probability 0.8-0.9 [1, 2]. Additional seismic forecasts of aftershocks $M \geq 6$ based on a foreshock and aftershock "scenario" is part of the presented method [1-4]. The results of these forecasts can be used to enhance seismic safety.

A prediction of the Middle Kuril Island earthquake, 15.11.2006, $Ms=8.2$ is the most recent success of the proposed method [3, 4].

This method's state-of-the-art and a long-term seismic forecast for Kamchatka and Kuril islands for 2009-2014 is presented. Explanations are given for the forecast preparation. A similar forecast for 2008-2013, including maps and tables, is published in [4]. The development of seismic processes in the Kuril-Kamchatka seismogenic zone is considered. This zone is divided into 20 areas in the present forecast. The most important conclusion to be drawn from the present long-term earthquake forecast is that very high earthquake hazard will persist during the next five years (from 2009 to January 2014) in the Petropavlovsk-Kamchatskiy area, where the probability of a disastrous earthquake causing shaking of intensity VII-IX is 48% during these years. Speedy measures must be urgently undertaken to accomplish necessary retrofitting in the main city of Kamchatka in order to insure residents' safety in case of a significant seismic event. These long-term earthquake forecasts have been important in previous years when arguments have been presented to the Government requesting retrofitting measures be taken to ensure seismic safety and protection [1].

The long-term earthquake forecast proposed here is also a long-term forecast of tsunami probability for various locations along the Kuril-Kamchatka arc.

The proposed method can be used for Japanese, Aleutian, and other island arcs and regions of the world that have similar structure and seismicity [1]. The retrospective long-term prediction for an earthquake near the coast of Hokkaido, 25.9.2003, $M=8.1$ has confirmed the possibility of applying this method in other regions of the world [2].

References

- Fedotov S.A. The Long-Term Earthquake Prediction for the Kuril-Kamchatka. Moscow: Nauka, 2005. 302 p. (In Russian. Introduction, Conclusion and Supplements are translated).
- Fedotov S.a., Solomatin A.V., Chernychev S.D. Long-term Earthquake Forecast for the Kuril-Kamchatka Arc for 2004-2008 and Retrospective Forecast of the $M=8.1$ September 25, 2003, Hokkaido Earthquake // Vulcanol. Seismol., 2004, No 5, pp. 3-32. (In Russian.)
- Fedotov S.A., Solomatin A.V., Chernyshev S.D. Long-term Earthquake Prediction for the Kuril-Kamchatka Arc for 2006-2011 and Successful Prediction for the Middle Kuril Island Earthquake, 15.XI 2006, $Ms=8.2$ // Journal of Volcanology and Seismology. 2007, Vol. 1, No 3, pp. 143-163.
- Fedotov S.A., Solomatin A.V., Chernyshev S.D. Aftershocks and the Rupture Zone of the $M_S = 8.2$, November 15, 2006 Middle Kuril Is. Earthquake and a Long-Term Earthquake Forecast for the Kuril-Kamchatka Arc for the Period from April 2008 to March 2013 // Journal of Volcanology and Seismology, 2008, Vol. 2, No. 6, pp. 375-394.

SEISMIC VELOCITY STRUCTURE AT THE VOLCANOES OF KATMAI, ALASKA, FROM LOCAL EARTHQUAKES AND AMBIENT NOISE

Matthew M. Haney¹, Stephanie G. Prejean¹, Rachel Murphy², and Cliff Thurber²

¹USGS Alaska Science Center, Alaska Volcano Observatory, Anchorage, AK, USA.

²Department of Geology and Geophysics, University of Wisconsin-Madison, Madison, WI, USA.

The seismicity and structure of the volcanoes in Katmai National Park - Martin, Mageik, Trident, Novarupta, Griggs, Snowy, and Katmai - have both fascinated and puzzled researchers (Goodliffe et al., 1991; Ward et al., 1991; Jolly and McNutt, 1999; Moran, 2003; Jolly et al., 2007). Questions remain on the details of shallow magma transport and the relationship between magma bodies and seismicity (Jolly et al., 2007). We apply the recently-developed seismic techniques of double-difference relocation and ambient noise tomography to add to what is known about this complex volcanic system.

Ambient noise tomography (ANT) is an emerging technique in seismology with the ability to provide 3D images of subsurface volcanic structure using relatively sparse seismic networks. The method relies on the principle that the cross-correlation of noise recordings at two different seismic stations reproduces an experiment in which one of the stations acts as an active source. Ambient seismic noise in the frequency band from 0.1 to 1 Hz is mostly composed of fundamental mode surface waves, of both Love and Rayleigh type. As a result, noise cross-correlations are sensitive to S-wave structure and act to complement P-wave images computed by local earthquake tomography (LET) or double-difference tomography.

We determine a 3D S-wave velocity image for the Katmai group of volcanoes along the Alaska peninsula from 60 days of continuous recordings in 2005 and 2006. A low-velocity zone (LVZ) at Katmai Pass, previously known from LET (Jolly et al., 2007) and station corrections (Ward et al., 1991), exists in the 3D model at depths within 2-3 km of the surface, as shown in Figure 1. That the LVZ is also apparent in P-wave velocity models suggests it is a shallow magma storage area for Trident volcano. These depths are consistent with the depth of an inflation source previously detected by InSAR (Lu et al., 1997; Lu et al., 2003). In contrast, low S-wave velocities under Martin volcano are likely fluid-related, given the lack of low P-wave velocities in images derived from LET. Interestingly, a deep (> 5 km), subtle LVZ imaged between Trident and Mount Katmai may represent remnants of the magmatic conduit system from the cataclysmic 1912 eruption of Novarupta. A deployment of 11 temporary broadband seismometers is currently in place around Katmai Pass and should provide more constraints on the structure of the deep LVZ.

In late 2008, Trident experienced its largest earthquake swarm in the past decade. Although the swarm was primarily characterized by brittle failure earthquakes in the shallow crust, roughly 15 deep long-period (DLP) events and many shallow tornillo-type long-period events occurred as well. The Katmai area has witnessed DLP events in the past (Power et al., 2004), but depth resolution of the DLP events was poor due to the relatively sparse permanent seismic network. The added station density provided by the temporary network should improve locations and source parameters of the DLP events from 2008. The observations of DLP events, shallow brittle-failure earthquakes, and tornillos together suggest that fluids are moving at depth and that the recent increase in seismicity may be related to magma recharge of the shallow low-velocity body the dense temporary network is designed to image.

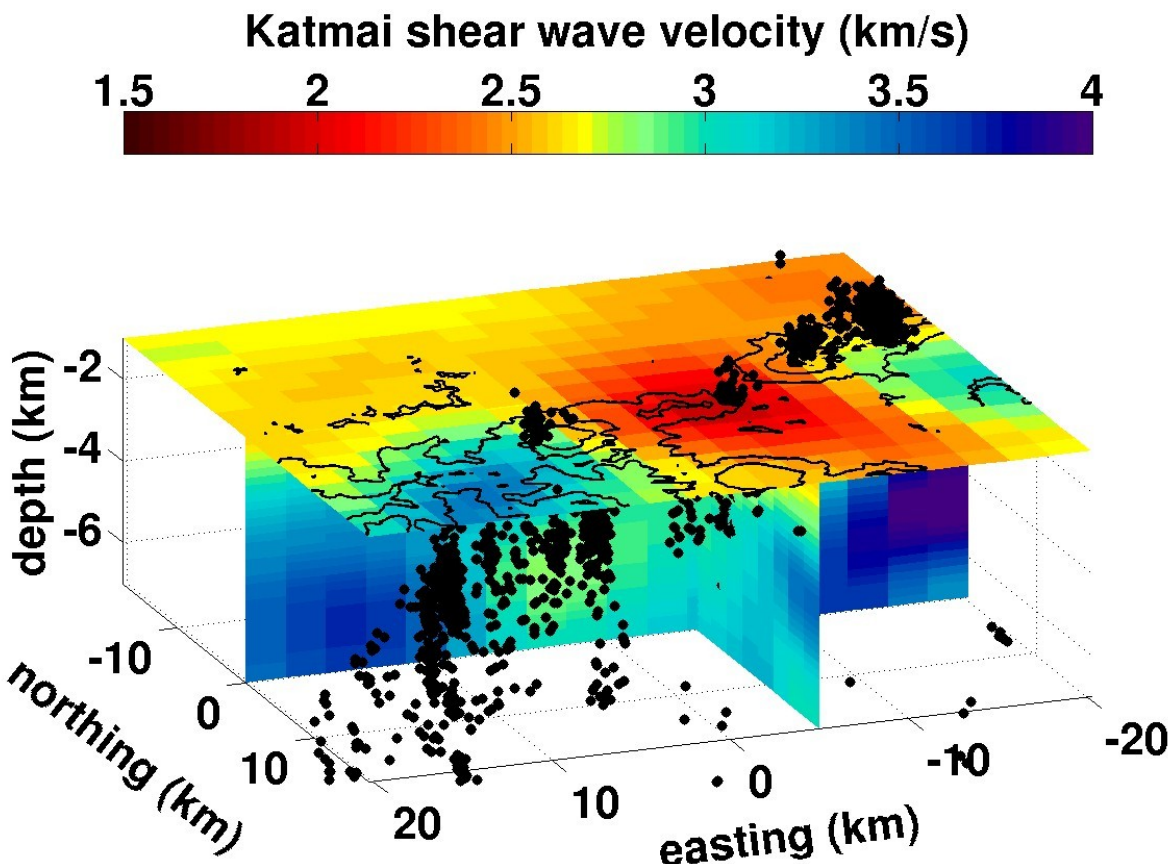


Figure 1. The seismicity and S-wave velocity structure in the vicinity of Katmai Pass, Alaska, plotted with elevation contours at 1 and 1.5 km above sea level. View is toward the southwest. This image is derived from ambient seismic noise, in contrast to local earthquakes. Katmai Pass is associated with a prominent low velocity zone within 2-3 km of the surface. Double-difference re-locations are shown by black dots.

Reference

- Goodliffe, A. M., D. B. Stone, J. Kienle, and P. Kassameyer, Geophysical Research Letters, 18, 1521-1524, 1991.
- Jolly, A. D. and S. R. McNutt, Journal of Volcanology and Geothermal Research, 93, 173-190, 1999.
- Jolly, A. D., S. C. Moran, S. R. McNutt, and D. B. Stone, Journal of Volcanology and Geothermal Research, 159, 326-342, 2007.
- Lu, Z., R. Fatland, M. Wyss, S. Li, J. Eichelberger, K. Dean, and J. Freymueller, Geophysical Research Letters, 24, 695-698, 1997.
- Lu, Z., C. Wicks, Jr., D. Dzurisin, J. Power, W. Thatcher, and T. Masterlark, Earth Observation Magazine, 12, 8-18, 2003.
- Moran, S. C., Bulletin of the Seismological Society of America, 93, 94-108, 2003.
- Power, J. A., S. D. Stihler, R. A. White, S. C. Moran, Journal of Volcanology and Geothermal Research, 138, 243-266, 2004.
- Ward, P. L., A. M. Pitt, and E. Endo, Seismic evidence for magma in the vicinity of Mt. Katmai, Alaska, Geophysical Research Letters, 18, 1537-1540, 1991.

GREAT EARTHQUAKES ALONG THE TRENCHES AND HUGE ACTIVE FAULTS TRAVERSING THE BACK ARC ISLANDS : 2004 SUMATRA-ANDERMAN EARTHQUAKE AND SUMATRAN FAULT

**Funiaki Kimata¹, Takeo Ito¹, Endra Gunawan¹, Agustan¹, Takao Tabei², Iruwan Meilano³,
Didik Sugiyanto⁴, Irwandy⁴**

¹⁾Nagoya Univ., Japan; ²⁾Kochi Univ., Japan; ³⁾ITB, India; ⁴⁾Syiahkula Univ., India

Fault Model of 2004 Sumatra—Anderman Earthquake

Many fault models have been proposed. Vigny et al. (2005) suggest a maximum slip distribution to the plate boundary of 50 km in depth. Basically, depth is estimated as the uncoupling zone. Subarya et al. (2006) estimate a large slip under the Aceh Basin although they introduced large displacements in the west coast of Aceh.

We estimate the fault slip distribution of Aceh segments of the 2004 Sumatra-Anderman Earthquake based on displacements detected in Sumatra (Fig.1). A slip greater than 20 m is estimated under the outer arc to wedge, which is located between active aftershock zones (Plamert et al., 2007) as shown in Fig.2

Post-Seismic Deformation and the Aceh GPS Network for Sumatran Fault System (AGNeSS)

We have repeated the GPS measurements in Aceh every year from 2005 until now and we have constructed a continuous GPS network to detect post-seismic deformation following the 2004 earthquake and the Sumatran fault in 2007. Large post-seismic deformations of >20cm/yr have been detected by GPS measurements, especially in north Aceh (Fig.3). In contrast, small deformations of <10 cm/yr have been observed in south Aceh, where, as estimated by coseismic deformation measurements, there is no large fault slip (Fig.1)

Sumatran Fault

The Sumatran Fault traverses Sumatra, and large earthquakes of M6-7 have occurred along this fault during the last 100 years. Fault slip rates of 1-4 cm/yr are estimated from the geological surveys. A large fault slip of 4 cm is estimated in north Aceh; however, there is no record of large earthquakes in this region. We suggest that creep movements or a large earthquake could occur in north Aceh in the near future. It is difficult to maintain continuous GPS measurements in Sumatra, but using these measurements we hope to make clear the strain accumulation in the Sumatran fault.

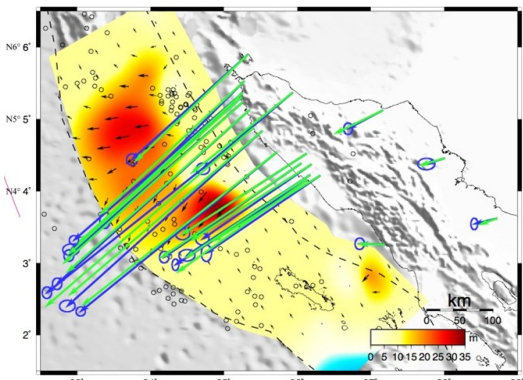


Fig.1 Co-seismic displacements and estimated fault slip distribution in the Aceh segment.

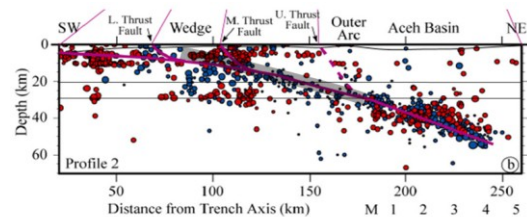


Fig.2 Cross section of aftershock distribution in the Aceh Basin. Grey band indicates the large fault slip distribution estimated by Irwan et al. (2007).

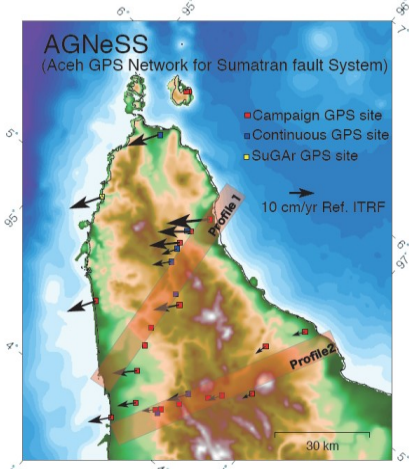


Fig.3 Horizontal displacement rates detected by GPS measurements since 2005 (Ito et al., 2008).

ABOUT THE NECESSITY OF REMOVING GROUPED EARTHQUAKES FROM THE CATALOGUE OF KAMCHATKAN EARTHQUAKES IN ORDER TO ESTIMATE SEISMICITY PARAMETERS

Anna Konovalova¹, Vadim Saltykov¹

¹Kamchatkan Branch of Geophysical Survey, RAS, Petropavlovsk-Kamchatsky, Russia.

Seismic processes include both independent and grouped (aftershocks, swarms) earthquakes. Aftershocks reflect relaxation of the environment after a large earthquake; therefore, aftershocks have characteristics that are distinct from the characteristics of background seismicity.

The recurrence graph slope, the b -value, is one of the most important parameters used to describe seismic conditions. In the present work, the influence of grouping events by their b -values on the assessment of seismicity parameters is considered.

As initial data, the catalogue of Kamchatkan earthquakes was used. The Molchan-Dmitrieva algorithm and additional clustering was applied to allocate groups of aftershocks to specific earthquakes.

The b -value was calculated using the method of maximal likelihood from the formula:

$$b = \log_{10} e \cdot \frac{1}{\sum_i^N \frac{M_i}{N} - M_0}$$

where N = number of seismic events with magnitude M_i in the area of space-time energy chosen for calculation, and M_0 = the minimal magnitude corresponding to the lowest level of reliable earthquake detection.

Calculations were conducted at several thresholds (or minimal numbers) of earthquakes, $N = 100, 50$, and 25 ; that means that the maximum level of a relative b -value error δ_b has been fixed at $0.1, 0.14$, and 0.2 , respectively. For all grouped earthquakes, the spatial area was estimated as the 2σ -ellipse centered on the epicenter according to a 2-D Gaussian distribution.

Within the limits of the allocated areas, b -values for the grouped and background events and for earthquakes from the full catalogue were compared among themselves.

For comparing calculated values of the recurrence graph slopes, the parameter Z was used:

$$Z = \frac{(b_2 - b_1)}{\sqrt{\sigma_2 + \sigma_1}}$$

where b_1 and b_2 = values for the earthquake groups being compared, and σ_1 and σ_2 = the values of the root-mean-square deviation of b_1 and b_2 , respectively.

A statistical analysis of Z distribution was conducted, validating our hypothesis H_0 that the compared b -values are equal. To double-check this conclusion, Kolmogorov-Smirnov's criterion was used: the empirical function of the distribution Z was compared to the normal distribution $N(0,1)$. In all three cases ($N \geq 100, 50$, and 25) the calculated significance value α varies from 0.15 till 0.01 . On the basis of the calculated significance values, our hypothesis is rejected.

As a result of statistical analysis, we conclude that there is a difference in b -values of background and grouped events. The size of distortions in calculating the b -value due to the grouped events when the full catalogue is used is estimated as the weighted average difference, Δ_b . A monotonic decrease of Δ_b values is correlated with a reduced number used to calculate the b -value of earthquakes; hence, the longest groups of seismic events will yield greater distortions. Thus, the expediency of additionally clearing the catalogue is demonstrated.

LONG-PERIOD GROUND MOTIONS FROM LARGE INTERPLATE EARTHQUAKES; THE 2003 TOKACHI-OKI EARTHQUAKE

Takahido Maeda¹, Tsutomu Sasatani²

¹*Institute of Seismology & Volcanology, Hokkaido Univ., Sapporo, Japan.*

²*Graduate School of Engineering, Hokkaido Univ., Sapporo, Japan.*

We study characteristics of long-period ground motions from the 2003 Tokachi-oki earthquake (25 September 2003 UTC; Mw=8.3 after the Global CMT Project). This earthquake is a large interplate earthquake occurring at the southern Kurile-Hokkaido arc. Long-period ground motion from this earthquake damaged huge oil tanks due to a sloshing phenomenon at Tomakomai about 200 km away from the epicenter (Hatayama et al. 2004; Koketsu et al. 2005). Damage to high-rise and large-scale structures due to long-period ground motion has been observed during past large earthquakes (e.g., the 1964 Niigata and 1983 Nihonkai-chubu earthquakes in Japan and the 1985 Michoacan earthquake in Mexico). We have re-realized from the 2003 Tokachi-oki earthquake that long-period ground motion has potential to cause serious damage to high-rise and large-scale structures even at a long distance.

The 2003 Tokachi-oki earthquake is the first M 8 class earthquake in Japan since the dense strong-motion networks have been deployed. K-NET (Kinoshita, 1998) and KiK-net (Aoi et al., 2000) of National Research Institute for Earth Science and Disaster Prevention are representative networks in Japan; the K-NET and KiK-net consist of more than 1000 and 550 stations, respectively. The numerous strong motion data from this earthquake provide a good opportunity for studying seismic source, propagation path and site effects on strong ground motion over the wide period range.

The characteristics of long-period ground motions are investigated using spatial distribution maps and attenuation relationships of peak ground velocity (PGV) value for four period ranges; wide band and three narrow bands (central periods of 10, 20, and 30 s). The attenuation relationships (Fig. 1) show the following trends: the wide-band PGV values are larger than the sum of the 10-s, 20-s and 30-s PGV values at distances (D) less than 200 km, while the wide-band PGV values are comparable to the sum of the 20-s and 30-s PGV values at $D>200$ km. These trends indicate that short-period waves (periods less than 10 s) control the wide-band PGV values at $D<200$ km, while long-period surface waves mainly contribute to wide-band PGV values at $D>200$ km. The spatial distribution maps for all kinds of PGV value (Fig. 2) show azimuth dependence; the PGV values in northern side of the epicenter are larger than those in southwestern side of the epicenter, when compared at a comparable distance. We find that these features result from the radiation pattern of long-period surface waves, that is, the source effect. A patchy pattern in the spatial distribution maps and a large scattering in the attenuation relationships of wide-band and 10-s PGV values are generated by the basin site effect. We examine the site effect of the Sarobetsu basin ($D\sim350$ km) located at the northern tip of Hokkaido, and find that 10-s period basin-transduced surface waves are generated at the basin and cause PGV values to be large.

The long-period ground motion from the 2003 Tokachi-oki earthquake is characterized by the source radiation pattern and various basin site effects. We should note that the PGV attenuation relationship for the 2003 Tokachi-oki earthquake is derived from a specific station configuration in northern Japan, and it is not appropriate to apply this attenuation relationship to other large interplate earthquakes occurring at different regions, as the general relationship.

References

- Aoi, S., K. Obara, S. Hori, K. Kasahara, and Y. Okada (2000). New strong-motion observation network: KiK-net, EOS Trans. AGU 81, F863.
- Hatayama, K., S. Zama, H. Nishi, M. Yamada, Y. Hirokawa and R. Inoue (2004). Long-period strong ground motion and damage to oil storage tanks due to the 2003 Tokachi-oki earthquake, *Zisin* 2 **57**, 83-103 (in Japanese with English abstract).
- Kinoshita, S. (1998). Kyoshin Net (K-NET), *Seism. Res. Let.* 69, 309-332.
- Koketsu, K., K. Hatayama, T. Furumura, Y. Ikegami, and S. Akiyama (2005). Damaging long-period ground motions from the 2003 Mw8.3 Tokachi-oki, Japan earthquake, *Seism. Res. Let.* **76**, 58-64.

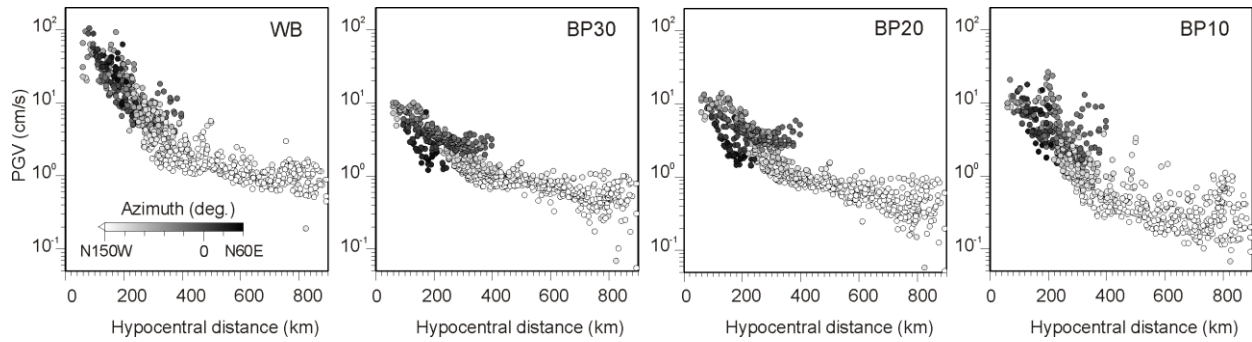


Figure 1. Attenuation relationships of the four kinds of PGV (peak ground velocity) value from the 2003 Tokachi-oki earthquake. Color scale indicates epicenter-to-station azimuth.

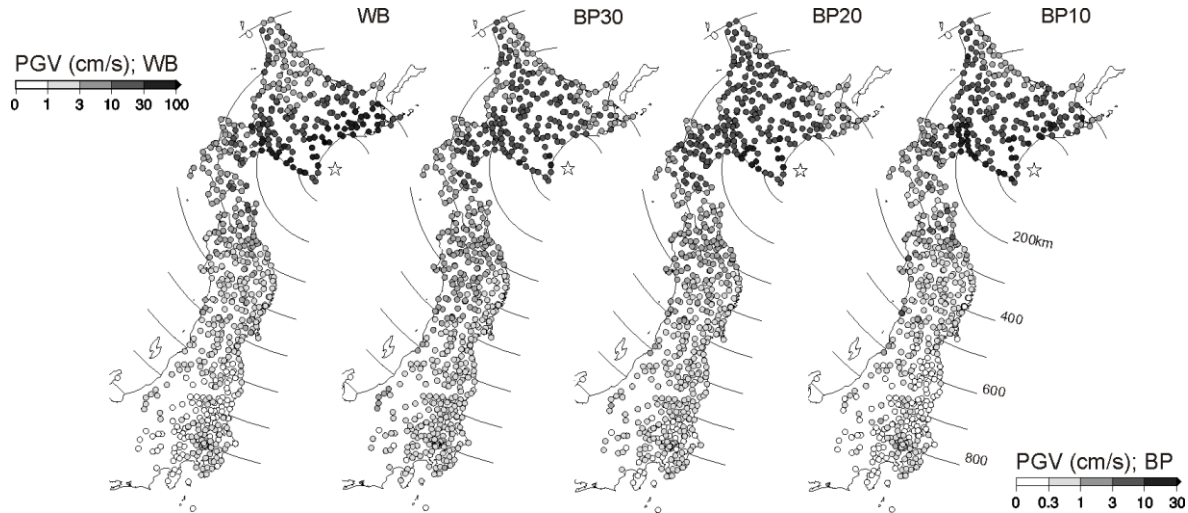


Figure 2. Spatial distribution maps of the four kinds of PGV (peak ground velocity) value from the 2003 Tokachi-oki earthquake. WB: PGV value from wide-band velocity seismograms. BP10, BP20 and BP30: PGV value from band-pass filtered velocity seismograms with a central period of 10, 20 and 30 s, respectively. An open star is a centroid epicenter determined by GCMT. Concentric circles indicate distances from the hypocenter. Note that the color scale is different between the WB and BP data.

STRONG CRUSTAL EARTHQUAKES IN CENTRAL ALEUTIAN ISLANDS IN 2006-2008: IMPLICATIONS FOR THE BLOCK ROTATION MODEL

Natalia A. Ruppert, Natalia P. Kozyreva, and Roger A. Hansen

Alaska Earthquake Information Center, University of Alaska Fairbanks, Fairbanks, Alaska, USA.

Between 2006 and 2008 six strong crustal earthquakes occurred in central and western Aleutian Islands. The series started with a M6.5 event on June 14, 2006 that occurred immediately west of Kiska Island and had a M6.0 aftershock. Two weeks later a M6.2 event occurred near Buldir Island. On April 15 and 16, 2008 a M6.4 and M6.6 earthquakes occurred in the Amchitka Pass area and on May 2, 2008 a M6.6 earthquake occurred between the Kanaga and Tanaga Islands. The events are located along a 450 km long segment of the Aleutian arc and all have strike-slip faulting mechanisms with varying orientations of the focal planes. The Alaska Earthquake Information Center reported hundreds of aftershocks for each event. Due to the seismic network limitations, however, the event locations are poorly constrained and the fault planes can not be easily determined.

A search of the Global CMT catalog produced a handful of crustal strike-slip events in the region. The most notable are the earthquakes that occurred after the great megathrust events in the region, such as a Ms7.2 event in 1966 that followed the M8.7 1965 Rat Islands earthquake and a series of strong crustal shocks (up to M6.6) near Atka Island following the M8.0 1986 Adak earthquake.

Geist et al. (1988) proposed a block rotation model for the central and western Aleutians. Five blocks of various sizes have been identified based on geomorphic evidence. Boundaries between the blocks were delineated based on the submarine fault-controlled canyons. Northern boundaries were defined as the southern edge of the corresponding summit basins, which were formed as result of rotation of the blocks. Southern boundaries were prescribed along the seaward edge of the arc massif. The block boundaries were meant to delineate regions of cohesive movement. They are bounded by zones that are significantly disrupted by normal and strike-slip faults.

The 2006-2008 crustal earthquakes and previously recorded shallow strike-slip events in the region are mostly located either near delineated boundaries of the Buldir, Rat and Delarof blocks or north of the crustal blocks.

In order to identify how the 2006-2008 earthquakes characterize the crustal block model, we used waveform cross-correlation and double-difference relocations to identify aftershock distribution and determine preferred fault planes. We conclude that while some earthquakes may be related to the motion along the block boundaries, most are located north of the identified blocks on NNE trending faults. The latter events may be manifestation of riedel shearing in the region north of the crustal blocks. Such shears are usually arranged en echelon, at inclinations of between 10 and 30° to the direction of relative plate motion.

RAPID FOREARC SUBSIDENCE AND BASIN FORMATION IDENTIFIES SOURCE AREAS OF GREAT EARTHQUAKES AND TRANSOCEANIC TSUNAMIS—EXAMPLE OF THE ANDREANOFOREARC, ALEUTIAN ISLANDS

David W. Scholl¹, Holly Ryan², Katie M. Keranen², Ray E. Wells², and Stephen H. Kirby²

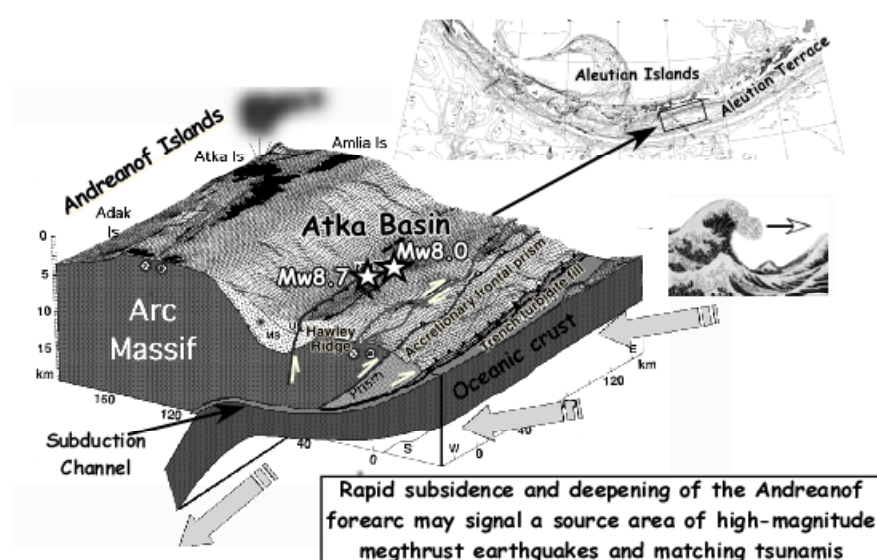
¹*Dept. Geology and Geophysics, University of Alaska Fairbanks, AK, USA.*

²*U.S. Geological Survey, Menlo Park, CA, USA.*

Observational information implies that the occurrence beneath the submerged forearc of prominent basins, crustal-scale splay and high-angle reverse faults, and large-scale growth structures, identify source regions of great subduction zone earthquakes and destructive tsunamis. The Atka Basin area of the Andreanof forearc of the Aleutian Islands displays these concerning characteristics. During the past 50 years two great megathrust earthquakes (1957 Mw8.7; 1986 Mw8.0) nucleated below the deeply submerged (4-5 km) Atka Basin sector of the Aleutian Terrace. During these events the highest slip (i.e., moment release) occurred beneath the basin

area. The 1957 rupture launched a large transoceanic tsunami.

Seismic data, dredging, and DSDP drilling document that the Andreanof forearc slope is rapidly subsiding and that the area of Atka Basin is a young, rapidly forming structural depression filled with 2-3 km of late Cenozoic deposits. It is fronted to seaward by Hawley Ridge, a rapidly rising, outer forearc



antiformal high. GPS studies (Cross and Freymueller, JGR, v. 113, 2008) attest that the subduction zone is effectively locked beneath the deepening Atka Basin and rising Hawley Ridge, but effectively unlocked to the east where the forearc basin of the terrace is inverted and large megathrust earthquakes have not been recorded.

It is not clear why the Atka Basin area is the locus of rapid subsidence and great earthquakes. But the coincidence of low-angle underthrusting of a rough seafloor, focused interplate coupling and subduction erosion, and a structurally strong sector of arc massif, are likely involved. The rupture propagation necessary to generate high magnitude earthquakes is facilitated by the insertion of a thick (>1 km), laterally continuous section of trench sediment into the subduction channel separating the arc massif from the underthrusting Pacific plate.

It can be posited that the occurrence of an actively subsiding forearc and deepening forearc basin may identify where high magnitude earthquakes repeatedly nucleate and launch matching tsunamis.

VOLCANIC AND NON-VOLCANIC DEEP LOW-FREQUENCY EARTHQUAKES OCCURRING IN JAPANESE ISLANDS

Hiroaki Takahashi¹, Jun'ichi Miyamura²

¹*Inst. Seismology & Volcanology, Hokkaido Univ., Sapporo, Japan.*

²*Japan Meteorological Agency, Tokyo, Japan.*

Deep low-frequency (DLF) earthquakes have been observed in active volcanoes with relatively deep focal depth. Several examples indicate that high DLF activity may signal unrest in active volcanoes (White, 1996). Studies of DLF source processes show that volumetric change induces DLF (e.g. Nakamichi et al., 2003). This suggests fluids like magma and supercritical water excite DLFs. The recent development of a high-sensitivity seismological network in the Japanese Islands allows us to examine the activity with homogeneous earthquake detectability.

We investigated DLF activity from 1997 to 2008 in the Japanese Islands using the Japan Meteorological Agency (JMA) hypocenter catalogue, which contains DLF flags. It has been confirmed that DLFs are distributed in any region as clusters. This implies that the DLF phenomenon is common in the Japanese subduction zone. Many active DLF clusters are identified in and around the quaternary volcanoes that exist throughout the whole area. Many non-volcanic DLF clusters have been detected in regions of northern Japan, where the Pacific (PA) slab is subducting with high speed and angle. Very few non-volcanic DLFs have been detected in central Japan, at the junction of the PA and Philippine Sea (PH) slabs. High non-volcanic activity has been observed in the western Honshu region where the hot PH slab is subducting with a low dipping angle. The high $^{3}\text{He}/^{4}\text{He}$ of spring water just above DLF clusters (Sano and Wakita, 1985) implies possible dehydrated water injection from the PH slab to the surface without melting. These regional characteristics might reflect the difference in tectonic settings due to differences in the subduction processes of the PA and PH plates.

Several examples of abrupt volcanic activities in non-volcanic areas in northern Japan have been recorded during the Quaternary. Takahashi (1986) indicates such 'new' and one-time-only volcanic events were due to drastic high-alumina basalt and calk-alkali andesite burst intrusion from the Moho to the surface. This suggests that non-volcanic DLFs at the Moho might indicate the possibility that future volcanism of non-volcanic clusters will be 'volcanic'. Several non-volcanic DLFs in western Honshu correspond to focal regions of large inland earthquakes without active faults. Ohmi and Obara (2002) indicate that precursor high DLF activity in the M7.0 focal region suggest possible water injection from Moho to Conrad which might trigger an eruption.

The lower limit of DLF cluster hypocenter depth generally coincides with that of the Moho. This may indicate that the structure of the upper mantle, lower crust, and their boundary strongly controls the occurrence of DLF. Depth distributions of each DLF cluster vary from region to region and volcano to volcano. For example, DLFs in Mt. Fuji are concentrated at the 15km depth while Mt. Iwate exhibits three DLF clusters at different depths. These differences may reflect differences in the magma supply system and/or chemical variations in the active magma system.

No clear correlation between DLF number and volcano activity index during 100 and 10,000 years, which are defined by JMA using observed and geological evidence, is recognized. This fact implies the possibility that DLF activity is not the precursor signal of shallow volcanic

activities such as eruptions. Several actual examples of volcano unrest with DLF activation, however, indicate that longer-period data will resolve this discrepancy.

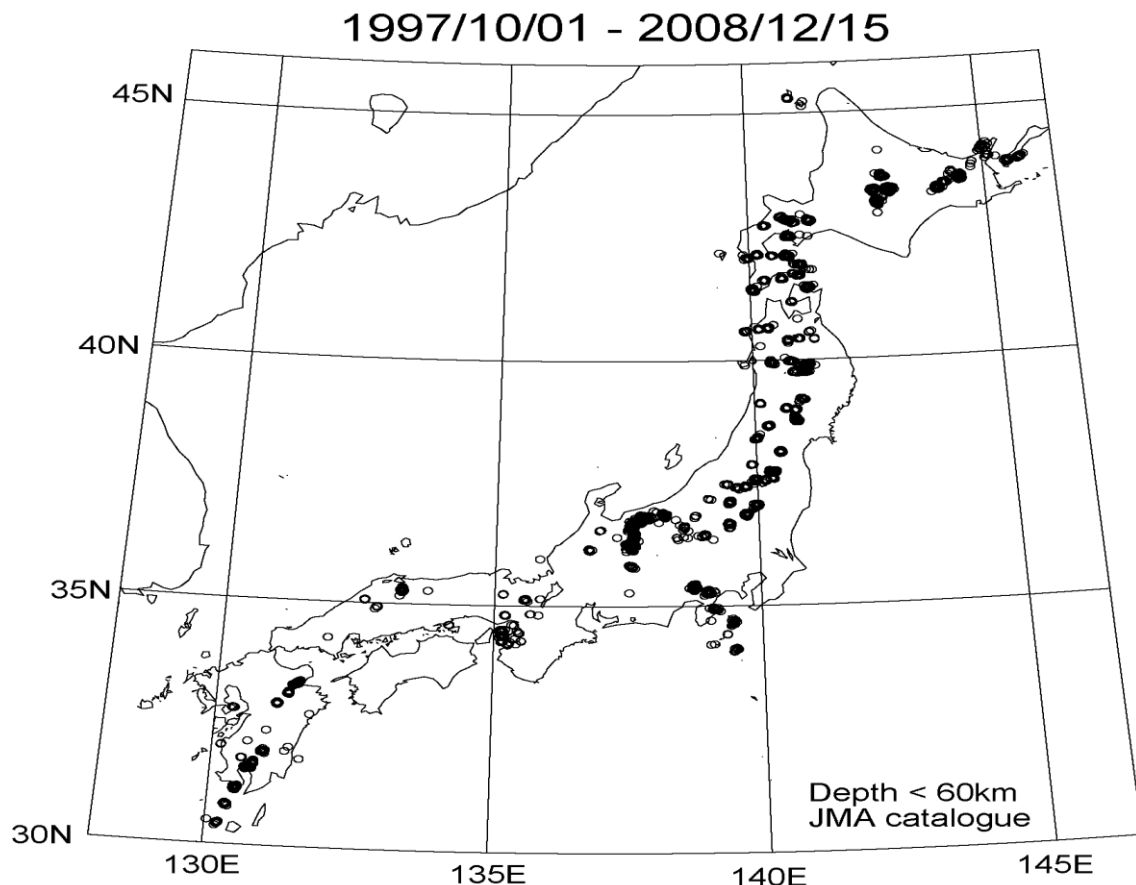


Figure 1. Epicenters of deep low-frequency earthquakes during this decade determined by JMA. Deep low-frequency tremors as showed by Obara (2002) are excluded.

DEVELOPMENT OF CRUSTAL DEFORMATION DATABASE

Teruhiro Yamaguchi, Minoru Kasahara, Hiroaki Takahashi, Muneo Okayama, Masamitsu Takada, Masayoshi Ichiyanagi

Institute of Seismology and Volcanology, Faculty of Science. Hokkaido Univ., Sapporo, JAPAN.

Introduction

We have developed a database, available on the web, of crustal deformation, using data collected continuously by strain-meters, tilt-meters, and other instruments in vaults and boreholes. One of its excellent features is the ease with which one can access and download data anywhere with a PC connected to the Internet. Another is its flexibility in accepting new data, which should be in the WIN format (Urabe, 1994). By using this technique, we can include any kind of data at different sampling levels in the database avoiding tedious steps.

Data Input System

One feature of this database is its ability to collect data from a variety of institutes. To achieve this, the server is connected to JDXnet (Takano et al., 2006). Data in WIN format are transmitted from an observatory to an institution; the accumulated data are also in the WIN format. Data are distributed between institutions via JDXnet. The server receives data being distributed via JDXnet and accumulates them (Fig.1). The sampling frequency of raw data is 100Hz, 50Hz, 20Hz, and 1Hz. The server preserves raw data, processes the re-sampling, and preserves 1/60Hz, 1/3600Hz data. The 1Hz data sampling is repeated every minute. The server processes the re-sampling once every 30 minutes. Moreover, locally archived data can be augmented by old data in the WIN format from other archives.

Data Output System

The following functions are presently available: 1) Data plots (graphics) for selected time periods from 1 second to 10 years; 2) data downloads for selected channels and periods; and 3) several data analyses, i.e., filtering, tidal analysis by using BAYTAP-G (Ishiguro et al, 1981; Tamura et al, 1991), and plane strain analysis. Figure 2 shows an example of plotted waves.

Summary

The Crustal Deformation Database, CDD, contains data from Hokkaido University, Tohoku University, Nagoya University, and Kyushu University dating back to 2004. We are trying to increase CDD participants with the goal of establishing a unified CDD of Japan.

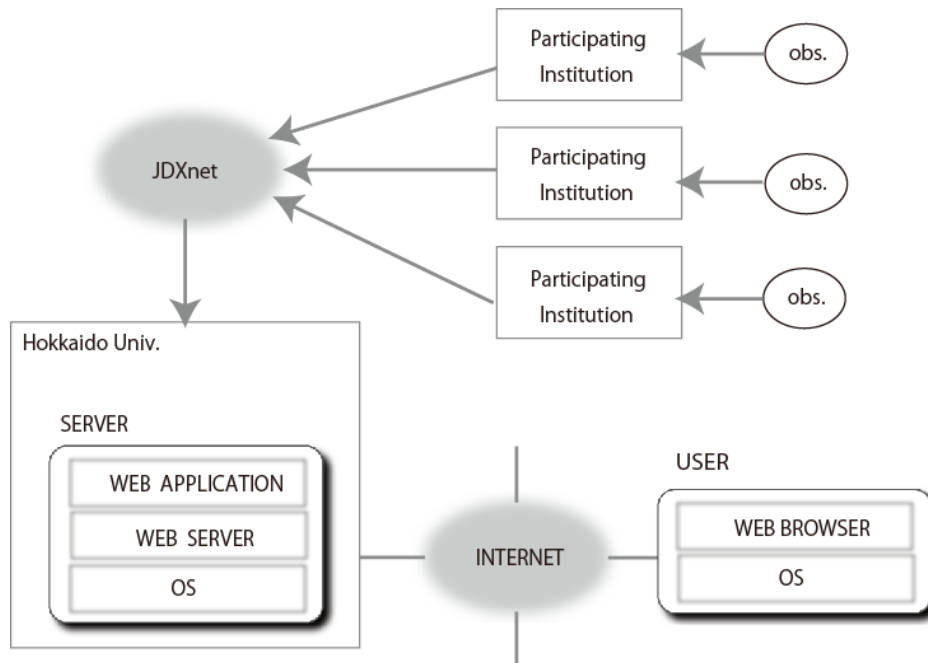


Figure1. Connectivity chart of the Crustal Deformation Database server.

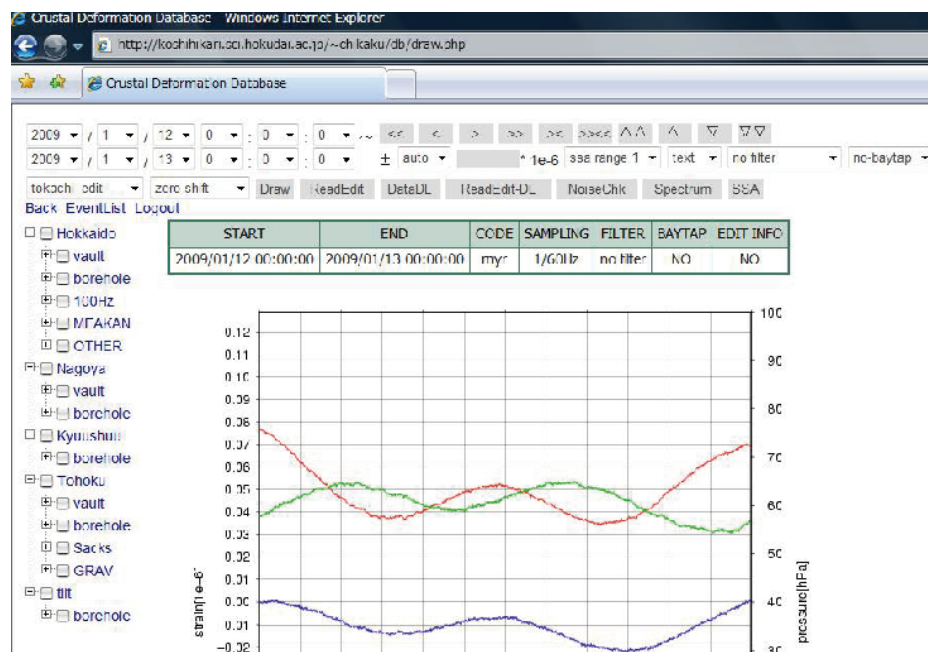


Figure 2. Example of plotted waves.

SUBDUCTION ZONE SEISMICITY AND STRUCTURE

POSTER PRESENTATIONS

MANTLE ANISOSTROPY IN ALASKA FROM SHEAR WAVE SPLITTING OBSERVATIONS

Anna Bellesiles¹, D. Christensen¹, G. Abers², X. Song³

¹*Geophysical Institute, University of Alaska Fairbanks, Fairbanks, AK, USA.*

²*Lamont-Doherty Earth Observatory of Columbia University, Palisades, NY, USA.*

³*University of Illinois at Urbana-Champaign, Urbana-Champaign, IL, USA.*

Seismic anisotropy observations were obtained from teleseismic SKS phases. Fast directions and delay times were determined for three different PASSCAL broadband experiments throughout Alaska. The first broadband experiment, BEAAR (Broadband Experiment Across the Alaska Range), was deployed from 1999 to 2001. BEAAR was deployed to study the crust, mantle wedge, and Pacific plate subduction zone under the Alaska Range. ARCTIC (Alaska Receiving Cross-Transects for the Inner Core) was deployed from 2004 to 2007, from Fairbanks to the Arctic Ocean, and was a northern extension of the BEAAR experiment. The third network, MOOS (Multidisciplinary Observations Of Subduction), is currently deployed and only the preliminary results were used in this study. MOOS is a southern extension of BEAAR and is deployed from Talkeetna, AK to the Kenai Peninsula. The splitting observations from the BEAAR network show a tight rotation of fast directions. Results from the northern portion of the network, above the mantle wedge, show fast directions along the strike of the subducting slab. In the southern portion of the network, above the shallow subduction zone, fast directions are subparallel to plate motion. The preliminary observations from the MOOS network indicate that anisotropic fast directions continue to be subparallel to plate motion as you move south toward the subduction zone trench. Similarly, the results from the ARCTIC network indicate that the fast directions seen in the northern portion of the BEAAR network continue north, with a slight NNW rotation. Thus shear wave splitting observations in Alaska fall into two distinct regimes separated by the subducting slab. Fast directions north of the slab are oriented along strike of the slab, while fast directions south of the slab are oriented in the direction of plate motion.

SWARMS VERSUS MAINSHOCK-AFTERSHOCK SEQUENCES: A SYSTEMATIC STUDY IN TERMS OF ENERGY

Branden Christensen¹, Stephen R. McNutt¹, Leah Burris²

¹*AVO, Geophysical Institute, Univ. of Alaska Fairbanks. Fairbanks, AK, USA.*

²*AEIC, Geophysical Institute, Univ. of Alaska Fairbanks. Fairbanks, AK, USA.*

The distinction between swarms and mainshock-aftershock sequences has generally been ambiguous; a magnitude difference of 0.5 to 1 between the mainshock and largest aftershock is usually the discriminator. Seismologists have assumed that the mainshock carries most of the energy, but this is true only if it is sufficiently large compared to the size and number of all the aftershocks. Therefore, energy is a logical, physical quantity on which to draw the distinction between a swarm and a mainshock-aftershock sequence. The two main factors affecting energy are the b-value and the magnitude separation (M mainshock - M largest aftershock). When plotting the minimum b-value at which the energy of the sequence (excluding the mainshock or largest event in the swarm) exceeds the energy of the mainshock alone against the magnitude separation, a linear relationship emerges. Pairings of b-value and mainshock-separation that plot above this line represent swarms (i.e., E -sequence > E -mainshock) and, conversely, pairs plotting below this line represent mainshock-aftershock sequences (i.e., E -mainshock > E -sequence). The current study employs this quantitative approach to investigate the fundamental properties of swarms and aftershock sequences for standard shear fracture earthquakes (i.e., low-frequency or long-period events are excluded). We assembled a data set of 88 seismic sequences from the literature and from a systematic search of Alaskan earthquake catalogs. 53 of these sequences occur within tectonic and 25 within volcanic fields on the plots. By plotting the b-value against the magnitude separation, no clear distinction arises between sequences occurring within these fields. Important systematic differences, however, do exist. The tectonic sequences differ from the volcanic sequences in that they have a broader range in magnitude and magnitude separations. Although a handful of volcanic sequences overlap the tectonic sequences at large magnitudes and magnitude separations, tectonic sequences generally have greater magnitudes and magnitude separations than volcanic ones. Tectonic and volcanic sequences vary in magnitude from 3.3 to 9.3 and 1.4 to 7, and magnitude separations from 0.1 to 2.9 and 0 to 1.8, respectively. The datasets share similar distributions in b-value. With the exception of 3 sequences, the b-values of tectonic and volcanic sequences are coincident and range from 0.6 to 1.7. With respect to the model, every tectonic sequence, irrespective of magnitude, and those volcanic sequences with $MMAG > 5$ plot in the mainshock-aftershock field. Those sequences that occurred in volcanic provinces with $MMAG < 5$, on the other hand, fall in all three fields. Of the 25 total volcanic sequences, 15 are re-classified as mainshock-aftershock sequences, 6 as swarms, and 4 cases are transitional (fall on or near the dividing line). According to the model, not all of the elevated levels of seismic activity previously classified as "swarms" were in fact swarms, but rather mainshock-aftershock sequences. Of the sixteen Aleutian sequences presented here, ten can be classified as mainshock-aftershock events, four as swarms and two fall on the dividing line. As suggested by the 2006 Kasatochi mainshock-aftershock sequence, which culminated in an eruption, those tectonic sequences occurring within volcanic regimes may be associated with igneous activity and need not be strictly tectonic in origin.

PROPERTIES OF STRONG GROUND MOTIONS OF OLYUTORSKOYE EARTHQUAKE OF APRIL 20, 2006 AND ITS AFTERSHOCKS FROM DIGITAL RECORDS

Olga Chubarova¹, Alexander Gusev^{1,2}, Victor Chebrov²

¹*Institute of Volcanology and Seismology Russ.Ac.Sci., Petropavlovsk-Kamchatskii, Russia.*

²*Kamchatka Branch , Geophysical Service, Russ.Ac.Sci., Petropavlovsk-Kamchatskii, Russia.*

The shallow-focus Olyutorskoye earthquake of April 20, 2006, $M_w = 7.6$ was the strongest earthquake ever to occur in the Koryak District in northeast Russia. Broadband digital records are studied of the main shock and its numerous aftershocks, obtained at local to regional distances.

In Figure 1 one can see the seismic network and the location of the main shock and the strongest aftershocks. The data on corrected peak accelerations, velocities, and displacements, along with Fourier amplitude spectra of the main shock and aftershock records were analyzed and some features of ground motion at individual seismic stations were revealed.

To determine the interdependence among peak amplitude, peak magnitude, and hypocentral distance, the data on peak accelerations and aftershock ground motion velocities are analyzed in detail based on the records of the two digital stations Tilichiki (TLC) and Kamenskoye (KAM). The data set of peak acceleration and velocities consists of 49 three-component records of events with local magnitudes $M_L=4.0 - 6.4$ and depths 0 - 22 km, obtained at hypocentral distances $R=34 - 237$ km.

As the first step of the analysis, the site effect correction for TLC with respect to the reference station KAM is determined based on comparison of coda wave spectra. Using this correction, TLC data are reduced to the reference (rock) KAM ground conditions.

At the second step, multiple linear regression is performed, resulting in construction of average relationships between peak amplitudes, local magnitude M_L , and distance R for the case of Koryak District. The results of regression are illustrated by Figure 2.

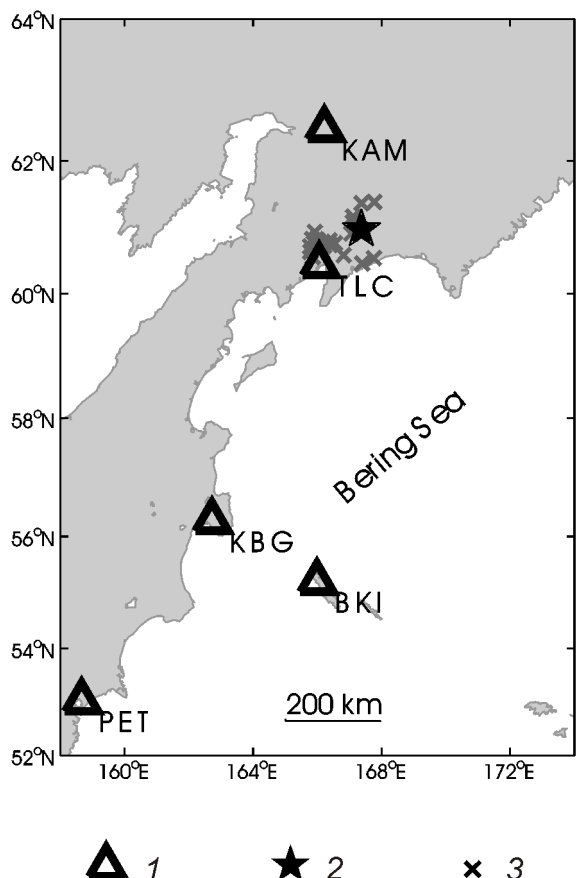


Figure 1. The area of study: digital seismic stations and epicenters. 1 - digital seismic stations; 2 - epicenter of the main shock of the Olyutorskoye earthquake; 3 - epicenters of aftershocks.

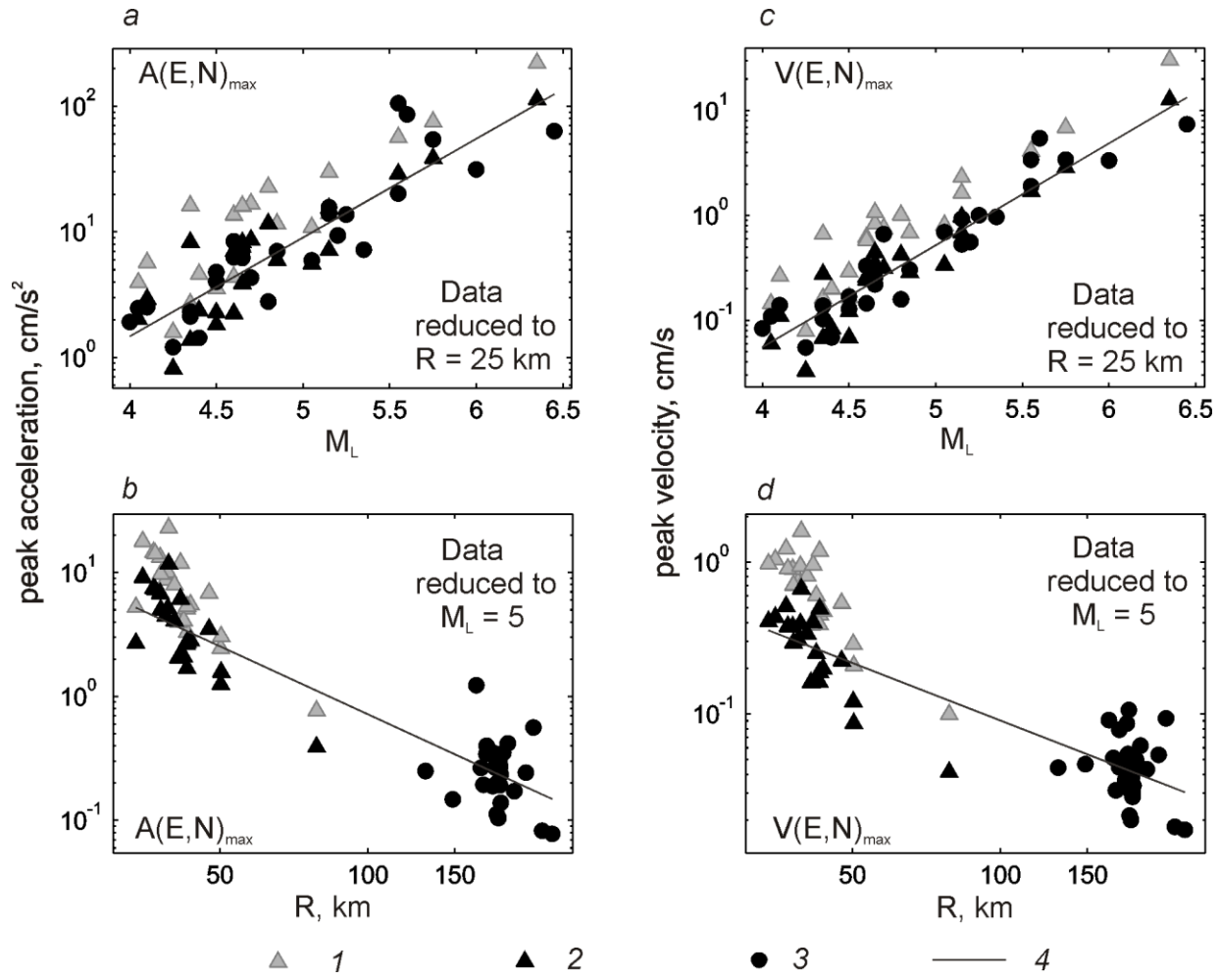


Figure 2. Peak horizontal acceleration A (a, b) and velocity V (c, d) as functions of magnitude and distance. To present the results of multiple regression in graphically clear form, data are reduced either to the standard value of hypocentral distance $R = 25$ km (a, c) or to the standard value of local magnitude $M_L = 5$ (b, d). 1 – data from station TLC, original; 2 – same data with site effect corrected (reduced to rock ground of KAM); 3 – data from station KAM; 4- lines of regression

The residual scatter of observed amplitudes is relatively low (r.m.s. residual of 0.22-0.25 decimal log units). It was revealed that for Koryak District earthquakes, the values of peak acceleration at $M_L = 5$, $R = 25$ km are considerably (2-3 times) lower, as compared to the conditions of eastern Kamchatka, western USA, or Japan. The possible cause of this anomaly is the low values of stress drop for aftershocks.

For the first time the analysis of strong-motion data has been carried out in Koryak District; the results will improve our understanding of seismic hazard in this weakly studied seismically active region located at the boundary of the North American plate and the Beringia mini-plate.

The study was supported by RFBR Grant 07-05-00775.

INVESTIGATING THE DEEP CRUSTAL SEISMIC STRUCTURE OF COLIMA VOLCANO, MEXICO

Matt Gardine and Michael West

Geophysical Institute, University of Alaska Fairbanks, Fairbanks, AK, USA.

We present early-stage results of velocity modeling and ray tracing at Colima Volcano, located in the western section of the Trans-Mexican Volcanic Belt - and one of North America's most active volcano centers. From January 2006 - February 2008, twenty broadband seismometers were deployed in a wide-aperture array around the volcano as part of the IRIS/PASSCAL supported Colima Volcano Deep Seismic Experiment (CODEX). Data from this deployment, integrated with data from the Mapping of the Rivera Subduction Zone (MARS) project, have been used to characterize both the regional seismicity and the seismicity of the volcano.

We used subduction-zone earthquakes (depths > 40 km) located by the arrays as well as selected, well-located regional crustal earthquakes to create a 1-D velocity model of the region. Using this model, longer arrival times were systematically seen at most stations close to the volcano. Variations in travel time arrivals seen across the CODEX network, combined with 1-D raytracing were used to show that there is initial evidence of a lower-velocity zone in the deep crust with a possible southwest-northeast trend near the volcano with depths of 20-40 km. Preliminary seismic tomography with the use of 3-D ray tracing helps to refine and better constrain the details of the low-velocity zone. Any other anomalies in the crust, with a particular emphasis on velocity variations within the deep (>20 km) crust, will also be investigated with the hope of achieving a better understanding of deep crustal processes underneath a prodigious subduction-zone volcano.

ANALYSIS OF DEEP SEISMICITY AT MOUNT SPURR, COOK INLET, ALASKA

Ophelia George, Michael West

Geophysical Institute, University of Alaska Fairbanks, Alaska, USA

Following centuries of quiescence, early 2004 -2006 marked a period of increased seismicity beneath the summit volcano of Mount Spurr. This increased seismicity coincided with an increase in heat flow and gas flux and has been interpreted to be the result of a magmatic intrusion (Coombs et al, 2006). A prominent feature of this increased seismicity was the occurrence of a large number of deep events. Deep seismic events are not uncommon to many volcanoes and are believed to be associated with fluid migration. A 2002 study by Power et al showed that DLP events are more prevalent at Mount Spurr than all the other Aleutian Volcanoes combined. While the presence of deep events is significant enough on its own the fact that these events share similar locations with those occurring during the 1992 eruption of Crater Peak, Mount Spurr's satellite volcano, provide impetus for the current study. This study endeavors to unravel the origin of these events and gain a better understanding on what role they may have played in the unrest.

For this study seismic data was obtained from the AVO catalogue of earthquakes occurring within 20 km of the summit and at depths greater than 20 km. Working towards the key goals, cross correlation analysis was conducted using several stations in the Spurr network. For detailed analysis, station SPU was utilized as it contained the most complete catalogue of deep events and its advantageous location provided waveforms with lower attenuation. Analysis was conducted both on waveforms occurring within the unrest period and those which occurred during the 1992 eruption of Crater Peak to investigate the location similarities. To find the dominant frequencies in these deep events a fast Fourier transform was performed on the data. Locations of earthquakes occurring during summer of 2005 were reassessed using dbloc2 to take advantage of broadband seismometers deployed during that period.

The cross correlation analysis indicated that even at low correlation coefficients few of the waveforms occurred in families. The exceptions were 2 families of 6 waveforms each occurring in June, 2005. Both these families occurred 42-46 km deep over a roughly 24 hour period starting at 18:33 UTC. The Fourier analysis showed that none of the events during the 2004-2006 unrest had a dominant frequency exceeding 2.3 Hz.

References

- Coombs, M.L., Neal, C.A., Wessels, R.L., McGimsey, R.G., 2006, Geothermal Disruption of Summit Glaciers at Mount Spurr Volcano, 2004-6: An Unusual Manifestation of volcanic unrest, U.S Geological Professional Paper 1732-B
- Power, J.P., Stihler, S.D, White, R.A., Moran, S.C., 2004, Observations of deep long-period (DLP) seismic events beneath Aleutian arc volcanoes 1989-2002, Journal of Volcanology and Geothermal Research, v 138, pg 243-266
- Angelis, S., McNutt, S.R. 2005, Degassing and hydrothermal activity at Mt Spurr, Alaska during summer of 2004 inferred from the complex frequencies of long-period events, Geophysical Research Letters, V 32, L12312

LOCATION OF B-VALUE ANOMALIES: PROCEDURE AND RESULTS

Anna Konovalova and Vadim Saltykov

Kamchatkan Branch of Geophysical Survey, RAS, Petropavlovsk-Kamchatsky, Russia.

One precursor of large earthquakes is reduction of the recurrence graph slope b -value. The b -value is defined on the basis of Gutenberg-Richter's law: $\lg N = \tau - bM$, where N is number of earthquakes with magnitude more than M .

The goal of the work presented here is to detect spatial zones where anomalous b -values are observed. In our approach, the statistical significance of b -value variations is more important than the absolute value of those variations. Changes over time of the b -value are presented and analyzed in the form of the dimensionless parameter Z_b , which measures the statistical significance of the current deviation of the b -value from its long-term (or background) values:

$$Z_b = \frac{(b_2 - b_1)}{\sqrt{\sigma_2 + \sigma_1}},$$

where b_1 and b_2 represent the values of the time intervals being compared, and σ_1 and σ_2 represent the values of the root-mean-square deviations of b_1 and b_2 , respectively.

Monitoring of b -value variations over time was carried out for the Kamchatka seismoactive zone. This work utilized data from the Kamchatkan regional catalogue of earthquakes that occurred from 1962-2008; this catalogue was created by the Kamchatkan Branch of the RAS Geophysical Survey.

Spatial scanning was conducted by defining cylindrical volumes with radius $R \leq 100$ km and height $H = 100$ km for the area $51^{\circ} - 57^{\circ}\text{N}$ and $156^{\circ} - 167^{\circ}\text{E}$. The number of earthquakes within an elementary cylindrical volume was fixed, but differed in various calculations: $N = 100, 200, 400$, and 800 . B -values were calculated for the time interval $T_1 = 1, 2, 3, 4, 6, 8$, and 11 years. For determining background b -values, the time interval T_2 was used: 1) 1962-2007, and 2) the double interval T_1 preceding T_1 .

Charts of Z_b -values are presented in figure 1. We consider the statistically significant reduction of b -value relative to background value to be an anomaly, and the reduced b -value area to be an anomalous zone. Anomalies with $Z_b \leq -3$ are especially interesting, because for these Z_b -values the statistical significance of the reduced b -value is at least $\alpha=0.01$.

The epicenters of strong earthquakes on Kamchatka from 1962-2008 are shown in figure 1 for comparison. They can be related to the revealed anomalies.

Figure 1 shows maps of anomalies with areas localized to within the limits of a $\text{Mw}(\text{HRV}) = 7.8$ earthquake that occurred on 05/12/1997 ($\text{UTC} = 11:26:51$, $\varphi = 54.64^{\circ}\text{N}$ and $\lambda = 162.55^{\circ}\text{E}$). A statistically significant reduction in recurrence graph slope was observed before this earthquake during more than 10 years (in view of a time window size of calculations). The area affected by this earthquake was estimated as the 2σ -ellipse of aftershock epicenter dispersion according to a 2-D Gauss distribution.

The approach presented here allows local temporal variations of b -value to be monitored in places where large earthquakes are possible.

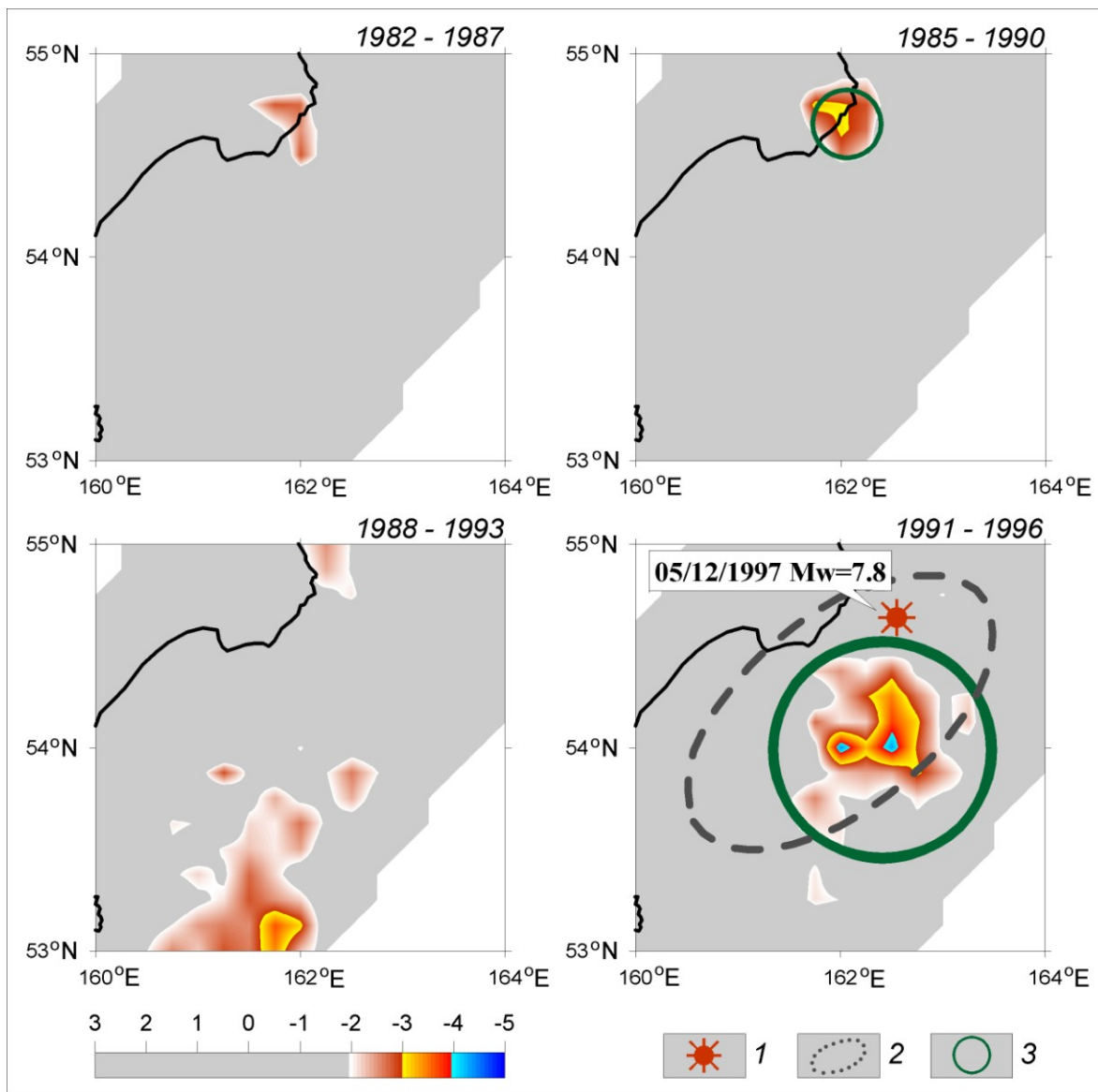


Figure 1. The maps of anomalies calculated in a sliding time window 6 years wide, with steps of 1 year and $N=200$. The color scale represents Z_b values that characterize the statistical significance and depth of the anomaly. 1: epicenter of the $M_w(HRV) = 7.8$ earthquake that occurred on 05/12/1997; 2: area of this earthquake's aftershock sequence; 3: the territory where earthquakes have generated is considered to be anomalous.

EXPERIENCE WITH REMOTE DETERMINATION OF ASH PLUME INITIATION AND HEIGHT USING LOCAL SEISMICITY AT SHEVELUCH AND KARYMSKY VOLCANOES, KAMCHATKA

Kozhevnikova T.Yu., Senyukov S.L.

Russian Academy of Science, Kamchatkan Branch of the Geophysical Survey (KBGS), Petropavlovsk-Kamchatsky, Russia

During the ongoing dome-building eruption at Sheveluch Volcano, we examined seismic records that accompany the production of ash plumes and associated pyroclastic flows related to gravitational and explosive dome collapse. We investigated seismic data from a single seismic station "SVL", which was located 8.5 km to the southwest of the volcano. Spectrograms from the seismic events show predominant frequencies from 1 Hz to 2-4 Hz, which is unusual for other volcanic earthquakes in the vicinity of Sheveluch. For the first time, due to continuous video observation we are able to correlate the amplitude of the seismic signal envelope with the ascent rate of the ash plume. We investigated short-lived (<10 minutes) ash plumes with heights from 500 m (1640 ft) to 15000 m (49180 ft) above the dome. We derived a formula to determine ash plume height using a sum of the seismic signal envelope values. The correlation coefficient $R^2=0.85$ for the 142 ash plumes registered by photo or video observation from 1998-2004. In 2002, 580 possible ash plumes at Sheveluch Volcano were detected seismically, and 104 of these were confirmed by visual and video observation. Clouds or darkness obscured the rest of the plumes. During 2002 we did not use our method to calculate ash plume height from seismic signal envelope. In 2003, on the basis of seismicity we detected 272 possible ash plumes in real time and sent this urgent information to participants in the KVERT project (Alaska Volcano Observatory, Institute of Volcanology and Seismology). Thirty-three plumes were confirmed by video observation, while clouds or night obscured the remainder. Similar data were obtained in 2004; 594 events were detected seismically, and only 39 of these were confirmed by video observation. Unfortunately, seismic station "SVL" was destroyed by eruption on February 27, 2005. In the autumn of 2005, three new seismic stations were installed in safer locations in the vicinity of Sheveluch. None of these stations have registered seismic records with the characteristic increasing frequency of 1 Hz to 2-4 Hz that accompany the production of ash plumes. So at the present time, it is not possible to accurately detect the seismic events that accompany the production of ash plumes. A new KBGS seismic station is needed, located closer to the active cone.

Karymsky Volcano has been in a state of constant eruption, including both dormant periods and periods of violent volcanic activity, from 1996 until the present time. KBGS has no video observation equipment located on this volcano. We investigated seismic records from the seismic station "KRY", which is located 1.5 km to the southeast of this volcano. All ash plumes that were confirmed visually began with a 1-1.5 Hz signal which increased to 2.5-4.5 Hz. We have derived a formula to determine ash plume height using the sum of the seismic signal envelope values. The correlation coefficient is $R^2=0.58$ for the 38 ash plumes, with heights from 50 m to 5000 m, registered by visual observation from 1999-2007. As part of the KVERT project we detected 138 possible ash plumes from Karymsky Volcano and sent this urgent information to the Tokyo VAAC, the Anchorage VAAC, the Alaska Volcano Observatory, and to others in 2005-2007.

Our empirical method offers a more reliable warning of ash clouds that can affect air traffic, especially during bad weather or when visual observations and confirmation are not possible.

MUTNOVSKY VOLCANO SEISMICITY STUDIED USING DATA FROM THE "MUTNOVSKY" SEISMIC STATION (KAMCHATKA, RUSSIA)

Yulia Kugaenko, Irina Nuzhdina, Victor Chebrov

Geophysical Survey of Russian Academy of Sciences, Kamchatkan Branch

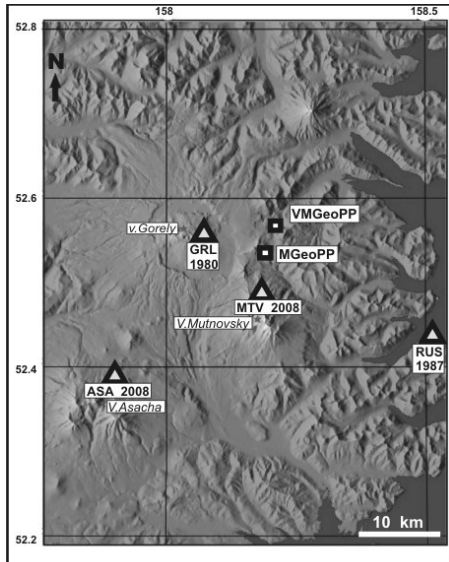


Fig.1. Seismic stations in the Mutnovsky-Gorely area. MGeoPP and VMGeoPP indicate the Mutnovsky and Vierhne-Mutnovsky Geothermal Power Plants, respectively.

development began, shallow earthquakes were detected immediately in zones of hydrothermal field development.

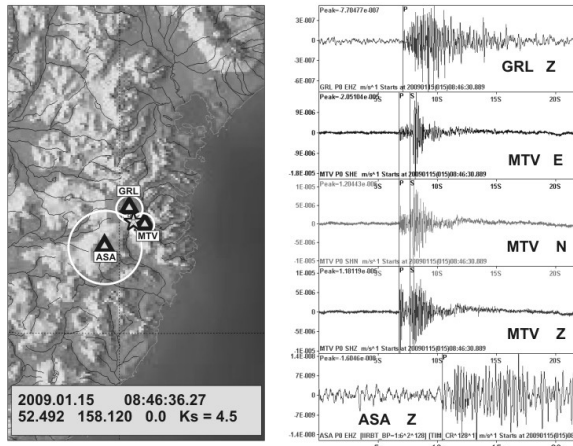


Fig.2. Location of a weak shallow earthquake in the fault zone between Mutnovsky and Gorely volcanoes as detected by a local seismic group.

Mutnovsky is one of the most active volcanoes of southern Kamchatka. It is a compound volcanic massif, formed of four coalescing stratovolcanoes of predominately basaltic composition. Mutnovsky Volcano contains crater lakes and very active fumaroles. Holocene activity has been characterized by mild-to-moderate phreatic and phreatomagmatic eruptions from the summit crater. During the last 200 years 16 eruptions were observed; they exhibited no periodicity and a mainly explosive character. The most recent weak eruptions occurred in 1960 and 2000. The eruption in 2000 was characterized as a phreatic explosion that has caused substantial changes in the volcano's topography. Mutnovsky's nearest "neighbors" are Gorely and Asacha volcanoes.

The developed Mutnovsky hydrothermal field is located to the north of Mutnovsky Volcano. The Verkhne-Mutnosky Geothermal Power Plant (VMGeoPP, 12 MW) has been operating since 1999, and the Mutnovsky GeoPP (MGeoPP, 50 MW) since 2001 (Fig. 1). Data from the Kamchatkan regional seismic network showed that after

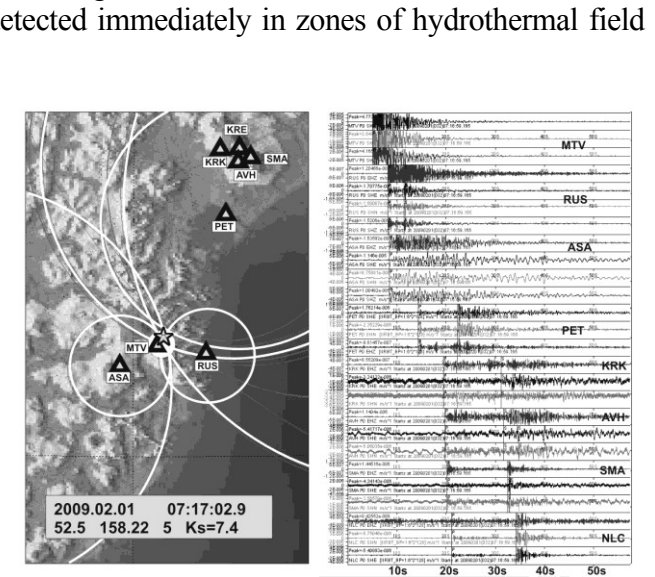


Fig.3. Earthquake location under the developed area of the Mutnovsky hydrothermal field detected by a regional seismic network and a new station on Mutnovsky.

In 2008 two regional seismic stations were constructed in the Mutnovsky area (Fig.1): **MTV** on Mutnovsky's northeast slope about 2 km from the active crater, and **ASA** north of Asacha Volcano.

At present the Mutnovsky Volcano region is under observation by four telemetric seismic stations (Fig.1). All stations are equipped with a three-component set of SM-3 seismometers ($T_s=1.2$ s) for detecting ground motion velocities in the 0.7-30 Hz frequency band. Real-time seismic data are transmitted by UHF radio to Petropavlovsk-Kamchatsky for processing. Thanks to new seismic stations we have additional information about local seismicity in the Mutnovsky-Gorely area:

1) Locating weak Mutnovsky Volcano regional earthquakes is possible now. We can distinguish between weak earthquakes originating in different parts of the area (Figs. 2, 3).

2) By analyzing **MTV** seismic records, different types of local seismic events were found. They differ by spectral composition and P-wave polarization (Fig.4).

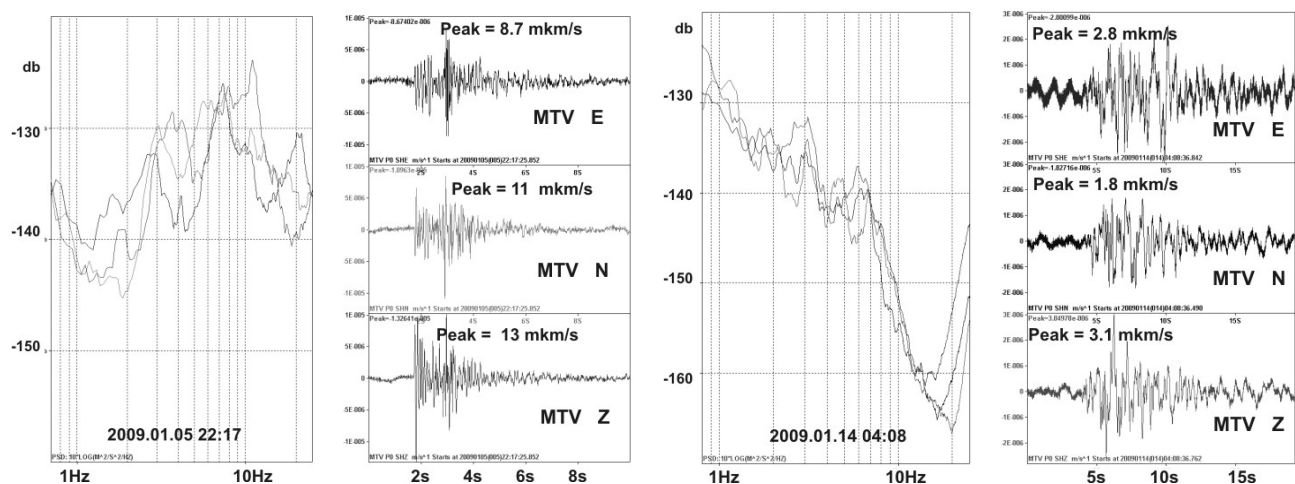


Fig.4. Weak local earthquakes from the Mutnovsky Volcano area and their power spectra. Left – a high-frequency tectonic earthquake from a fault zone between Mutnovsky and Gorely volcanoes. Right – a low-frequency earthquake, presumably located under Mutnovsky Volcano (SE of the **MTV** station)

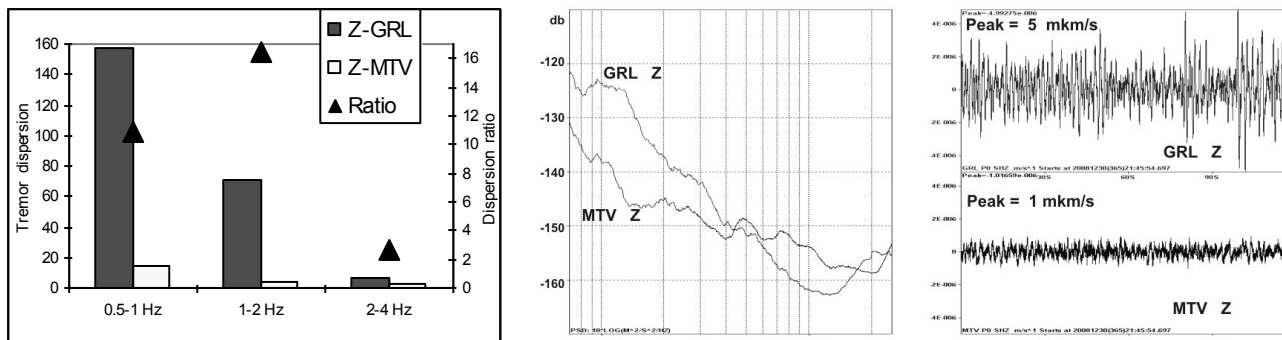


Fig.5. Left - analysis of volcanic tremor seismic records in three frequency bands. We use tremor dispersion as a parameter for estimating signal energy. Right - seismic records of volcanic tremor and power spectra (Z-channels from **MTV** station on Mutnovsky and **GRL** station on Gorely volcanoes, Dec.30, 21-45).

3) A volcanic tremor connected with Gorely Volcano has been detected (Fig.5), but to accurately locate the real tremor source it will be necessary to carry out additional studies using the broad-band seismic array.

4) A connection between some local earthquakes and development of the Mutnovsky hydrothermal field (Fig.3) northeast of **MTV** has been confirmed.

SEISMICITY OF KLUCHEVSKOY VOLCANO (KAMCHATKA, RUSSIA) BETWEEN 1999-2008: SPATIO – TEMPORAL ANALYSIS OF THE EARTHQUAKES

Nuzhdina I.N., Senyukov S.L.

Kamchatka Branch of the Geophysical Survey of the RAS

Petropavlovsk-Kamchatsky, 683006, RUSSIA, e-mail: sva08@emsd.ru

Kluchevskoy Volcano ($56^{\circ} 04'$ N, $160^{\circ} 38'$ E, height 4750 m) is the most active and powerful basaltic volcano of the Kuril-Kamchatka volcanic area. This volcano produced 4 summit eruptions between 1999-2008 with ash plumes and lava flows. During this time, ~40000 earthquakes were located within 7 km distance of the volcano. We carried out a spatio-temporal analysis of these earthquakes. The B-value and a seismic energy center were investigated for the seismic precursor study of the eruptions in the terminal crater. Before all 4 terminal crater eruptions of Kluchevskoy Volcano, the amount of seismic energy center lift was fixed, from a depth of ~30 km to crater level. Last lifting was used as a seismic precursor for successfully predicting the summit eruption of this volcano in 2008.

A MOMENT TENSOR ESTIMATION ALGORITHM BASED ON A NEW METHOD OF SYNTHETIC SEISMOGRAM CALCULATION

Victor Pavlov, Iskander Abubakirov

Kamchatkan Branch of Geophysical Survey of RAS, Petropavlovsk-Kamchatsky, Russia.

An algorithm for seismic moment tensor (SMT) estimation of large earthquakes ($M_w \approx 8$) is proposed. The radiation of an extended source at low frequencies is approximated by radiation of a point source with a symmetric-triangular time function of adjustable duration. For fixed point source depth and duration, SMT is calculated by linear inversion of observed seismograms band-filtered in the period band of 60-120 seconds. The best estimate of SMT is found by systematic search over depth and duration. The coefficients for SMT components are Green's functions which are calculated in advance.

To calculate Green's functions a new algorithm is applied based on matrix impedance for computing unknown depth functions and stress-motion vectors, that are included in the solution representation of the problem. The impedance is a matrix that transfers motion vector to stress vector by multiplication. For a layered half-space with homogeneous isotropic elastic layers, impedance and motion vector are calculated by analytic formulas excluding a possibility of accuracy loss. The algorithm is effective for any layers and frequencies.

Practical estimation of SMT was performed for the five largest earthquakes that occurred during the last fifteen years in the Far East of Russia ($M_w=7.6-8.3$). Comparison with CMT solutions shows that tensor orientations ("mechanisms") are in good agreement, whereas our M_w estimates are somewhat lower, by 0.2 units on the average.

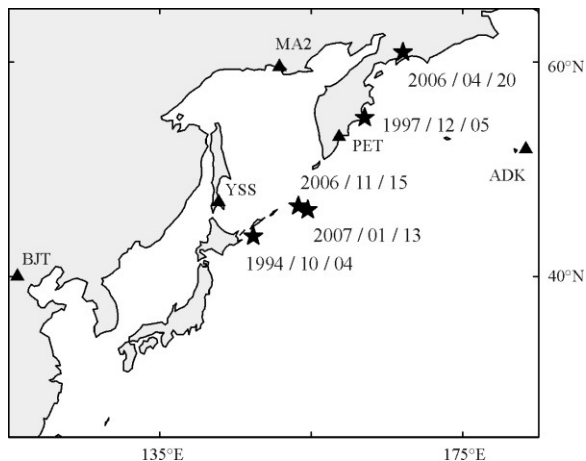


Fig. 1 – Earthquake epicenter (asterisks) and station (triangles) locations. Data from three stations are used for an earthquake: PET, YAK, BJT for the 1994/10/04 event; MA2, YSS, ADK for the 1997/12/05 event; MA2, PET, YSS for the 2006/04/20, 2006/11/15 and 2007/01/13 events.

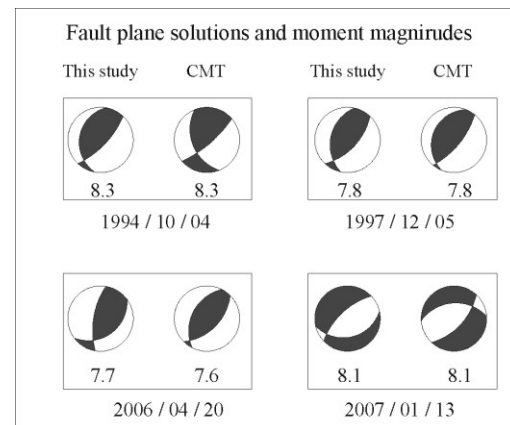


Fig. 2 – Fault plane solutions and moment magnitudes M_w for four of five events. For event 2006/11/15 see Figs. 3 and 4.
A lower hemisphere stereographic projection is used.

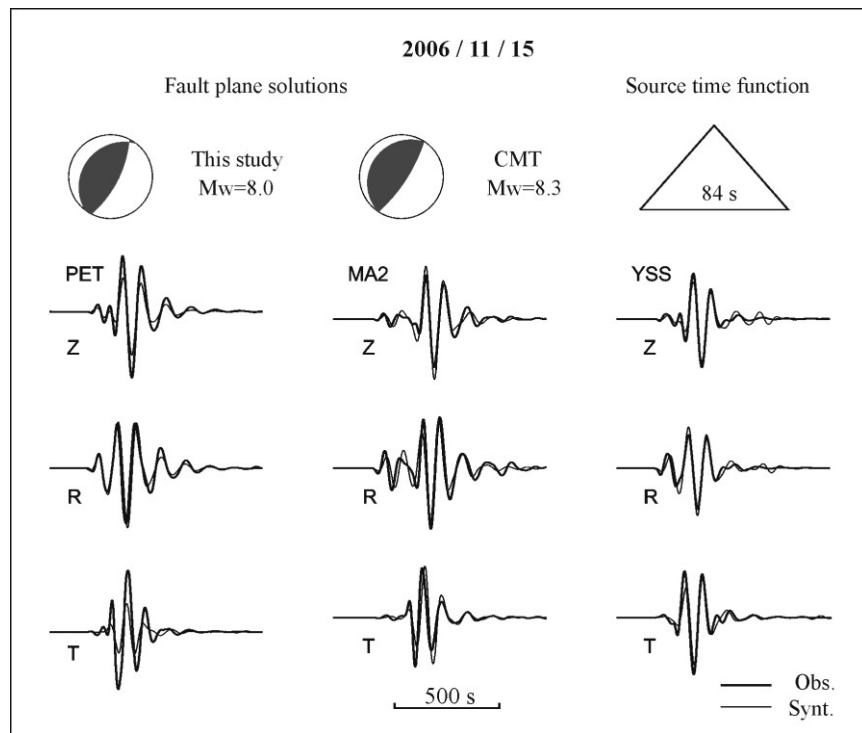


Fig. 3 – Fault plane solutions, moment magnitudes M_w , and waveforms for the event on 2006/11/15.

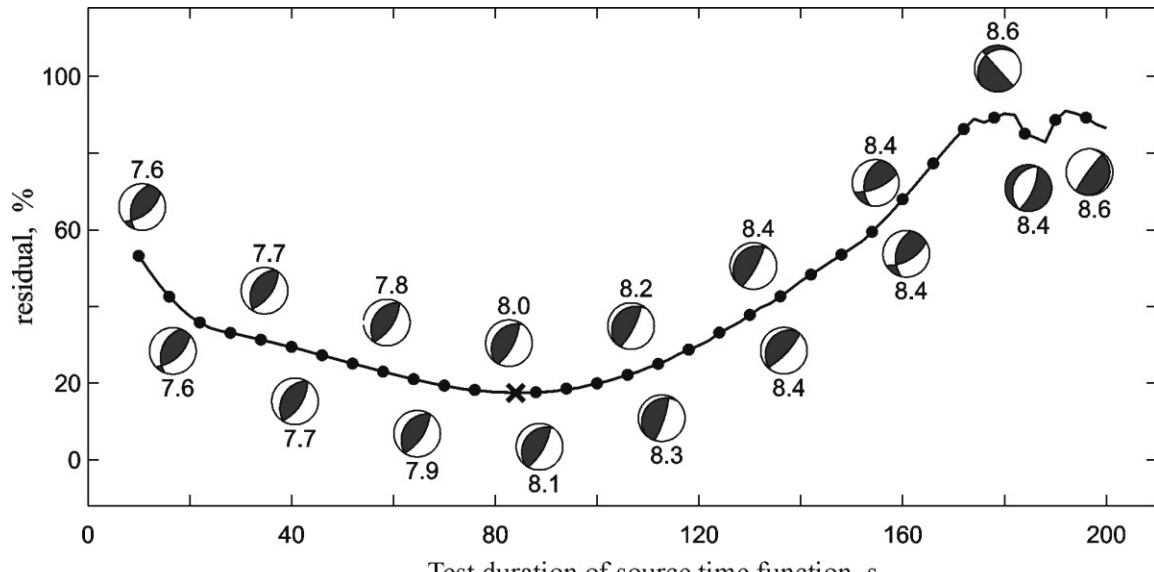


Fig. 4 – Dependence of the results on the duration of source time function for the event on 2006/11/15.

Reference

Pavlov V.M. Matrix impedance in synthetic seismograms calculation in a layered isotropic half-space. Fizika Zemli, 2009, in press

PRECURSORY ANOMALIES IN PARAMETERS OF MULTI-SCALE SEISMICITY BEFORE LARGE CRUST EARTHQUAKE $M_w=6.8$ AND KARYMSKY SEISMO-VOLCANIC CRISIS ON JANUARY 1-2, 1996 IN KAMCHATKA, RUSSIA

Vadim Saltykov, Yulia Kugaenko, Nadezhda Kravchenko

Kamchatkan Branch of Geophysical Survey of RAS, Petropavlovsk-Kamchatsky, Russia

Karymsky is an andesitic volcano on the Kamchatka Peninsula, Russia ($54.05^{\circ}N$, $159.43^{\circ}E$, summit elevation 1486 m; Fig. 1). It is one of the most active volcanoes of Kamchatka's eastern volcanic zone. Karymsky is a symmetrical stratovolcano constructed within a 5-km-wide caldera that formed during the early Holocene. Post-caldera eruptions at the volcano began about 5300 years ago. Historical eruptions have been Vulcanian or Vulcanian-Strombolian with moderate explosive activity and occasional lava flows from the summit crater. In the 20th century Karymsky had 7 periods of continuous Strombolian eruptive activity, each lasting from 4 to 15 years. The 1996- ongoing eruptive cycle started with simultaneous eruption of andesite from the Karymsky summit vent and basalt from a new vent formed in the northern part of the Academia Nauk caldera.



Fig.1. Karymsky Volcano in November, 2008. Photo A.Sokorenko.

The Karymsky seismo-volcanic crisis is the series of paroxysmal seismic and volcanic events that occurred in the Kamchatka East Volcanic Belt on January 1-2, 1996: the summit eruption of Karymsky Volcano, the freatomagmatic eruption in the Academia Nauk caldera lake, and a significant earthquake swarm with the largest event, $M_w=6.8$, on January 1, 1996. This seismic event was named The Karymsky Earthquake. It is the strongest crustal earthquake recorded in Kamchatka since instrumental observations began.

Significant anomalies in seismicity parameters at different levels of energy were detected before the Karymsky seismo-volcanic crisis occurred on January 1-2, 1996. As a multi-scale seismicity we use earthquakes from the Kamchatkan regional seismic catalog and microseismicity (seismic noise with amplitude about 10^{-9} - 10^{-12} m and frequency band that includes the first decades of Hz). Retrospectively we calculated the spatial distribution of the *RTL* (Sobolev et al., 1996) parameter and the Z-function (Wyss and Habermann, 1988) for detection of seismic process dynamics (Fig. 2). For microseismicity analysis the original method was used; it is based on seismic noise response to tidal influence (Saltykov, 1997).

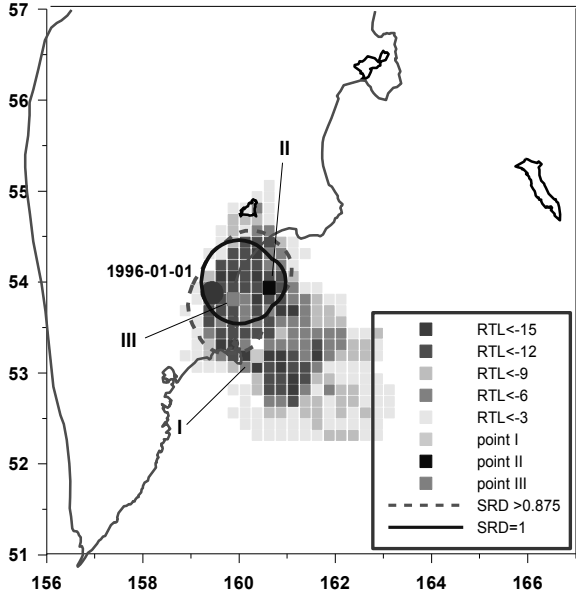


Fig.2. Superposition of *RTL*- and *Z*-anomalies. Seismic quiescence precursors, measured by two methods based on different approaches, are in agreement. Our attempt to join two independent methods (*RTL* and *Z*-test) for detecting seismic quiescence during the run-up to the Karymsky seismovolcanic crisis is successful.

Precursory seismic quiescences detected by two independent methods (*RTL* and *Z*) are synchronous in time and demonstrate spatial agreement. The duration of the detected anomaly is about 4 years. The volume of the anomaly can be estimated as $(1-3)\cdot 10^6 \text{ km}^3$. The physical model for connecting a crustal earthquake with large anomalies in subduction seismicity is not yet clear. The fact that the two methods yield nearly identical results strongly suggests that the observed precursory quiescence is real. Synchronous *RTL* and *Z* anomalies before tectonic-magmatic activation were detected for the first time.

An anomaly in seismic noise response to tidal influence lasting about 1 month was detected at a distance of about 140 km from the Karymsky earthquake epicenter. The parameters of this anomaly detected before the crustal Karymsky earthquake differ from those for subduction earthquakes in 1992-2008 attended with similar effects. In 1992-2007, HFSN synchronization with Earth tides was detected for 32 regional earthquakes with $M_w \leq 7.9$, ≤ 400 km from the epicenter and ≤ 200 km deep.

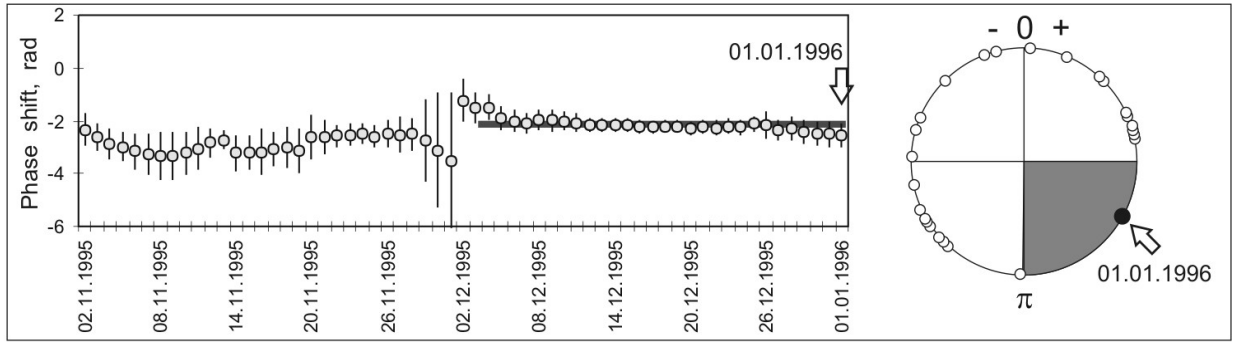


Fig.3. Left: $\Delta\varphi$ stabilization before the Karymsky seismo-volcanic crisis. Right: circular pattern with $\Delta\varphi$ distribution.

An irregularity in the $\Delta\varphi$ distribution was revealed. The $\Delta\varphi$ value for the Karymsky crustal earthquake on 01.01.1996 (hatched sector) differs from that of many other subduction-type earthquakes. The estimation of probability of less than 2 points appearance in the hatched sector (if the hypothesis of regular $\Delta\varphi$ distribution on the circle is accepted) gives a value less than 3×10^{-3} . The distribution irregularity assumes the informative character of the $\Delta\varphi$ stabilization level.

Here we have demonstrated the possibility, in principle, of detecting seismic anomalies before large crustal earthquakes, connected with long-term volcanic-tectonic activation.

RFBR grant 07-05-00225.

STAGES OF ACOUSTIC RESPONSE IN LABORATORY MODELING OF TIDAL INFLUENCE UPON SEISMICITY

Vadim Saltykov ¹, Andrey Patonin ²

¹Kamchatkan Branch of Geophysical Survey of RAS, Petropavlovsk-Kamchatsky, Russia.

²Geophysical Observatory "Borok", Institute of Physics of the Earth of RAS, Borok, Russia.

Introduction.

Seismic radiation varies through a wide range of seismic energy, ranging from seismic emissions (high-frequency seismic noise, HFSN) to earthquakes. Some features of external influence response to the different scales allow us to consider the medium as a single whole seismoactive object. Earth's tide is a clear example of an external excited field.

The tidal topic has a long history in seismology. Results obtained by different scientists are contradictory, and often ambiguous. We suggest that the inconsistency of tidal effect manifestation is a possible cause of these discrepancies. In view of the aforesaid it is significant that tidal effects on weak seismicity and HFSN are seen more strongly in the preparatory stage of large earthquakes [Rykunov et al., 1998; Saltykov et al., 2004, 2007].

It is presumed that a metastable medium has a greater tidal sensitivity; examples include sources of prepared earthquakes and extensive near-surface zones of micro-fissuring and dilatancy, which appear during source formation and propagate for long distances [Alekseev et al., 2001; Goldin, 2004, 2005]. Features common to the observed effects allow us to suggest the existence of a tidal modulation mechanism, which is similar on different seismic scales. Modeling these processes can improve our understanding of the nature of tidal effects.

Laboratory experiment.

Results of rock sample destruction experiments under controlled conditions are presented. Acoustic emission (AE) pulses act as an analogue of seismic events. Tides are simulated by weak long-period variations added to quasi-stationary subcritical loading.

The results of tidal modeling confirmed the known AE intensity synchronization with external periodic influence, with large (5-10%) variations of loading [Lockner, Beeler, 1999; Ponomarev et al., 2007]. But real, natural tidal strain-and-stress variations are much smaller, closer to tenths of a percent. Therefore, investigating the influence of **weak** modulations upon deformed rock is one of our primary goals.

We used the INOVA software-programmable electro-hydraulic system [Patonin, 2006], which enables a variety of experimental procedures, among them programmable modulatory action. Axial deformation with stable strain rate and additional action of meander with specified period and amplitude was the chosen mode of operation. The correlation between background and periodic strains suggests strong relationships between maximum tectonic and tidal strains.

Results.

For detecting the periodic AE modulation loading we used a procedure based on Rayleigh criteria of uniformity, and we considered the uniformity of AE impulse distribution over time intervals defined as multiples of the loading period. The predominant phase of periodical loading, corresponding to maximal AE activity, was calculated in a sliding time window.

In all experiments we observed instability of modulation effects, and we distinguished the following stages:

1. synchronization of AE and periodic loading in the initial part of the test;
2. absence of synchronization in the elastic stage; and
3. resumption of synchronization during plastic deformation.

Phase stability corresponding to maximal AE activity was discovered in the initial and plastic deformation stages. The absolute values of phase for initial loading and during plastic deformation are different.

Conclusion.

We believe that the primary result of our experiments is to reveal the stages of AE response to weak periodic loading. The different stages of AE response are connected to different states of rock samples during loading and destruction. The observed effects of synchronization can be considered to be an analogue of the tidal modulation of HFSN and the appearance of “tidal” seismicity in the source zone of prepared large earthquake.

This investigation was supported by RFBR, grant 08-05-00692.

MODELING OF SEISMIC WAVES PROPAGATION IN AN INHOMOGENEOUS THREE-PHASE MAGMA

Samoilenko S.B.¹, Gordeev E.I.^{1,2}, Melnik O.E.³

¹*Institute of Volcanology and Seismology, FEB RAS, Petropavlovsk-Kamchatsky, Russia.*

²*Kamchatka Branch, Geophysical Service, RAS, Petropavlovsk-Kamchatsky, Russia.*

³*Institute of Mechanics, Moscow State University, Moscow, Russia.*

Magma in the volcanic vent is considered as a non-equilibrium three-phase system, consisting of viscous liquid melt with dissolved gas, bubbles of evolved gas, and solid crystal phase. The governing equations of the system contain equations of mass balance, momentum conservation, equations of state, and a dynamic equation for bubbles. Solution of these equations in a quasi-stationary case yields the distribution of pressure, temperature, concentrations, densities, and velocities of different phases etc. In order to study the propagation of the small-amplitude waves in the considered medium, governing equations are linearized and reduced to a hyperbolic system with variable parameters and additional viscous terms. The analysis of the dispersion equation of the linearized system reveals two kinds of waves that have different propagation speeds and decrements. The numerical solution of the problem agrees with the analytic results and brings to light some features of wave propagation in the non-homogeneous medium. The main goals of the study are to determine the solid phase influence on the wave propagation pattern, and to examine whether standing waves and resonance phenomena can take place in the volcanic vent.

MEASURING TEMPORAL CHANGES IN SEISMIC VELOCITY AT BEZYMIANNY VOLCANO USING AMBIENT NOISE CROSS-CORRELATION

Ashley Shuler¹, Göran Ekström¹, Michael West², Sergey Senyukov³

¹Lamont-Doherty Earth Observatory, Columbia University, Palisades, NY, USA.

²Geophysical Institute, Alaska Volcano Observatory, University of Alaska Fairbanks, Fairbanks, AK, USA.

³Kamchatka Branch of Geophysical Services, Institute of Volcanology and Seismology, Petropavlovsk-Kamchatsky, Russia.

Bezymianny Volcano is an active stratovolcano located in the Kluychevskoy volcanic complex on the Kamchatka Peninsula in eastern Russia. Since its dramatic sector collapse eruption in 1956, the volcano's activity has been characterized by nearly twice annual Plinian eruptions accompanying ongoing lava-dome growth. Since mid-2006, the volcano has been monitored by a broadband seismic array as part of the ongoing NSF Partners in Research and Education (PIRE) program. The seismic array is currently composed of 8 stations within 10 kilometers of the active dome. Four of these stations are located on the edifice of the volcano itself.

Bezymianny's frequent eruptions make it an excellent laboratory for studying processes related to explosive volcanism. Recent studies at Piton de la Fournaise Volcano (Brenguier et al., 2008) have shown that precursors to eruptions can be detected by measuring the spatially homogeneous relative velocity change over consecutive time intervals. Specifically there, a negative relative velocity perturbation is seen a few days prior to an eruption. This is attributed to inflation of the volcano, which will increase the travel time for seismic energy traveling between two stations located over the inflating region. At Piton de la Fournaise, the size and duration of the precursory relative time perturbation related to the magnitude of the impending eruption. Furthermore, the use of an array allowed the location of inflation to be determined. In this project, we implement this method to determine if similar variations in seismic velocity can be seen prior to eruptions at Bezymianny volcano.

For our work, we use cross-correlations from the vertical component of different receiver pairs to estimate the Green function between the two stations, using the frequency band 0.1-1.5 Hz to sample the upper few kilometers of the volcano. We compute the relative time perturbation by comparing a reference cross-correlation function to a cross-correlation function from a 10-day moving time window. Preliminary results for the October 2007 explosive eruption and the November 2007 dome collapse are inconclusive, in part as only three stations were installed at that time. However, data covering the August 2008 explosive eruption have been retrieved recently for 5 stations. These questions will continue to be addressed as more data becomes available in future field seasons.

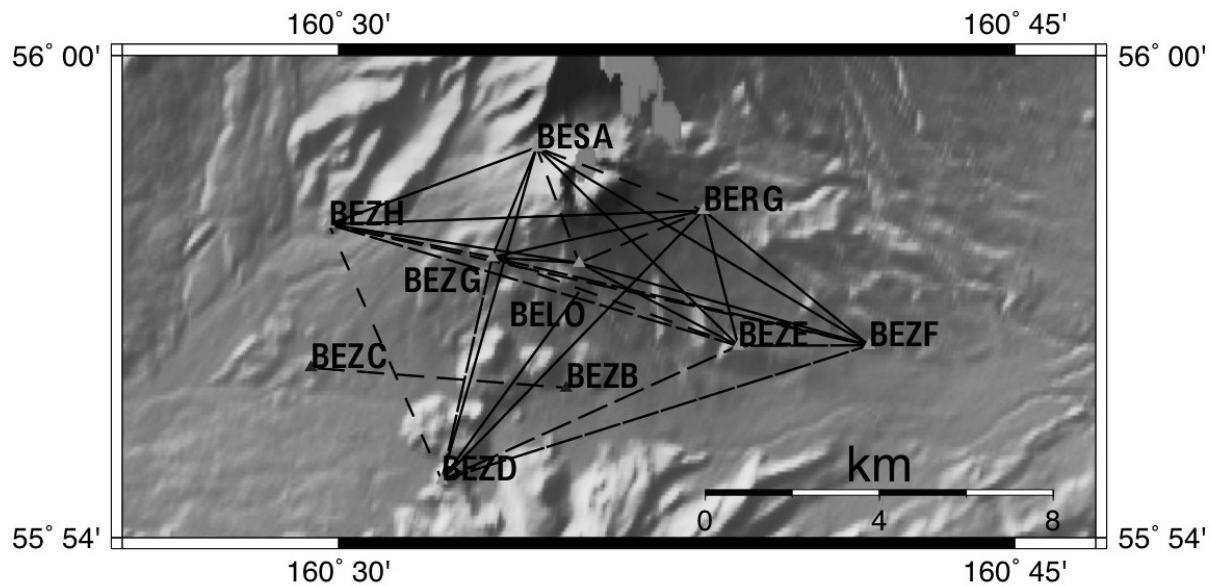


Figure 1. Seismic network at Bezymianny Volcano overlain on SRTM topography. Lines show station paths for which there is available data. Dashed paths indicate that data covering an eruption is available for that station pair.

References:

- Brenguier, F., Shapiro, N.M., Campillo, M., Ferrazini, V., Duputel, Z., Coutant, O., Nercessian, A., 2008. Towards forecasting volcanic eruptions using seismic noise. *Nature Geoscience* 1. doi:10.1038/ngeo104.

ON THE PROBLEM OF CALCULATING SEISMIC WAVE ENERGY

Alexander Storcheus

Institute of Volcanology & Seismology, Petropavlovsk-Kamchatskiy, Russia.

E-mail: sav@kscnet.ru

Seismic energy is one of the major dynamic characteristics of seismic waves. Accurate determination of seismic energy is important, not only to characterize the intensity of shaking but for research on physical parameters of earthquake sources. Calculations of the seismic energy of body waves have customarily used the following formula (*Wiechert et al., 1912*):

$$E^{P,S} = 8\pi R^2 c \rho \exp(kR) \frac{\sin \Delta \sin e_0}{de_0/d\Delta} \sum_n \frac{A_i^2}{T_i^2 t_e}, \quad (1)$$

where: R = distance to epicenter, km; c = speed of seismic waves; k = attenuation factor; ρ = density of medium; A_i = amplitude of a seismic wave; T_i = period of a seismic wave; t_e = duration of earthquake; Δ = distance, degrees; and e_0 = outgoing wave angle. This formula assumes that: 1) seismic energy from a source is radiated as elastic vibrations in an elastic medium; 2) energy from the source is transferred along rays; 3) vibrations are harmonious, and 4) body seismic wave energy radiates from a source in a spherically symmetric pattern

In modern literature (*Kogan S.Ya., 1975*) the seismic energy is the integral of a power flux

$$q \text{ through a surface } \Omega: E(\Delta) = \int_{-\infty}^{\infty} \int q d\vec{\Omega} dt. \quad (2)$$

It is accepted, as a rule, that it is possible to take the integral in infinite limits of time t because only those moments of time for which displacement of points on Ω is not equal to zero will contribute. From the aforesaid it follows that the seismic energy of an earthquake would be calculated as the summary energy of each oscillation (Fig. 1). However, such a method of calculating seismic energy contradicts the four above-enumerated assumptions.

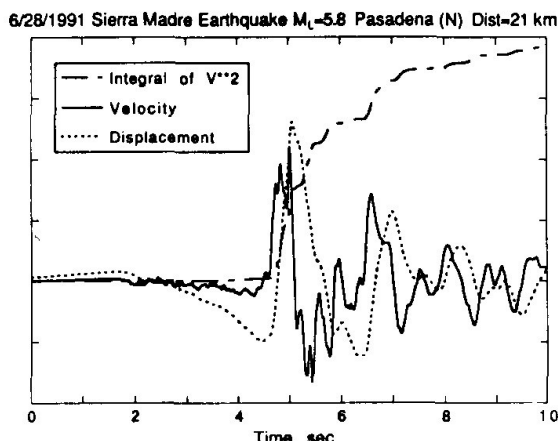


Figure 1. A typical seismogram (displacement and velocity) and the integral of the squared velocity. (From *Kanamori et al., 1993*)

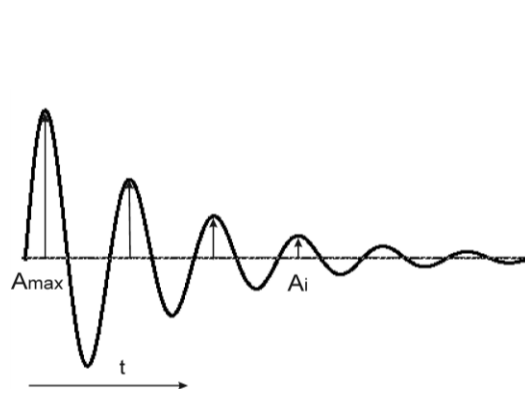


Figure 2. The quasinsoidal signal simulated form of an earthquake.

Analysis of how well the seismic energy calculations meet assumptions 1-4 reveals:

1) These formulas can be used to calculate seismic energy in viscous-plastic, but not in elastic media (the latter contradicts Assumption 1). If energy is not lost, seismic vibrations in an ideally elastic medium would continue indefinitely and the seismic vibrational energy calculated under these formulas would be infinitely large; moonquakes are an example. Moonquakes may continue for ≥ 4 hours. Calculating seismic energy using these formulas yields more kinetic energy than their source possessed (i.e. the result of a falling spacecraft).

2) Summarizing $(A_i/T_i)^2$ along t_e means taking into account the energy of refracted and reflected waves, which contradicts assumptions 2 and 4.

The original energy of seismic vibrations has been considered as elastic deformations of the medium in some volume around the future failure; after a rupture or crack appears, it was represented by the oscillatory motion of the surrounding medium. The kinetic energy of movement at a balance point is equal to the potential energy of elastic deformations before the motion began. It is known from physics that the amplitude of harmonious oscillations of particles in a medium changes according to the law: $A = A_{max} * \sin(\omega t)$; $\omega = 2\pi/T$, while for damping oscillations, $A = \exp(-at) * A_{max} \sin(\omega t)$ (Fig. 2). The kinetic energy of harmonious oscillations is proportional: $E \sim (1/T)^2 \int [A_{max} \sin(\omega t)]^2 dt$; $t = 0 \div T/2$, while for damping oscillations, kinetic energy is: $E \sim (A/T)^2_{max}$. As a result of these calculations, Wiechert's formula is transformed to:

$$E^{P,S} = 6\pi R^2 c \rho \exp(kR) \frac{\sin \Delta}{de_0/d\Delta} \left(\frac{A}{T} \right)_{max} T. \quad (3)$$

For the same reason it is a mistake to calculate the integral in Eq. (2) over infinity.

Using Eq. (3) the causation of a magnitude $M = M(A/T)$ seismic event with seismic energy E can be determined analytically. The causation of earthquake energy and magnitude in seismology is known as the empirical formula of Guttenberg-Richter: $M = a * Ks - b$, where

$Ks = \lg E$. Taking into account: $M \left(\frac{A}{T} \right) = \lg \left(\frac{A}{T} \right)_{max}$, $R = 100$, and using Eq. (3), we find:

$$M_S \left(\frac{A}{T} \right) = 0.5Ks - 0.5\lg C_1 \text{ or } Ks = 2 M_S \left(\frac{A}{T} \right) + \lg C_1; \quad (4)$$

where C_1 = the factor before $\left(\frac{A}{T} \right)_{max}$ in Eq. (3). For Kamchatkan earthquakes the coefficient a

in the Guttenberg-Richter equation was solved empirically as $a = 0.5$ which agrees with its value in Eq. (4) which was determined analytically.

Formulas (3) and (4) are applicable not only for earthquakes with a one-impulse source but also for artificial explosions of atomic bombs and other explosives.

Cited literature:

1. Kanamori H., Mori J., Hauksson E., Heaton T., Hutton L., Jones L. (1993) Determination of earthquake energy release and M_L using TERRASCOPE. Bull. Seism. Soc. Am. 83(2): 330-346
2. Kogan S.Ya. (1975) Seismic energy and methods of its determination. Moscow. Science. P. 152
3. Wiechert E., Zoppritz K., Geiger L., Guttenberg B. (1907-1912) Uber Erdbebenwellen Nachr. K. Asses. Wiss. Göttingen, Mathem.-Phys., Kl.

FOCAL REGIONS OF GREAT EARTHQUAKES AND A SEISMIC GAP IN THE CENTRAL KURIL ISLANDS FROM HISTORICAL GEOPHYSICAL DATA

Hiroaki Takahashi, Takahiro Maeda, Minoru Kasahara

Inst. Seismology & Volcanology, Hokkaido Univ., Sapporo, Japan.

Determining the focal regions of great earthquakes in a subduction zone is very important for earthquake forecasting based on the seismic gap hypothesis. Fedotov (1965) first examined focal regions in the Kuril subduction zone and pointed out several seismic gaps where source regions of great earthquakes would be located in the near future. Most seismic gaps were filled by the occurrence of great earthquake events during the 20th century. But there is still a large gap in the central Kuril area between the locations of the 1915 and 1918 ~M8.0 earthquakes.

On November 15, 2006, an awaited earthquake (Mw8.3) occurred there. An outer-rise earthquake on January 15, 2007 (Mw8.1) followed. Slip distributions and aftershock distribution of the 2006 event seemingly filled the gap described above. To confirm this, we reexamined characteristics of these first two events of the 21st century. Seismic intensities, seismograms, and tsunami data were recorded by the Japan Meteorological Agency and the International Latitude Observatory of Mizusawa. Comparisons of data from the 1915, 1918, 2006, and 2007 earthquakes have been made. The magnitudes of these events, between 7.8 and 8.3, are almost the same. This suggests that a tsunami should have been produced if each source was shallow. It is reaffirmed, however, that the 1915 event did not generate an observable tsunami while the other events excited large ones. This fact implies that the focal depth of the 1915 earthquake was not shallow. Low seismic intensity also indicates that the 1915 earthquake was not a typical interplate earthquake on a shallower plate boundary.

According to the above facts, we propose that the 1915 earthquake was a deep-focus event in the northeastern Okhotsk Sea. The intensity distributions of the 1915, 1971 (M7.0), and 2008 (Mw7.7) deep focus events are similar. Comparing seismograms from the 1915 and 2008 earthquakes also supports this hypothesis. We believe this solution explains the conditions of large, low-intensity seismic movement, without tsunami. The epicenter location was estimated from the distribution of preliminary tremor durations observed at several seismic stations in the Japanese Islands. We conclude that there is still a seismic gap with M>8.0 between the 1952 and the 2006 great Kamchatkan earthquakes (M9.0).

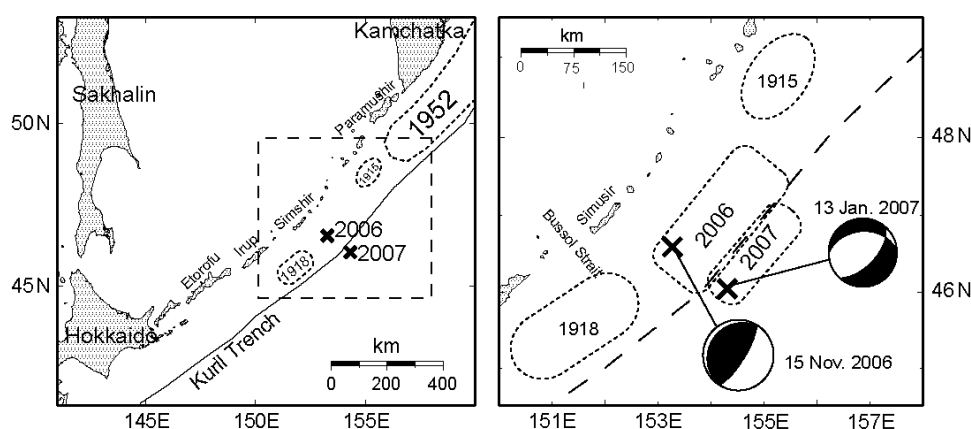


Figure 1. Focal regions of the 1915, 1918, 1952, 2006, and 2007 earthquakes modified by Fedotov (1965). CMT solutions are from GCMT.

REPEATING EARTHQUAKES ACTIVITY IN THE HYUGA-NADA REGION, SOUTHWEST JAPAN, HIGH ANGLE SUBDUCTION ZONE

Yusuke Yamashita¹, Hiroshi Shimizu¹, Kazuhiko Goto²

¹*Institute of Seismology and Volcanology, Faculty of Science (SEVO), Kyushu University, Shimabara, JAPAN.*

²*Nansei-Toko Observatory for Earthquakes and Volcanoes (NOEV), Faculty of Science, Kagoshima University, Kagoshima, JAPAN.*

1. Hyuga-nada

The Hyuga-nada region, a high-angle subduction zone belong the Kyushu-Ryukyu arc (Fig.1 and Fig. 2), is one of the most seismically active area in Japan and earthquakes with magnitude from 6.5 to 7.5 usually occur at 10-20 years interval. Recently, in the southern part of Hyuga-nada, two large earthquakes occurred on October 19, 1996 (MJMA=6.9) and December 2, 1996 (MJMA=6.7). In this region, the Philippine Sea Plate (PHS) subducts northwestward beneath the Eurasian Plate at a rate of about 5cm/year [Seno *et al.* (1993)]. This region is located between Nankai Trough, which is a very strong interplate coupling zone and Ryukyu trench, which seems to be a very weak interplate coupling zone. In particular, the regions from off coast of Shikoku to the Bungo channel and Hyuga-nada have large variation of seismicity. Also, it has been indicated that interplate coupling spatially changes from the north over the south according to the analysis of geodetic data by the GPS observation [e.g., Nishimura *et al.* (1999); Watabe and Tabei (2004)].

In the Hyuga-nada, the temporal seismological observation using Ocean Bottom Seismometers (OBSs) has been carried out every year for about two months since 2000 by Kyushu University, Kagoshima University, University of Tokyo, Tohoku University, and Nagasaki University. As the result, the details of hypocenter distribution, focal mechanism solutions and seismic velocity structure were revealed. Uehira *et al.* (2006) indicated that reverse fault type earthquakes and normal fault type earthquakes have occurred by the almost same frequency in and around plate boundary of Hyuga-nada. Tahara *et al.* (2008) suggest that an aseismic slip area correspond to the high poisson's ratio region.

Therefore it is considered that Hyuga-nada is one of the best regions for understanding what controls the and strength of interplate coupling.

2. Repeating earthquakes analysis

Recently, in NE Japan, the study on the estimation of asismic (quasi-static) slip on the plate boundary using small repeating earthquakes is progressing [e.g., Igarashi *et al.* (2003);

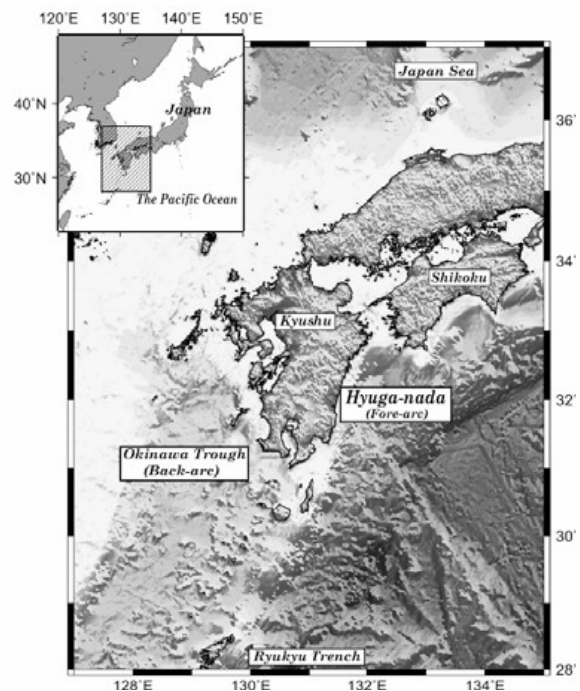


Fig.1. Topography map in SW Japan.

Uchida *et al.* (2003)]. Small repeating earthquakes which occurred on the plate boundary are thought to be caused by repeated rupture of small asperities surrounded by stably sliding area [Igarashi *et al.* (2003)]. Thus, we can estimate the amount of quasi-static slip from the cumulative slip of small repeating earthquakes. This method can estimate the spatio-temporal variation of quasi-static slip at the accuracy which is higher than the analysis of land-based GPS data. As a result of using this method, the relationship between the quasi-static slip and interplate earthquakes has been gradually revealed. Uchida *et al.* (2004) suggested that the rupture of large asperity may be triggered by the acceleration of quasi-static slip. In other words, the spatio-temporal variation of quasi-static slip on the plate boundary of subduction zone is thought to be important for understanding of the earthquake process and development of earthquake prediction. From this viewpoint, we investigate the repeating earthquakes activity in the Hyuga-nada region.

3. Method

In this study, repeating earthquakes are selected on the bases of waveform similarity and the cumulative slip of repeating earthquakes (quasi-static slip amounts) is estimated by using relationship between slip (d ; cm) and seismic moment ($M0$; $\text{dine} \cdot \text{cm}$) proposed by Nadeau and Johnson (1998). We used the vertical component of short-period seismograms at 27 stations, and calculated cross correlation coefficients of waveforms for all earthquake pairs with epicenter separations less than 50 km in and around Hyuga-nada for the period from June 1994 to November 2008. Selected events are larger than M 2. Time window was set for 40 seconds from one second before P wave onset. The total number of selected events and calculated pairs are about 19,000 and 20,000,000, respectively.

We treated an earthquake pair as a pair of repeating earthquakes when the calculated cross correlation coefficients of two waveforms were larger than 0.95 at two or more stations (Igarashi *et al.* [2003]). If the two pair shared the same event, they were grouped into the same group of repeating earthquakes.

The preliminary results show that few repeating earthquakes distribute in the asperities in the Hyuga-nada region. We will estimate the spatio-temporal variation of quasi-static slip after checking carefully whether these repeating earthquakes are interplate earthquakes or not.

Acknowledgments. In this study, we have used the data of Kyushu University, Kagoshima University, University of Tokyo, Kochi University, and Japan Meteorological Agency

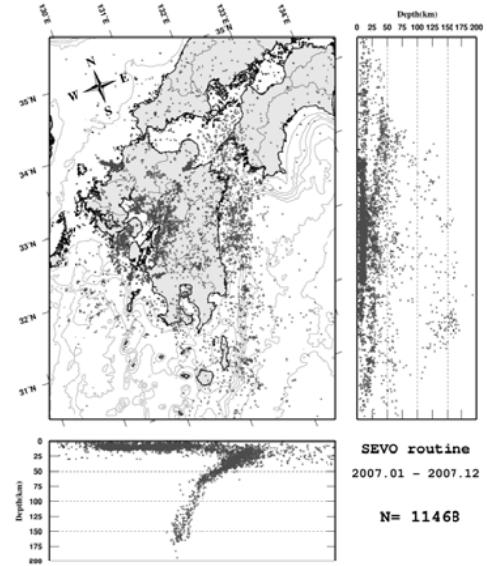


Fig. 2. Hypocenter distribution in and around Hyuga-nada.

VOLCANO GEOPHYSICS

ORAL PRESENTATIONS

MAGMA CHAMBER MODEL BENEATH UNZEN VOLCANO INFERRED FROM GEODETIC AND SEISMIC DATA

Yuhki Kohno¹, Satoshi Matsumoto², Takeshi Matsushima², Kenji Uehira², Kodo Umakoshi³, Hiroshi Shimizu²

¹*Institute of Seismology and Volcanology (ISV), Hokkaido University, Japan.*

²*Institute of Seismology and Volcanology (SEVO), Kyushu University, Japan.*

³*Faculty of Environmental Studies, Nagasaki University, Japan.*

Measuring volcanic ground deformation enables us to determine how subsurface structure has altered; such changes indicate inflation or deflation of magma chambers beneath a volcano, and therefore changes in magma supply. Spatial variation of geodetic data is affected by changes in both the shape of and the pressure exerted by a magma body. At the same time, the relative stress field change, as estimated by focal mechanisms, also disturbs the stress field in the region around the magma chamber. A model describing the shape and internal pressure of a magma chamber can be constrained by both ground deformation and the focal mechanism. The purpose of this study is to estimate the magma supply system in detail using geodetic and seismic data simultaneously.

Unzen Volcano, located in the middle of Kyushu Island, Japan, erupted during 1990-1995, accompanied by pyroclastic flows and the formation of a lava dome at the summit. In this research, we investigated the magma supply system of the volcano using dense seismic and geodetic observations that were carried out in this area during the eruption. We took into account a precise leveling survey which has been conducted for many years in and around the volcano for setting our boundary condition of magma chamber shape in order to determine spatial and temporal variations. This leveling survey has been conducted since 1991 on the north flank of the volcano, and since 1986 on the western coast of the peninsula.

The point source model, which is based on leveling and GPS data, can explain the general features of crustal deformation data. However, the model does not represent well the spatial variation of crustal deformation. The discrepancy between the model and data suggests that the point source assumption is not applicable and realistic pressure sources should be modeled. Therefore, we searched for the best solution to explain the data by using the finite element method (FEM) for a major source. To build our final model, a grid search procedure was adopted to determine the source shape. The result showed that an oblate spheroid with a dip oriented to the south showed good correlation with observational data. This shape supports the idea that magma ascends easily to a shallower chamber.

Deviatoric stress tensors for a focal region around Unzen Volcano were also estimated using the stress tensor inversion method, because high seismic activities prior to the beginning of the eruption seem to have been significantly related to ascending magma. Contrary to our expectation, we found that the stress field in the hypocenter area exhibited no change, even during eruption.

Comparing the stress using the optimal solution inferred from geodetic data, stress tensors were calculated by FEM. We found stress disturbance induced by increasing or decreasing pressure of the magma chamber only in the region closest to the chamber. From these results we can conclude that the body of the magma chamber did not reach the focal area; thus, the earthquake swarm was generated by a volatile substance. Such substances can weaken the bedrock when they soak into the rocks.

GEODETIC OBSERVATIONS AT ANATAHAN VOLCANO, NORTHERN MARIANA ISLANDS

Takeshi Matsushima¹, Takao Tabei², Tsuyoshi Watanabe³, Setsuya Nakada⁴, Yuichi Morita⁴, Fukashi Maeno⁴, Atsushi Watanabe⁴, Jun Oikawa⁴, Teruyuki Kato⁴

¹Institute of Seismology & Volcanology (SEVO), Kyushu Univ., Shimabara, Japan.

²Applied Sci., Kochi Univ., Kochi, Japan.

³Research Center for Seismology, Volcanology and Disaster Mitigation (RCSVDM), Nagoya Univ., Nagoya, Japan.

⁴Earthquake Research Institute, Univ. of Tokyo, Tokyo, Japan.

Anatahan (788 m ASL) is one of the most active volcanoes of the Northern Mariana Islands on the Izu-Bonin-Mariana islands arc, which is located at the margin of the Philippine Sea plate and the Pacific plate. The island of Anatahan stretches for 9 km from east to west and 4 km from north to south. The sparse vegetation on the most recent Anatahan lava flows indicates that they are of Holocene age, but the first historical eruption of Anatahan did not occur until May 2003, when a large explosive eruption took place forming a new crater inside the eastern caldera. Formerly inhabited, Anatahan now has no population because of the eruptions. We have carried out GPS surveys at Anatahan Island village since 1998. Soon after the eruption started in May 2003, we continued the GPS survey and geological inspection at Anatahan (Nakada et al., 2005). Watanabe et al. (2005) showed three deformation Mogi sources located along a westward-dipping conduit from the eastern active crater.

In 2008 we started a new seismic and geodetic observation campaign at Anatahan with the purpose of understanding what goes on inside the volcano. In this presentation, we will focus on the geodetic results of our observations.

We established four new GPS benchmark pillars on the island. Including one old benchmark at the village, we set a total of five GPS receivers to detect the crustal deformation of the volcanic island. The campaign lasted for about 24 hours because of limitations on the helicopter flight schedule. We also set a ground-tilt meter with a continuous recording system to detect crustal movement at the south rim of the west crater. The second GPS campaign was held in January 2009, and the tilt data were retrieved successfully. The analyzed data suggest an inflation of the deformation source under the western crater and a depression under the active eastern crater during the 2008-09 period.

We also carried out InSAR analyses of Anatahan Island using ALOS-PALSAR data in order to detect crustal deformation of the volcano. We found no remarkable deformation due to magma activity inside the volcano during the period of 2007-08; however, in the interferogram we found a non-interference area and a 2-20cm uplift around the non-interference area extending southwest to south of the active eastern crater. As a result of our geological inspection of these areas, we found the thickness of the 2008 volcanic ash deposit was consistent with the value of the uplift. Thus, the 2-20cm thick ash deposit appears like an uplift of the volcano surface in InSAR analyses, while a deposit more than 20cm thick changes surface conditions so much that non-interference areas in the interferogram map are affected.

References

Nakada et al., Geological aspects of the 2003-2004 eruption of Anatahan Volcano, Northern Mariana Islands, *J. Volcanol. Geotherm. Res.*, 146, 226-240, 2005.

Watanabe, T. et al., Geodetic constraints for the mechanism of Anatahan eruption of May 2003, *J. Volcanol. Geotherm. Res.*, 146, 77-85, 2005.

A CONCEPTUAL MODEL OF AKUTAN VOLCANO, ALASKA, INFERRED FROM OBSERVATIONS OF SEISMICITY AND GROUND DEFORMATION: 1996 - 2009

J.A. Power¹, Z. Lu², S.G. Prejean¹, C. Wicks³, D. Dzurisin²

¹USGS, ASC, AVO, 4210 University Dr., Anchorage, AK 99508, USA.

²David A. Johnston Cascades Volcano Observatory, USGS, 1300 SE Cardinal Court, Building 10, Suite 100, Vancouver, WA 98683-9589, USA.

³USGS, 345 Middlefield Rd. MS 977, Menlo Park, CA 94025-3591, USA.

Akutan Volcano in the central Aleutian Arc has experienced one strong earthquake swarm and associated deformation episode followed by persistent lower-level seismicity since monitoring began in the early 1990s. Integration of these long-term data sets, including multi-temporal interferometric synthetic aperture (InSAR) images and refined earthquake hypocenters, allows us to develop a conceptual model of the Akutan magmatic system that should assist in forecasting the next eruption and addressing associated hazards.

In March 1996, Akutan Volcano was the source of a powerful swarm of volcano-tectonic (VT) earthquakes composed of more than 200 shocks greater than magnitude 3.5 ($M_{max} = 5.1$) that produced an estimated total cumulative seismic moment of 2.7×10^{18} N m. Extensive ground cracks striking N70W and extending discontinuously across the island from near Lava Point (the most recently active satellite vent) to the southeast side of the island formed in association with this swarm. The most extensive cracks formed a zone 500 m wide and 3 km long on the NW flank of the volcano between the summit and Lava Point. In this area, local graben structures show vertical displacements of 30 to 80 cm, suggesting the cracks formed in response to uplift and extension. Both C-band ERS and L-band JERS images that span the time of the swarm reveal a complex island-wide pattern of deformation. The western part of the island moved upward as much as 70 cm, while the eastern part moved downward a similar amount.

The most plausible interpretation is that the 1996 seismic swarm and associated ground deformation at Akutan resulted from an intrusion of magma beneath the northwest flank of the volcano. Modeling of the observed deformation field suggests inflation on the northwest side of the volcano results from intrusion of a dike to within ~0.4 km of the surface. Deflation on the island's eastern side is modeled as several dislocation planes that might represent depressurization of a known hydrothermal system in this area. In spite of the high level of volcanic unrest in 1996, no magmatic eruption has occurred at Akutan in association with or since this episode. The seismic moment and ground deformation observed at Akutan in 1996 greatly exceed many sequences that precede eruptions at other volcanoes. Remarkably, no observed increases in fumarolic activity or gas emission and no obvious periods of volcanic tremor or long-period seismic events were observed in association with the 1996 unrest. Lack of these common eruption precursors played an important role in correctly diagnosing the unrest and formulating public warnings and advisories issued by the Alaska Volcano Observatory (AVO).

Since 1996, AVO has located more than 1,600 earthquakes near Akutan Volcano. Most of the hypocenters fall into one of three groups: (a) a prominent shallow cluster beneath the eastern side of the island near the center of subsidence in 1996, (b) a west-northwest trending group that aligns with the 1996 ground cracks and extends across the island, and (c) a small cluster of low- and mixed-frequency events that locate at mid-crustal depths beneath the volcano's southwest flank. Larger earthquakes during 2003-2008 beneath the volcano's western flank show dominantly strike-slip motion, while those beneath the volcano's summit caldera indicate normal

and strike slip faulting. Remarkably a few hypocenters on the island's southeast side show reverse mechanisms.

These observations suggest that Akutan Volcano is situated at the intersection of two rift zones. The orientation of these rift zones might be controlled partly by the inferred direction of maximum principal stress resulting from the convergence of the North American and Pacific plates. The deeper low- and mixed-frequency earthquakes to the southwest suggest this area as a possible source region for Akutan magmas.

REAL TIME EARTHQUAKE PROCESSING AT VOLCANOES: WHAT IS AND ISN'T FEASIBLE

Michael E. West

Alaska Volcano Observatory, Geophysical Institute, University of Alaska Fairbanks, Fairbanks, AK 99775; west@gi.alaska.edu

This presentation offers case studies of automated earthquake location and real time analyses from Okmok, Redoubt and other north Pacific volcanoes. By examining different types of seismic networks and different types of volcanic behavior, the objective is to provide examples of what can be expected from real time earthquake processing using standard techniques. We examine minimum station criteria, the potential for S waves, prospects for locating low frequency earthquakes, and how preliminary locations may be sufficient for some types of analysis.

Earthquake analysis at volcanoes is in many ways a more challenging exercise than its regional and teleseismic counterparts. Many volcano networks have a small number of seismic stations deployed in inherently noisy locations. In the US, most volcanoes still rely on short period, vertical component sensors. Data quality is often compromised by extremely high attenuation and scattering, compounded by infrequent access for remote repairs. The close receiver distances at volcanoes present a further limitation by not allowing sufficient differentiation of P and S waves. With S waves buried early in the P wave coda it can be extremely challenging for an algorithm (or analyst) to extract a meaningful S wave arrival.

In light of these challenges, it can seem futile to carry out automated earthquake processing. However, volcanic earthquakes are interpreted differently than regional earthquakes. These differences make it possible to use large numbers of, perhaps poor quality, earthquakes to tease out patterns and provide rapid notification of volcanic activity. Specifically: (1) knowledge that a swarm is occurring is often more important than the precise location of the swarm; (2) occasional false triggers are less important when seismicity rates are high; and (3) many procedures for estimating source types, event rates, and waveform patterns are robust to questionable locations.

TSUNAMIS AND TSUNAMI HAZARDS

ORAL PRESENTATIONS

TSUNAMI AND PALEO-EARTHQUAKE HISTORY OF THE SOUTH-CENTRAL ALASKAN SEGMENT OF THE ALEUTIAN SUBDUCTION ZONE DETERMINED AT VALDEZ, ALASKA

James Begét^{1,2} and Jason Addison²

¹*Alaska Volcano Observatory, Univ. of Alaska-Fairbanks. Fairbanks, AK, USA.*

²*Dept. Geology and Geophysics Univ. of Alaska-Fairbanks. Fairbanks, AK, USA.*

The 1964 Alaska earthquake on Friday, March 27 had a moment magnitude of 9.2 and registered 8.4 on the Richter scale, making it the most powerful in North American history and the third most powerful ever measured. Shaking occurred across south-central Alaska for almost five minutes, collapsing buildings and generating a major tsunami. Numerous local tsunamis were simultaneously produced by submarine landslides and caused most of the 131 deaths during this event. A tsunami as much as 67 m high was generated at Valdez, Alaska by a submarine landslide from the Shoup Bay moraine and a smaller tsunami was produced by a landslide beneath the old Valdez townsite.

Tsunami deposits from the 1964 events and prehistoric paleotsunami deposits were identified during this study at sites near Shoup Bay, at Saw Island in the Valdez Marine Terminal, and at a site near Solomon Gulch. Paleotsunami deposits are distinctive sediments found in certain geologic settings that record deposition by large prehistoric tsunamis. Large tsunamis are usually coeval with great earthquakes, and the history of tsunamis in the Valdez area is interpreted as a proxy record of past great earthquakes. Multiple accelerator mass spectrometry radiocarbon dates and conventional radiocarbon dates indicate major prehistoric earthquakes also created large tsunamis in the Valdez area ca. 950-1000 yr B.P., ca. 3800 yr BP. and ca. 4300 yr BP. A large landslide near the VMT dated to 5800 yr BP may have been triggered by a still older earthquake.

The tsunami dated to ca. 950-1000 yr BP was higher and affected a larger inland area at the eastern end of Port Valdez than the historic 1964 tsunami. The 950-1000 yr BP tsunami was probably caused by submarine landslides from the Shoup Bay Moraine and the Valdez River and Lowe River fan deltas. Some of the extensive submarine landslide deposits on the floor of Port Valdez appear to pre-date the 1964 earthquake, and may be correlative with the 950-1000 yr BP event. The tsunamis at 3800 and 4300 yr BP may also have been larger than the 1964 event, but were not as large as the 950-1000 yr BP event. Based on the much higher wave-runup and more extensive tsunami deposits, we speculate the 950-1000 yr BP earthquake may have been larger than the 1964 earthquake.

Seismic engineering for the Valdez Marine Oil Terminal in the Valdez area was based on an assumption that future earthquakes will resemble the 1964 event, and an educated guess that such events will recur only every few thousand years. The actual duration between great earthquakes in the Valdez area has apparently varied between ca. 500-2800 years, with some evidence suggesting previous earthquakes and tsunamis may have been larger than the 1964 event. However, even assuming a repeat of the shortest interval found between prehistoric earthquakes, another giant subduction zone earthquake similar to the 1964 event is unlikely to occur for hundreds of years.

MULTIPLE PALEO-SUBMARINE LANDSLIDE DEPOSITS TRIGGERED BY EARTHQUAKES ON THE ALASKAN MEGATHRUST AT PORT VALDEZ, ALASKA

Ryan, H.F.¹, Lee, H.J.¹, Haeussler, P.J.², Alexander, C.R.³, and Kayen, R.E.¹

¹U.S. Geological Survey, Menlo Park, CA.

²U.S. Geological Survey, Anchorage, AK.

³Skidaway Institute of Oceanography, Savannah, GA.

Submarine slope failures at Port Valdez triggered by the 1964 M9.2 great Alaskan earthquake generated some of the highest tsunami wave heights observed in Alaska (> 50 m). Debris flow deposits from the slope failures are imaged on very high-resolution bathymetry (Fig. 1) and high-resolution sub-bottom profiles (Fig. 2). These deposits appear as large, relatively intact blocks up to 40 m high visible on the seafloor and as acoustically opaque units on sub-bottom profiles, which are locally lens-shaped and may truncate reflectors below. The largest tsunami wave heights are associated with the failure of the Shoup Glacier terminal moraine in western Port Valdez. The damage to the town of old Valdez (previously located at the eastern end of Port Valdez), however, was primarily the result of the failure of the fiord-head delta, which generated a much smaller tsunami than observed at Shoup Bay.

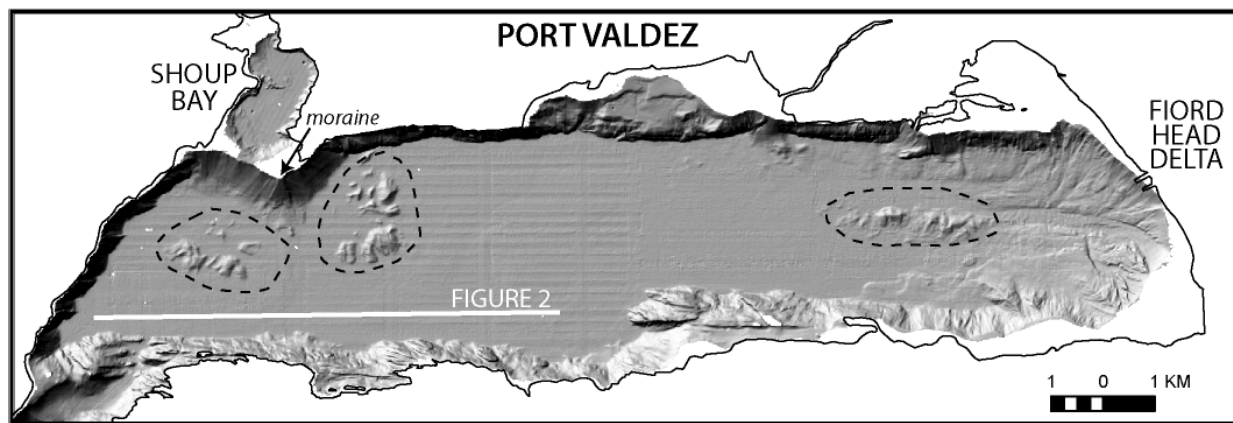


Figure 1. Multibeam imagery of Port Valdez showing landslide features (outlined by dashed lines) that contributed to tsunamis generated during the 1964 Alaskan earthquake.

Beneath the 1964 debris lobes, 5 additional acoustically opaque units are imaged on sub-bottom profiles; the opaque units are intercalated with layer-parallel reflectors (Fig. 2). We interpret these units as debris lobe deposits from paleo-submarine landslides that were triggered by earthquakes on the Alaskan megathrust. Debris lobe 2 is assigned to the timing of the penultimate earthquake (913-808 yrs B.P., Carver and Plafker, 2008), based on time-averaged sedimentation rates calculated for Port Valdez and the thickness of the layer-parallel reflectors between the debris lobes. Debris lobe 2 has a similar spatial distribution to debris lobe 1, although it is not as thick as the 1964 lobe. The older, deeper, debris lobes are thinner, less extensive, and separated by thinner sequences of parallel-layered reflectors than those deposited during the 1964 and penultimate events. In addition, the older debris flow lobes did not involve the failure of the Shoup Glacier terminal moraine. We postulate that variations in the thickness and spatial extent

of the debris flows are related to differences in the recurrence interval between and/or magnitude of megathrust earthquakes, modulated by variations in climatic conditions. The retreat of Valdez Glacier and the concomitant build-up of the fiord-head delta sediment combined with longer recurrence intervals between earthquakes may result in more extensive delta failures and thus thicker debris lobe deposits. The retreat of Shoup Glacier from its terminal moraine in the 1700s and also perhaps during the Medieval Warm Period (ca. 850-1200 A.D.) may have facilitated failure of the Shoup Glacier moraine during the more recent megathrust earthquakes.

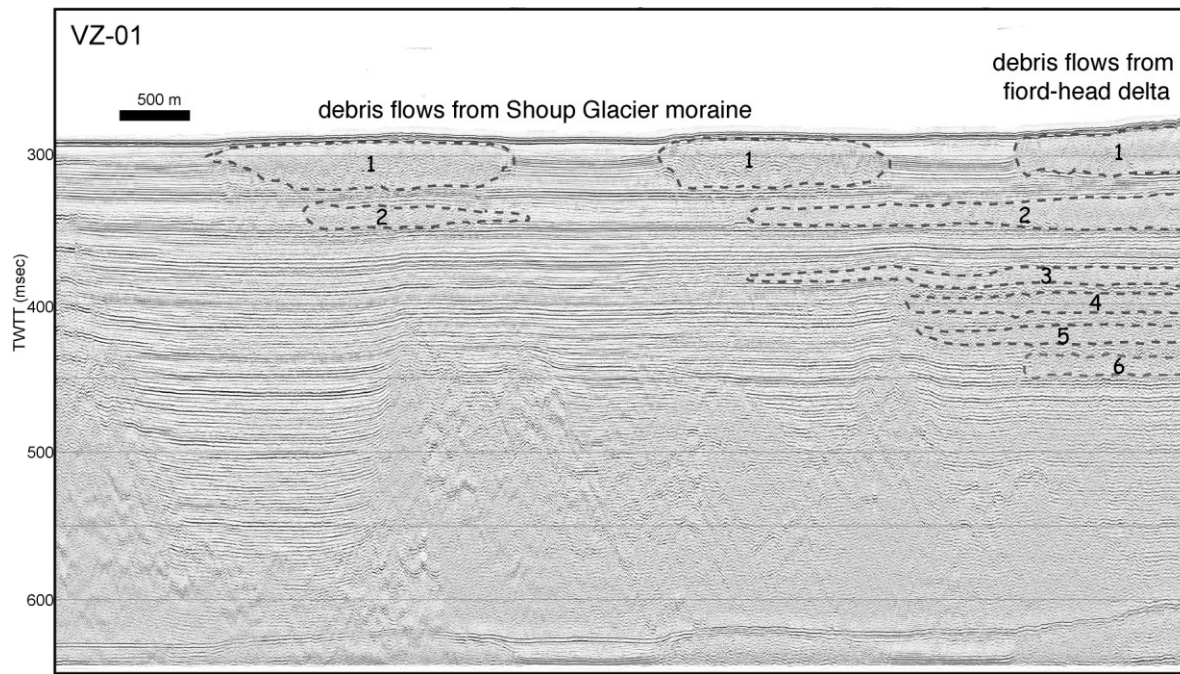


Figure 2. Mini-sparker profile showing acoustically transparent units that are attributed to debris flow deposits triggered by megathrust earthquakes. Debris flow 1 was deposited at the time of the 1964 earthquake, debris flow 2 during the penultimate event. Location of profile shown in Figure 1.

Carver G., and Plafker G., 2008, Paleoseismicity and neotectonics of the Aleutian subduction zone – an overview, *in* Freymueller J. T., Haeussler, P. J., Wesson, R. L., Ekström, G., eds., Active Tectonics and Seismic Potential of Alaska: Geophysical Monograph Series 179, American Geophysical Union, Washington, 350 pp., ISBN 978-0-87590-444-3, AGU Code GM1794443.

SIZES AND SLIP DISTRIBUTIONS OF THE 2006–2007 GREAT KURIL EARTHQUAKES FROM GPS COSEISMIC OFFSETS

Grigory M. Steblov^{1,2}, Mikhail G. Kogan², Boris V. Levin³, Nikolai F. Vasilenko⁴, Alexander S. Prytkov³, and Dmitry I. Frolov⁴

¹*Institute of Physics of the Earth, Russian Academy of Sciences, Moscow, Russia.*

²*Lamont-Doherty Earth Observatory, Columbia University, Palisades, New York, USA.*

³*Institute of Marine Geology and Geophysics, Far Eastern Branch, Russian Academy of Sciences, Yuzhno-Sakhalinsk, Russia.*

⁴*Ioffe Physico-Technical Institute, Russian Academy of Sciences, St.Petersburg, Russia.*

The Kuril subduction zone is one of the most seismically active regions on the Earth. It had been the last major subduction zone totally unexplored by methods of space geodesy before we started GPS observations in 2005. The 2006-2007 earthquake doublet in the central Kurils with moment magnitudes of 8.3 and 8.1 occurred in the segment of the subduction zone where such strong events had not been observed since 1915. It is probably the strongest doublet (thrust faulting on a subduction interface followed by normal faulting beneath the outer rise) ever observed by seismic and space geodetic methods simultaneously. Several months before the first event in the pair, the Kuril GPS Array was installed over the whole length of the Kuril subduction zone, so that we were able to capture coseismic offsets and monitor postseismic time-dependent deformation for a period of about two years since the first event. The work was performed in collaboration with Columbia University and the University of Alaska Fairbanks on the US side, and with the Institute of Marine Geology and Geophysics and the Geophysical Service, both organizations administered by the Russian Academy of Sciences (RAS), on the Russian side. In mid-2007, two survey-mode GPS (SGPS) sites in the central Kurils were upgraded to a continuous mode; in mid-2008, the third SGPS site in the central Kurils was upgraded to a continuous mode, so that now the array comprises eight continuously recording stations from Hokkaido to Kamchatka. To access the Kurils, we benefited from using cruises of the NSF-sponsored ship supervised by the University of Washington and from cruises sponsored by RAS.

Seismic, geodetic, and tsunami observations at several subduction zones provide evidence that slip is nonuniform over the earthquake. It is generally recognized that the maximum slip occurs within fault regions called asperities, patches that repeatedly break in earthquakes. Inversions of seismic and tsunami data resolve the rapid slip that occurs during seismic and tsunami periods. By contrast, the offsets measured with GPS are sensitive to the total slip comprising both rapid and slow components. There are large variations in the sizes and slip distributions of both events in the doublet estimated from several seismological and tsunami inversions. Here we present the expanded analysis of geodetic moments and slip distributions of the 2006–2007 Kuril earthquakes determined from GPS coseismic offsets by *Steblov et al.* [2008]. Our analysis was improved in the following aspects: (1) the inversion grid was extended to the southwest, beyond the region characterized by aftershocks; (2) more accurate daily station positions were estimated due to the most recent improvement of the GAMIT/GLOBK software; and (3) the preseismic and postseismic time series were modeled in several variants using the longer time series available to us now.

Our updated results confirm the analysis of *Steblov et al.* [2008] with respect to sizes and slips of both events in the central Kurils doublet: geodetic moments significantly exceed seismological moments, and the highest-slip patches from the 2006 and 2007 earthquakes are

adjacent to each other. For the 2006 event, we confirm that the region of the highest slip outlines a shallow ruptured zone expanding from the trench bottom downward to a depth of only 22 km, i.e., at the lower edge of the model fault plane dipping 16° . A shallow rupture is also indicated by the location of the GCMT earthquake centroid near the trench. We attribute the shallow seismogenic fault in the central Kurils to the absence of the accretionary prism that controls the upper aseismic zone. With respect to the 2007 event, we revised our initial estimated depth of the rupture from 50 km to 25 km, a fraction of the total thickness of the bent oceanic lithosphere. Our earlier estimate of 50 km contradicts the observed postseismic offsets of stations in the near field of earthquake ruptures.

Reference

- Steblov, G.M., M.G. Kogan, B.W. Levin, N.F. Vasilenko, A.S. Prytkov, and D.I. Frolov (2008), Spatially linked asperities of the 2006-2007 great Kuril earthquakes revealed by GPS, *Geophys. Res. Lett.*, 35, doi:10.1029/2008GL035572.

GENERATING TSUNAMI SOURCES FOR THE JAPAN-KURIL-KAMCHATKA AND ALEUTIAN-ALASKAN SUBDUCTION ZONES, AND FORECASTING THE THREAT FOR THE WEST COAST AND ALASKA TSUNAMI WARNING CENTER'S AREA OF RESPONSIBILITY.

Kara Sterling, William Knight, Paul Whitmore

West Coast and Alaska Tsunami Warning Center, Palmer, AK.

The Alaska Tsunami Forecast Model (Kowalik and Whitmore, 1991) is used at the West Coast and Alaska Tsunami Warning Center (WC/ATWC) to forecast maximum tsunami wave amplitudes for our Area of Responsibility (AOR), with the focus here being on sources in the Japan-Kuril-Kamchatka and Aleutian-Alaska Subduction Zones. Potential tsunami sources are generated using hypothetical thrust events of magnitudes, M_w : 7.5, 7.9, 8.2, 8.6, 9.0, 9.2, and 9.5. Great earthquake parameters for the tsunami sources are derived following Papazachous et al. 2004, and regional considerations are discussed. The tectonic uplift is calculated following Okada's (1985) static dislocation formulae, and the resulting tsunami is propagated using the shallow water equations of motion.

Using the Alaska Tsunami Forecast Model, the development of a tsunami threat database is underway. The Tsunami Forecast and Threat Database (TFTD) will be called upon during an event to access pre-defined initial Warning/Watch/Advisory regions based upon the threat, as determined by the forecasted maximum tsunami amplitudes. A summary of the results from the TFTD for Kuril-Kamchatka Subduction Zone sources upon Alaska can be seen in Figure 1. The threat from volcanic sources to the WC/ATWC's AOR along with current monitoring techniques and warning procedures will also be reviewed.

Reference

- Kowalik, Z. and Whitmore, P. M., 1991. An investigation of two tsunamis recorded at Adak, Alaska, *Science of Tsunami Hazards*, **9**, 67-83.
- Okada, Y., 1985. Surface deformation due to shear and tensile faults in half-space, *Bulletin of the Seismological Society of America*, **75**, 1135-1154.
- Papazachos, B. C., E. M. Scordilis, D. G. Panagiotopoulos, C. B. Papasachos, and G. F. Karakaisis, 2004. Global Relations Between Seismic Fault Parameters and Moment Magnitude of Earthquakes, *Bulletin of the Geological Society of Greece*, **XXXVI**, 1482-1489.

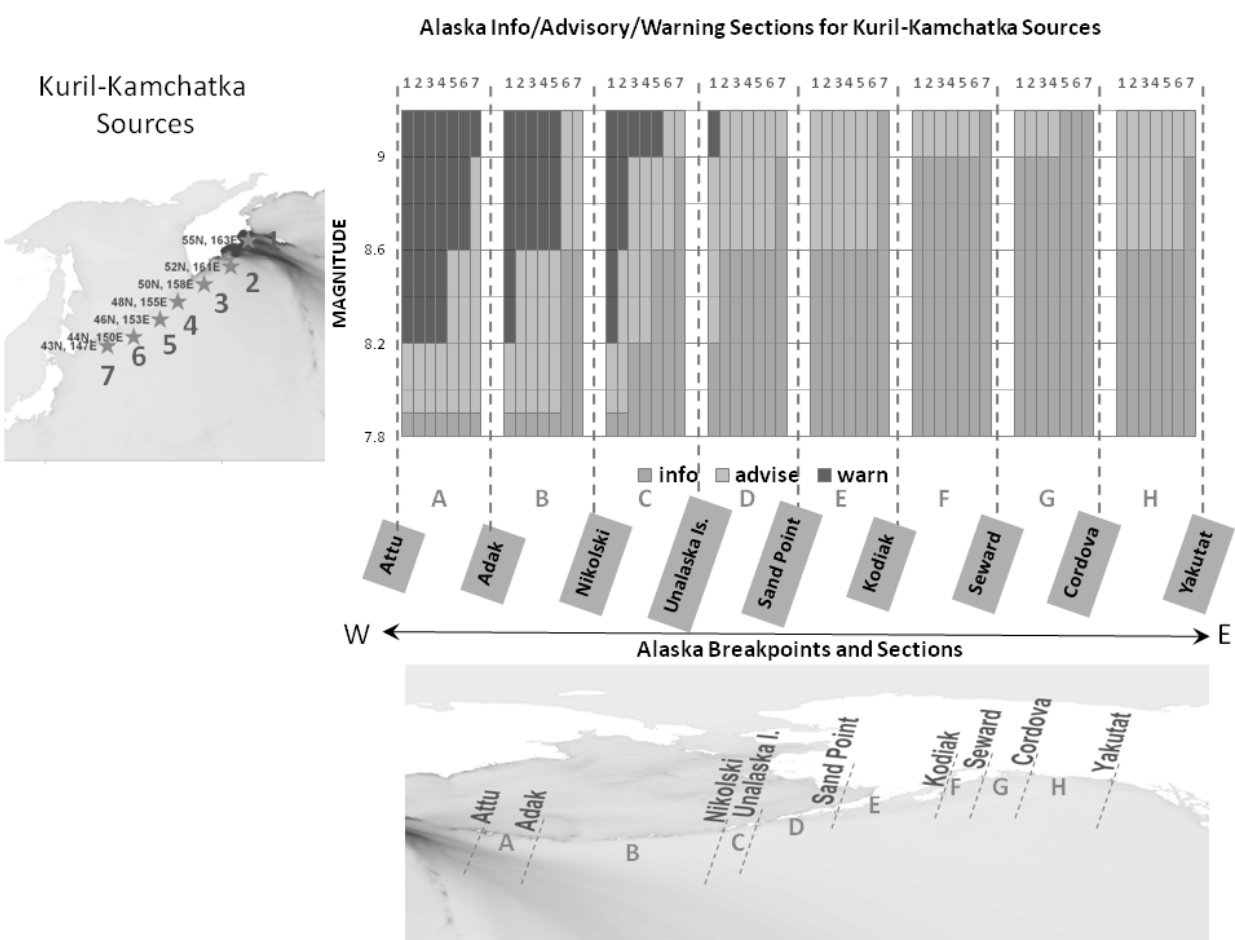


Figure 1: For earthquake sources in the Kuril-Kamchatka Subduction Zone, the bar chart summarizes initial Warning, Advisory, and Information Only, sections for Alaska based upon the forecasted tsunami amplitudes.

NEAR-FIELD MODELING OF THE 1964 ALASKA TSUNAMI: A SOURCE FUNCTION STUDY

Elena Suleimani, Dmitry Nicolsky, Roger Hansen

Geophysical Institute, University of Alaska Fairbanks, Fairbanks, AK, USA.

The Alaska Earthquake Information Center conducts tsunami inundation mapping for coastal communities in Alaska. For many locations in the Gulf of Alaska, the 1964 tsunami generated by the $M_w 9.2$ Great Alaska earthquake may be the worst-case tsunami scenario. We use the 1964 tsunami observations to verify our numerical model of tsunami propagation and runup; therefore it is essential to use an adequate source function of the 1964 earthquake to reduce the level of uncertainty in the modeling results. It was shown that the 1964 coseismic slip occurred both on the megathrust and crustal splay faults (Plafker, 1969). The analysis of the eyewitness arrival times of the highest observed waves in Kodiak and Kenai Peninsula showed that the initial tsunami wave was higher and closer to the shore, than it would be if it was generated by slip on the megathrust (Plafker, 2006). That resulted in a hypothesis that crustal splay faults were a major contributor to vertical displacements that generated local tsunami waves.

We conduct a numerical study of different source functions of the 1964 tsunami to test whether the crustal splay faults had significant effects on local tsunami runup heights and arrival times. We consider the following source models of the 1964 earthquake: the slip model by Johnson et al. (1996) developed by joint inversion of the far-field tsunami waveforms and geodetic data; the model by Ichinose et al. (2007) based on the combined inversion of seismic, tsunami and geodetic data; and the recent model by Suito and Freymueller (2008, submitted). The last one extends the Montague Island fault farther along the Kenai Peninsula coast and thus reduces slip on the megathrust in that region. Although in the far field all source functions produce very similar waveforms, which are also in good agreement with the tide gage records, the near-field amplitudes and arrival times differ substantially. In order to study the near-field tsunami effects, we construct embedded telescoping bathymetry grids around tsunami generation area to calculate tsunami arrival times and sea surface heights for all source models of the 1964 earthquake and use available observation data to verify model results.

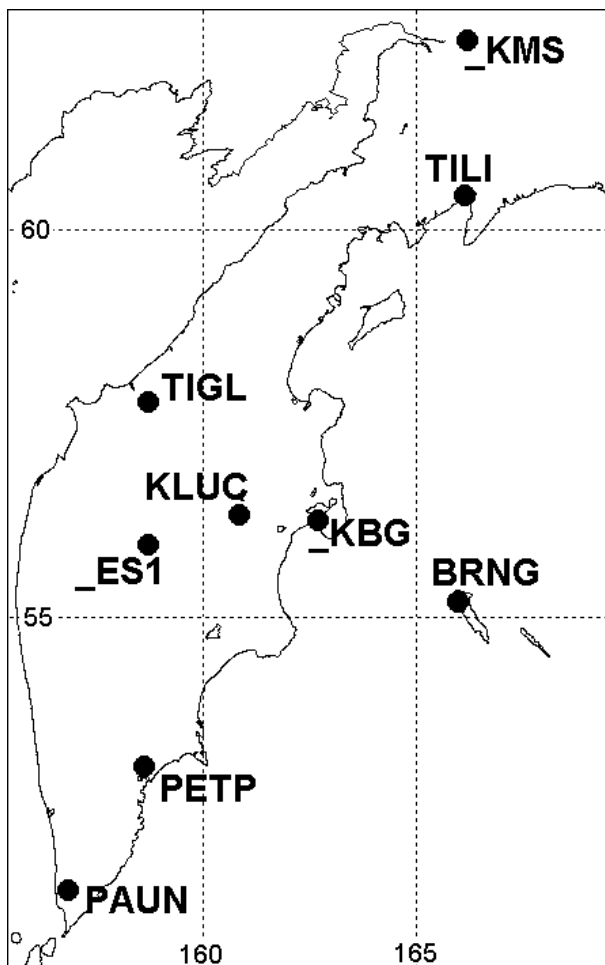
**SUBDUCTION ZONE TECTONIC PROCESSES,
VOLCANO GEOPHYSICS, TSUNAMIS AND TSUNAMI
HAZARDS**

POSTER PRESENTATIONS

CHARACTERISTIC PROPERTIES OF TIME SERIES OF CONTINUOUS GPS POINTS ON KAMCHATKA (2000-2008).

Vilory Bakhtiarov,

Kamchatsky Branch of Geophysical Service RAS, Petropavlovsk-Kamchatsky, Russia.



The structure of GPS time series is not uniform. A time series can include gaps, offsets after antenna change, or changed GPS points; these irregularities cannot be excluded by geodetic methods, co-seismic offsets, et cetera. These offsets were excluded from GPS time series with the purpose of correctly determining velocities, for example, changes of velocities over time, and analyzing fine row structure, for example, to determine the periodical component.

Offsets were excluded using an original interactive program based on continuity of observation rows. The information about offsets is included in a time series as time interval and 3 NEU offsets. Initial visualization as correct rows is possible by consecutively including an offset table.

Initial and correct time series from the main permanent points of the Kamchatka GPS network (Fig. 1) are considered. Horizontal and vertical velocities and accelerations are presented.

Co-seismic offsets and post-seismic time deformations of Olutorskoe earthquake (Koryakia, 20.04.2006, Mw=7.6) are discussed on the basis of GPS points _KMS and TILI.

OVERVIEW OF GEODYNAMIC MODELS FOR NEOGENE ALASKA OROGENESIS

Jeff Benowitz¹, Paul Layer¹, Stephanie Perry², Paul Fitzgerald²

¹*Geophysical Institute, University of Alaska Fairbanks, Fairbanks, AK, 99775,*

e-mail ftjab@uaf.edu

²*Dept. of Earth Sciences, Syracuse University, Syracuse, NY 13244.*

Neogene (~25 Ma to present) tectonic activity throughout Alaska, from the Brooks Range in the far north, to the Chugach/St. Elias mountains along the southern Alaska subduction margin, has been documented by thermochronometric techniques and geologic field mapping. One of the most active regions is the ~650 km long Alaska Range which cuts through the center of the state paralleling the Denali Fault system and has been the subject of several previous thermochronometric studies and ongoing investigations (Fig. 1).

However, the exact timing and amount of orogenic exhumation of the Alaska Range as a whole is not well constrained by a spatially sparse thermochronometric data set and our new data indicate that the timing is different for different parts of the range. The amount of glacial ice cover on many of the major faults systems and the rugged nature of high topography which limits the amount of detailed structural work in the region make it difficult to collect comprehensive geologic data to guide geodynamic interpretations. Although the mechanisms and timing of this activity is poorly understood, it is clear that Neogene topography formation at the Alaska southern margin and inboard is correlated with processes at Alaska's southern margin subduction zone Such as the northward transport of allochthonous terranes and the subduction of the anomalously thick Yakutat microplate.

It has been proposed that block rotation negative buoyancy related to flat-slab subduction and/or orogenic float are responsible for Neogene Alaska orogenesis. The role major strike-slip faults systems, like the Denali Fault and the Fairweather Fault play in topography formation have also been questioned. What is not known is which of these proposed geodynamic models (or other explanations) are responsible for the formation of topography across Alaska. More likely different geodynamic processes are responsible for topography formation for different time-space coordinates.

Before models can be tested and further refined, it is important to look at the constraints that thermochronometric and geologic data place on these models. In this presentation we will look at several questions including: What is the current state of data and where are the data gaps? What should the various models predict regarding Alaska Range uplift and deformation? Where are the disconnects between field observations and model predictions. Although we will not attempt to answer the 'big questions' in Alaska subduction/topography interactions, we will discuss the current state of knowledge of the neotectonic history of southern Alaska, the role that major fault systems play and the current state of proposed geodynamic models.

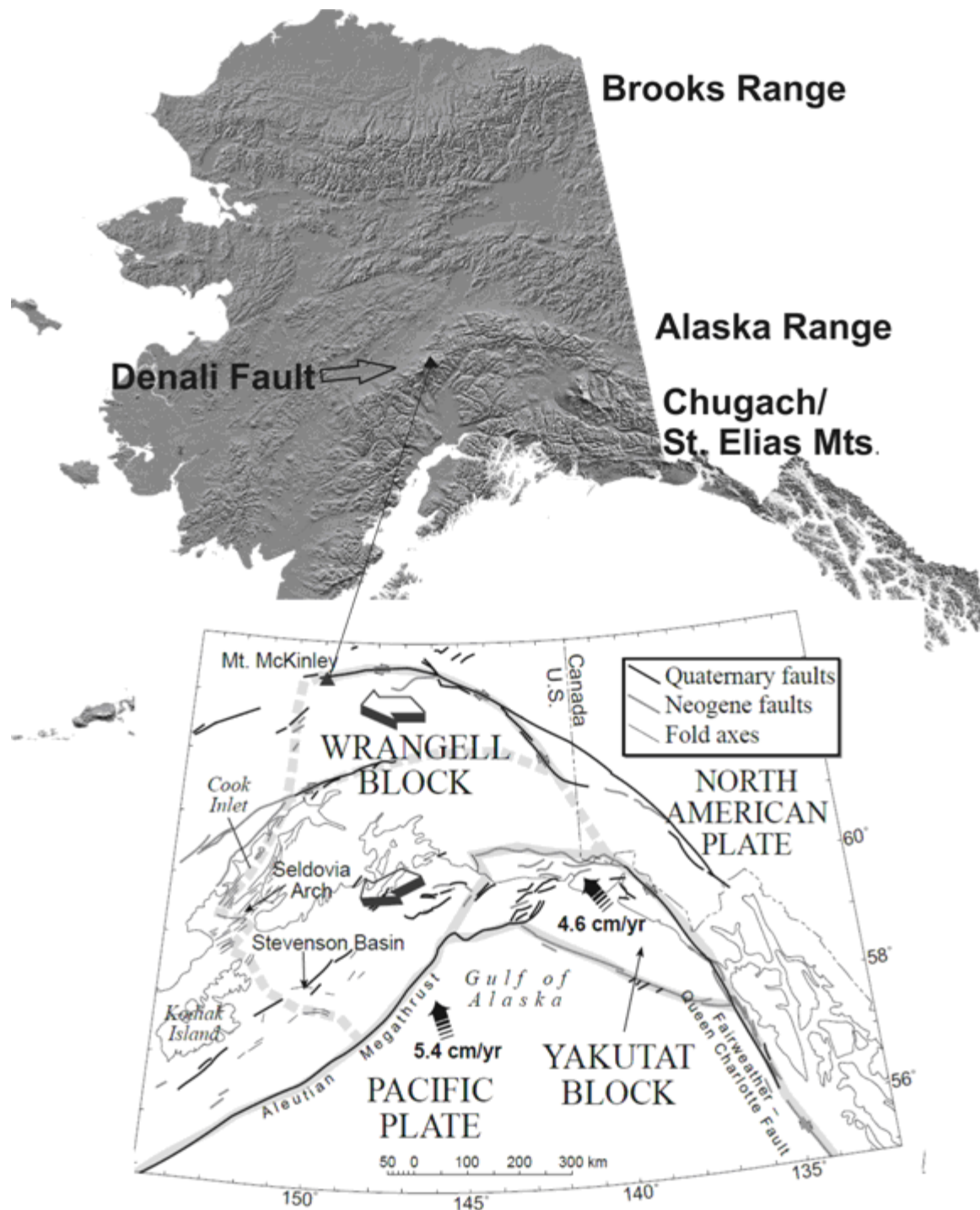


Figure 1. DEM of Alaska. Tectonic Model of Alaska from: Bruhn and Haeussler, 2006. Deformation driven by subduction and microplate collision: Geodynamics of Cook Inlet basin, Alaska, Geol. Soc. Am. Bull., 118(304), 289-303.

SEISMIC NETWORK DEVELOPMENT FOR THE RUSSIAN FAR EAST: VIEW OF A TSUNAMI WARNING SYSTEM

Chebrov V.¹, Droznin D.¹, Gusev A.¹, Mishatkin V.², Sergeev V.¹, Shevchenko Y.¹, Chebrov D.¹

¹Kamchatka Branch of Geophysical Survey of Russian Academy of Science, Petropavlovsk-Kamchatskiy, Russia.

²Geophysical Survey of Russian Academy of Science, Obninsk, Russia.

Until recently only 3 seismic stations, "Petropavlovsk-Kamchatski", "Yuzhno-Sakhalinsk", and "Severo-Kurilsk", were available to warn of possible tsunamis in the Russian Far East; these stations, supervised by the Geophysical Survey of the Russian Academy of Science (GS RAS), were equipped with out-of-date analog equipment. In addition, the "Petropavlovsk-Kamchatski" and "Yuzhno-Sakhalinsk" stations had data from broadband IRIS stations available to them, as well as data from their analog devices, to measure earthquake properties. The so-called "magnitude-geographical criterion" is the basis of deciding whether the possibility of a tsunami exists. Previously, a decision as to whether an earthquake posed tsunami danger was made by each seismic station independently, without sharing data among a network of stations.

In 2006, within the framework of a federal program, the concept of a seismic subsystem of the Tsunami Warning System (SS TWS) in the Russian Far East was developed. It is expected that by 2010 a number of subsystems will be created: a network of 11 specialized seismic stations, a system of communication for data transmission, and information-processing centers (IPCs) to handle the data from this network of seismic stations.

All specialized TWS seismic stations are equipped with the same broadband gauges of seismic signals (Guralp): CMG-3ESPC, 0.0083-40 Hz velocimeters are used, with CMG-5, 0-100 Hz accelerometers. Two types of seismic stations are specialized for TWS: auxiliary (regional) and base stations. Auxiliary TWS seismic stations are intended to protect coastal settlements or sites of low tsunami danger against local tsunamis; as a rule they are equipped with velocimeter and accelerometer, and serve to optimize the SS TWS. Base seismic stations are intended to protect coastal settlements, significant objects, and sites of high tsunami danger against local tsunamis; they form the basis of the SS TWS.

The base SS TWS seismic station is a seismic group with sizes 15 km and more. The central station of the group is equipped with a velocimeter and an accelerometer, while remote stations have only accelerometers. The central station is also equipped with a system of gathering and processing the seismic data in automatic and automated modes, and a system of technological communication with remote stations. Each group of accelerometers is intended to enable rapid decision-making when the threat of a tsunami looms (in safe points) after a strong earthquake in a zone up to 200-300 km distant. Quickly estimating the amplitudes of seismic waves or automatically estimating macroseismic intensity using specialized methods of data analysis can be accomplished even when station data are incomplete. If necessary, decision-making will be carried out on this basis only.

Along with data from specialized TWS seismic stations, when deciding whether to issue a Tsunami forecast real-time data from the global IRIS network, regional networks, and local GS RAS networks and (or) results of their processing are used.

In the remote Far East region a full-scale system of data transmission is constructed based on satellite liaison channels. A system organized in this way provides continuous transmission of

three-component seismograms from each station. Allocated DSL channels can be reserved for use, if needed. The IRIS-station data are provided by USGS via the Internet.

The processing of signals on the seismic network is developed at the regional GS RAS IPC. Regional IPCs in Petropavlovsk-Kamchatski and Yuzhno-Sakhalinsk simultaneously seek to answer the question of whether a tsunami is likely to occur. They use data from all seismic stations involved in survey of the tsunami warning. The results of processing from all IPCs are automatically reflected in the situational panel of every IPC and will be used to control each stage of decision-making. Realizing this method of data processing and deciding whether a tsunami is likely is accomplished by enabling equal and full access of all IPCs to the data from all seismic stations and the results of processing by other IPCs. Thus, on the basis of real-time satellite liaison channels a uniform information space is realized that preserves the functional performance of all IPCs even if one fails due to catastrophic earthquake, technical problems, etc.

In 2008 the first stage of an SS TWS entered into experimental operation. It includes two basic stations with groups of accelerometers ("Petropavlovsk-Kamchatskiy" and "Yuzhno-Sakhalinsk"), an auxiliary station ("Vladivostok") equipped with groups of accelerometers, and a regional "Petropavlovsk-Kamchatskiy" IPC. Each specialized station is equipped with a broadband Guralp velocimeter, the CMG-3ESPC (120). The basic "Petropavlovsk" station represents a seismic group with remote stations as distant as 10-25 km. The basic "Yuzhno-Sakhalinsk" station represents a seismic group with remote stations as distant as 25-70 km. The regional "Petropavlovsk" IPC is organized on the basis of the KB GS RAS computer network; equipped with an automated operator workplace, it carries out data gathering and data processing, presents processing results, allows algorithm debugging and the formation of warnings. The first-stage SS TWS software package includes the following components: the "Real-Time Display" program, the interactive DIMAS processing program, and the "FTSL" program enabling a fast, tentative estimation of strong earthquake parameters at IPC level in automatic mode.

At the first stage of SS TWS experimental operation the created algorithms and software are adjusted and tuned, at both the basic station and the IPC levels. An extensive network of seismic stations contribute data to test the first stage SS TWS operation, including specialized stations "Petropavlovsk-Kamchatskiy", "Yuzhno-Sakhalinsk", and "Vladivostok"; regional stations "Krutoberegovo", "Bering", "Palana", "Esso", and "Tilichiki"; and IRIS stations PET, TIXI, YAK, YSS, BILL, INCN, MAJO, ADK, and MIDW. The SS TWS communication system uses special satellite communication channels, via allocated optical and DSL Internet channels, and allocated hard-wired lines.

Judging by results of experimental first-stage SS TWS operations, reaction time for strong earthquakes ($M > 6.0$) with epicentral distance up to 200 km from the station does not exceed 7 minutes. Reaction includes estimating earthquake parameters and preparing a warning message for dispatch under the pre-arranged notification scheme.

In 2009 it is planned to create specialized SS TWS stations: basic stations "Severo-Kurilsk" and "Ust-Kamchatsk", and auxiliary stations "Nikolsky", "Tilichiki", and "Oha". In 2010 it is planned to create more specialized SS TWS stations: basic station "Yuzhno-Kurilsk", and auxiliary stations "Malokurilsky" (Shikotan Island) and "Kurilsk". In addition, it is planned to create a network of accelerometers on Kamchatka and Sakhalin from which data also will be accessible in real time. The purpose is to decrease the reaction time of the system to the strongest Kamchatka and Kuriles earthquakes by enabling a fast, tentative estimation of their parameters.

At the end of the certification procedure, data from these specialized stations will be freely shared with all users of the Pacific Ocean region TWS services.

ALGORITHMS AND SOFTWARE FOR REAL-TIME PROCESSING OF SEISMIC SIGNALS FOR A TSUNAMI WARNING SYSTEM

Droznin D., Chebrov D.

Kamchatka Branch of Geophysical Survey of Russian Academy of Science, Petropavlovsk-Kamchatskiy, Russia.

A Tsunami Warning System, which has been developed and introduced in the Russian Far East, processes seismic signals using two methods: interactively in the automated mode, and without operator intervention in the completely automatic mode. Automated processing is carried out by operators at seismic stations and in the Regional Information-Processing Centers. Specialized software programs for the Operator's Workplace include:

Real-Time-Display

The real-time-display software program is a flexible, real-time data viewer that connects as a client to the data acquisition server. It provides a real-time data time-series display of any number of user-selectable channels that are being received, provides a sound alarm based on user threshold settings, and collects data in a short-ring buffer for fast interactive processing in near-real-time.

Display Interactive Manipulation and Analyses of Seismograms (DIMAS)

This program was designed to assist the operator of a seismic station to make an initial analysis of the station's waveform data, quickly determine the main parameters of a seismic event, and create an earthquake report which can be forwarded to national data centers.

Current Status Network Monitor

The Current Status Network Monitor is an HTTP plug-in to data acquisition systems. The status monitor serves up html pages and provides an up-to-date digitizer status report to the user. The CGI script allows access to 4-hour seismic plots gathered from instruments. Automatic processing is carried out in real time by a system that operatively estimates the parameters of an earthquake source. This specially-designed program complex has functioned in an experimental operations mode and has been named the Fast Tsunami Source Localization (FTSL) algorithm.

Structurally the FTSL represents a set of program units (modules) which solve a number of subtasks. Input to and output of these program units is standardized. Modules are called by the main manager, which prepares the system to begin work, traces the data quality, logs detected earthquakes and their parameters, and detects possible errors in the program complex functioning. The programs share a similar method of construction, allowing for flexible detection and processing of seismic signals. Also, a wide field remains for subsequent modernization, both within the limits of an extended production string, and in the form of escalating the quantity of analysis algorithms at all hierarchical levels.

At the present time, a rather simple algorithm for detecting and estimating parameters has been realized, aimed at the fastest acquisition of epicenter coordinates. However, despite its simplicity, the technology includes elements of self-checking when new data are received (especially when data from new stations are included). In particular, it allows improbable magnitude values to be reliably excluded.

Earthquake detection is carried out using variations of the well-known algorithm STA/LTA. We have demonstrated that when tsunamigenic earthquakes (high signal/noise ratio) are detected, this method allows reliable results to be achieved.

In the process of data accumulation at each station, the following information is taken from the record of the detected earthquake: a source azimuth, the arrival time of an S-wave, the arrival time of a surface wave maximum, and the magnitude, M_S . P-wave arrival time is determined during the detection of the seismic event. Although the opportunity exists to estimate epicenter coordinates using the arrival times of P- and S-waves, the current priority remains to define epicenter coordinates on azimuths on a source, because this is the fastest method. For estimating an azimuth on the source, 10-15 seconds of earthquake record are sufficient; thus, the first estimation of coordinates is generated practically at once after a P-wave arrives at the second station.

To determine M_S , we intend to use a modified scale based on 20-second periods that was offered by A.A. Gusev, and is now in development. The Tsunami Warning System uses the beta-version of this scale. The scope of this new scale begins with epicentral distances within one degree of an arch of the big circle.

The described system has been applied in a regional network of 5-6 stations, including Kamchatka regional network stations, and also the IRIS global network, for earthquakes $M > 6.0$ on Kamchatka, the Kuril Islands, and in Japan; within five minutes of detecting the first arrival, this network allows us to assess coordinates of an epicenter to within 100 km, and to estimate M_S to within 0.1-0.2.

These results have been achieved using archival records of the strongest earthquakes since 1993, and also in experimental operations mode since 2008.

ACCRETIONARY TECTONICS OF SOUTHERN ALASKA CONSTRAINED BY GPS

Julie Elliott¹, Jeff Freymueller¹, and Chris Larsen¹

¹*Geophysical Institute, University of Alaska, Fairbanks, AK, USA.*

The eastern end of the Aleutian subduction zone marks the transition from normal subduction to a complex collisional boundary involving the Pacific plate, the southern Alaska block, and the Yakutat block, an allochthonous terrane actively accreting to the southern Alaskan margin. This collision plays a leading role in the tectonics of southern Alaska. The eastern asperity of the 1964 earthquake may be related to the interface between the buoyant Yakutat block and southern Alaska. The dextral Fairweather fault, which generated several M>7 earthquakes during the past century, forms the eastern boundary of the Yakutat block. The northeast edge of the block is demarcated by the St. Elias orogen, which hosts over half of North America's 25 highest peaks. Previous studies established high rates of motion for the Yakutat block, but insufficient data prevented the development of a detailed, comprehensive regional tectonic model for this crucial area. We present a GPS dataset that spans the region and use that data to constrain relative block motions and fault slip rates in southern Alaska.

In southeast Alaska, extremely large, northwest-directed GPS velocities are observed along the coast west of the Fairweather fault. Inboard of the Fairweather fault, GPS velocities have smaller magnitudes and display a clockwise rotation. Further east, within the Canadian Cordillera, GPS velocities have a small but distinct motion relative to North America. The Yakutat block moves to the northwest at a rate of over 45 mm/yr relative to North America, resulting in nearly 40 mm/yr of NW-SE-directed convergence between the block and southern Alaska. Compared with the Pacific plate, the velocity of the Yakutat block is slower and more westerly.

The highest strain rates in the region occur across Icy Bay and the western edge of the Malaspina Glacier. Rates there approach -1 microstrain/yr, a value higher than that observed in the Himalaya. Lower, but still significant, strain rates of about -0.2 microstrain/yr extend north from Icy Bay to the region surrounding Mount St. Elias. These strain rates suggest that the current deformation front between the Yakutat block and southern Alaska is located within the Icy Bay area. Our preliminary modeling indicates that multiple NW- and N- directed thrust faults in Icy Bay, along the western edge of the Malaspina Glacier, and between Icy Bay and Mount St. Elias are required to explain the GPS observations. Over 50% of the relative convergence between the Yakutat block and southern Alaska may be accommodated by slip on these faults.

The second major focus of compressive strain in the St. Elias orogen is centered over the Yakataga fold-and-thrust belt. Strain rates there are in the range of -0.40 to -0.50 microstrain/yr. Little significant strain is seen across the Bagley icefield or to the north of that feature. These results suggest that most of the convergence between the Yakutat block and southern Alaska is currently accommodated on structures located south of the Bagley icefield, specifically in the Icy Bay, upper Malaspina/Mount St. Elias, and Yakataga fold-and-thrust belt regions.

A POINT IN A VOLCANIAN ERUPTION: DECOMPOSING THE CONTINUOUS GPS RECORD OF THE 2008 KARYMSKY ERUPTION USING WAVELETS

Ronni Grapenthin¹, Jeffrey T. Freymueller¹, Vilory Bakhtiarov², Sergey Serovetnicov²

¹*Geophysical Institute, Univ. of Alaska Fairbanks, AK, USA.*

²*Kamchatkan Branch of Geophysical Service of RAS, Petropavlovsk-Kamchatskiy, Russia.*

On 25 July 2008, an international group of scientists witnessed three discrete explosions of Karymsky Volcano, Kamchatka. The events occurred at 14:11, 14:39, and 15:11 local time (UTC+13). A continuous GPS site (KRMS) located at the base of the edifice recorded this period of unrest with a 30 s sampling rate. Its horizontal distance to the vent is about 0.5 km. Since the recorded data is a superposition of contributions from many processes as well as noise we use wavelet analysis to decompose the signal.

In wavelet analysis a signal is represented by scaled and translated versions of a so-called mother wavelet; a short, oscillating wave of finite energy. This technique resolves a problem inherent to Fourier analysis and its descendants which assume (periodic) signals that are, at least over short periods, not time dependent, as well as reasonably smooth. When monitoring natural processes this assumption is a limiting factor to interpretations of the frequency representation of a signal. The fixed window length in a windowed Fourier approach biases the distribution of energy over the frequency range and lacks the ability to point out self-similarities within the signal. Post-seismic relaxation, for example, shows a pattern of exponential decay with a relaxation time depending mostly on the size of the preceding earthquake, the viscosity of the mantle, and distance of the observer to the epicenter. Given relatively noisy data such features might be hidden in Fourier transform based spectrograms and require filtering that adds more assumptions to the analysis process.

Employing wavelet analysis we are able to decompose non-periodic, time dependent signals with sharp peaks and discontinuities such as steps based on scale. For the KRMS data we use these characteristics to eliminate tide load contributions as well as noise from the data and to isolate the signal related to the volcanic events of July 25, 2008.

GRAVITY ANOMALY OVER THE NORTHERN HOKKAIDO REGION, NORTHERN JAPAN

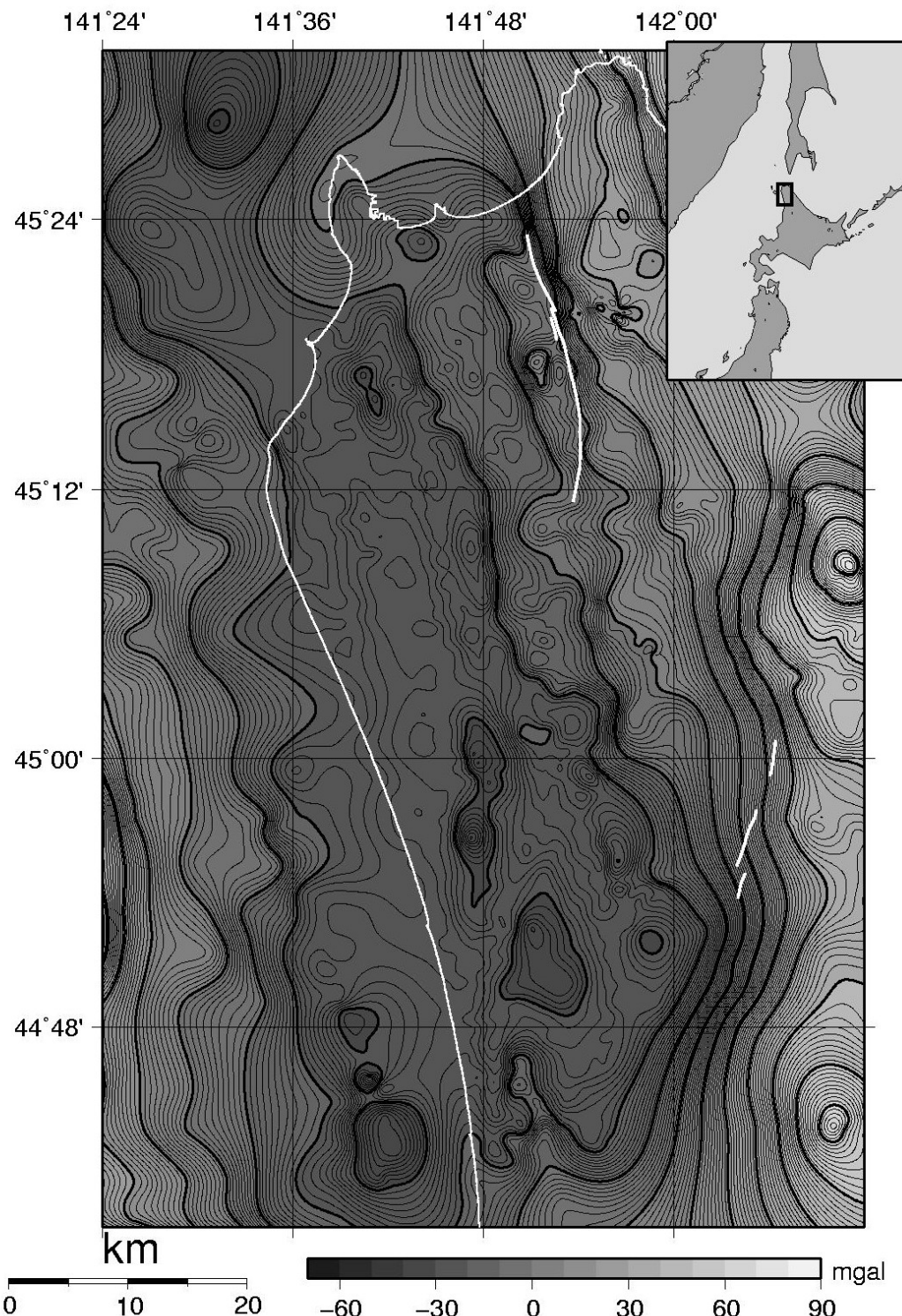
Ryo Honda, Minoru Kasahara and Toru Mogi

Institute of Seismology and Volcanology, Graduate School of Science, Hokkaido University.

The northern part of Hokkaido Island (the Dohoku region) exhibits relatively high seismicity. According to recent research, this region is recognized as the boundary between the Okhotsk and the Amurian plates, and strain concentration has been reported based on triangulation and GPS observations (GSI Japan, 1997; Takahashi *et al.*, 1999). However, no intraplate earthquakes larger than M_{JMA} 6 were observed in the Dohoku region until the 2004 Rumoi-Nanbu earthquake (M_{JMA} 6.1) occurred, and another large intraplate earthquake may occur in the future. The CMT of the earthquakes ($M_{JMA} > 5$) observed in the Dohoku region is strike-slip and thrust type, owing to the east-west compression. Active faults have also been reported by geologic and topographic researchers. Recurrent thrust-type faults, which are dominant in this region, generate positive Bouguer gravity anomalies over the hanging wall side, and horizontal gravity gradients above fault lines. Plentiful gravity observation data have been collected in this region for the purpose of oil and mineral exploration. However, these data exist as a handwritten paper document, and they have not been released to the larger scientific community. Therefore, we have been taking gravity measurements in this region since 2007. These new data demonstrate the data yield an improved picture of the gravity anomaly distribution over the Japan Sea side of the Dohoku region, clearly indicating that the lineament of a large horizontal gravity gradient coincides with the Horonobe Fault (Research Group for Active Faults, 1991). This may indicate a cumulative faulting in the same place.

References

- Geographical Survey Institute of Japan, 1997, [〈http://vlDb.gsi.go.jp/〉](http://vlDb.gsi.go.jp/) .
Takahashi, H., M. Kasahara, F. Kimata, S. Miura, K. Heki, T. Seno, T. Kato, N. Vasilenko, A. Ivashchenko, V. Bahtiarov, V. Levin, E. Gordeev, F. Korchagin and M. Gerasimenko, 1999. Velocity field around the Sea of Okhotsk and Sea of Japan regions determined from a new continuous GPS network data, *Geophys. Res. Lett.*, **26**, 2533-2536.
Research Group of Active Faults of Japan, 1991, "Active Faults in Japan", Univ. of Tokyo Press, pp. 1-437 (in Japanese with English abstract).



DIRECT MEASUREMENTS OF TSUNAMI EROSION BY THE KURIL BIOCOMPLEXITY PROJECT: THE 2006 AND 2007 KURIL ISLAND EVENTS

Breanyn MacInnes¹, Joanne Bourgeois¹

¹*Earth & Space Sciences, Univ. of Washington. Seattle, WA, USA.*

The tsunamis produced by the 15 November 2006 Kuril earthquake (Mw 8.1-8.4) and the 13 January 2007 earthquake (Mw 7.9-8.1) changed the coastal geomorphology in the central Kuril Islands. The Kuril Biocomplexity Project conducted pre- and post-tsunami surveys of the islands that included topographic profiles measured before the tsunamis (2006) and reoccupied afterwards (2007). Comparison of these profiles and our observations allow us the confidence to attribute many changes to the tsunamis, in spite of an absence of eyewitness accounts in the central islands.

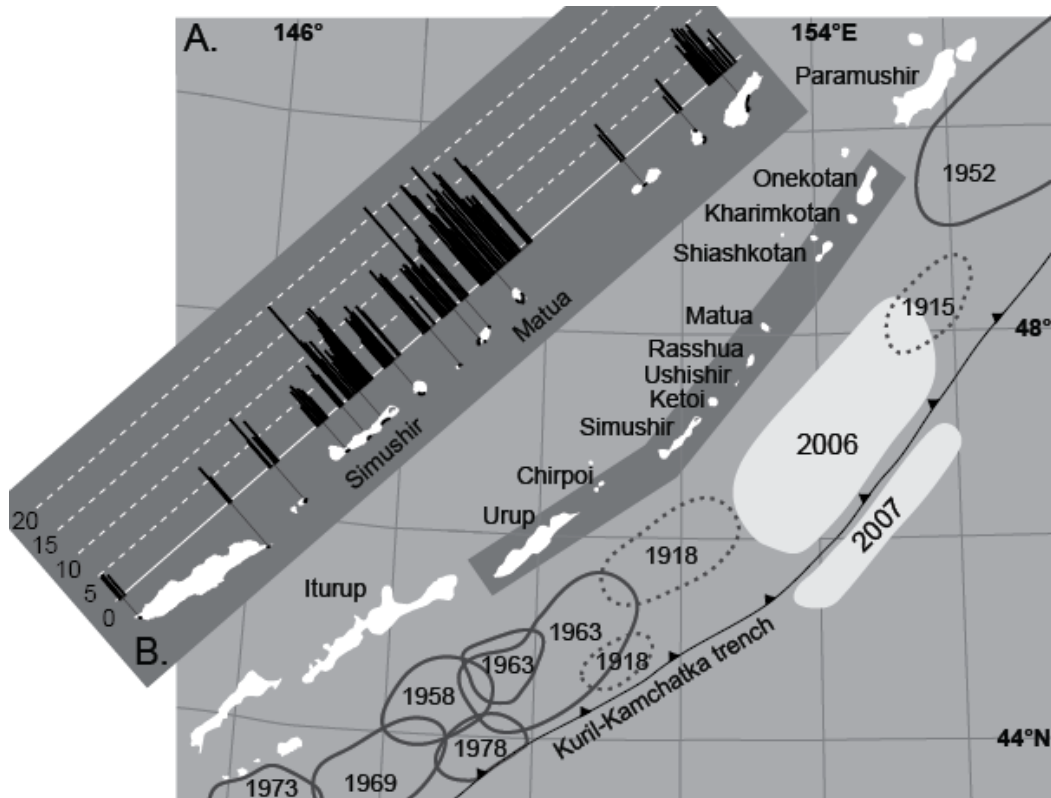


Figure 1: A: Location of the 2006 and 2007 Kuril Island earthquakes as well as other historical tsunamigenic earthquakes in the region. B: Runup observations (in meters) collected by the Kuril Biocomplexity Project and the Institute of Marine Geology and Geophysics, Yuzhno-Sakhalinsk in the 2007 and 2008 field seasons.

While effects on many shorelines were dramatic, areas with low runup, <8 m, experienced limited geomorphic change, primarily confined to the beach or stream channels. Erosion on vegetated sections of coast occurred only as patches (usually <1-3 m in diameter). The volume of sediment per profile removed from coasts with low runup ranged from 5 m³ to 50 m³, dominantly occurring on unvegetated beaches.

Regions with high runup, >15 m, experienced massive erosion that dramatically altered the coastline and will be observable for decades to centuries. The tsunami removed ~200 m³ of sediment per profile in high runup regions. Continuous deep erosion of vegetation and sediment occurred on the seaward 100-200 m of the coast, including landward widening of the beach from back-beach cliff retreat (Fig. 2). The tsunami removed seaward-most beach ridges, reduced others in size, and eroded seaward-facing slopes primarily by stripping young, sandy sediment off the surface.

The 2006 and 2007 tsunamis produced net offshore sediment transport in the Kuril Islands. The amount of sediment eroded by the tsunami far outweighed the amount deposited on land in all cases studied; in eight cases with measured volumes of both erosion and deposition, the amount of tsunami-transported sand preserved on the coastal plain was usually <10% of that eroded. Even where the tsunami was the smallest, erosion the least, and deposition the most extensive, three times more sediment was removed from the coast then deposited on land. The tsunami was dominantly erosive in the Kuril Islands because the high-relief topography of the coastline accelerated tsunami outflow.

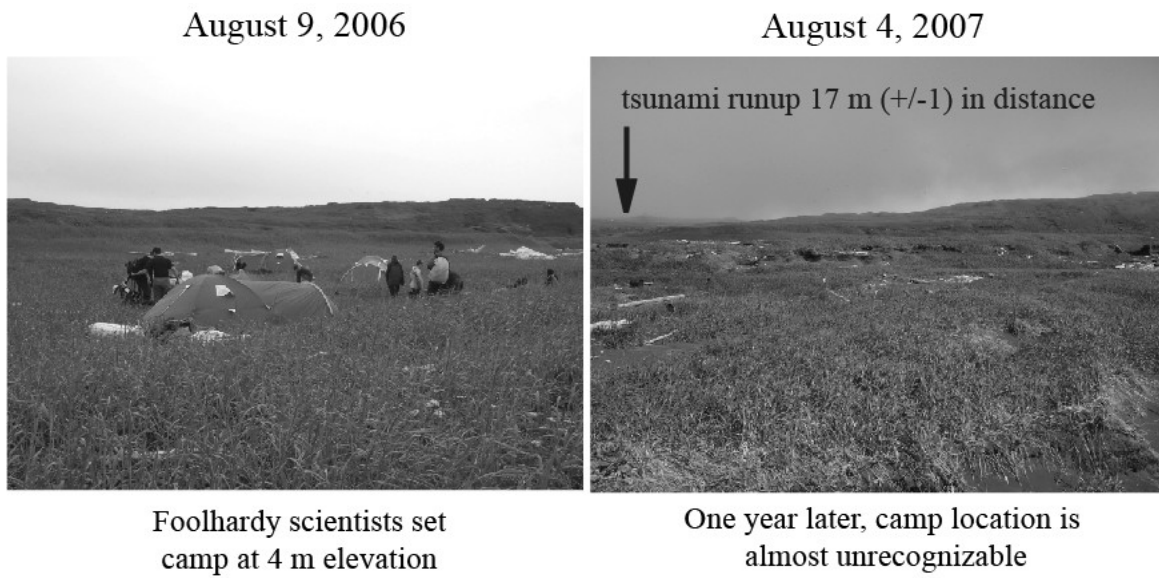


Figure 2: Images from before and after the 2006 and 2007 Kuril Island tsunamis. The location where the photographer stood for the 2006 image had become the beach in 2007. (Photos: Misty Nikula).

PROSPECTS FOR RECONSTRUCTING THE HISTORY OF GREAT EARTHQUAKES AND TSUNAMIS IN THE CENTRAL ALEUTIANS

Alan Nelson

Geologic Hazards Team, U.S. Geological Survey, Golden, CO USA.

Despite being one of the most seismically active plate boundaries and the source of some of the largest historical earthquakes and accompanying tsunamis, the earthquake prehistory of the Aleutian arc is little known. In the eastern Aleutian-Alaska subduction zone, where the orthogonally subducting plate dips gently beneath a wide forearc, signs of as many as nine plate-boundary earthquakes in the past 5000 years have been identified at tens of sites spanning 650 km of the subduction zone. But in the central and western Aleutian arc, where convergence increases from right oblique to strike-slip in the far west and the forearc is faulted into rotating blocks, the record of prehistoric earthquakes and tsunamis remains unstudied. Is the series of great earthquakes that ruptured much of the subduction zone in the mid-twentieth century a repeat of a pattern common in the past? Are the 1957, 1965, and 1986 M8 earthquakes of this series, each of which ruptured several structural segments of the arc and spawned high tsunamis, typical or unusual? Can even greater central Aleutian earthquakes send higher tsunamis across the Pacific?

Paleoseismology has answered similar questions for other plate boundaries, but most paleoseismic techniques are difficult to apply at subduction zones where plate boundaries lie tens to hundreds of kilometers offshore. Indirect methods of identifying signs of great subduction earthquakes and their tsunamis center on identifying (1) sudden shoreline uplift or subsidence during earthquakes caused by regional strain release in the overriding plate or slip on shallow faults within it, or (2) the deposits or erosional effects of tsunamis generated by seafloor displacement during earthquakes. The identification and dating of seismically induced turbidites in forearc canyons offers the greatest potential for developing long, arc-wide earthquake chronologies, but the vast resources needed for such research has limited its application. Other techniques common in paleoseismology, such as identifying paleoliquefaction features that record strong ground motion or dating slip on shallow surface faults, have been used infrequently at subduction zones.

Prospects for identifying great earthquakes using uplifted shorelines are quite limited in the central Aleutians. The optimism of a few decades ago that each marine terrace on a subduction-zone coast records a separate plate-boundary earthquake has waned with the recognition that many terraces were raised partly through interseismic processes, that many record slip on shallow crustal faults that may or not be synchronous with plate-boundary earthquakes, and that those that do record a single earthquake may only record the greatest earthquakes. Most central Aleutian islands lie well arcward of modeled areas of regional forearc uplift during plate-boundary earthquakes. Even the islands closest to the trench—Chirikof, the outermost Shumagins, and the Sanaks—are no closer to the trench than southwest Kodiak Island, which was just arcward of the zone of coseismic uplift in 1964. Oblique subduction and steepening plate-boundary dips westward along the arc suggest that regional zones of coseismic uplift and subsidence have been narrower than in the eastern arc. Winslow and Johnson used elevations as high as 44 m from inferred marine terraces at 120 locations in the Shumagin Islands and adjacent Alaska Peninsula with 54^{14}C ages on peat overlying marine surfaces to deduce local relative sea-level histories for the past 12,000 years. Inconsistencies in apparent uplift rates across

the island group were inferred to result from differential uplift on fault-bounded blocks, but rates are too high to be explained by slip on shallow faults.

Prospects for identifying and dating coseismic subsidence in the central Aleutians are better than for identifying uplift because (1) past zones of regional coseismic subsidence may encompass some southerly islands, (2) some of these islands have tidal marshes likely to preserve a record of sudden subsidence, and (3) new microfossil methods of reconstructing relative sea-level changes (precision ≤ 0.2 m) allow previously undetectable changes to be measured. For example, Shennan and Hamilton used fossil diatom floras to infer that subsidence during seven great earthquakes of the past 4000 years at Cook Inlet was similar to or less than that in 1964. Limited high-resolution Google Earth air photos of parts of some islands show <500-m-wide tidal marshes at the heads of some inlets and fringing lagoons behind barrier beaches. Gilpin developed an earthquake history from evidence at similar, more abundant sites on Kodiak Island. Small lakes at elevations of 2–25 m are common on some islands (for example, Sanak) and a detailed relative sea-level history might be reconstructed if cores could be obtained from an elevational succession of lakes.

Surely the best prospects for identifying signs of great earthquakes in the central Aleutians lie with detailed mapping of tsunami deposits. Google-Earth photos show many islands have several or more inlets with 300–3000-m-wide beach ridge sequences and/or adjacent 3-to-25-m-high lakes or sphagnum bogs. Detailed studies of much larger beach ridge complexes in Hokkaido and Kamchatka revealed the deposits of 15 high tsunamis in 6000 years and as many as 50 in 7000 years, respectively. In southern Oregon, a 150x400-m, 6-m-high lake contains a 5000-yr record of 12–13 local tsunamis. In a unusually thorough series of studies on the Norwegian coast, deposits from the tsunami generated by the 3200-km³ Storegga submarine slide were traced in 18 isostatically raised lake basins. As has been done on many subduction-zone coasts, careful site selection combined with thorough stratigraphy should allow the deposits of unusual storm tides or distant tsunamis to be distinguished from the deposits of Aleutian tsunamis. Distinguishing large local tsunamis generated by volcano flank collapse or submarine landslides—such as the 1946 tsunami that obliterated buildings at Scotch Cap on Unimak Island—from tsunamis produced by regional seafloor displacement will depend on the characteristics, number, and location of sites that can be studied. Many islands, such as the outer Shumagins, Unalaska, and Atka, are ringed with narrow inlets whose differing orientations could help determine tsunami source directions (assuming access to suitable trench-facing inlets).

An effective way to identify tsunamis accompanying great earthquakes is to correlate deposits of high tsunamis with times of sudden coastal subsidence identified through paleogeodesy studies in tidal marshes. As shown by the detailed studies of tsunami history in Japan and Kamchatka, widespread Aleutian tephras have the potential to provide far more accurate correlations of tsunami deposits and times of subsidence than ¹⁴C-based correlations of similar deposits at subduction zones such as Cascadia and south-central Chile. Although many Aleutian tephras are undated, thorough AMS ¹⁴C, ¹³⁷Cs, and ²¹⁰Pb dating of tephra sequences in key sections should allow the field characteristics of some tephras to be used to extend late Holocene timelines widely. Subsequent lab analysis of tephras may allow correlations over greater distances of hundreds of kilometers.

TSUNAMI MODELING AND INUNDATION MAPPING IN ALASKA: CURRENT STATUS OF THE PROJECT

Dmitry Nicolsky, Roger Hansen, Elena Suleimani, David West
Geophysical Institute, University of Alaska Fairbanks, AK, USA.

The Alaska Earthquake Information Center (AEIC) participates in the National Tsunami Hazard Mitigation Program by evaluating and mapping potential tsunami inundation of coastal Alaska. We develop hypothetical tsunami scenarios based on parameters of potential underwater earthquakes and landslides for specified coastal communities. We perform simulations for each of the source scenarios using AEIC's recently developed and tested numerical model of tsunami wave propagation and runup. The modeling results are then delivered to the community for local tsunami hazard planning and construction of evacuation maps.

Making maps that communicate information effectively and are easily distributed is a challenge for any hazard mitigation campaign, particularly when the Geographic Information System (GIS) source data are generally inaccessible to the public. Delivery of tsunami hazard information is especially challenging in Alaska, where coastal communities are difficult to access and have very limited resources for disaster planning. Though our modeled results are still formally distributed in professional GIS formats and static illustrations, we have found the simplicity and flexibility of the KML platform to be useful in education and circulation to a wider audience, namely to residents and officials in at-risk communities. With a reasonably well-equipped computer, an internet connection, and free Google Earth software, residents can explore dynamic 3-D tsunami visualizations of their own community, gaining a strong impression of what to expect and how to react in the case of tsunami.

STRONG SUBDUCTION-ZONE EARTHQUAKES AND TSUNAMIS ALONG SOUTHERN KAMCHATKA AND THE NORTH KURIL ISLANDS DURING THE LATE HOLOCENE

Tatiana Pinegina¹, Joanne Bourgeois²

¹*Institute of Volcanology & Seismology, Petropavlovsk-Kamchatskiy, Russia.*

²*Earth & Space Sciences, Univ. of Washington. Seattle, WA, USA.*

Tsunamigenic earthquakes in subduction zones can be classified into three types depending on source location: typical interplate earthquakes, intraplate earthquakes (including outer-rise events, intraslab events in the downgoing plate, and crustal earthquakes in the overlying plate, if the sources are under water); and tsunami-earthquakes at the shallow extension of the interplate seismogenic zone beneath the accretionary wedge (Satake and Tanioka, 1999). The type of earthquake and earthquake parameters influence the tsunami intensity and tsunami height particularly in the zone nearest to the source (Geist and Dmowska, 1999). The majority of disastrous tsunamis arise during the largest interplate earthquakes. Since large displacement is possible with comparatively low shear modulus during tsunami-earthquakes, these earthquakes also are capable of generating powerful tsunamis on the nearest coasts.

Tsunami deposits from different types of tsunamigenic earthquakes are also different--more with regard to their horizontal, vertical and map distribution--less their content, which relies strongly on available sediment source. For example, distance of tsunami penetration (that is, *inundation*) and therefore of tsunami deposits from a great interplate earthquake can be significantly greater than inundation from a tsunami earthquake, even if vertical runup is comparable, because the wavelengths are different. Moreover, intraplate earthquakes usually generate only local tsunamis with shorter inundation and lower runup; thus tsunami deposits from intraplate earthquakes are limited to the first 10s to 100s of meters from the shore. Even if runup is locally high in these cases, the distance along the coast where high runup can be observed is comparatively short (also see Okal and Synolakis, 2004).

Detailed study of tsunami deposits along hundreds of km of coastline can help to clarify which type of earthquake has caused a disastrous tsunami (for example, Nanayama et al., 2003). To differentiate tsunamis from the different sources, we use the following criteria: 1) elevation of the tsunami deposits above sea level; 2) distance from the shoreline where tsunami deposits pinch out; 3) thickness of tsunami deposits along a line perpendicular to the shore; 4) presence of erosional features at the base of tsunami deposits; 5) possibility of correlation of the same tsunami layer from excavation to excavation in the same locality; and 6) possibility of correlation of the same tsunami layer at the different localities. The latter exercise is the most challenging (e.g., see Martin et al., 2008)

During our paleoseismological investigations along Kamchatka and the northern Kurils (field seasons 1997-2008), we have correlated, compared and analyzed data from multiple historical and prehistorical tsunami deposits. Based on cumulative results, we have selected the most disastrous tsunamis and identified also less significant events. The strongest two historical tsunamis on Kamchatka and the northern Kurils occurred in A.D. 1952 (Mw ~9.0) and A.D. 1737. Our tsunami-deposit data allow us to conclude that the sources of both earthquakes were comparable in size and that their sources approximately coincided spatially. [See also MacInnes Kamchatka 1952 JKASP abstract herein.]

We have also established that during the last ~1000 years, at least 2-3 catastrophic tsunamis (in addition to 1952 and 1737 events), have occurred along southern Kamchatka and the northern Kurils, or one event per 200-250 years on average. For the last ~1500 years in the same region 5-6 strong tsunamis were identified, or 1 event per 230-280 years on average. We think that all these events were produced by interplate earthquakes with $M_w \sim 8.5$ -9.0. Other tsunami layers, which are not correlated between coastal sites, may be connected with smaller ruptures, possibly even landslides.

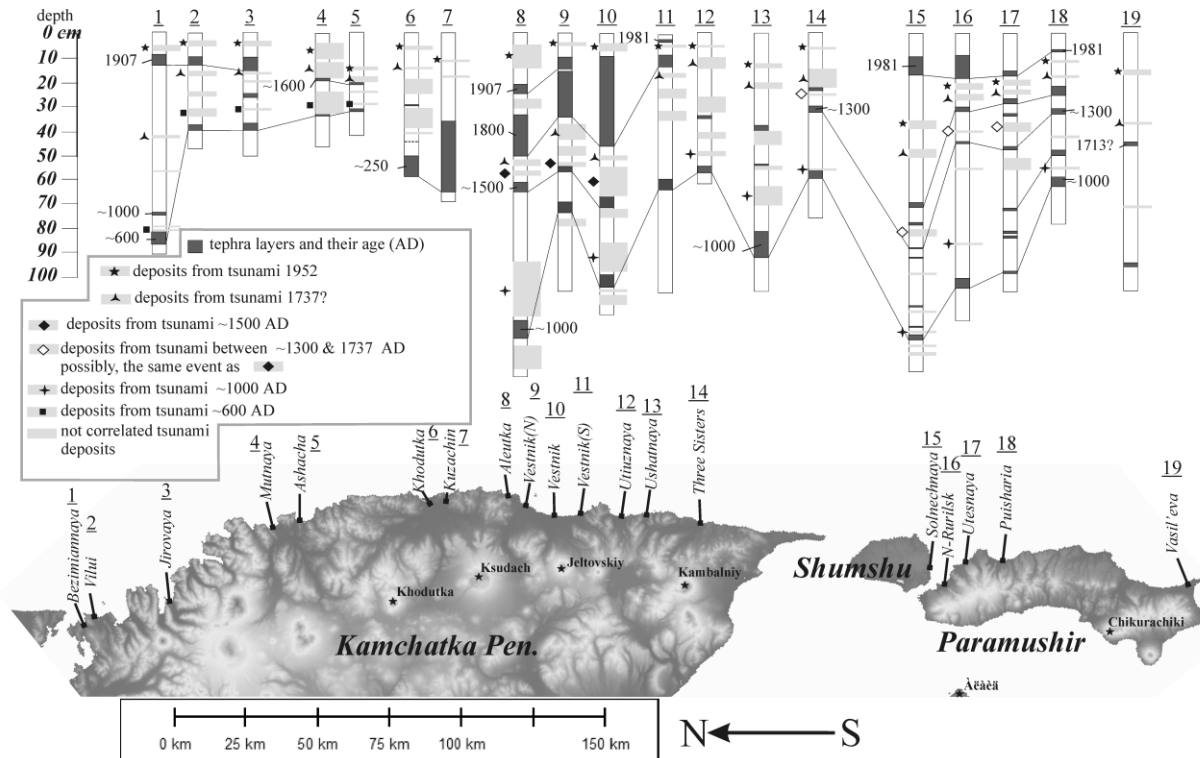


Fig.1. Correlation of most prominent tsunami deposits for the last ~1000-1500 years

References

- Geist, E.L. and Dmowska, R., 1999. Local tsunamis and distributed slip at the source, *Pure and Applied Geophysics*, v. 154, p. 485-512.
- Martin, M.E., Weiss, R., Bourgeois, J., Pinegina, T.K., Houston, H., and Titov, V., 2008, Combining constraints from tsunami modeling and sedimentology to untangle the 1969 Ozernoi and 1971 Kamchatskii tsunamis, *Geophysical Research Letters*, v. 35, L01610, doi:10.1029/2007GL032349
- Nanayama, F., K. Satake, R. Furukawa, K. Shimokawa, B. F. Atwater, K. Shigeno and S. Yamaki, 2003. Unusually large earthquakes inferred from tsunami deposits along the Kuril Trench. *Nature*, v. 424, p. 660-663.
- Okal, E.A. and Synolakis, C.E., 2004. Source discriminants for near-field tsunamis, *Geophys. J. Internat.*, v. 158, p. 899-912.
- Satake K, Tanioka Y, 1999, Sources of tsunami and tsunamigenic earthquakes in subduction zones, *Pure and Applied Geophysics*, v. 154, p. 467-483.

INVESTIGATION OF PRE-, CO-, AND EARLY POST-SEISMIC CRUSTAL DEFORMATIONS CAUSED BY OLUTORSKOE (20.04.2006, Mw=7.6) AND GREAT KURIL (15.11.2006, Mw=8.3; 13.01.2007, Mw=8.1) EARTHQUAKES FROM KINEMATIC ANALYSIS OF 30-SEC GPS DATA

Nikolay Shestakov^{1,2}, Vilory Bakhtiarov³, Vasily Levin³, Nikolay Titkov³, Sergey Serovetnikov³, Nikolay Vasilenko⁴, Alexander Prytkov⁴, Dmitry Frolov⁵

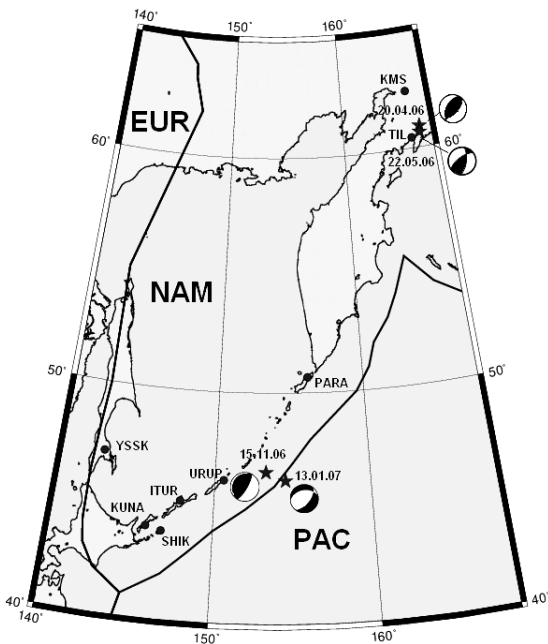
¹Institute of Applied Mathematics FEB RAS, Vladivostok, Russia.

²Far Eastern National University, Vladivostok, Russia.

³Kamchatsky Branch of Geophysical Service RAS, Petropavlovsk-Kamchatskiy, Russia.

⁴Institute of Marine Geology and Geophysics FEB RAS, Yuzhno-Sakhalinsk, Russia.

⁵Ioffe Physico-Technical Institute, RAS, St. Petersburg, Russia.



In 2006-2007 three great earthquakes occurred in the Russian Far East: Olutorskoe earthquake (Koryakia, 20.04.2006, Mw=7.6) and two Kuril earthquakes (central part of the Kuril Islands Arc, 15.11.2006, Mw=8.3 and 13.01.2007, Mw=8.1). The first earthquake was probably the result of the collision of the North American plate with the hypothesized Beringia microplate. The two Kuril events can be associated with the subduction process between the Pacific and North American plates.

Crustal deformations associated with these earthquakes were previously investigated by analyzing the averaged daily positions of the Kamchatsky GPS Network (KAMNET) sites (Levin *et. al.*, 2007), the Kuril GPS Array (Steblov *et. al.*, 2008), and the northern part of the GPS Earth Observation Network (GEONET) of Japan (Takahashi and Kasahara, 2007). Significant horizontal co-seismic displacements up to a few decimeters caused by the main shock were found for the

stations nearest to the epicenters of the first two earthquakes. Small co-seismic offsets (10 mm and less) caused by the first Kuril earthquake (15.11.2006) were detected even at distant GPS stations located 900-1200 km from the epicenter.

In this study, we used a pseudo-kinematic analysis to investigate the short-term pre-, co- and early post-seismic deformations produced by the above-mentioned great earthquakes. We analyzed 30-sec GPS data recorded by two KAMNET stations (TIL, KMS) closest to the epicenter of the Olutorskoe earthquake and GPS data obtained by 5 stations of the Kuril GPS Array (PARA, URUP, ITUR, SHIK, KUNA) and the IGS station YSSK (see Figure 1). We utilized the GPS data recorded one week before and one week after the seismic event. The day in which the earthquake occurred was also included in our analysis. The GPS data recorded for the greatest aftershock of the Olutorskoe earthquake (22.05.2006, Mw=6.2) were also analyzed.

The BERNSE 5.0 software was used for GPS data processing. We estimated every epoch horizontal positions of each station by using the PPP (Precise Point Positioning) processing strategy implemented into the BERNSE software. Resolution of phase ambiguities was not applied.

Our analysis did not clearly show any pre-seismic movements preceding seismic events. All GPS stations, even distant sites, recorded the horizontal offsets related to surface wave propagation, despite the significant quasi-periodic variations of epoch to epoch station's positions. Surface wave signals were detected for all the earthquakes, including the largest aftershock of the Olutorskoe earthquake. The nature of quasi-periodic variations is also an object of great interest because they incorporate a lot of information about atmosphere, internal mass movements, and so on. It seems that the character of such variations for some stations slightly changes shortly before and after seismic events. However, this suggestion still requires further investigation.

We also tried to resolve horizontal co-seismic offsets for all sites where they were visually detected. We used the decomposition of initial signal before and after the event in order to remove quasi-periodic variations of epoch-to-epoch station positions (Kuleshov and Fishchenko, 2003). Our estimates of co-sesmic offset for the main Olutorskoe earthquake shock show a good agreement with static estimates (within 3 mm) and reveal a near-absence of early afterslip. No significant offsets were detected after the largest aftershock of this seismic event.

In contrast to Steblov *et. al.* (2008), we estimated the eastward co-sesmic offset at URUP station related to the 15.11.2006 Kuril event as approximately equal to 46 mm (~75% of the total offset), with a following afterslip approximately equal to 12-20 mm. This afterslip was released during the next 1.9 days after the main shock. We did not reliably resolve co-seismic offsets for other stations of the Kuril GPS Array due to their small size. We also did not detect a significant postseismic slip at any of the other GPS stations. The next great Kuril earthquake (13.01.2007) did not produce significant co-seismic slip or afterslip at any station of the Kuril GPS Array.

It is very important to install and operate high-rate GPS/GLONASS systems on the Kuril Islands, Sakhalin, and Kamchatka, together with broad-band seismic stations in order to have access to information about different geophysical processes in the Kuril-Kamchatka-Aleutian subduction zone.

References

- Kuleshov E.L., Fishchenko V.K. (2003) Wavelet transform used in optimal estimation of stochastic process trend, *Avtometriya*, 39(1): 86-94.
- Levin V.E., Bakhtiarov V.F., Pavlov V.M., Titkov N.N., Serovetnikov S.S. (2007) Preliminary geodynamic investigation results of the Olutorskoe earthquake 20(21) April 2006 by data of Kamchatka GPS network, Spec. issue about Olutorskoe earthquake 20(21) April 2006, First investigation results, Petropavlovsk-Kamchatsky: KB RAS, 251-262 (in Russian).
- Steblov G.M., Kogan M.G., Levin B.V., Vasilenko N.F., Prytkov A.S., Frolov D.I. (2008) Spatially linked asperities of the 2006–2007 great Kuril earthquakes revealed by GPS, *Geophys. Res. Lett.*, 35, L22306, doi:10.1029/2008GL035572.
- Takahashi H., Kasahara M. (2007) Geodetic constraint on the slip distribution of the 2006 central Kuril earthquake, *Earth Planets Space*, 59: 1095– 1098.

Acknowledgments. We thank Prof. E.L. Kuleshov for constructive discussion about the GPS time series processing. A.V. Mischenko provided his code for decomposition of GPS time series. The GMT software was partially used to plot the figure. This study was supported by grants from the FEB RAS № 09-III-B-08-480, 09-III-A-08-441, 09-III-A-08-438, and RFFI № 08-05-00197-a.

IMPROVEMENT IN DETECTING VOLCANIC EVENTS WITH DESDynI MISSION

Sang-Ho Yun, Scott Hensley, Paul Rosen, Paul Lundgren

Jet Propulsion Laboratory, California Institute of Technology, Pasadena, CA, USA.

Synthetic Aperture Radar Interferometry (InSAR) has revolutionized the study of volcanic deformation providing millimeter-scale accuracy of ground displacement measurements at tens of meters spatial sampling over the volcanic edifice and the surrounding area. This often provides more than enough spatial coverage and resolution to estimate the model parameters of the magma chamber at depth. However, the sparse sampling of InSAR measurements in time (24- to 46-day revisit period) can significantly limit its ability to resolve shorter time scale transient events, one of the keys to understanding the mechanism dynamics of magmatic systems.

Volcanic eruption events have wide ranges of duration from a day to tens of years. During the past 108 years (from 1900 to the end of 2008), about 3800 volcanic eruptions were recorded worldwide (Siebert and Simkin, 2002). Among them we identify about 1200 (31%) eruption events that lasted for a month or less, and about 500 (13 %) eruption events lasted for a week to a month. The eruption events that lasted for a month or more may also have had short-term transient signatures at the beginning. Sometimes the events are intermittent, and the eruption records show only the first and the last dates of the whole period. Thus, when it comes to transient activities that potentially have caused ground deformation, a much larger number of events would fall into these categories.

These short-term events are the ones that the DESDynI mission (the future U.S. L-band SAR satellite) would significantly improve our ability to capture their transient behavior with its proposed 8-day revisit period. Because most eruptions undergo pre-eruptive inflation and co-eruptive deflation, a month-long sampling interval of the existing missions is prone to severe aliasing when imaging the short-term events. Simulating volcanic intrusion and eruption events with geophysical modeling techniques, we demonstrate how different interpretations can be inferred from an event depending on how frequently the measurements are made. We also explore two different orbiting scenarios of 8-day repeat versus 24-day repeat with 8-day shift.

References

- Siebert L, Simkin T (2002-). Volcanoes of the World: an Illustrated Catalog of Holocene Volcanoes and their Eruptions. Smithsonian Institution, Global Volcanism Program Digital Information Series, GVP-3, (<http://www.volcano.si.edu/world/>).

GEOTHERMAL POWER

ORAL PRESENTATION

TAPPING GEOTHERMAL ENERGY IN ACTIVE VOLCANIC ENVIRONMENTS: LESSONS FROM WORLDWIDE PRODUCTION AND PLANS FOR MT. SPURR GEOTHERMAL DEVELOPMENT

Lucien Y. Bronicki and Brigitte A. Martini

Ormat Inc., 6225 Neil Rd., Reno, NV, 89511, USA.

More than one third of the energy from Ormat-owned and operated geothermal power plants is extracted from fields located in or directly adjacent to active volcanic environments. The last 40 years has seen Ormat grow its wholly-owned and operated geothermal energy production portfolio to over 500 MW, with a total of over 1200 MW worldwide production that includes sales of power units and turn-key power plants to other geothermal producers. Its combined cycle steam/binary plants have logged more than 19 million turbine hours of operation at very high capacity factors; greater than 70% of installed US capacity since 2000 has been Ormat technology. Unlike other geothermal companies, Ormat is a vertically-integrated geothermal and recovered energy-based equipment, services and power provider that designs, develops, builds and manufactures most of the equipment used in its plants. Part of this integration also includes its busy exploration arm that is charged with prospecting and proving up geothermal reservoirs for development. Ormat has worked in 24 countries and deployed power plants and units on all seven continents; many of these plants have been on the flanks of active volcanoes including, Puna on Hawai'i (30 MW), Amatitlan in Guatemala (20 MW) and Momotombo in Nicaragua (30 MW).

The high potential for geothermal power generation in active volcanic environments continues to lead exploration groups back to hot spots and the proverbial Ring of Fire over and over, but the attendant hazards of these resources must always be weighed against the possible power generation. Three different Ormat-operated geothermal fields, two in Central America and one in Hawai'i, are discussed with special emphasis on their original exploration and development as well as their specific hazards (eg. slow moving lava flows, high energy pyroclastic flows and earthquakes). Hazard preparedness plans for each site are outlined including details on Ormat associations with local, state and federal agencies (such as the Puna geothermal plant relationship with the Hawaiian Volcano Observatory-HVO).

In September of 2008, Ormat leased close to 36,000 acres on the southern flank of the eastern Aleutian Mount Spurr complex within the Kenai Peninsula Borough in the state of Alaska. This geologically young volcano with activity stretching over the past 250,000 years to the present is similar to other active arc volcanoes that have been exploited for geothermal power over the past several decades including those in Kamchatka, New Zealand, Japan, the Philippines, Indonesia and Central America. Much of the Mt. Spurr edifice is covered in glacial ice and snow and hence large portions of the geology here remain enigmatic. The recent activity in 1953 and 1992 (including thick ash fall and debris flows in 1953 and ash falls, lahars, pyroclastic flows and ballistic showers in 1992) both issued from the Crater Peak vent located approximately 3.5 km to the south of the main Summit vent (Waythomas and Nye, 2002); in turn Ormat leases begin just to the south of Crater Peak and extend down the flanks approximately 8.5 km covering portions of the Chakachatna River in the south. From the west at Chakachamna Lake to the east at Straight Creek, the geothermal leases stretch to just under 20 km in an east-west direction.

The relative inaccessibility (roadless and high-latitude short field seasons) of Mt. Spurr makes initial exploration of the Ormat leases more challenging, lengthy and expensive than

exploration activities at most of our other lease-sites. Previous exploration work in the mid-1980's (Wescott et al., 1985) built on previous basic mapping, petrologic and geochemical efforts and has provided an excellent starting point for our upcoming exploration activities; however there is more data to collect, interpret and synthesize into a geothermal system model for Mt. Spurr. Our initial 2009 reconnaissance plans include an expansion of the aqueous geochemical sampling efforts, focusing on not only the previously discovered hot spring and thermal seeps on the southern flank of Mt. Spurr, but also continued sampling of creeks issuing from beneath the glaciers that cover the edifice to the west and east. Encouraging geochemistry (Neal et al., 2006) from the Kid glacier suggests that additional sampling might reveal further information about sub-glacial geology and thermal manifestations. Besides drilling, geochemical sampling and geothermometer calculations are our best proxy for assessing the possible geothermal reservoir. We also plan to acquire high resolution aerial photography and/or satellite imagery of the entire Mt. Spurr region to aid in future geologic mapping and site-development activities. Higher level site-intensive exploration (geophysics and gradient drilling) will be guided by this initial 2009 reconnaissance and will not commence until the 2010-2012 timeframe.

In addition to standard geothermal exploration (geology, geochemistry, geophysics and drilling), Mt. Spurr will require additional attention to hazard assessment; this information will receive paramount weighting within the development models of the possible geothermal reservoir. The on-going monitoring and assessment studies of the Alaskan Volcano Observatory and affiliated personnel of the University of Alaska system serve as a baseline from which Ormat will move forward in siting and designing the possible future geothermal power plant. The co-occurrence of Ormat leases with lahar and pyroclastic flows is of primary concern in addition to possible flooding in the Chakachatna River Valley. Ormat plans to work closely with state and federal agencies in maintaining and possibly augmenting volcanic hazard monitoring systems such as seismic stations, tilt-meters, satellite-based thermal and radar measurements and on-site gas detectors and web-cams. Though new infrastructure (roads and transmission lines) and highly innovative partially autonomous power plant designs will make the Mt. Spurr development far more accessible and safe, Ormat fully appreciates the active volcanic nature of its leases.

- Neal, C.A., McGimsey, R.G., Dixon, J.P., Manevich, A. and Rybin, A., 2009, 2006, Volcanic activity in Alaska, Kamchatka, and the Kurile Islands: Summary of events and response of the AVO: USGS Scientific Investigations Report 2008-5214, 102p.
Waythomas, C.F. and Nye, C.J., 2002, Preliminary Volcano-Hazard Assessment for Mount Spurr Volcano, USGS Open File Report 01-482.
Wescott, E.M., Turner, D.L., Nye, C.J., Motyka, R.J. and Moore, P., 1985, Preliminary report on geothermal resource investigations at Mt. Spurr, Alaska: ADGGS Public Data File 85-65.

**COMPARATIVE STUDY OF BEZYMIANNY,
SHIVELUCH, AND MOUNT ST HELENS VOLCANOES –
RESULTS OF PIRE-KAMCHATKA PROJECT**

ORAL PRESENTATIONS

EVOLUTION OF DEPOSIT CHARACTERISTICS OF BLAST-GENERATED PYROCLASTIC DENSITY CURRENT WITH DISTANCE FROM VOLCANO: KEY TO TRANSPORTATION/DEPOSITION MECHANISMS OF THE BEZYMIANNY, 1956 AND MOUNT ST. HELENS, 1980 EVENTS

Alexander Belousov¹, Marina Belousova^{1,2}, Amanda B. Clarke³, Barry Voight⁴, Kim Genereau³

¹*Academia Sinica, Taipei, Taiwan.*

²*Institute of Volcanology and Seismology, Petropavlovsk, Russia.*

³*Arizona State University, Tempe, USA.*

⁴*Pennsylvania State University, State College, USA.*

Directed blasts generate very energetic, high-velocity pyroclastic density currents (PDCs), which travel long distances and leave peculiar deposits. Understanding factors which govern propagation of blast-generated PDCs as well as mechanisms of particle transport and deposition are important due to the extreme destructive potential and world-wide distribution of blast-prone volcanoes. We report results of detailed stratigraphic investigations in the NW sector of the 1980 Mount St. Helens (USA) blast deposit. The new data are compared to the data collected along the axis of the 1956 Bezymianny (Kamchatka, Russia) blast deposit. Characteristics of both blast deposits, despite very strong local variability, demonstrate similar trends with distance from vent. In general, the deposits become thinner, finer grained, and better sorted; percentage of juvenile clasts increases, while average density of constituent rock clasts (both juvenile and accidental) decreases. This proves the ability of blast-generated PDCs to effectively sort clasts with respect to size and density, and therefore suggests low particle/gas ratio in comparison to conventional pyroclastic flows. One remarkable feature of both deposits is that the proximal-to-distal changes in all major lithologic parameters demonstrate an abrupt discontinuity at distances ~2/3 of the total distances traveled by the PDCs (~18 km at Bezymianny and 15 km at Mount St. Helens). We hypothesize that in the proximal zone the PDCs were driven mostly by momentum obtained from gravitational collapses of the parental explosions, while in the distal zone they were driven mostly by the density difference between the PDCs and surrounding air ('density current' sensu stricto). The momentum was the source of energy supporting high turbulence in the proximal zones, allowing the blast clouds to transport exceptionally big (boulderly) rock fragments as well as to severely erode and incorporate the substratum. After dissipation of the momentum, the PDCs continued to travel due only to density contrast with the atmosphere. Accordingly, the velocity, turbulence intensity, and hence transport capacity (expressed in dimensions and concentration of rock fragments) and erosive action of the PDCs abruptly diminished, as reflected in deposit characteristics.

COMPOSITIONAL TRENDS AT BEZYMIANNY VOLCANO

Pavel Izbekov and PIRE team

Geophysical Institute, University of Alaska Fairbanks

Frequently erupting active volcanoes are unique natural laboratories, which allow the dynamics of short-term magma processes investigated. It appears that a composition of magma system may change at timescales as short as several weeks, e.g. the 1996-present eruption of Karymsky volcano, Kamchatka (Eichelberger & Izbekov, 2000; Izbekov et al, 2004). Such variations would remain unnoticed without sampling of eruptive products, which time of eruption is known precisely. Time-series of samples, each of which represents a snapshot of compositionally changing magma system, may help to distinguish magma processes that drive volcanic eruptions.

Bezymianny volcano, Kamchatka has been in a state of almost continuous eruptive activity since October 1955. On March 30, 1956 a sudden collapse of the edifice triggered a devastating directed blast followed by a vigorous Plinian eruption, which destroyed the summit of the volcano and formed a 1.3-km-wide crater. Within weeks the volcano started rebuilding its edifice through extrusion of the dome in the middle of the crater, intermittent collapses of the dome, and associated block-and-ash flows. By mid 70s, as the volume of the dome increased, the dome-building extrusive activity became complemented by short explosive events with pyroclastic flows and surges followed by effusions of lava flows. By late 90s the explosive eruptions became remarkably regular with 1-2 events per year. Importantly, all recent eruptions occurred from the crater at the summit of the dome. It appears that the mechanism through which Bezymianny rebuilds its edifice changed remarkably with time from purely extrusive dome growth to explosive-effusive eruptions from the central vent since the beginning of the new millennium.

The whole-rock composition of erupted magmas changed from 60.9 wt. % SiO₂ in 1956 to 56.8 wt. % SiO₂ in October 2007. Although the overall trend shows the decline in SiO₂, there was at least one 10-yr-long period (1993-2004), during which SiO₂ concentration gradually increased. The SiO₂ trend correlates with changes in mineral abundances and mineral compositions. Hornblende, abundant in March 30, 1956 magma, almost disappeared by mid 60s. Clinopyroxenes, exceptionally rare in 1956 products, became more abundant and their crystals became larger with time.

Detailed study of plagioclase stratigraphy showed that despite significant compositional variations, the minimum An content in plagioclase phenocrysts remains nearly the same for the entire sequence of the eruptive products. Core-to-rim compositional profiles of plagioclase phenocrysts commonly show repeated dissolution boundaries followed by abrupt jumps in An content up to 80 mol. % and gradual returns to compositional plateaus at 48-50 mol.%. Since plagioclase composition is very sensitive to variations of pressure, temperature, melt composition, and water content, such repeated pattern may be best explained by the presence of a buffer. One of the most likely candidates for such a buffer could be the persistent presence of a substantial volume of the 1956 magma, which composition, temperature, and pressure have not been modified by neither the withdrawal of its portion in 1956, nor by periodic basaltic replenishments.

GEOCHEMICAL TRACING OF VOLCANIC GASES AT BEZYMIANNY AND SHIVELUCH VOLCANO: IMPLICATIONS FOR MAGMATIC PLUMBING SOURCES

Theresa M. Kayzar¹, Bruce K. Nelson¹, Pavel E. Izbekov², Marina Belousova^{3,4}, Alexander Belousov^{3,4}, and PIRE Research Team

¹*Department of Earth and Space Sciences, University of Washington, Seattle WA, USA.*

²*Geophysical Institute, University of Alaska, Fairbanks AK, USA.*

³*Institute of Earth Sciences, Academia Sinica, Taipei, Taiwan.*

⁴*Institute of Volcanology and Seismology, Petropavlovsk-Kamchatsky, Russia.*

In magmatic systems, volcanic gases have an important role in eruption generation, eruptive behavior, and the evolution of melts and magma chambers. However, volcanic gases are transient and, therefore, identifying their magmatic sources and quantifying gas flux through melts has proven difficult. Here we present a geochemical approach to understanding gas migration in two systems: Bezymianny and Shiveluch volcanoes in Kamchatka, Russia.

Uranium-series isotopes provide insight into volcanic gas behavior because many of the nuclides in the uranium decay chain are volatile in nature. Notably, the decay product of ²²⁶Ra is ²²²Rn, a noble gas. During gas migration in melt, ²²²Rn moves with the gas phase, fractionating the radioactive equilibrium between its parent, ²²⁶Ra, and its daughter product, ²¹⁰Pb. Recent research suggests that (²¹⁰Pb)/(²²⁶Ra) can be used to study gas motion and magma recharge in volcanic systems (Berlo et al. 2004, Reagan et al. 2006, Kayzar et al. 2009). However, in order to trace volcanic gases with the ²²⁶Ra-²²²Rn-²¹⁰Pb decay chain, analyzed volcanic samples must be less than 50 years old to preserve disequilibrium. Therefore, the use of this technique requires access to historically erupted products.

Bezymianny and Shiveluch volcanoes have had abundant strong explosive eruptions over past 50 years. Therefore, the systems are likely driven by a voluminous, possibly continuous, supply of magma and volatiles making them appropriate sites for an investigation of volcanic gas behavior. Bezymianny and Shiveluch erupt magmas of different compositions and character. Bezymianny typically erupts crystal-rich andesite and basaltic andesite with minor evidence for magma mingling, whereas Shiveluch erupts largely andesite to dacite compositions with abundant xenoliths, basaltic enclaves, and signatures of open system behavior. The two systems also erupt on different timescales. Bezymianny has erupted approximately twice every year since the 1970's in a somewhat predictable fashion; however, Shiveluch eruptions are much less predictable and occur sporadically during adjustments and collapse of a growing dome. Therefore, gas signatures can be interpreted in a variety of contexts by an investigation of only two volcanic centers. There are very few samples that have been analyzed for uranium-series disequilibrium from these volcanic centers. However, published data suggest that different styles of gas transfer occur at Bezymianny and Shiveluch. Shiveluch material was reported to have (²¹⁰Pb)/(²²⁶Ra) of 1.523 (a 50% ²¹⁰Pb excess) implying large volumes of gas accumulation (Turner et al. 2004). (²¹⁰Pb)/(²²⁶Ra) values reported for Bezymianny, however, are near equilibrium (0.862-1.055) (Turner et al. 2007). Therefore, there appears to be no gas motion relative to melt in the Bezymianny volcanic system.

Bezymianny and Shiveluch volcanoes are the focus of a United States-Russia Partnership for Volcanological Research and Education, a large interdisciplinary project funded by the NSF PIRE program to understand explosive volcanism. The PIRE-Kamchatka project has funded our field studies at Bezymianny volcano for three years and at Shiveluch volcano for one year. We present preliminary U-Th-Ra-Pb results from a time-series of recent samples (younger than 50 years) from both Bezymianny and Shiveluch volcanoes. We interpret new (^{210}Pb)/(^{226}Ra) data and suggest hypotheses for the role that gas motion plays in the context of two contrasting volcanic systems. In addition, results from the PIRE-Kamchatka project provide seismic, geodetic, petrological, as well as direct gas sampling results to constrain our interpretations of geochemical gas signatures.

MODELING OF THE ERUPTION DYNAMICS OF A SILICIC VOLCANO

Melnik, Oleg E.^{1,2}, Alexey A. Barmin¹, R. Stephen. J. Sparks²

¹*Institute of Mechanics, Moscow State University.*

²*Research Centre for Environmental and Geophysical Flows, Department of Earth Sciences, Bristol University.*

Silicic volcanoes show different styles of eruptive activity with different timescales, repeatability, and intensity. The most common style of activity is represented by slow lava dome or lava flow effusion. This activity may be interrupted by a single or a sequence of explosive eruptions of different magnitudes. Vulcanian blasts may occur in sequences with repose periods of hours to days; the duration of individual events may be only minutes. Usually between these blasts a lava dome continues to grow, but sometimes it becomes totally devastated by explosions. Larger-scale events, including Plinian eruptions and direct blasts, usually lead to significant changes in the morphology of the upper conduit system and interrupt lava dome growth leading to significant repose periods, sometimes years or decades long. Mathematical models have been developed for different styles of eruptive activity.

Lava dome eruptions can display fairly regular alternations between periods of high and of low or no activity. The time scales for these alternations are typically months to years. We have developed a transient model of magma flow in a conduit from an open-system magma chamber with continuous replenishment. The model considers gas exsolution, bubble growth, gas escape through the magma, kinetics of decompression-induced crystallization, and latent heat effects. The system is described by a 1D transient set of partial integro-differential equations containing mass conservation, momentum, and energy equations. The model accounts for elasticity of the chamber wallrocks, compressibility of bubbly magma, and heat exchange between the hot basaltic magma entering the chamber and silicic magma in the chamber. Crystal growth kinetics is calibrated using experiments on decompression-induced crystallization for a rhyolitic melt representing the composition of the Soufrière Hills Volcano (Montserrat).

A steady-state solution for the system is sigmoidal, with three steady regimes corresponding to fixed conditions inside the chamber. The difference in discharge rates between these regimes can be several orders of magnitude. Calculations based on the transient model show the presence of periodic variations in discharge rate due to the transition from a stable regime, when discharge rate is low and crystals grow efficiently leading to high magma viscosity, to another stable state, when discharge rate is high and crystallization is negligible leading to low magma viscosity; periodic behavior occurs when influx rate to the chamber corresponds to the intermediate unstable regime. The influence of principal parameters, such as magma temperature, water content, conduit diameter, chamber size, phenocryst size, and magma rheology, is studied.

The system shows strongly nonlinear responses to the variation of governing parameters. Small changes in magma temperature, water content, conduit diameter, and phenocryst size can result in large changes in eruption intensity, including transitions between effusive and explosive activity. When the system is in high discharge rate regime, gas escape through the magma becomes insufficient and the system can reach conditions favorable for explosive activity.

The process of the development of explosive eruption followed by collapse of a growing lava dome is described by means of a 1D transient multiphase flow model. Diffusion delay of volatile exsolution, viscosity distribution around the bubble, and pressure disequilibrium between bubbles and melt are taken into account. Parameter distributions obtained from the calculations of

slow magma ascent prior to the dome collapse are used as initial conditions. The simulations reveal a spectrum of behaviors, from sustained to short-lived highly non-equilibrium Vulcanian-style explosions lasting a few tens of seconds, through longer-lasting eruptions that can be sustained for tens of minutes, and finally to eruptions that can last hours or even days. Behavior is controlled by a mass-transfer parameter, ω , which equals $n^{2/3}D$, where n is the bubble number density and D is the diffusivity. The parameter ω is expected to vary between 5×10^{-5} and 0.5 s^{-1} in nature, and reflects a time-scale for efficient diffusion. The spectrum of model behaviors is consistent with variations in styles of explosive eruptions of silicic volcanoes. In initial stages peak discharges occur over 10-20 seconds and then decline to low discharges. If a critical bubble overpressure is assumed to be the criterion for fragmentation, then fragmentation may stop and start several times in the declining period causing several pulses of high intensity discharge. In cases of strong disequilibria the fluxes can decrease to negligible values while other processes, such as gas escape through permeable magma, prevent explosive conditions from becoming re-established so that explosive activity stops and dome growth can start. For cases closer to the equilibrium the eruption can evolve towards a quasi-steady sustained flow, never declining sufficiently for gas escape to become dominant.

Although proposed models allow us to explain many observed phenomena during different stages of an eruption of a silicic volcano, there is no model for the evolution of a silicic volcano that can represent changes in eruption styles and intensity. In any case, due to non-linearity of the system, using such a model as a forecasting tool remains problematic because small changes in governing parameters can lead to dramatic change in eruption dynamics. A better approach is to treat parameters in a probabilistic way with uncertainties and distributions and run ensemble type simulations to detect possible trends in eruption dynamics. A similar approach is used in climate prediction modeling.

The work was supported by the Russian Foundation for Basic Research (projects 07-01-12041, 08-01-0016), an NERC grant, UK, and the PIRE project.

References

- Barmin, A, Melnik, O, and Sparks, RSJ. Periodic behavior in lava dome eruptions, *Earth and Planetary Science Letters*, **199**, 173-184, 2002.
- Mason, RM, Starostin, AB, Melnik, OE and Sparks, RSJ. From Vulcanian explosions to sustained explosive eruptions: The role of diffusive mass transfer in conduit flow dynamics, *Journal of Volcanology and Geothermal Research*, **153 (1-2)**, 146-165, 2006. ISSN: 0377-0273
- Melnik, OE, Barmin, A and Sparks, RSJ. Dynamics of magma flow inside volcanic conduits with bubble overpressure buildup and gas loss through permeable magma, *Journal of Volcanology and Geothermal Research*, **143 (1-3)**, 53-68, 2005. ISSN: 0377-0273
- Melnik, OE and Sparks, RSJ. Controls on conduit magma flow dynamics during lava dome building, *Journal of Geophysical Research: Solid Earth*, **110 (2) B02209**, 1-21, 2005. ISSN: 0148-0227

TIME CONSTRAINTS FOR MAGMA SUPPLY IN BEZIMYANNY AND SHIVELUCH VOLCANIC SYSTEMS

Pavel Plechov¹, Vasily Shcherbakov¹, Alexandra Tzay¹, Madeleine Humphreys²

¹*Geological Department, Moscow State University, Moscow, Russia.*

²*Department of Earth Sciences, University of Cambridge, United Kingdom.*

The width of reaction rims between phenocrysts and surrounding melt represents incomplete mineral-melt reactions; we used these widths for determining time constraints on magma supply in hybrid volcanic systems (Bezymyanny and Shiveluch). Opacitic rims around hornblende from Bezymyanny (March 1956 eruption) and complex rims around olivine from Shiveluch (2001-2004 eruption) allowed estimations of 1) time between magma chamber supply and eruption, and 2) frequency of new magma intrusion into the shallow level magma chamber.

According to the proposed model [1], the generation of the hornblende opacitic rims is the result of Hb disequilibrium with surrounding melts that occurs due to the magma mixing or to abrupt changing of P-T-x conditions. There are two stages in the generation of the reaction rims.

1. During the first stage, minerals attain equilibrium with the surrounding melt by diffusion exchange of the components. If equilibrium is attained then a polymimetal rim is not present and a zonal outer rim is formed as a result of reequilibration. If the stability limit of the mineral has been reached, phenocrysts are replaced with polymimetal aggregates and a reaction rim starts to form.

2. In the second stage, the reaction rim spreads to the center of the grain. Diffusion exchange between hornblende and melt proceeds through the newly-formed polymimetal rim.

The thickness of the rim is a function of the time of reaction between hornblende and melt [1]:

$$x(t) = \sqrt{D(t - t_0)} \quad (1)$$

where x = thickness of the rim, t = period of time during which the mineral reacts with the surrounding melt, t_0 = "rest time" during which rim is not generated, and D = coefficient of proportionality which characterises the speed of the process.

"Rest time" (t_0) reflects the duration of the first stage of disintegration; it is controlled by the velocity of diffusion in mineral. t_0 for olivine, characterized by the high-speed diffusion of Fe and Mg, is close to 0 [2], but for hornblende t_0 may reach a few days [3].

The experimentally defined coefficient D [2,3] is greater by two orders of magnitude than coefficients of diffusion in hornblende and olivine and corresponds to the rates of diffusion in melt within one order of magnitude. Growth of the opacitic rim in hornblende is controlled by diffusion in the interstitial melt within the rim. The reaction of replacing hornblende with a plagioclase – pyroxene – magnetite aggregate leads to a 5% decrease in volume. Interstices formed as a result of hornblende breakdown are filled with melt, which creates an environment for component transportation. Diffusion in rim interstitial melt is slower than diffusion in surrounding melt because: 1) there is a nonlinear path inside the reaction rim, 2) some channels are not permeable to components throughout their length, and 3) small channel dimensions could produce an additional interaction of components with channel walls.

We determined the maximum range of D for hornblende breakdown (2.7×10^{-16} to 2.0×10^{-15} m²/s) and t_0 (2–5 days) from experimental data [3]. The time required for developing the hornblende breakdown rims (Fig.1a) during the March 30, 1956 eruption of Bezymyanny Volcano was calculated using the maximum and minimum possible t_0 and D values and evaluated

to be 4–37 days. This evaluation allowed us to revise the interpretations of the events preceding this eruption. The hot magma injection into the chamber that induced hornblende opacitization could have taken place in February or March 1956, while the eruptive activity of the volcano occurred on October 22, 1955, and a series of eruptions associated with ash falls continued until late November. Hence, the volcanic events in 1955 were not directly related to processes in the chamber before the March 30, 1956 eruption and required a separate batch of the magma supply before October 22, 1955, i.e. magma supply frequency could be estimated for the 1955–1956 period as 2 times per year. This estimate is consistent with estimations from plagioclase zoning study (Shcherbakov et al., this volume) for the 2000–2007 eruptions.

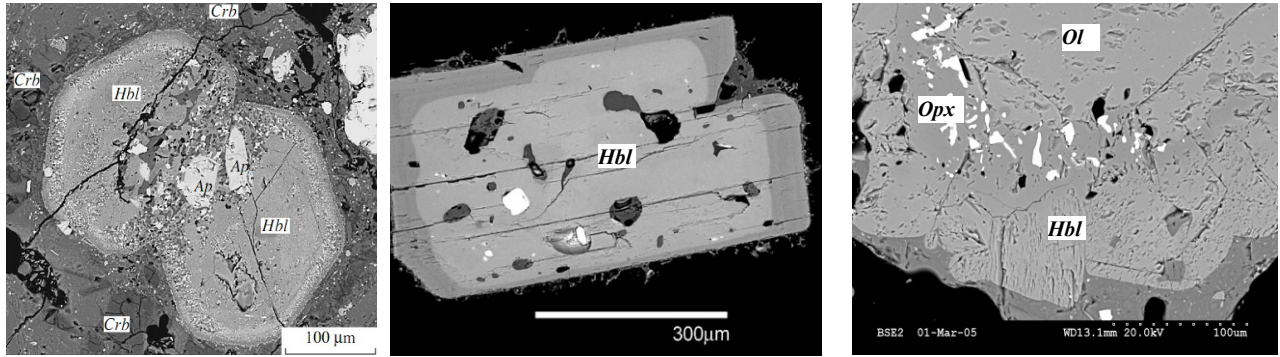


Fig. 1. Rims around phenocrysts in Bezymyanny and Shiveluch lavas. a) An opacitic rim around hornblende (Bezymyanny, March 1956)[1]; b) a Mg-rich rim around hornblende without breakdown (Shiveluch, 2001)[4]; c) a complex reaction rim around olivine. The rim consists of two parts. The external part of the rim consists of hornblende; the internal part is made up of orthopyroxene-magnetite aggregates. The width of the internal rim is constant, whereas the external rim width is more variable (Shiveluch, July 2002)[4]. Mineral symbols: Hbl—hornblende, Ol—olivine, Opx—orthopyroxene, Ap—apatite, Crb—cristobalite.

In products of the 2001–2004 eruption of Shiveluch Volcano there is no evidence for hornblende breakdown (Fig. 1b). Moreover, hornblende is present in the reaction rim around olivine (Fig. 1c). Possibly the magma supply under Shiveluch Volcano is more similar to the magma of the shallow chamber than is the supplying magma beneath Bezymyanny Volcano.

We obtained timescales of 13–50 days for formation of the inner rim and 61–1361 days for formation of the whole reaction rim [4], using an experimentally determined coefficient for a rhyodacitic melt at $T = 885^\circ\text{C}$ and $P = 150\text{ MPa}$ ($1.02\mu\text{m}^2/\text{h}$) as a minimum estimate, and the growth rate of olivine reaction rims in Arenal Volcano ($2.95\mu\text{m}^2/\text{h}$) as a maximum value [2]. The value of 13–50 days obtained from internal rim widths could reflect the length of time for which the olivine–amphibole interface was unstable, though it is not clear whether the experimentally obtained growth rate is appropriate for this solid–solid reaction. This timescale is consistent across all samples, and might represent the time of magma ascent below the amphibole stability limit (approximately 50–100 MPa) [4]. The estimate of 2 months to >4 years based on total rim widths reflects the residence time of the olivine xenocrysts in the system, i.e. the time between injection of basalt and eruption, under either mechanism. Rim widths from this sample indicate magma influx 470–1361 days prior to eruption (i.e. approximately August, 1997 to February, 2000). Samples shv202002 and PK-02/3a were erupted a year later, in June 2002. Rim widths from these samples indicate magma influx 9 weeks to 1 year previously (i.e. during the same

extrusive episode, June 2001 to May 2002). Thus, frequency of magma recharge for the Shiveluch volcanic system is estimated as 0.3-1 times per year.

References

1. Plechov P., Tzay A., Scherbakov V., and Dirksen O. (2008) "Horblendes in andesites of 30 March 1956 Bezymyanniy eruption and conditions of their opacitization", Petrology, 16(1),19-35.
2. Coombs M.L. and Gardner J.E. (2004) "Reaction rim growth on olivine in silicic melts: Implications for magma mixing," Am. Mineral. 89, 748–759.
3. Rutherford M.J. and Hill, P.M. (1993) "Magma ascent rates from amphibole breakdown: An experimental study applied to the 1980–1986 Mount St. Helens eruptions," JGR, 98, 19667–19685.
4. Dirksen O., Humphreys M.C.S., Plechov P., Melnik O., Demyanchuk Y., Sparks R.S.J., and Mahony S. (2006) "The 2001-2004 dome-forming eruption of Shiveluch Volcano, Kamchatka: Observation, petrological investigation and numerical modelling", JVGR, 155(3-4), 201-226.

EXPERIENCE OF PREDICTING EXPLOSIVE ERUPTIONS AT BEZYMIANNY VOLCANO (RUSSIA, KAMCHATKA)

Senyukov S.L.

Kamchatka Branch of Geophysical Surveys RAS, Petropavlovsk-Kamchatsky, Russia, ssl@emsd.ru

Bezymianny Volcano is located in Kamchatka, Russia ($55^{\circ} 58' N$, $160^{\circ} 35' E$, 2869 m). The last catastrophic eruption occurred on March 30, 1956, after 900-1000 years of quiescence. Since 1956 the volcano has produced 1-2 explosive eruptions per year. Ash plumes rose to from 6 km to 15 km above sea level.

Seismic precursors were registered before some eruptions from 1956 to 1994, but no eruptions were officially predicted using seismic data. The Kamchatka Branch of Geophysical Survey (KBGS) of the Russian Academy of Science began processing data from volcanic earthquakes in 1992. During 1996-1999, seismic monitoring was improved significantly: 1) new telemetered stations were installed, 2) seismic data were converted to digital format, and 3) custom seismic processing software was written. KBGS began to monitor the activity of Kamchatkan volcanoes in 2000 (<http://www.emsd.ru/~ssl/monitoring/main.htm>) using real-time seismic, visual (or video), and satellite (NOAA, AVHRR) data. Seven eruptions of Bezymianny Volcano were recorded and investigated from February 2000 to February 2004. The first variant of an individual algorithm for Bezymianny eruption prediction was established in May 2004. This algorithm was determined as a formalized scheme of decision-making about the eruption possibility in near-real-time based on collected seismic and satellite data.

During 2004-2008, using this algorithm 7 out of 8 eruptions were successfully predicted in real time within 1-7 days prior to eruption. It was determined that successful prediction of Bezymianny eruption depends on activity at nearby Kluchevskoy Volcano. According to seismic data, the magma systems of Bezymianny and Kluchevskoy volcanoes possibly interact. The original algorithm for predicting Bezymianny eruptions has been modified according to all collected experience.

**COMPARATIVE STUDY OF BEZYMIANNY,
SHIVELUCH, AND MOUNT ST HELENS VOLCANOES –
RESULTS OF PIRE-KAMCHATKA PROJECT**

POSTER PRESENTATIONS

THREE-DIMENSIONAL DEGASSING STRUCTURES IN THE UPPER CONDUIT OF ANDESITE-DACITE VOLCANIC SYSTEMS – BEZYMIANNY, RUSSIA, UNZEN, JAPAN, OBSIDIAN DOME AND MOUNT ST. HELENS, USA

Leslie D. Almberg^{1,2}, John C. Eichelberger³, Jessica F. Larsen^{1,2}, Florian Fusseis⁴

¹*Geophysical Institute, Univ. of Alaska Fairbanks, Fairbanks, AK, USA.*

²*Geology & Geophysics, Univ. of Alaska Fairbanks, Fairbanks, AK, USA.*

³*US Geological Survey, Volcano Hazards Program, Reston, VA, USA.*

⁴*Multiscale Earth System Dynamics, Univ. of Western Australia, Perth, WA, Australia.*

Magmas that were volatile saturated at depth may erupt as dense, degassed lavas or domes. How this can occur in high viscosity magmas is a matter of contention, as it requires maintaining magma permeability down to very low porosity or rapid gas loss and collapse of a degassed melt before it cools below the glass transition. Different mechanisms have been proposed for efficient degassing down to very low porosity in effusive eruptions including fragmentation along conduit walls, development and subsequent collapse of a permeable foam, or coalescence of bubble chains within the magma.

Here we present three-dimensional visualizations of degassing structures formed within the upper conduits and domes of four volcanic systems: Bezymianny, Russia, Unzen, Japan, Mount St. Helens and Obsidian Dome, USA. Our findings from X-ray computed tomography reconstructions and percolation modeling of samples retaining ~1-15 vol.% vesicularity from conduit core and cryptodome samples indicate that gas loss at depth is more efficient in sheared regions (anisotropic) than those that contain no evidence for shearing (isotropic). Preferential vesicle orientation is interpreted as an indication of shear direction and determined via stereonet projections of first tensors measured in 3D space.

In the case of the Obsidian Dome intrusive samples, we see a progression from low to high vesicularity (0.5, 2.5, 12.2 vol.%) and decreasing anisotropy with increasing distance from the conduit wall into the center of the dike. The Mount St. Helens high- and low-density (2.0 and 4.5 vol.% voids, respectively) cryptodome samples exhibit the same inverse relationship between vesicularity and anisotropy. There is no significant density or vesicularity difference between the three Bezymianny cryptodome samples (3.0 ± 0.1 vol.%), which were emplaced at near surface conditions. Within the Unzen conduit zone at 1500 m depth, alteration has obscured degassing structures, however remnant bubble chains and microscopic pockets of foam were found via SEM (scanning electron microscope) investigations.

The lava domes of Unzen and Obsidian Dome reveal degassing structures not observed elsewhere within the volcanic systems under investigation. Unzen contains a mere 4.5 vol.% ragged, concave void clusters concentrated in and around fractured phenocrysts. By contrast, a sample from 17.22 m within the Obsidian Dome contains 15.2 vol.% oblate spheroid vesicles within alternating bands of high and low vesicularity on the scale of ~2.5 mm.

Our observations from these four volcanic systems support the hypothesis that degassing down to low porosities in high-viscosity crystalline magmas is achieved via bubble chains, with their development promoted by magma shearing. This conclusion does not, however, undermine the validity of the other models, which may more accurately describe degassing behavior at times within the eruptive cycle or at locations within the conduit system not considered by this study. For example, complete degassing to zero vesicularity obsidian was not investigated.

VOLCANIC AND CHEMICAL GEOLOGY OF SHIVELUCH VOLCANO: THREE PHASES OF EVOLUTION

Natalia Gorbach¹, Maxim Portnyagin², Vera Ponomareva¹.

¹Institute of Volcanology and Seismology, Petropavlovsk-Kamchatsky, Russia.

²IFM-GEOMAR, Kiel, Germany.

Shiveluch Volcano, at the junction of the Kurile-Kamchatka and Aleutian island arcs, is one of the largest and most active Kamchatka Peninsula volcanoes. It has no analogs with respect to the amount of erupted andesites among all Quaternary Kamchatka volcanoes. The volcano's Holocene eruptive history was reconstructed in detail using tephrachronology and radiocarbon dating (Ponomareva et al., 2007). Data on Late Pleistocene activity, however, is very limited (e.g., Menyailov, 1955; Melekestsev et al., 1991). Here we present new results of a systematic geological and geochemical investigation of all volcanic complexes comprising Shiveluch edifice. Three major phases of Shiveluch volcanic evolution were distinguished: (1) Initial, (2) Stratocone, and (3) Late phases.

The Initial Phase deposits are voluminous, stratified, partly-consolidated, coarse agglomerate tuffs with thickness ranging from ~2000 m in the central Old Shiveluch edifice to 900-1000 m 7 km away. Initial Phase deposits are lithologically similar to the Holocene pyroclastic density currents covering the volcano's southern flank (Ponomareva et al., 2007). The similarity of lithological rock types, close scale of spatial distribution, and gentle dipping indicate similarity between initial and Holocene volcanic activity periods. Small-volume lava flows are intercalated in the upper Initial Phase pyroclastic deposits.

Predominant Initial Phase eruptive products are magnesian *Hbl-Pl* and *Hbl-Px-Pl* andesites with moderate Mg#=53.0-54.6 mol%, Cr=46-72 ppm, and Ni=5-29 ppm content at SiO₂=57.5-62.5 wt%. Small volume lavas are high-magnesian *Ol-Cpx-Pl* basaltic andesites (Mg#=58.8-63.7 mol%, SiO₂=53.9-55.0 wt%, TiO₂=0.76-0.87 wt%, Al₂O₃=15.1-16.5 wt%, K₂O=1.2 wt%). These high-Mg basaltic andesites, erupted at Initial Phase end, contain magnesian olivine phenocrysts Fo₉₀₋₉₂ with high Ni (0.36-0.45 wt%) concentration.

The Stratocone Phase had a complex eruptive history including at least two construction stages, forming the **Main Summit** and the **Baidarny Spur**. The Main Summit was built by a series of thick andesitic lava flows compositionally identical to Initial Phase andesites. The Main Summit edifice was affected by the subsequent sector collapse forming a horseshoe-shaped caldera (Melekestsev et al., 1991) or crater (Ponomareva et al., 2006). The Baidarny Spur lava series originated from several eruptive centers situated 3-5 km southwest of the Main Summit. Major Baidarny Spur rock types are high-Al *Px-Pl±Ol* basaltic andesite lava flows and co-genetic dykes (Mg#=52.1-56.1 mol%, SiO₂=54.2-55.4 wt%, TiO₂=0.87-0.96 wt%, Al₂O₃=17.0-17.6 wt%, K₂O=0.9-1.3 wt%). The high-Al basaltic andesites differ remarkably from typical Shiveluch andesites, with lower SiO₂ and higher Al₂O₃ at a given Mg#. Trace element concentrations are, however, similar in both groups, indicating common parental melts but different conditions of crustal evolution.

The Late Phase built the Young Shiveluch lava and dome complex and pyroclastic deposits and the Karan satellite dome complex. In comparison to Initial and Stratocone phases of Old Shiveluch, the Late Phase is less voluminous and more compositionally heterogeneous. Young Shiveluch pyroclastic deposits are *Hbl*-bearing andesites with SiO₂=56-64% wt% (Ponomareva, et al., 2007). The Young Shiveluch and Karan lava complex includes high

magnesian *Hbl-Pl*, *Px-Hbl-Pl* andesites, *Ol-Hbl-Pl±Px*, *Ol-Px-Pl±Hbl* andesite and basaltic andesites. We also found hybrid lava flows, generated by mixing mafic basaltic andesite and evolved silicic andesite magmas. Late Phase rocks generally have the highest Mg# (57.7-64.4 ppm) Cr (108-307 ppm) and Ni (18-78 ppm) of all Shiveluch rocks, slightly elevated Na, and more strongly fractionated REE patterns than older rocks with similar SiO₂ contents.

Shiveluch's lava series originated via a combination of fractional anhydrous and hydrous mineral assemblage crystallization, crustal assimilation, and magma mixing processes. The high-Mg basaltic andesite suite shows general trends of increasing incompatible lithophile element concentrations (e.g. Ba, K, Th) and decreasing compatible trace element concentrations (Ni, Cr) with decreasing MgO. Transition from basaltic andesite to andesite accompanies the change from incompatible to compatible behavior of TiO₂, FeO, and Sr as the result of Fe-oxide and plagioclase crystallization. Similar changes are observed for Ba, K, Rb, Zr, HREE, and Y with decreasing MgO. The most evolved Shiveluch rocks exhibit U-shaped patterns of normalized HREE concentrations, most likely due to compatible HREE and amphibole behavior. Fractionation of an amphibole-rich assemblage can explain HREE depletion of Shiveluch magmas and their pseudo-adakitic (Castillo, 2006) signature, clearly expressed as abundant amphibole phenocrysts in younger andesites.

Many Shiveluch rocks show evidence of magma mixing: macroscopic mingling and mixing textures in Late Phase rocks, large plagioclase composition range within single samples, reverse, complex plagioclase phenocryst zoning, two amphibole generations in some rocks, reverse orthopyroxene zoning, and Mg-rich olivine phenocrysts present in evolved rocks. Field observations and mineralogical and geochemical data indicate an increased role of magma mixing during the volcano's evolution. Also, Shiveluch andesites contain many inclusions of recrystallized, partially melted crustal (mainly amphibolites and gabbros) and mantle rocks suggesting that wall rock may have been assimilated during magma evolution.

Our data show complex magma generation processes beneath Shiveluch. A plausible model to explain these observations assumes residual silicic melts generated by incomplete crystallization of wet basaltic melts periodically injected into a deep crustal hot MASH zone and periodic eruption of MASH zone material (e.g. Annen et al, 2006). Basaltic Baidarny Spur andesites likely originated from the other, extinct volcanic center, which did not share a magma plumbing system with Shiveluch. A remarkable result of this study is evidence for an increasing magma mixing role during the volcano's evolution, suggesting more frequent basaltic magma injections into the crustal MASH reservoir under Shiveluch during the Holocene, perhaps reflecting more efficient postglacial deep mantle magma generation.

This research was supported by FEB RAS, grants 06-III-B-08-369, 07-III-Д-08-095, 09-III-A-08-422 and the KALMAR project, which funded geochemical and mineralogical investigations.

References

- Annen C., Blundy J.D., Sparks R.S. J. (2006) The genesis of intermediate and silicic magmas in deep crustal hot zones. *Journal of Petrology*, 47: 505–539.
- Castillo P.R. (2006) An overview of adakite petrogenesis. *Chinese Sci. Bull.* 51: 257-268.
- Melekestsev I.V., Volynets O.N., Ermakov V.A., Kirsanova T.P., and Masurenkov Yu.P. (1991) Shiveluch Volcano. In: Fedotov S.A., Masurenkov Yu.P. (Eds.). *Active volcanoes of Kamchatka*. 1, pp. 84-92, Nauka Press, Moscow.

- Menyailov A.A. (1955) Shiveluch Volcano, its geologic structure, composition and eruptions. Trudi Laboratori Vulkanologii, 9, 264 pp (in Russian).
- Ponomareva V.V., Melekestsev I.V., Dirksen O.V. (2006) Sector collapses and large landslides on Late Pleistocene-Holocene volcanoes in Kamchatka, Russia. Journal of Volcanology and Geothermal Research 158: 117-138.
- Ponomareva V.V., Kyle P., Pevzner M.M., Sulerzhitsky L.D., Hartman M. (2007) Holocene eruptive history of Shiveluch Volcano, Kamchatka Peninsula, Russia. In: Volcanism and Subduction: The Kamchatka Region. Eichelberger J., Gordeev E., Izbekov P., Lees J. (Eds), AGU Geophysical Monograph Series, 172: 263-282.

LITHOLOGICAL CHARACTERISTICS OF BEZYMIANNY VOLCANO PYROCLASTIC DENSITY CURRENTS THAT OCCURRED FROM 2005-2008

Oxana Krivomazova

Institute of Volcanology and Seismology FED RAS, Piip 9, Petropavlovsk-Kamchatsky, Russia.

This work shows the results of studying granulometric and component composition and lithological characteristics of the density currents of Bezymianny Volcano ($55^{\circ} 58' N$, $160^{\circ} 35' E$) pyroclastic flows from 2005-2008. Samples from pyroclastic flows after eruptions that occurred on November 30th, 2005, December 24th, 2006, and May 12th, 2007, and samples from an avalanche on November 5th, 2007 were collected in 2007. These samples were studied using a sift data method, and also using the "Analyze 22" compact laser analyzer. The results of our analyses were processed using the "Pascal" program. Histograms created using these data indicate that we can split these deposits into two types: one with bimodal, and one with polymodal granulometric distribution. The deposits which conform to the second type of distribution (histograms are polymodal) contain a large percentage of an altered material, indicating that dome collapses have played an essential role in forming these deposits. The deposits which conform to the first type of distribution (histograms are bimodal) contain a small quantity of an altered material, indicating that collapse played an insignificant role in forming these deposits. The deposits from the eruption of November 5th, 2007 differ sharply from all other deposits studied. Histograms of the granulometric structure of these deposits exhibit a strongly pronounced polymodal character, and the material is found in an exclusively altered fragment that confirms the collapse genesis of the November 5th, 2007 deposits.

MAJOR AND VOLATILE ELEMENTS IN GLASSES FROM LARGE EXPLOSIVE KAMCHATKA ERUPTIONS CORRELATE WITH DEPTH TO SUBDUCTING PLATE

Kuvikas O.V.,^{1,4} Portnyagin M.V.,^{2,3} Ponomareva V.V.⁴

¹*Kamchatka V. Bering State University, Petropavlovsk-Kamchatsky, Russia.*

²*Institute of Geochemistry and Analytical Chemistry, Moscow, Russia.*

³*Leibniz Institute of Marine Sciences, IFM-GEOMAR, Kiel, Germany.*

⁴*Institute of Volcanology and Seismology, Petropavlovsk-Kamchatsky, Russia.*

At least 40 large ($>1 \text{ km}^3$ of tephra) and many small explosive Holocene eruptions have occurred in Kamchatka. Tephras from strong eruptions are widely distributed and serve as time-markers in stratigraphic research. In previous studies, tephras from various volcanic centers were recognized based on K_2O content in bulk samples (Braitseva et al., 1997) and volcanic glass (Ponomareva et al., 2004). In our study we assess multi-component systematics of volcanic glass from major Kamchatka tephras. We use results to 1) fingerprint tephra from different sources, 2) compare silicic magmas across/along the volcanic arc, and 3) understand the processes governing silicic melt generation in Kamchatka.

Within the framework of the German-Russian project KALMAR, we analyzed 94 volcanic glass samples from major Kamchatka tephras. Analyses were conducted at IFM-GEOMAR (Kiel, Germany) with a JEOL JXA 8200 microprobe using one analytical protocol (15 keV accelerating voltage, 6 nA current, 5 μm beam size). Smithsonian Institution glass reference standards (Jarosevich, 1980) were used. High-sensitivity (H-type) crystals were used to analyze volatiles and rare elements (Ca, Fe, Mg in silicic glasses), significantly improving analytical precision for these elements compared to conventional analyses. As a result we obtained a new self-consistent database of ~ 2500 high-quality glass analyses of known source and age. Here we report pilot results from analyzing this database.

There is large compositional variability in volcanic glasses from different Kamchatkan volcanic zones and centers. Some spatial geochemical trends are, however, evident from our database. For example, mean glass compositions from different volcanoes demonstrate increased K_2O content and a decrease in FeO , MgO , CaO and Cl/K ratios from the volcanic front toward the rear-arc, i.e. with increasing depth to the subducting plate (Fig. 1). With regard to the increasing concentrations of incompatible elements (e.g., K) and decreasing Cl/K from the volcanic front to the rear-arc, the trends of silicic melts are qualitatively similar to those reported for mafic rocks and primitive melt inclusions in olivine (e.g., Volynets, 1994; Portnyagin et al., 2007), yet absolute concentrations of K_2O are higher in silicic melts and Cl/K ratios are lower. This suggests that crystal fractionation of mantle basaltic melts is the main mechanism of silicic melt generation in Kamchatka while assimilation of crustal rocks plays a relatively minor role. Reconciling the spatial geochemical zoning evident from our data and massive crustal assimilation involved in the origin of silicic melts (e.g., Bindeman et al., 2004) requires us to consider re-melting of rocks formed within the same volcanic center.

Most volcanoes in Kamchatka produce tephras with glass compositions that plot along single fractionation trends. Clear exceptions are Ksudach, Khangar, Shiveluch, and Bezymianny volcanoes. Significant variability of glasses from individual volcanoes can be related to variable extent of crustal assimilation, compositional heterogeneity of parental melts, and different conditions of crystallization; i.e. glass from minor Bezymianny tephra erupted on Oct. 14, 2007 differs dramatically from glass found in pumice from the 2400 yr BP large eruption; it has lower

Al_2O_3 and higher K_2O , FeO , and TiO_2 at given SiO_2 content. We suggest that these compositional peculiarities reflect low (near-surface) pressure conditions of magma fractionation in recent years (probably after 1956) that promoted frequent weak eruptions rather than larger ones driven by high water pressure in a deeper magma chamber.

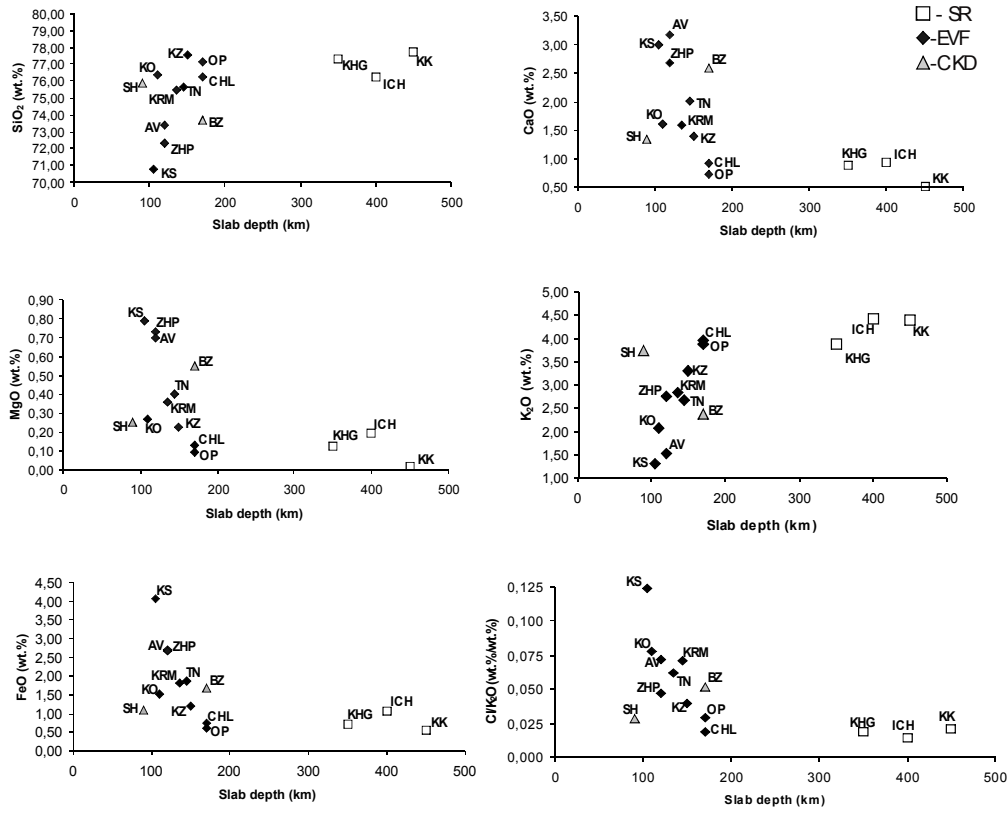


Fig.1. Across-arc variations of major volcanic glass elements. Symbols: SR (Sredinny Range), EVF (Eastern Volcanic Front), CKD (Central Kamchatka Depression). Abbreviations for volcanoes: KO (Kurile Lake Caldera), AV (Avachinsky), KS (Ksudach), KRM (Karymskaya Caldera), ICH (Ichinsky), KHG (Khangan), KZ (Kizimen), OP (Opala), BZ (Bezymianny), SH (Shiveluch), TN (Taunshits), ZHP (Zhupanovsky), KK (Kekuknaisky), CHL (Chasha Lake).

References

- Braitseva O.A., Ponomareva V.V., Sulerzhitsky L.D., Melekestsev I.V., Bailey J., Holocene key-marker tephra layers in Kamchatka, Russia. Quat. Res. 47:125-139, 1997.
- Jarosewich E.J., Nelen J.A., Norberg J.A., Reference samples for electron microprobe analysis. Geostandards Newsletter, 4: 43-47, 1980.
- Ponomareva V., Bourgeois J., Braitseva O., Kozhurin A., Kyle P., Pinegina T., Tibaldi A., Major Holocene Marker Ash Layers on Kamchatka Peninsula, NW Pacific, and their Implication for Dating Paleoseismic Events, Eos Trans. AGU, 85(47), Fall Meet. Suppl., Abstract V21, 07, 2004.
- Portnyagin M.V., Hoernle K., Plechov P.Y., Mironov N.L., Khubunaya S.A., Constraints on mantle melting and composition and nature of slab components in volcanic arcs from volatiles (H_2O , S, Cl, F) and trace elements in melt inclusions from the Kamchatka Arc. Earth Planet. Sci. Lett. 255: 53-69, 2007.
- Volynets, O.N., Geochemical types, petrology and genesis of Late Cenozoic volcanic rocks from the Kurile-Kamchatka island arc system. Int. Geol. Rew. 36(4): 373-405, 1994.

A COMPARISON OF VOLCANIC SO₂ EMISSIONS FROM BEZYMIANNY, SHIVELUCH, AND MOUNT ST. HELENS VOLCANOES

Taryn Lopez¹, Sergey Ushakov^{2,3}, Timothy Clark⁴ and Pavel Izbekov¹

¹*Alaska Volcano Observatory, Geophysical Institute, UAF, Fairbanks, Alaska, U.S.A.*

²*Institute of Volcanology and Seismology, Petropavlovsk-Kamchatsky, Russia*

³*Kamchatka Volcano Eruption Response Team, Petropavlovsk-Kamchatsky, Russia*

⁴*United States Army Geospatial Center, Alexandria, Virginia, U.S.A.*

Bezymianny (Kamchatka, Russia), Shiveluch (Kamchatka, Russia), and Mount St. Helens (Washington, U.S.A.) volcanoes are the focus of a five year National Science Foundation supported Participants in International Volcanological Research and Education (PIRE) program involving fifty graduate students and research scientists from the United States, Russia, and Japan. The project's goal is two-fold, 1) to introduce graduate students to international collaborative research, and 2) to use a multi-disciplinary approach to investigate the response of magmatic systems to edifice collapse. Volcanic gas chemistry is one of the disciplines integral to the PIRE program. Herein, we present preliminary findings of sulfur dioxide (SO₂) emissions from the target volcanoes measured during the 2007 and 2008 field seasons.

Measurements of absorption of ultraviolet (UV) light by SO₂ at Bezymianny, Shiveluch, and Mount St. Helens volcanoes were collected during 2007 and 2008 using a FLYSPEC UV spectrometer system. These data were automatically converted to SO₂ column densities (parts per million meter) by the FLYSPEC operating software, according to the Beer Lambert law. Measurements were collected in scanning mode, in which a series of samples were collected along a cross-section of the volcanic plume by rotating the FLYSPEC on a tripod. These column density measurements, along with simple trigonometry and wind speed estimates, were used to calculate SO₂ emission rates from the target volcanoes.

Preliminary results find SO₂ emission rates ranging from 60 - 460 (+/- 50%) tonnes per day (t/d) for Bezymianny; 10 – 70 (>100%) t/d for Shiveluch; and from below detection limit to 10 (+/- 30%) t/d for Mount St. Helens. Poor plume viewing geometry at Shiveluch volcano prevented the entire plume cross-section from being measured as the lower portion of the plume was hidden from view. Therefore, the values presented here should be considered under-estimates and actual emission rates from Shiveluch could be as much as an order of magnitude larger. The above emission rates will be reprocessed using well constrained plume widths and plume speeds, as determined by coincident plume thermal infrared videos, to reduce error and more accurately constrain the emission rates from the target volcanoes.

The variability of SO₂ emission rates seen among the target volcanoes may be attributed to volcanic activity at the time of sample collection, sampling limitations such as in the example of Shiveluch, and differences in the underlying magmatic systems, including magma composition, degassing state, and volume and depth of magma. Additional FLYSPEC measurements will be collected in 2009 to further characterize the SO₂ emissions from the target volcanoes. Finally, through integration of these emission data with other volcanic gas measurements, as well as seismic, geodetic, and petrologic datasets, we aim to constrain the variables controlling the underlying magmatic systems at Bezymianny, Shiveluch, and Mount St. Helens volcanoes, and elucidate magmatic system response to edifice collapse.

EDIFICE PRESSURE PRIOR TO THE 30 MARCH, 1956 ERUPTION OF BEZYMIANNY VOLCANO, KAMCHATKA, RUSSIA

Owen K. Neill^{1*}, Julia E. Hammer¹, Pavel E. Izbekov², Marina G. Belousova³, Alexander B. Belousov³, Amanda B. Clarke⁴, Barry Voight⁵

¹*Department of Geology & Geophysics, University of Hawaii – Manoa, 1680 East West Road, Honolulu, HI, 96822, USA. *okneill@hawaii.edu*

²*Geophysical Institute, University of Alaska – Fairbanks, 903 Koyukuk Drive, Fairbanks, AK, 99775-7320, USA.*

³*Institute of Volcanology and Seismology, 9 Piipa Boulevard, Petropavlovsk-Kamchatsky 683006, Russia.*

⁴*School of Earth and Space Exploration, Arizona State University, P.O. Box 871404, Tempe, AZ, 85287-1404, USA.*

⁵*College of Earth and Mineral Sciences, Pennsylvania State University, University Park, PA, 16802*

This study attempts to constrain pressure within the volcanic edifice of Bezymianny volcano prior to the 1956 blast. Pressure is determined by back-solving H₂O solubility equations with established compositional and thermometry data¹ in concert with new assessments of H₂O in matrix melt. The range of lithostatic pressures expected within the edifice is indicated by the shaded region of Figure 1. The Moore et al. (1995) solubility model² indicates corresponding melt H₂O contents of up to 1.86 wt %. The hypothesis – that the pressure inside the dome is equal to lithostatic pressure – is evaluated by comparing dissolved H₂O concentrations in Bezymianny interstitial glasses with the expected range. If dissolved H₂O contents exceed lithostatic values, the solubility diagram allows assessment of magmatic overpressure prior to eruption. Magma pressurization is difficult or impossible to quantify using geophysical methods, yet is a critical input for dynamical models of volcanic processes involving edifice failure and initiation of volcanic blasts (e.g. [3],[4]).

Low glass contents of Bezymianny blast material preclude direct analysis of H₂O in the glass with microbeam or manometric techniques. However, taking the total H₂O content of Bezymianny material as the sum of water H₂O in glass and hornblende, glass H₂O are determined using the phase percentages along with whole rock and hornblende H₂O analyses. The percentages of glass and hornblende are determined through point-counting (e.g.[5]), whole-rock H₂O content are determined through Karl Fischer Titration (e.g. [6]), and hornblende H₂O content are determined by manometry (e.g. [7]). Glass contents range from 39 weight % in highly vesicular blast material to 7 weight % in highly crystalline samples. Hornblende has an average proportion of 6-7 weight % across all samples, and is not correlated with sample crystallinity. Bulk rock H₂O contents range from 0.05 – 0.35 weight %, with highly crystalline samples showing lowered bulk water contents. The following equation relates the previous parameters, and can be used to calculate the H₂O content of glass in Bezymianny blast material:

$$H_2O_{wt.\%}^{Glass} = \frac{H_2O_{wt.\%}^{WR} - (H_2O_{wt.\%}^{HBDE} * Mode_{wt.\%}^{HBDE})}{Mode_{wt.\%}^{Glass}}$$

These glass H₂O contents are then used to calculate intra-edifice pressure using the Moore et al. (1995)² solubility model mentioned previously.

References

1. Kadik, A. A., Maksimov, A. P., and Ivanov, A. P. (1986) Physicochemical Crystallization Conditions and Genesis of Andesites. Nauka, Moscow [in Russian].
2. Moore, G., Venneman, T., and Carmichael, I.S.E. (1995) Solubility of water in magmas to 2 kilobars. *Geology*, 23: 1099-1102
3. Esposti Ongaro, T, Widiwidjayanti, C., Voight, B., Clarke, A.B., and Neri, A. (2008) Simulating the Initial Dynamics of the 18 May 1980 Mount St.Helens Blast. *Eos: Transactions of the American Geophysical Union*, 89(53), Fall Meet. Suppl., Abstract V34A-07.
4. Esposti Ongaro, T, Clarke, A.B., Neri, A., Voight, B., and Widiwidjayanti, C. (1995) A high-performance 3D multiphase flow code to simulate directed blasts and their pyroclastic density currents: example from the Boxing Day event, Montserrat. Programme and Abstracts, Soufriere Hills Volcano — Ten Years On, Scientific Conference, Montserrat.
5. Van der Plas, L., and Tobi, A. C., (1965) A chart for judging the reliability of point counting results. *American Journal of Science*, 263: 87-90.
6. Westrich, H. R. (1987) Determination of water in volcanic glasses by Karl-Fischer titration. *Chemical Geology*, 163: 335-340.
7. King P.L., Vennemann T.W., Holloway J.R., Hervig R.L., Lowenstern J.B., and Forneris J.F. Analytical techniques for volatiles: A case study using intermediate (andesitic) glasses. *American Mineralogist* 2002 87: 1077-1089.

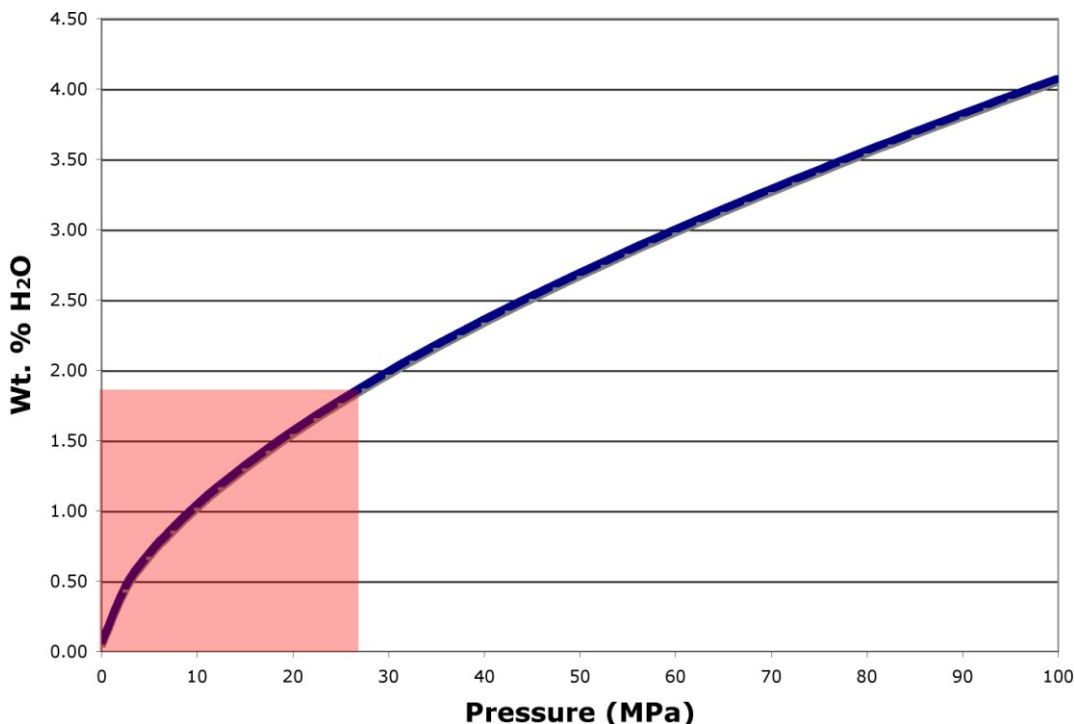


Figure 1: Solubility of water in 1956 Bezymianny melt. Shaded region represents estimated lithostatic values within dome magma prior to the 1956 blast.

PRELIMINARY 1-D VELOCITY MODEL OF BEZYMIANNY VOLCANO (KAMCHATKA, RUSSIA), USA-RUSSIA PIRE PROJECT

Senyukov S.L., Droznina S.Ya.

*Kamchatka Branch of the Geophysical Survey RAS, Petropavlovsk-Kamchatsky, Russia,
e-mail: ssl@emsd.ru*

Bezymianny Volcano ($55^{\circ} 58' N$, $160^{\circ} 35' E$, 2869 m) is located in the central part of the Kluchevskaya group of volcanoes southwest of Kluchevskoy. Bezymianny Volcano's last catastrophic eruption occurred on March 30, 1956, after 900-1000 years of quiescence. Since 1956 the volcano has produced 1-2 explosive eruptions per year, with ash plumes that rose to from 6 km to 15 km above sea level.

Seven new iron bunkers were installed near Bezymianny during 2006-2007 as part of the USA-Russia PIRE project. Eight to nine self-contained seismic stations and one self-contained acoustic station were installed under the auspices of this project in 2007-2008. Joint processing of data from the KBGS telemetered stations and from the PIRE stations has allowed us to:

- 1) calculate a 1-D velocity model of Bezymianny Volcano;
- 2) relocate the volcanic earthquake centers; and
- 3) create a model of the magma system of Bezymianny Volcano and explain the mechanism of Bezymianny's eruptions.

GPS MONITORING OF BEZYMYANY VOLCANO, KAMCHATKA IN 2006-2009

Sergey Serovetnikov, Vilory Bahtiarov, Nikolay Titkov

Kamchatka Branch Geophysical Service, Petropavlovsk-Kamchatsky, Russia.

Bezymianny Volcano produces a strong explosive eruption 1-2 times each year. A 10-point GPS network has been created in the area around this volcano. This network is installed half way around the south side of the Klyuchevskoy volcano group; we require a dense network in order to reach any conclusions about the depth of pressure sources.

Permanent GPS stations based on two-way Trimble NETRS GPS receivers are the backbone of the GPS network. Each station uses a reinforced concrete pylon with a forced centering antenna mount device. The GPS receiver and batteries are installed in a metallic enclosure. The station's power system consists of 18V battery assembly made of 1.5V 300Ah "BAKEN" elements. The total capacity of the power system enables self-contained operation of a GPS station for 380 days. GPS data are recorded to a 2 GB flash memory unit. GPS stations are not equipped with data communication equipment, and downloading data is possible only 1-2 times a year during on-site technical support visits. Technical support workers are brought by helicopter, or travel on foot in the summer season.

Important data about terrestrial crust deformation were received at the end of 2006 by the permanent GPS station BZ09, located 1.5 km from the Bezymianny Volcano crater. During this period of observations, on December 24 2006, Bezymianny Volcano produced a strong explosive eruption with pyroclastic flows. The explosive event caused a strong motion of the GPS station BZ09, especially in the north-south direction. The most interesting results, however, were obtained for a few weeks before and after the eruption. Fifteen days prior to the explosion the moving rate of BZ09 increased gradually, then jumped abruptly during the course of explosion, after which gradually returned to the pre-eruptive moving rate within 25 days. The observed changes of movement rates characterize the processes of eruption preparation, explosive eruption, and post-eruption relaxation at Bezymianny Volcano on December 24, 2006. Some Bezymianny GPS network stations installed close to the volcano have recorded similar observations, but with smaller amplitudes of deformation.

During 2007-2009 Bezymianny Volcano produced 4 strong eruptions. The Bezymianny GPS network continues to detect deformations associated with Bezymianny and Klyuchevskoy volcanic activity. Today the Bezymianny GPS network includes 7 permanent GPS stations and 7 campaign observation points.

PETROPHYSICAL PROPERTIES OF VOLCANIC ROCKS OF BEZYMIANNY VOLCANO, KAMCHATKA, FAR EASTERN RUSSIA

Violetta Shanina

Lomonosov Moscow State University, Moscow, Russia.

Bezymianny Volcano is one of the most active on Kamchatka. It received much attention after its 1956 eruption; during its active period, lava and pyroclastic flows and an extrusive dome formed on its slopes (Braitseva et al., 1990). Presently this volcano is characterized by the regular periodicity of its eruptions (1-2 per year). Not all volcanologists recognize the necessity of studying the physical and physical-mechanical properties of volcanic rocks, but the engineer-geologists have been interested in Bezymianny Volcano for a long time (e.g. Ladygin et al., 2004, 2008); for more than 20 years Ladygin's student, O. Girina, has devoted most of her time to it (Girina, 1988, 1991, 2001). Only the unusual productivity of this young volcano, on whose slopes almost every year one or two new pyroclastic flows can be found, allows young science students to get acquainted with an active volcano, to conduct valuable field work and to publish their first articles.

I visited Bezymianny Volcano for the first time in the summer of 2008 within the framework of the PIRE project. Our group was engaged in studying the pyroclastic flows of recent years. In addition, I studied Dismembered Dome at the contact with the extrusive dome Lokhmaty. The former is characterized by a continuous change from unaltered andesites to products of their hydrothermal alteration toward the contact. This sequence of alteration products may provide additional constraints on the hydrothermal processes related to dome emplacement. Previous studies by Ladygin, Girina, and others suggested that the rocks comprising extrusive domes of Bezymianny Volcano are characterized by low density ($r: 2.19 \text{ g/cm}^3$ on average), velocity of longitudinal waves (V_p and V_{pw} : 2.65 km/sec in dry conditions, and 3.45 km/sec in water-saturated conditions), average durability (R_c and R_{cw} : 82 and 68 MPa, respectively), porosity ($n: 18.8\%$), and magnetic susceptibility ($\alpha: 23.7 \times 10^{-3} \text{ SI}$) (Blyumkina, Shanina, 2009).

The unaltered rocks of the extrusive Dismembered Dome (andesite, specific density 2.69 g/cm^3) differ from rocks of other domes by greater density (2.40 g/cm^3) and smaller porosity (10.8%) and magnetic susceptibility ($29.7 \times 10^{-3} \text{ SI}$); the velocity of longitudinal waves are equal (2.70 km/sec in dry conditions and 3.55 km/sec in water-saturated conditions). The altered varieties of Dismembered Dome rocks have lower density (2.29 g/cm^3) and magnetic susceptibility ($15.5 \times 10^{-3} \text{ SI}$), but higher velocity of longitudinal waves (up to 3.30 km/sec in dry conditions and 4.20 km/sec in wet conditions). This is most likely due to the occurrence of new minerals, which fill pores; a similar effect was observed by the author during experiments studying the hydrothermal transformations of rocks.

We investigated the properties of juvenile pyroclastic flow materials erupted in 2005 and 2007. The rocks are two-pyroxene andesites, light grey in color, porous, and porphyritic, with pyroxene and plagioclase crystals less than 2-3 mm in size. These rocks have minimal density (1.42 g/cm^3 on average), nearly 50 % porosity (from which more than 30% represent open pores), very low hygroscopic humidity ($< 0.1\%$), low longitudinal wave velocity (1.45-1.75 km/sec), and with parameters of durability detailed in Table 1.

On the basis of the characteristics presented above it is possible to conclude that the physical and physical-mechanical properties of extrusive dome andesites strongly differ from

those of pyroclastic flow andesites. This difference is connected to the different genesis of these rocks, and can serve as an additional criterion for definition and division of rocks.

Table 1. Petrophysical properties of pyroclastic flow juvenile materials.

Year	r, g/cm ³	rs, g/cm ³	n, %	W, %	Vp, km/sec	Vp w, km/sec	Rc, MPa	Rcw, MPa	Rstr, MPa	$\alpha \cdot 10^{-3}$ SI
2005	1.20	2.70	55.5	29.0	1.65	2.35	94	43	10	18.5
2006	1.72	2.74	37.4	16.1	1.45	2.30	103	128		26.4
2007	1.42	2.72	46.6	23.0	1.45	2.50	66	45	12	22.3

Blyumkina M.Y., Shanina V.V. Petrophysical properties of Bezymianny Volcano sopka (Kamchatka). Planet Earth: Urgent questions of geology through the eyes of young scientists and students. 2009. pp. 142-146. http://geo.web.ru/pubd//2009/04/14/0001182159/2_39.pdf.

Braitseva O.A., Melekestsev I.V., Bogoyavlenskaya G.E., Maksimov A.P. Volcano Bezymianny: history of formation and dynamics of activity. 1990. Volcanology and Seismology. № 2. p. 3-22.

Girina O.A. Types of pyroclastic deposits of Besymyanny Volcano and criteria of their diagnostics. Volcanology research in Kamchatka. P.-Kamchatskiy. 1988. pp. 9-14.

Girina O.A. Pyroclastic deposits of the Besymyannyi eruption in October 1984. Volcanology and Seismology. 1991. V.12(3):407-417.

Girina O.A. Pyroclastic deposits of andesitic volcanoes and diagnostics of their genetic types. Geodynamics and volcanic processes of the Kurile-Kamchatka Arcs. Petropavlovsk-Kamchatskiy, 2001. pp. 253-266.

Ladygin V.M., Girina O.A., Frolova J.V. Kondrashov I.A. The lava flows of Bezymianny Volcano, Kamchatka. 4th International Biennial Workshop on Subduction Processes Emphasizing the Japan-Kurile-Kamchatka-Aleutian Arcs. 2004. pp. 63-64.

Ladygin V.M., Frolova J.V., Girina O.A., Blyumkina M.E. Petrophysical properties of Bezymianny Volcano (Kamchatka) and their dependence on genesis. The ninth "Physical-Chemical and Petrophysical Research in Earth Sciences" conference, Moscow, 7-10 October 2008, pp. 192-196

The author expresses gratitude to J. Frolova and V. Ladygin for their kindness and ready willingness to help students

PLAGIOCLASE ZONING AS AN INDICATOR OF PROCESSES IN MAGMA SYSTEM BENEATH BEZMYANNY VOLCANO, KAMCHATKA.

Vasily Shcherbakov¹, Pavel Plechov¹, Pavel Izbekov²

¹ Geological department of Moscow State University, Moscow, Russia

² Geophysical Institute, University of Alaska, Fairbanks, AK, USA

Bezmyanny Volcano is located in the Central Kamchatka Depression and is part of the Kluchevskaya group of volcanoes. It is one of the most active andesitic volcanoes in the world. More than 17 large explosive events have occurred since the catastrophic 1956 eruption. The latest decade has been characterized by frequent (1-2 times per year) significant explosive events accompanied by continuous extrusive dome growth. Frequent eruptions allow us to study dynamic changes in the magmatic system as they are recorded in eruptive products.

Plagioclase composition is very sensitive to temperature, pressure, and water content of coexisting melt. Due to very slow interdiffusion of Si and Al in plagioclase, its zoning is often preserved in very fine detail. The complex zoning of plagioclases from eruptions in 2000-2007 was used to determine changes of conditions in the magmatic system.

Zoning of all phenocrysts consists of three main elements (Fig. 1). *Oscillatory zones* have approximately constant composition of 50-60 mol% An with small frequent variations of ± 5 mol% An. *Resorption zones* show abrupt jumps in anorthite content with evidence of intensive dissolution. *Normal zones* reflect sequential crystallization of plagioclase with decreasing anorthite content. Zoning of the majority of phenocrysts consists of the following alternation: *oscillatory zoning*→*resorption zoning*→*normal zoning*→*oscillatory zoning*. The outermost parts of phenocrysts usually consist of resorption and normal zoning.

Frequent resorption of plagioclase, in our view, is caused by periodical replenishment of magma chamber by hotter magma. Magma system recharge at Bezymianny may have triggered every eruption during the 2000-2007 period (1-2 magma injections per year), and causes the crystallization of calcium-rich rims around plagioclase. Models of plagioclase-melt equilibria show that crystallization of plagioclase with anorthite content more than 75 mol.% requires mixing with significant amount of mafic magma. The involvement of mafic material is also suggested by the presence of xenocrysts of olivine and products of its breakdown.

Temperature determined by clinopyroxene-orthopyroxene equilibrium show long term heating of magma from $\sim 890 \pm 20^\circ\text{C}$ in 1956 [1] to $\sim 930 \pm 20^\circ\text{C}$ in 2006. Hornblende breakdown and magnesium rich rims around orthopyroxene also indicate a rise in temperature. Calculations of plagioclase-melt equilibria show that liquidus temperature of anorthite-rich plagioclase (observed in resorption zones in rims) is higher than liquidus temperature oscillatory zones for $\sim 100^\circ\text{C}$. This temperature gap is consistent with temperatures of crystallization of groundmass (950 - 1050°C).

Plagioclases from each eruption show a good correlation of rim zoning within eruption groups. They crystallized during the pre-eruptive period after magma recharge. The same T-P history of all phenocrysts from this period is caused by the small volume of magma which ascends to the surface. Poor correlation of plagioclase rims from the May 9th 2006 eruption is caused by the larger volume of erupted magma, in which intensive parameters may differ in widely-separated areas. Uncorrelated zoning of plagioclase cores from a single eruption seems to be the result of a large magma chamber where each phenocryst may have an individual T-P history, but a quantitative estimation of the volume required for this to occur is not possible yet.

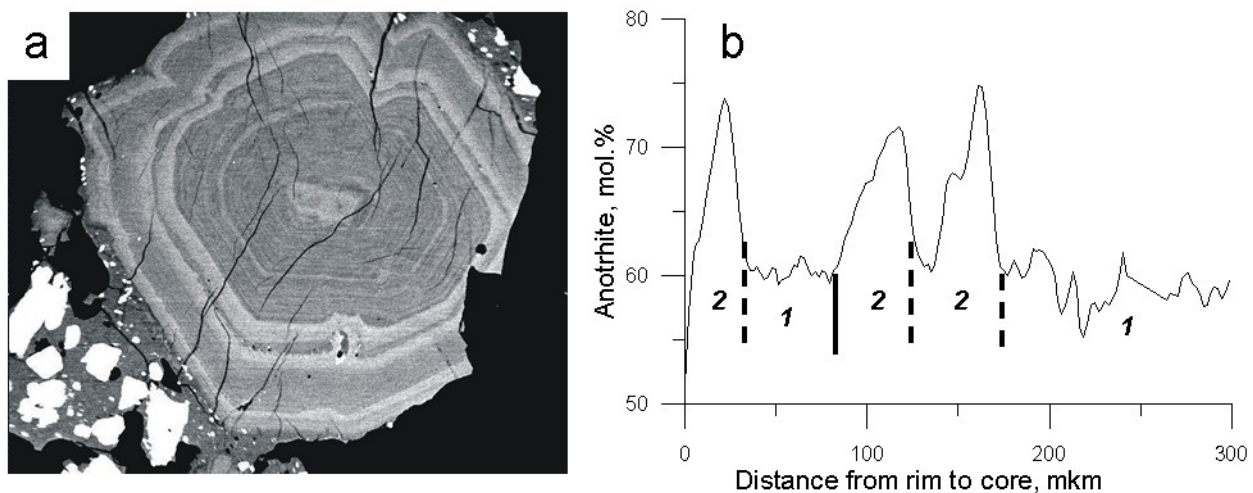


Fig. 1. Typical zoning of plagioclase phenocryst from Bezymyanny andesites. a – BSE image, b – plagioclase composition profile. Dashed lines – zones of resorption, 1 – oscillatory zoning, 2 – normal zoning.

Literature:

1. Plechov P., Tzay A., Scherbakov V., Dirksen O. (2008) "Hornblendes in andesites of 30 March 1956 Bezymyanniy eruption and conditions of their opacitization", Petrology, 16(1): 19-35.

PETROLOGIC INSIGHT INTO THE MAGMATIC SYSTEMS AT BEZYMIANNY AND SHIVELUCH VOLCANOES, KAMCHATKA, RUSSIA

Jill Shipman¹, Pavel Izbekov¹, and John Eichelberger²

¹*Geophysical Institute, Alaska Volcano Observatory, University of Alaska Fairbanks, Fairbanks, AK, USA.*

²*Volcano Hazards Program, U.S. Geological Survey, Reston, VA.*

Bezymianny and Shiveluch volcanoes of the northern Kamchatka Peninsula, Russia have experienced catastrophic collapse (1956 and 1964, respectively), plinian eruption and subsequent dome building and intermittent explosive activity similar to the well-known sequence at Mount St. Helens, WA that began in 1980. As part of the international collaborative study into the comparison between these systems, we present results of petrologic studies of bulk chemical trends, crystal size distributions (CSD), and crystallization temperatures at Bezymianny and Shiveluch. These three systems exhibit contrasting petrologic trends over the decades since their initial paroxysmal eruptions that are not yet fully understood.

X-ray fluorescence analysis was conducted on a PANalytical Axios XRF at the University of Alaska Fairbanks Advanced Instrumentation Laboratory on glass beads for samples at Bezymianny and Shiveluch volcanoes. Bezymianny exhibits a bulk chemical trend toward more mafic compositions from 61.0 wt. % SiO₂ ($\sigma = 0.3$) in 1956 to 56.5 wt. % SiO₂ ($\sigma = 0.1$) in 2007. On a finer scale, there are periods of apparent pulsatory behavior where the composition temporarily shows a reverse trend with an increase in wt. % SiO₂. Shiveluch however, exhibits a bulk trend toward increasing wt. % SiO₂ since its catastrophic eruption in 1964. Compositions range from 60.6 wt. % SiO₂ ($\sigma = 0.2$) in 1964 to 64.2 wt. % SiO₂ ($\sigma = 1.0$) in 2007.

CSDs have been calculated for plagioclase in representative samples from Bezymianny and Shiveluch volcanoes, based on digitized intersections using the method of Higgins and Roberge (2003) with CSD Corrections v1.38 software (Higgins, 2000, 2002, 2006). An initially steep negative slope in crystal size vs. ln population density of the CSD suggests an initial period of nucleation and growth. This initial period of growth is typically followed by a flattening of the slope, which is consistent with partial solution and textural coarsening as a result of mafic magma injection.

Crystallization temperatures were determined for the Bezymianny sample suite from 1955 to 2007 using both co-existing Fe-Ti oxides and two-pyroxene methods. Analyses were conducted on a Cameca SX-50 Electron Microprobe at the University of Alaska Fairbanks Advanced Instrumentation Laboratory. Totals for Fe-Ti oxides were then recalculated according to Stormer, 1983. Temperature and oxygen fugacity were calculated using both the QUILF program (Andersen and Lindsley, 1993) and an online Fe-Ti oxide geothermometer (Ghiorso and Evans, 2008). Two pyroxene temperatures were also calculated with an online utility from Moscow State University using the calibration by Wells, 1977. Temperatures for 1956 blast material were found to range from 900°C – 950°C ($\pm 30^\circ\text{C}$ uncertainty of geothermometer calibration). From 1956 to 2007, a general warming trend is observed with an increase to 1050°C $\pm 30^\circ\text{C}$. Crystallization temperatures also exhibit the apparent pulsatory behavior of the bulk chemical trend.

Bezymianny's correlated chemical and temperature trend can be understood as reflecting continued mafic recharge subsequent to the initial collapse-blast-plinian sequence, with reversals perhaps reflecting intervals of minor differentiation. The invariant character of Mount St Helens

chemistry with time may reflect an absence of such recharge. However, the increase in silica content of Shiveluch magma despite clear evidence of mafic recharge poses a paradox.

References

- Andersen, D. J., D. H. Lindsley, et al. (1993). "QUILF - a Pascal Program to Assess Equilibria among Fe-Mg-Mn-Ti Oxides, Pyroxenes, Olivine, and Quartz." Computers & Geosciences **19**(9): 1333-1350.
- Ghiorso, M. S. and B. W. Evans (2008). "Thermodynamics of Rhombohedral Oxide Solid Solutions and a Revision of the Fe-Ti Two-oxide Geothermometer and Oxygen-barometer." American Journal of Science **308**: In press.
- Higgins, M. D. (2000). "Measurement of Crystal Size Distributions." American Mineralogist **85**(9): 1105-1116.
- Higgins, M. D. (2002). "Closure in Crystal Size Distributions (CSD), Verification of CSD Calculations, and the Significance of CSD Fans." American Mineralogist **87**(1): 171-175.
- Higgins, M. D. and J. Roberge (2003). "Crystal Size Distribution of Plagioclase and Amphibole from Soufriere Hills Volcano, Montserrat: Evidence for Dynamic Crystallization - Textural Coarsening Cycles." Journal of Petrology **44** (8): 1401-1411.
- Higgins, M. D. (2006). Quantitative Textural Measurements in Igneous and Metamorphic Petrology, Cambridge University Press.
- Stormer, J. C. (1983). "The Effects of Recalculation on Estimates of Temperature and Oxygen Fugacity from Analyses of Multi-component Iron Titanium-Oxides." American Mineralogist **68**(5-6): 586-594.
- Wells, P. R. A. (1977). "Pyroxene Thermometry in Simple and Complex systems." Contributions to Mineralogy and Petrology **62**: 129-139.

INVESTIGATING THE PLINIAN PHASE OF THE 1956 BEZYMIANNY ERUPTION USING MICROTEXTURAL ANALYSIS OF PYROCLASTIC FLOW DEPOSITS

Wendy K. Stovall¹, Bruce F. Houghton¹, PIRE Team (2006)

¹*University of Hawai‘i at Mānoa, Geology and Geophysics Department, Honolulu, HI USA.*

A sector collapse of Bezymianny volcano, Kamchatka, Russia in March 1956, resulted in a directed blast followed by a Plinian explosive eruption. Material from the eruption covered 500 km² east of the main volcanic edifice. During August 2006, samples were collected from the upper portion of the 1956 pyroclastic flows and from the fines depleted Layer B of the directed blast. The pyroclastic flow deposits are representative of the ejecta collapsing from the Plinian column and clasts incorporated during turbulent flow. Layer B is associated with the direct blast and is representative of the cryptodome that grew prior to the 1956 eruption. The density distribution of clasts from the pyroclastic flow deposit is bimodal and the total population ranges between 1200 – 2700 kg/m³. Material from Layer B is unimodal skewed towards a lower density tail and correlates to the higher density mode in the pyroclastic flow deposit (1800 – 2800 kg/m³). Microtextural analysis of clasts from the pyroclastic flow yield size data and vesicle number densities that give clues to the mechanisms behind the Plinian phase of the eruption. Comparison of these data to the Plinian phases of other explosive eruptions, such as Mount St. Helens 1980, Mount Mazama 7700 B.P., Novarupta 1912, Askja 1875, Taupo 186, and Etna 122 B.C., help us to understand the pre- and syn-eruptive rheology of the magma driving the 1956 Bezymianny eruption.

PRACTICAL APPLICATIONS OF MULTIPLET BEHAVIOR AT MOUNT ST. HELENS, WASHINGTON AND BEZYMIANNY VOLCANO, RUSSIA

Weston A. Thelen¹, Michael West², Stephen D. Malone¹

¹*Earth & Space Sciences, Univ. of Washington. Seattle, WA, USA.*

²*Geophysical Institute, Univ. of Alaska, Fairbanks. Fairbanks, AK, USA.*

Multiplets, or groups of earthquakes with similar waveforms, are a common occurrence on a variety of volcanoes exhibiting unrest. Multiplets were present during many eruptive periods at Mount St. Helens and Bezymianny Volcanoes. We have constructed a catalog of sets of multiplets using triggered data from the 1980-1986 Mount St. Helens eruption, and continuous data from eruptions in 2004 at Mount St. Helens and 2007 at Bezymianny Volcano. Here we look at all of the multiplets occurring during a given time period and characterize each multiplet individually based on the events within that group. Events are defined to be part of a multiplet when 9 seconds around the event trigger is similar at a cross-correlation value of 0.7 on 2 or more stations. Prior to explosions at Bezymianny in 2007 and Mount St. Helens in 2004, the percentage of total seismicity (PTS) that consists of multiplets declined, while the average amplitudes and standard deviations of those averages increased. The lifetimes of multiplets were also shorter prior to explosions, ranging from hours to days. During dome extrusion or periods of relative stability, some vigorous multiplets had lifetimes of weeks. One difference between the two volcanoes is the behavior in the number of contemporary multiplets. At Mount St. Helens during the 2004 eruption, the number of multiplets occurring at the same time increased prior to explosive activity and was variable during explosive activity and dome building. At Bezymianny Volcano in October 2007, the number of contemporary multiplets decreased dramatically prior to large explosions and was generally higher during periods of background activity.

The number, characteristics, and behavior of the multiplets occurring during a certain time were largely dictated by the state of material in the shallow conduit. At Mount St. Helens prior to 1983, there was weak multiplet development related mostly to deep seismicity after the 1980 eruption and prior to the 1982 eruption. After 1983 at Mount St. Helens, multiplet development occurred during periods of spine extrusion and around eruptions when the volume extrusion rate was lower, allowing for more complete degassing and crystallization of magma in the shallow conduit. During the 2004 eruption at Mount St. Helens, there was vigorous multiplet development prior to and accompanied by extrusion of a solidified plug at the surface. Bezymianny shows far fewer and less vigorous multiplets than Mount St. Helens, particularly prior to large explosions.

By comparing the state of the shallow conduit at both volcanoes during their most recent eruptions, we can gain insight into the processes generating multiplets. Our interpretation of the observations above is concentrated on the area immediately around the conduit. Conceptually, the relatively unstable environment prior to explosions possesses large and chaotic stress gradients brought about by elevated overpressures within the conduit. The large complex stress field activates sources on a variety of fractures and cracks surrounding the conduit. As a result, the PTS of multiplets should be low because no dominant, repeating stress is present to drive the generation of multiplets. Likewise multiplets that do occur will be short-lived. In systems without a solidified extrusive plug, the low number of contemporaneous multiplets with high average amplitudes prior to an eruption may suggest high stress concentrations over a small area. The most striking difference between large explosive eruptions and dome-forming eruptions at Bezymianny and Mount St. Helens is the dramatic difference in PTS of multiplets. In explosive eruptions the PTS of

multiplets is low, usually below 20%. Dome forming eruptions that include a partially solidified plug, like Mount St. Helens (1983-1986, 2004-2008) often possess more vigorous and long-duration multiplets with PTS of multiplets often exceeding 50%. In an eruption that includes a solidified extrusive plug, a high number of contemporaneous multiplets may be a sign of increased slip along several patches around the outside of the conduit or repeated readjustment of the plug through a constriction in the conduit. Regardless of the actual source mechanism of the multiplets, the extrusion of a solidified plug appears to improve the efficiency of multiplet development.

INFLUENCE OF MAGMA-WALLROCK HEAT TRANSFER ON ERUPTION DYNAMICS

Yulia Tsvetkova, Oleg Melnik

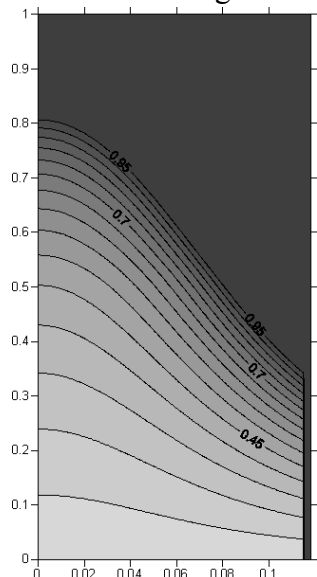
Institute of Mechanics, Moscow State University, Russia.

There is a set of models of magma flow in volcanic conduits which predicts oscillations in magma discharge during extrusion of lava domes [1,3,4,5,6]. These models neglect heating and deformation of surrounding rocks and use 1D approximation of the flow in the conduit. In the case of continuous extrusive eruptions we cannot neglect heat transfer to wall rocks because magma ascends slowly and convective heat transfer is comparable to conductive. An axis-symmetrical model for these eruptions was considered in [5]. Here magma flow is investigated with an account of heat exchange between surrounding rocks and magma and different dependencies of viscosity on temperature and crystal concentration. Stick-slip conditions were applied for the wall. The model assumes a parabolic velocity profile, and the flow is quasi-static and quasi one-dimensional. At the top of the conduit the pressure is assumed to be fixed; chamber pressure changes according to magma influx and out flux [1].

$$\frac{dP_{ch}}{dt} = \frac{E}{V_{ch}}(Q_{in} - \lambda)$$

When magma viscosity depends only on temperature no oscillatory behavior was found by simulations. Magma discharge trends asymptotically to the value of Q_{in} . Elastic deformation of surrounding rocks decreases the time required to approach this asymptotic value and decreases oscillations in discharge rate. These results are in contradiction with [4] where constant wall temperature is assumed. In our model, heat flux to wall rocks decreases with time and the cause of oscillations discovered in [3, 4] disappears.

In earlier models that account for crystal growth kinetics the temperature was allowed to change due only to the release of latent heat of crystallization. Heat transfer leads to cooling of the outer parts of the conduit, resulting in high crystal contents (Fig 1) and high magma viscosities. Changes in viscosity result in changes in discharge rate. For the non-isothermal case



there is no motion during most of the cycle (Fig 2) and a portion of magma solidifies at the top of the conduit, forming a plug. During the repose period chamber pressure grows due to influx of fresh magma, and magma discharge rate starts to increase. Influx of hot magma into the conduit leads to a decrease in friction resulting in a jump in discharge rate that leads to depressurization of the magma chamber. When the discharge rate decreases, the magma solidifies again. For an isothermal model with the same parameters, the discharge rate monotonically trends to the value of Q_{in} .

Accounting for heat transfer between magma and surrounding rocks is shown to have a major influence on eruption dynamics for the case of extrusive eruptions. The model must be developed further to overcome 1D simplification in description of conduit flow dynamics.

Fig.1. Crystal concentration in the conduit. Area where crystal concentration equals 1 is a plug.

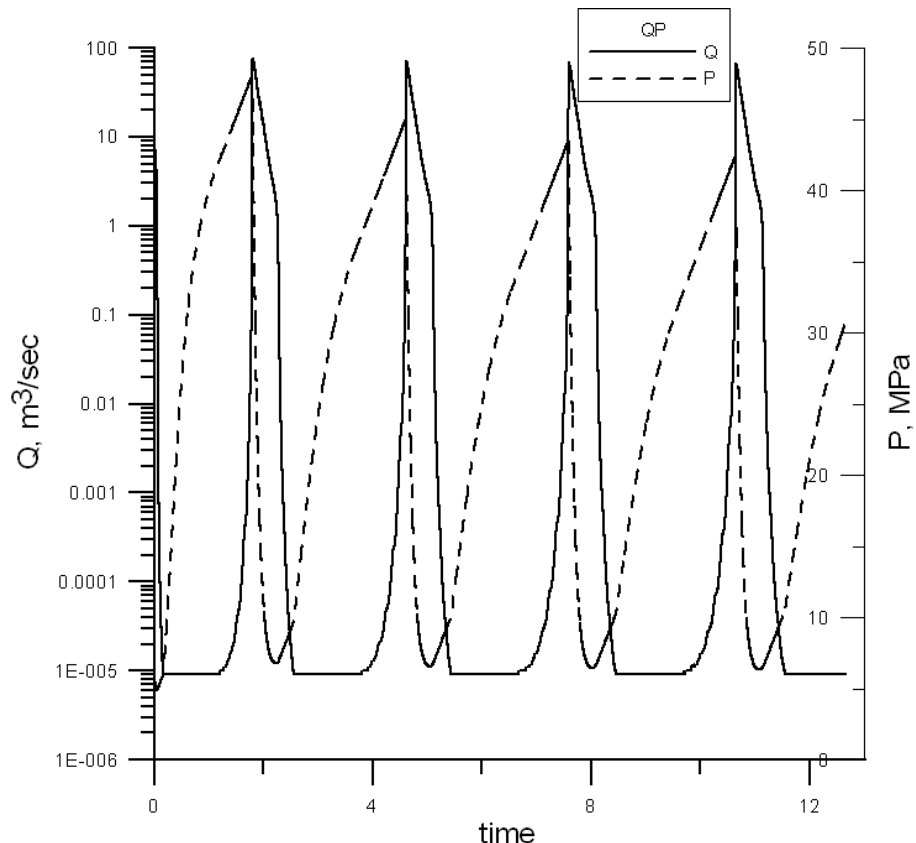


Fig.2. Evolution discharge rate and pressure. Dashed line is pressure and solid line is discharge rate.

References

1. Barmin, A., O. Melnik, R.S.J. Sparks, Periodoc behavior in lava dome eruptions, 2002, Earth and Planetary Science Letters 199:173-184
2. Bruce, P.M., H.E. Huppert, Thermal control of basaltic fissure eruptions, 1989, Letters To Nature, 342.
3. Maeda, I., Nonlinear visco-elastic volcanic model and its application to the recent eruption of Mt.Unzen, 2000, Journal of Volcanology and Geothermal Research, 95:35-47
4. Whitehead, J.A., K.R. Helffrich, Instability of flow with temperature dependent viscosity: A model of magma dynamics, 1991, Journal of Geophysical Research, 96(B3): 4145-4155
5. Costa, A., G. Macedonio, Nonlinear phenomena in fluids with temperature-dependent viscosity: An hysteresis model for magma flow in conduits, 2002, Geophysical Research Letters, 29(10):1402
6. Iverson, R., Dynamics of seismogenic volcanic extrusion resisted by a solid surface plug, Mount St. Helens, 2004–2005, A Volcano Rekindled: The First Year of Renewed Eruption at Mount St. Helens, 2004-2006.

FIFTEEN YEARS OF SPACEBORNE THERMAL OBSERVATIONS AT BEZYMIANNY: DOME GROWTH, PRECURSORS AND EXPLOSIVE ERUPTIONS

S. M. van Manen¹, J. Dehn²

¹*Volcano Dynamics Group, The Open University, Milton Keynes, UK.*

²*The Alaska Volcano Observatory, Fairbanks, Alaska, USA.*

Fifteen years worth of Advanced Very High Resolution Radiometer (AVHRR) data are used to shed light on processes occurring at Bezymianny. This volcano is one of Kamchatka's most dangerous volcanoes with fifteen eruptions in the last decade that have dispersed ash into North Pacific air routes. All known episodes of increased activity for which data are available are detected. Understanding the processes involved in dome growth and edifice failure at Bezymianny is essential to forecasting explosive eruptions and increasing aviation safety in the region. Methods aimed at predicting explosive volcanic eruptions have primarily focused on seismic data, however, volcanic dome building episodes commonly show increases in extrusion rate prior to erupting explosively. These increases in extrusion rate will result in an increase in the radiated thermal flux, which can be detected by satellites. The ability to identify, quantify and understand these increases will hold the key to predicting explosive eruptions at these volcanoes. Bezymianny shows complex oscillatory behaviour in its thermal signal on a variety of time scales that can be linked to a systematic process leading to explosive conditions, followed by extrusion. This process is strongly influenced by three main parameters: (1) magma supply rate, (2) magma properties and (3) edifice properties. Three different types of precursors to explosive behaviour have been identified at Bezymianny: (1) no change in background thermal levels (2) increases in radiant temperature 1-5 days prior to explosion and (3) increases in radiant temperature that result in sensor saturation up to 15 days prior to explosion. These different styles of precursory activity relate back to processes occurring on the ground, such as increased degassing or pre-explosive extrusion. Using these precursory patterns a basic algorithm is able to provide a retrospective early warning for 95% of explosions that have occurred during the past fifteen years. This algorithm can be integrated with the existing Okmok II algorithm to provide early warnings in the future. We conclude that the monitoring and analyzing of radiant thermal flux can potentially be applied successfully to forecast explosive events accompanying dome-building eruptions at other volcanoes around the world.

THE KURILE BIOCOMPLEXITY PROJECT

ORAL PRESENTATIONS

PALEOTSUNAMI STUDIES IN THE CENTRAL KURIL ISLANDS—PRELIMINARY REPORT BASED ON THREE KURIL-BIOMPLEXITY-PROJECT FIELD SEASONS

Joanne Bourgeois¹, Tatiana Pinegina², Breanyn MacInnes¹, M. Elizabeth Martin¹, Ekaterina Kravchunovskaya², Nadezhda Razzhegaeva³, Vera Ponomareva² & KBP teams

¹*Earth & Space Sciences, Univ. of Washington, Seattle, WA, USA.*

²*Institute of Volcanology & Seismology, Petropavlovsk-Kamchatskiy, Russia.*

³*Pacific Institute of Geography FEB RAS, Vladivostok, Russia*

The entire JKASP region provides unparalleled opportunity for the study of paleotsunamis because of prolific volcanic ash production upwind of tsunami-susceptible coastlines, leaving a record of marker tephra layers intercalated with tsunami deposits. Moreover, virtually all these north-Pacific shorelines have experienced one or more locally generated historical tsunamis. A modern analogue is very useful to calibrate the relationship between deposit distribution and earthquake source (as in Martin et al., 2008). Ideally, in order to produce probabilistic earthquake and tsunami hazard analyses in areas with short historical records, a paleotsunami record should include marker time lines such as tephra layers, and datable material such as peat and charcoal, as well as a well-studied modern tsunami analogue.

The 2006 (and 2007 and 2009) central Kurils earthquakes filled a seismic gap that had been previously interpreted by some as a non-seismic region. Now, in addition to a major post-tsunami survey (MacInnes et al., 2009 and submitted), we have conducted three field seasons of paleotsunami research focused in the central Kurils. As early as summer 2006, before the 15 Nov 2006 Mw ~8.3 interplate earthquake and ensuing tsunami, we knew this region experienced large tsunamis, based on prehistoric deposits. However, erosion and deposition from the 2006 tsunami presented us with a clear-cut modern analogue for our work on prehistoric cases.

We have applied the tephra-tsunami-deposit approach outlined in Bourgeois et al. (2006) to examine paleotsunami records from northern Kamchatka to the southern Kurils (see also Pinegina JKASP abstract). Herein we present a *preliminary* report on the central Kurils paleotsunami record (Figure 1). It is clear that many large tsunamis, some larger than 2006, have affected the central Kurils in the last 2000 years. Further work requires correlation of tephra with Nakagawa et al.’s geochemical analyses (Nakagawa et al. JKASP abstract and unpublished reports), review of all our sections and notes, and then statistical analysis in order to quantify the record, in particular paying attention not only to runup, but also to inundation.

References

- Bourgeois, J., Pinegina, T., Ponomareva, V., Zaretskaia, N., 2006. Holocene tsunamis in the southwestern Bering Sea, Russian Far East, and their tectonic implications: *Geological Soc. America Bulletin*, v. 118, p. 449-463.
- MacInnes, B.T., Pinegina, T.K., Bourgeois, J., Razhegaeva, N.G., Kaistrenko, V.M., Kravchunovskaya, E.A., 2009, Field survey and geological effects of the 15 November 2006 Kuril tsunami in the middle Kuril Islands, *Pure and Applied Geophysics* v. 166, DOI 10.1007/s00024-008-0428-3
- Martin, M. E., R. Weiss, J. Bourgeois, T. K Pinegina, H. Houston, and V. V. Titov, 2008. Combining constraints from tsunami modeling and sedimentology to untangle the 1969 Ozernoi and 1971 Kamchatskii tsunamis, *Geophys. Res. Lett.*, v. 35, L01610. doi:10.1029/2007GL032349

	URUP	CHRPOI	N. SIMUSHIR	USHISHIR	RASSHUA	MATUA	SHLASHKOTAN
	S	S	N	98 110 109 100,101		\$ Bay	\$ Bay
> 5 m	> 9 m	> 7 m.	> 10 m	> 5 m no	> 7 m no	> 5 m no	> 10 m no
A.D. 2006	no	no	*	*	*	*	*
~500 rcybp
~1000 rcybp
~2000 rcybp
~2400 rcybp	x	x	x	x	x	x	x

~500-800 rcybp

~1000 rcybp?

~2000 rcybp?

~2400 rcybp

Figure 1. PRELIMINARY summary of paleotsunami deposits (shown as dots) in the central Kuril Islands, counted between marker tephra (shaded horizontal bars), whose ages are *also still preliminary*. Each dot in a column represents an interpreted tsunami deposit. Presence or absence of the 2006 tsunami deposit is noted. Columns are organized by island and by runup elevation of a site. Some columns are single key excavations, others are composites. An X within a tephra layer means it was not present in that particular set of excavation(s), but the tephra is known to occur at that locality. A plus (+) sign, means the number of dots is a minimum above an unseen tephra layer. Rcybp means radiocarbon years before present. Vertical shading indicates the excavation did not extend deeper than a certain ash layer.

Participation in the Kuril Biocomplexity Project was made possible in part by US NSF grant ARC-0508109; Ben Fitzhugh, PI, and various logistical and financial support from: Univ. of Washington; Hokkaido University Museum; Historical Museum of Hokkaido; Sakhalin Regional Museum; and the Far East Branch of the Russian Academy of Sciences (IMGG: Yuzhno-Sakhalinsk, IVGG: Petropavlovsk-Kamchatsky, NEISRI:Magadan). Thanks to our may surveyors, diggers and helpers for the paleotsunami work. A more complete list of participants can be found at: <http://depts.washington.edu/kip/KBPpublic/KBPpeople/People.shtml>

SOME MULTI-DISCIPLINARY RESULTS FROM THE 2006, 2007 AND 2008 EXPEDITIONS OF THE KURIL BIOMULTIDISCIPLINARITY PROJECT

Ben Fitzhugh¹, Joanne Bourgeois², Mike Etnier¹, Erik Gjesfield¹ and KBP teams

¹*Anthropology, Univ. of Washington, Seattle, WA, USA.*

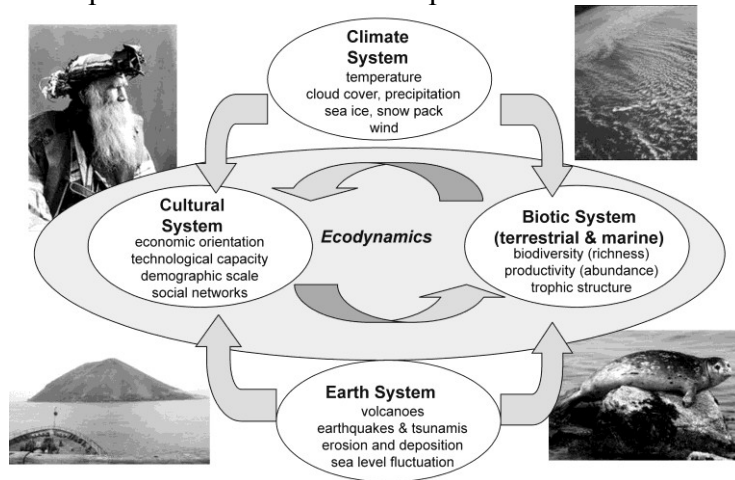
²*Earth & Space Sciences, Univ. of Washington, Seattle, WA, USA.*

The Kuril Biocomplexity Project (<http://depts.washington.edu/kip/index.shtml>) is an NSF-funded, multi-disciplinary research project led by the University of Washington and being conducted by a team of American, Japanese and Russian scholars and students, examining a 5000-year history of human-environmental interactions along the Kuril Island chain. After a preliminary study in 2000, major field expeditions occurred in summers 2006, 2007 and 2008. Field study focused on archaeology, zooarchaeology, volcanology, geomorphology and paleoseismology/tsunami studies, with samples also collected for paleoenvironmental and paleoclimate analysis, and geodesy. These disciplines are brought together in KBP to try to understand the dynamic relationships of natural and social processes in Kuril history.

Our 2006 and 2007 summer expeditions bridged a winter doublet of great earthquakes in the central Kurils, with at least one large tsunami (MacInnes et al., 2009; JKASP abstract). Moreover, KBP facilitated installation of permanent and campaign GPS stations (Steblov et al. 2008; JKASP abstract), including the first two remote sites to record continuously for a year (2007-2008), in the central Kurils.

Before KBP expeditions, work on Kurils volcanic history had been primarily on the larger southern and northern islands. For KBP, teams led by A. Rybin (JKASP abstract; also Kozlov, Zharkov) focused on active volcanism and on edifice structure, and teams led by Y. Ishizuka (2000, 2006) and M. Nakagawa (2007, 2008; JKASP abstract) focused on Holocene eruptions. All archaeological and paleoseismological excavations also have recorded and sampled tephra layers. Several new marker layers have been identified in the central Kurils.

Archaeological work has confirmed human occupation through the Kurils back to 2500 - 3000 rcybp. Population densities were highest between 2500 and 800 BP, but apparently occupations were discontinuous between these dates. Evidence, so far not completely analyzed, hints at pulses of high-intensity occupation through the chain followed by periods of low levels of activity. There is a gap in dated occupations throughout the islands minimally between 300 and 600 rcybp, possibly correlated with the Little Ice Age, and terminated by appearance of Ainu culture in the Kurils. This gap may partially be explained by increased volcanism on Hokkaido during this time; however, we have found that the Ushishir caldera eruption ca. 2100 rcybp did not significantly affect central Kurils settlement on the resolvable time scale, and other factors remain to be considered.



Schematic representation of system components for modeling the historical ecology of the Kuril Islands and similar contexts

With regard to preservation of archaeological materials, tsunamis in the Kurils are likely net-erosive of coastal sediments (MacInnes JKASP abstract), selectively removing archaeological evidence from low areas of coast. We have found most sites above 20 meters and on the Okhotsk side. A dearth of Ainu occupation may be explained by a more typically mobile lifestyle, nearshore camping, and greater loss of record to coastal erosion, but still indicating somehow smaller population densities than earlier. A model of tsunami frequency on different sections of coastline may help to determine the probability of preservation back through time. Preliminary results on tsunami frequency are reported by Bourgeois et al. (JKASP abstract)

The primary means of livelihood in the Kurils has been maritime hunter-gatherer, with each site having a unique assemblage of fauna. Relative contribution of each of the major groups of marine mammals (seals, fur seals and sea lions, and sea otters) appears to be site-specific. Likewise, dominant bird species varies by site (e.g., sea eagle at Ainu Creek; albatross at Rasshua 1). Many archaeological materials were locally generated. However, an obsidian source has not been found in the Kurils, and recovered obsidian can be sourced to Kamchatka and Hokkaido (Phillips and Speakman, 2009; Phillips JKASP abstract). Preliminary work on pottery indicates tempering agents are more typically sandy south of Chirpoi than north, suggesting locally manufactured, rather than traded, ceramics.

Preliminary theoretical work suggests alternative approaches to dealing with environmental risks in isolated environments. We are using geographical variability to scale predictions between the more and less isolated parts of the Kurils. These approaches are leading us to look for evidence of social networks and technological intensification as alternative strategies in the most isolated locations. Results from this project are providing insights into the dynamics of human-environmental interactions in remote island environments as well as the sensitivities of insular ecosystems to human occupation, volcanic eruptions, tsunamis, and climate change.

References

- MacInnes, B.T., Pinegina, T.K., Bourgeois, J., Razhegaeva, N.G., Kaistrenko, V.M., and Kravchunovskaya, E.A., 2009, Field survey and geological effects of the 15 November 2006 Kuril tsunami in the middle Kuril Islands, *Pure and Applied Geophysics* v. 166, DOI 10.1007/s00024-008-0428-3
- Phillips, S.C. and R.J. Speakman, 2009d. Initial source evaluation of archaeological obsidian from the Kuril Islands of the Russian Far East using portable XRF. *Journal of Archaeological Science* 36(6): 1256-1263.
- Steblov, G.M., Kogan, M.G., Levin, B.V., Vasilenko, N.F., Prytkov, A.S., and Frolov, D., 2008, Spatially linked asperities of the 2006-2007 great Kuril earthquakes revealed by GPS: *Geophysical Research Letters* v. 35, L22306, doi:10.1029/2008GL035572

Participation in the Kuril Biocomplexity Project was made possible in part by US NSF grant ARC-0508109; Ben Fitzhugh, PI, and various logistical and financial support from: Univ. of Washington; Hokkaido University Museum; Historical Museum of Hokkaido; Sakhalin Regional Museum; and the Far East Branch of the Russian Academy of Sciences (IMGG: Yuzhno-Sakhalinsk, IVGG: Petropavlovsk-Kamchatsky, NEISRI:Magadan).

A more complete list of participants can be found at:
<http://depts.washington.edu/ikip/KBPpublic/KBPpeople/People.shtml>

TSUNAMI DEPOSITS CAN DISTINGUISH THE DISTRIBUTION OF SLIP DURING THE 1952 KAMCHATKA EARTHQUAKE

Breanyn MacInnes¹, Robert Weiss², Joanne Bourgeois¹

¹*Earth & Space Sciences, Univ. of Washington, Seattle, WA, USA.*

²*Dept. Geology and Geophysics, Texas A&M University, College Station, TX, USA*

Of utmost interest to the tsunami-modeling and tsunami-hazard-assessment communities is the degree to which earthquake characteristics need to be considered in producing reliable runup and inundation models. Geist (2002) theorized that earthquake characteristics such as slip distribution along a rupture strongly affect near-field tsunamis. Therefore, tsunami models that use generic uniform earthquake ruptures could be misleading in predicting tsunami runup in the near field.

Sediment records of tsunamis from the near field of paleo-earthquakes provide the best available proxy of tsunami characteristics because tsunami deposits can be used as an approximation of paleotsunami runup and inundation. Tsunami deposits provide the basic information that 1) a tsunami must have reached the location of the deposit and 2) the farthest inland deposit location is a minimum estimate of runup and inundation. As such, tsunami deposits can be used to determine regional variations in the magnitude of a tsunami.

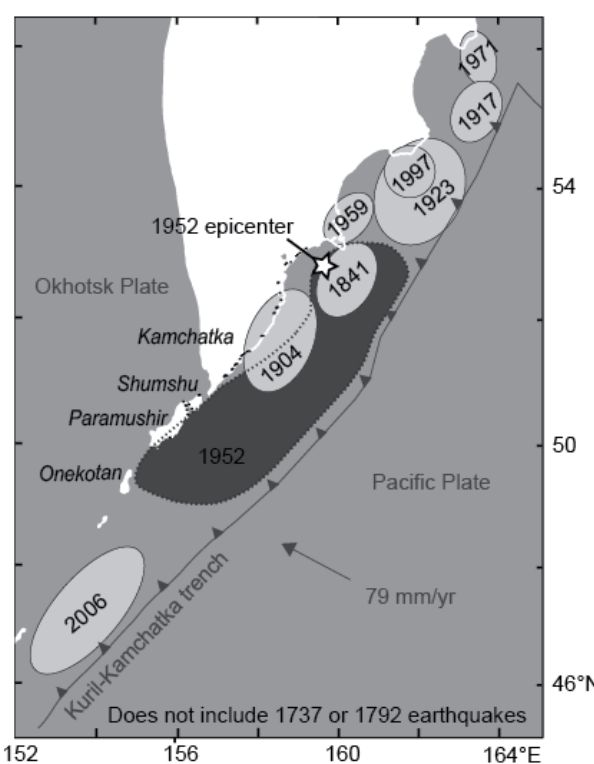


Figure 1: The generally accepted rupture area of the 1952 earthquake is approximately 700 km long--from northern Onekotan Island (49°N) to Shipunskii Cape (52.5°N)--and 150-200 km wide.

Our study uses the 1952 Kamchatka earthquake (M_w 8.8-9.0) (Fig. 1) and tsunami to explore the effect that internal distribution of slip within an earthquake has on tsunami runup in the near-field. We compare modeled tsunamis from this event with deposits in order to determine locations of higher slip during the earthquake. The 1952 Kamchatka earthquake produced a tsunami with extensive deposits, which we have identified and mapped along the Pacific coasts of central and southern Kamchatka and the northern Kuril Islands.

Our investigation of tsunami deposits, combined with catalogued observations of the tsunami, estimates minimum runup of the 1952 Kamchatka tsunami throughout the near-field.

The tsunami runup was 15-20 m in southern Kamchatka and northern Kuril Islands while only ~5-10 m in other near-field regions (Fig. 2).

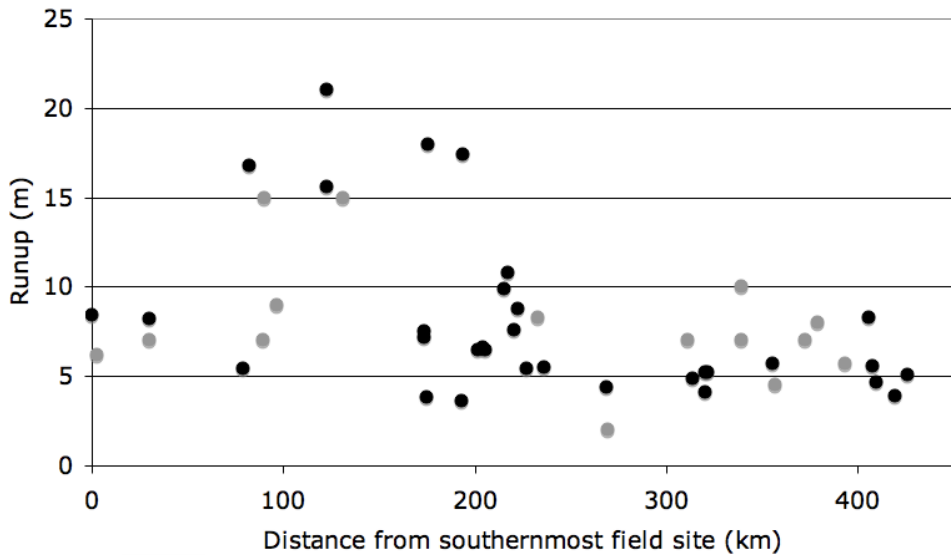


Figure 2: Estimations of tsunami runup from 1952 Kamchatka tsunami using deposits (black) and catalogued (grey) observations. The x-axis is the distance from S. Paramushir. The northern Kuril Islands are from 0-100 km. Southern Kamchatka begins at 131 km. Petropavlovsk-Kamchatski is at 395 km.

To relate tsunami deposits to earthquake slip, we used the MOST tsunami model (Titov and Synolakis, 1995; 1998) to propagate tsunami from seafloor deformation caused by potential slip distributions for the 1952 event. Only large-scale variations in slip distribution were apparent in near-shore tsunami variability for an earthquake of this size. However, the observed difference in tsunami runup from north to south can only be produced when slip is concentrated adjacent to southern Kamchatka. The location of high slip is comparable to asperities found by Bürgmann et al. (2005) suggesting that for the case of Kamchatka, a larger tsunami in southern Kamchatka are likely to reoccur during the next large Kamchatka earthquake.

References

- Bürgmann R, Kogan MG, Steblov GM, Hillel G, Levin VE, Apel E, 2005, Interseismic coupling and asperity distribution along the Kamchatka subduction zone: *Journal of Geophysical Research- Solid Earth*, 110, B07405.
- Geist, EL, 2002, Complex earthquake rupture and local tsunamis, *Journal of Geophysical Research*, 107, doi:10.1029/2000JB000139
- Titov, VV and Synolakis, C.E., 1995, Modeling of breaking and nonbreaking long-wave evolution and runup using VTCS-2. *Journal of Waterways, Ports and Ocean Engineering*, v. 121, p. 308-316.
- Titov, VV and Synolakis, CE, 1998, Numerical modeling of tidal wave runup, *Journal of Waterway, Port, Coastal and Ocean Engineering*, v. 124, p. 157-171.

TEPHROSTRATIGRAPHY OF KURIL ISLANDS: EVALUATION OF HOLOCENE ERUPTIVE ACTIVITY OF KURIL ARC

Mitsuhiko Nakagawa¹, Akira Baba¹, Yoshihiro Ishizuka², Takeshi Hasegawa¹, Ayumi Kosugi¹

¹*Earth & Planetary System Science, Hokkaido Univ., Sapporo, Japan*

²*Geological Survey of Japan, Tsukuba, Japan*

Kuril Islands extends for 1200 km in length from Kamchatka to Hokkaido, and is composed of many active volcanoes, 32 of which have erupted during the last 200 years. However, organized volcanological research of the islands except for several volcanoes has not been carried out since 1970's. In 2000 and 2007, the international (Japan, Russian and US) scientific cruises were carried out. The project was supported by JSPS and NSF funds. We also appreciate Russian Academy of Science, Far Eastern Branch. In this study, we present the result of tephrastratigraphy in the islands to evaluate frequency and types of volcanic eruption during Holocene.

We landed 15 islands from Urup in southern Kuril to Shumshu in northern Kuril to investigate tephrastratigraphy at 49 sites. We identified 274 tephra units sandwiched between soil layers. Using thickness, grain size, mineral assemblage and chemical compositions of glass shards of each unit, we could recognize 155 eruption units. Combined with these data, we determined 19 source volcanoes for the 155 units. During these analysis, we also found 13 marker tephra layers, 12 of which are newly recognized. Although these tephra layers are distributed at several neighbor islands far from each source volcano, three layers can be considered to be widespread tephra recognized at distal islands more than 300 km far from its source. These are KO tephra (Kuril Lake tephra: 7.6 ka) from southern Kamchatka, Zv-Su tephra (Zavaritskii - Shumshu tephra: 8.0 ka) from Zavaritskii caldera in central Kuril, and CKr tephra (Central Kuril tephra: 2.4ka) possibly from Medvehii caldera in southern Kuril. We determined carbon 14 ages of 39 samples, and also estimated eruption age of other units by using thickness of soil layers. Based on these data, we reveal eruption history of major volcanoes in Kuril Islands during Holocene. Although a dormant period longer than 500 years could not be obviously recognized in volcanoes of Kuril, it seems that the intensity and/or frequency of eruptive activity has fluctuated during Holocene. Most remarkable period was from 10 to 7 ka, in which explosive and large eruptions had occurred from Hokkaido to Kamchatka, resulting in the formation of 6 calderas, Mashu in Hokkaido, L'vinaya Past in southern Kuril, Zavaritskii in central Kuril, Tao-Rusyr in northern Kuril, and Kuril Lake and Karimsky in Kamchatka. In addition, considerable large scale plinian eruptions had occurred in several volcanoes from Hokkaido to Kamchatka during from 3 to 1 ka. The activity during these two periods might be influenced by regional tectonic events.

HAZARDS, MONITORING AND RISK REDUCTION

ORAL PRESENTATIONS

KAMCHATKAN VOLCANIC ERUPTION RESPONSE TEAM (KVERT) PROJECT IN 2006-2009

Olga A. Girina¹ and Christina A. Neal²

¹*Institute of Volcanology and Seismology FED RAS, Russia.*

²*US Geological Survey, Alaska Science Center, Alaska Volcano Observatory USGS, USA.*

The Kamchatkan Volcanic Eruption Response Team (KVERT) is a collaborative project of scientists from the Institute of Volcanology and Seismology, the Kamchatka Branch of Geophysical Surveys, and the Alaska Volcano Observatory (IVS, KB GS and AVO).

The purpose of KVERT is to reduce the risk of costly, damaging, and possibly deadly encounters of aircraft with volcanic ash clouds. To reduce this risk KVERT collects all possible volcanic information and issues eruption alerts to aviation and other emergency officials.

KVERT was founded by Institute of Volcanic Geology and Geochemistry FED RAS in 1993 (in 2004, IVGG merged with the Institute of Volcanology to become IVS). KVERT analyzes volcano monitoring data (seismic, satellite, visual and video, and pilot reports), assigns a Level of Concern Color Code for aviation and issues reports on eruptive activity and unrest at Kamchatkan (since 1993) and Northern Kurile (since 2003) volcanoes.

KVERT receives seismic monitoring data from KB GS (the Laboratory for Seismic and Volcanic Activity). KB GS maintains telemetered seismic stations to investigate ten of the most active volcanoes in Kamchatka and one on the North Kurile Islands. Data are received around the clock and analysts evaluate data each day for every volcano to determine the number and type of seismic events at these monitored volcanoes.

Satellite data are provided to KVERT from several sources. AVO conducts satellite analysis of the Kuriles, Kamchatka, and Alaska as part of its daily monitoring and sends the interpretation to KVERT staff. KVERT interprets MODIS and MTSAT images and processes AVHRR data to look for evidence of volcanic ash and thermal anomalies. KVERT obtains visual volcanic information collected by volcanologists on field trips and pilots, and from web-cameras that monitor Klyuchevskoy (established in 2000), Sheveluch (2002), Bezymianny (2003) and Koryaksky (2009) volcanoes.

KVERT staff work closely with staff of AVO, AMC (Airport Meteorological Center) at Yelizovo Airport and the Tokyo Volcanic Ash Advisory Center (VAAC), the Anchorage VAAC, and the Washington VAAC to release timely eruption warnings. Information about volcanic unrest based on seismic data from KB GS, satellite information from AVO and KVERT, or visual data from a variety of sources is shared by email among IVS, AVO and KB GS to facilitate evaluation of possible activity. After confirmation, urgent information is sent by email to government agencies, aviation services, and scientists (>300 users) located throughout the North Pacific region. KVERT staff also notify AMC and other emergency agencies in Kamchatka by telephone. KVERT Information Releases are formal written notifications that are sent by email to these same users to announce Color Code changes and significant changes in activity. These statements are posted on the KVERT and AVO web sites. AVO sends KVERT Information Releases by facsimile.

During the period from 2006 to March 2009, many eruptions of Kamchatkan and Northern Kurile volcanoes were potentially dangerous for aviation: six significant events have occurred at Bezymianny (two in 2006, three in 2007, and one in 2008), two at Klyuchevskoy (2007 and 2008), one at Koryaksky (2008-2009) and two at Chikurachki (2007 and 2008). Eruptions of Karymsky and Sheveluch volcanoes have continued essentially uninterrupted throughout the 2006-2009 period.

USING INSAR TO MAP AND STUDY DEFORMATION OF ALEUTIAN VOLCANOES

Zhong Lu and Dan Dzurisin¹, Chuck Wicks², and John Power³

¹*US Geological Survey, Cascades Volcano Observatory, Vancouver, WA 98683-9589, USA;*

lu@usgs.gov, dzurisin@usgs.gov

²*USGS, Menlo Park, CA 94025, USA; cwicks@usgs.gov*

³*USGS, Alaska Volcano Observatory, Anchorage, AK 99508, USA; jpower@usgs.gov*

With its global coverage and all-weather imaging capability, interferometric synthetic aperture radar (InSAR) has become an increasingly important technique for studying magma dynamics at volcanoes in remote regions such as the Aleutian Islands. The spatial distribution of surface deformation data derived from InSAR images enables the construction of detailed mechanical models to enhance the study of magmatic processes. This paper summarizes various deformation processes at Aleutian volcanoes observed with InSAR, including: (1) volcanic inflation and magma intrusion, (2) deformation preceding seismic swarms at several active and quiescent Aleutian volcanoes, (3) persistent volcano-wide subsidence at calderas that last erupted hundreds of years ago, (4) magma intrusion and associated tectonic stress release at active volcanoes, (5) subsidence caused by a decrease in pore fluid pressure in active hydrothermal systems, and (6) lack of expected deformation associated with recent eruptions at frequently active volcanoes. Among the inferred mechanisms are inflation/deflation of crustal magma reservoirs, pressurization/depressurization of hydrothermal systems, tectonic strain, thermal-elastic contraction of young lava flows, etc. Our work demonstrates that deformation patterns and associated magma supply mechanisms in the Aleutians are diverse and vary both in space and time. These findings provide a basis for improved models and better understanding of magmatic plumbing systems in the Aleutians.

APPLICATION OF UAVSAR TO ACTIVE U.S. VOLCANOES

Paul Lundgren¹, Zhong Lu², Charles Wicks³, Scott Hensley¹

¹*Jet Propulsion Laboratory, California Institute of Technology, Pasadena, CA, USA.*

²*US Geological Survey, Cascades Volcano Observatory, Vancouver, Washington, USA.*

³*US Geological Survey, Menlo Park, CA, USA.*

Surface deformation measurements represent one of the key types of measurements for understanding volcanic processes and hazards. Surface deformation of volcanoes often precedes other signs of renewed volcanic activity. In some cases this new deformation occurs without leading to an immediate eruption. In other cases new deformation can precede an eruption on time scales of months to hours, depending on the scale and mechanism of eruption and the characteristics of the volcano. Synthetic aperture radar (SAR) interferometry (InSAR) from satellites has proven an important observational tool for measuring volcano-wide deformation at tens-of-meter spatial resolution with centimeter-level accuracy. By giving a fairly complete picture of the surface deformation, InSAR can be very important for constraining potentially complex deformation processes, often comprised of more than one source and/or source type. A significant limitation of current satellite based SAR systems is their relatively long repeat intervals. Immediately before volcanic eruptions deformation may evolve over time scales significantly shorter than the approximately one month repeat intervals of current SAR satellites. UAVSAR, an airplane based SAR system, provides a measurement system that can complement satellite based observations by providing rapid revisits to active volcanoes to better understand their pre-eruption deformation, time-transient co-eruption deformation evolution, and for better hazard mitigation.

We have a recently funded proposal to apply UAVSAR to volcanoes in the United States that span a range of volcano types and levels of activity: Yellowstone, WY, Long Valley, CA, Kilauea, HI, and many volcanoes in the Cascades, Alaska, and the central and eastern Aleutians. We will compare UAVSAR InSAR observations with satellite based InSAR from Envisat, ALOS, and Radarsat to assess the applicability of UAVSAR to each volcano. The selected volcanoes represent most of those currently active in the US and span a variety of deformation processes. Together these volcanoes represent test sites for developing UAVSAR as an operational tool for volcano studies and hazard mitigation. Each of these volcanoes covers a unique portion of the volcano “spectrum” with a range of deformation amplitudes and time spans expected within the time span of this project. In addition, for the first time, high-resolution UAVSAR images will be systematically collected to facilitate geomorphology studies and other volcanological investigations. Since this year (2009) represents the first summer season of observations, we will present the capacity of UAVSAR system, calibration results, preliminary observations and future plans.

REMOTE SENSING OF VOLCANIC THERMAL FEATURES: EXPLORING THE LIMITS OF SUB-PIXEL THERMAL FEATURE MEASUREMENT USING ASTER TIR DATA

R. Greg Vaughan¹, Laszlo P. Keszthelyi¹, Ashley Gerard Davies², Henry Heasler³, Cheryl Jaworowski³, David J. Schneider⁴, Jacob B. Lowenstern⁵

¹*US Geological Survey, Astrogeology Science Center, Flagstaff, AZ, USA.*

²*Jet Propulsion Laboratory, California Institute of Technology, Pasadena, CA, USA.*

³*National Park Service, Yellowstone National Park, WY, USA.*

⁴*US Geological Survey, Alaska Volcano Observatory, Anchorage, AK, USA.*

⁵*US Geological Survey, Volcano Hazards Program, Menlo Park, CA, USA.*

Volcanoes commonly exhibit anomalous thermal behavior before explosive eruptions; therefore volcanic thermal features are studied and monitored for potentially predictive applications. Space-based thermal infrared (TIR) remote sensing tools are capable of monitoring volcanic thermal features on a global scale. However, TIR satellite observations used for continuous or semi-continuous monitoring necessarily have large pixels (90 to 1000 m per pixel), making most volcanic thermal features sub-pixel in scale. Information about the characteristics of sub-pixel thermal features is important for interpreting TIR image data. For example, a 90-m pixel that contains a 60-m diameter crater lake ($\sim 2800 \text{ m}^2$) with 50 °C water will have about the same thermal infrared spectral radiance value (and pixel-integrated temperature) as a pixel with an 80 m² fracture in a lava dome exposing 700 °C lava. The ability to periodically determine the difference between these situations is important in evaluating the potential hazards posed by a volcano.

Multispectral thermal infrared (TIR) satellite data, such as from the Advanced Spaceborne Thermal Emission and Reflection Radiometer (ASTER), can be used to derive surface temperatures as well as resolve the characteristics of some sub-pixel scale thermal features. Key questions regarding the use of such data for these measurements include: 1) How large does a hot sub-pixel feature, of a certain temperature, need to be for ASTER TIR data to resolve a thermally mixed pixel? 2) How large does a hot sub-pixel feature, of a certain temperature, need to be to saturate an ASTER TIR pixel? 3) What assumptions and sources of error have the greatest effect on the results of sub-pixel thermal feature analysis? Using examples of ASTER data over volcanic thermal features with a wide range of temperatures (e.g., the Mount Erebus lava lake, the Mount St. Helens lava dome, and Yellowstone hot spring pools) I will show some results of sub-pixel thermal feature analysis and help answer these questions.

PREDICTING VOLCANIC ASH CLOUD MOVEMENT ACROSS THE NORTH PACIFIC USING THE PUFF DISPERSION MODEL

Peter Webley and Ken Dean

Geophysical Institute, University of Alaska Fairbanks, Fairbanks, AK, USA.

There are over 100 active volcanoes in the North Pacific (NOPAC) region, most of which are located in uninhabited areas. These volcanoes erupt many times per year, for example from 1970 to the present there have been over 150 separate volcanic ash clouds reaching at least 20,000 ft and ejecting ash to a range of altitudes and jeopardising aircraft safety. Dispersion models play a pivotal role in forecasting the movement of volcanic ash clouds thus complementing remote sensing data and visual observations from the ground and aircraft. Puff is a three dimensional dispersion model primarily designed for forecasting volcanic ash dispersion and is used by the Alaska Volcano Observatory and other agencies. Here we show how Puff is used to monitor potential active volcanoes at elevated alert status volcanoes and those with current in eruption, sixteen potentially active volcanoes within the NOPAC region, ten more within the Pacific ring of fire and a total of 31 worldwide (<http://puff.images.alaska.edu>). The predictions are generated automatically every three hours for the NOPAC region and every six hours for the other volcanoes. Predictions are made for initial ash plumes ranging from 4 to 20 km and for a 24 hr forecast period. This information is then made available via the Puff website, updating automatically without any user interactions. We will discuss the usefulness of these simulations during operational crises and show examples from several volcanic eruptions in the last few years of how the Puff simulations complement locally collected satellite observations of volcanic ash clouds.

THE KURILE BIOCOMPLEXITY PROJECT

HAZARDS, MONITORING AND RISK REDUCTION

INTERDISCIPLINARY STUDIES

POSTER PRESENTATIONS

LARGE SCALE FAILURES AND DEBRIS AVALANCHE DEPOSITS OF VOLCANOES OF KURILE ISLANDS

Alexander Belousov¹, Marina Belousova²

¹*Institute of Earth Sciences, Academia Sinica, Taipei, Taiwan.*

²*Institute of Volcanology and Seismology, Petropavlovsk, Russia.*

Investigations of air and space images of Kurile Islands supplemented by observations during two research cruises have allowed us to identify 40 well-preserved horseshoe-shaped scars formed by large-scale collapses. The collapses occurred at active (33 cases) as well as extinct volcanoes (7 cases). Widths of breaches of the most of the scars (30 cases) range from 0.5 to 2 km indicating moderate volumes of the failures - around 1 km³. Three largest 3 to 4 km-across scars (which were formed by failures with volumes about 5 km³) belong to Milne, Sinarka and Stokap volcanoes. Most of the failures occurred on andesitic volcanoes which dominate in the region. At least 3 volcanoes (Harimkotan, Ekarma and Mendeleev) experienced multiple (3 or more) failures. Few failures occurred on dominantly basaltic stratovolcanoes (Alaid, Brouton

and possibly Atsonupuri). Most of the collapsed volcanoes of Kurile arc have strong hydro-thermal alteration of rocks inside their horseshoe-shaped scars, and their debris avalanche deposits contain large proportion of clayey material. This suggests that weakening of rocks composing volcanic edifices caused by hydrothermal alteration played leading role in gravitational destabilization of the volcanoes. In 50% of cases of volcanic failures in Kuriles were followed by magmatic activity - the horseshoe-shaped craters are partially filled by younger volcanic cones. This indicates that the failure surfaces intersected upper parts of feeding channels of active volcanoes – possibly the failures were triggered by magma intruding into the volcanic edifices. Apart from failures on volcanoes there are multiple rather large scale (>0,01 km³) failures along sea cliffs of the islands which involved volcanic rocks. These cases are transitional

to non-volcanic failures. Debris avalanches of all of the studied failures traveled far beyond the shore line of Okhotskoye Sea or the Pacific Ocean and thus their exact lengths and drop heights are unknown. Entering of the debris avalanches into the sea obviously generated tsunamis. The studied failures have Late Pleistocene – Holocene ages; and one historical case - failure of Harimkotan volcano on January 8, 1933 with the volume 0.4 km³. The failure generated tsunami up to 20 m high with 2 reported victims on nearby Onekotan Island. The failure followed by strong 5-days-long Plinian eruption with deposition of pyroclastic flows and subsequent dome growth during several months.

PROCESSES OF RELIEF FORMATION IN THE CONTINENT-OCEAN BORDER ZONE (COMMANDOR ISLANDS)

Bulochnikova Anna

Moscow State University, Geographic Department, Moscow, Russia.

Geographic position is of primary importance in the formation of natural systems in any region of the world. A region's location defines the relief that can form. Transition zones are located in regions of passage from the Eurasian continent to the Pacific Ocean. The problem of passage from the continent to the ocean remains incompletely explained. There are many theories which explain this phenomenon differently, but specific processes must govern the morpholithogenesis. Volcanism, seismicity, and moving of earth blocks are the major influences on relief formation.

Islands arcs and single islands are typical border zone land forms, but the processes by which these relief islands form are not well understood. By studying these islands we hope to elucidate how the fundamental factors and conditions that influence their formation are correlated in space and time. Some small islands react dramatically to changes of climate, tectonic situation, sea level, and other processes, which take place on both the global and the local level. Therefore discovering the details of formation and developmental history, and the peculiarities of the morpholithogenetic process will allow us to develop some rational schemes for understanding these unique natural systems.

The northwestern part of the Pacific Ocean is still a poorly-known region because of its isolation. We used laboratory methods for some tasks because some characteristics of this region remain poorly defined, for example in our geomorphological analysis of the Moneron (northeastern Japan Sea), Bering, and Mednij (southwestern Bering Sea) islands. The goal of this research was to update the developmental history and relief exposure features, and to understand the formation of an incoherent blanket in the transition zone. The morphometric analysis was the basis of the method we used. First, a digital relief model was created on the basis of the topographic map, then a series of special maps were built of gypsometry, slopes, river basins, block tectonics, etc. Following this, the statistical analysis of the distribution of altitude and declination was carried out. The result of these activities was a morphological description of the islands. The next stage was to conduct the block and basin analysis. The essence of these methods is to learn the characteristics of the drainage networks, to calculate the river basin parameters (area, stream length, etc.), to apportion the blocks and to analyze the distribution of their characteristics (height, area, etc.). These methods allow us to discover all details of the construction and development of a territory's structure, and to estimate and describe the main structure of the morpholithogenesis during different stages of modern relief formation.

MONITORING VOLCANIC ACTIVITY IN THE KURIL ISLANDS

Chibisova M.V. and Rybin A.V.

Institute of Marine Geology and Geophysics FEB RAS, Yuzhno-Sakhalinsk, Russia.

The Kuril Islands are the external manifestation of tectonic processes on the boundaries of Eurasian and Pacific lithosphere platforms or subduction zones. The formation of the Kuril arc as a structural element on the surface of the Earth began 10-15 million years ago. Therefore, this is a very young structure in terms of geological time. The islands are formed mainly by volcanic edifices or the products of their destruction. The modern relief of the Kuril Islands gives evidence of great volcanic processes.

In the Kuril Islands during the last 45 thousand years not fewer than 12 giant explosive eruptions occurred connected with the formation of the calderas, with a total volume of erupted pyroclastic material of nearly 720 km³.

During the historical period (last 300 years) on the territory of the Kuril Islands there have been 28 great and catastrophic eruptions. Because the islands have been sparsely populated during this period the harm from these eruptions was not as considerable as what commonly occurred after such eruptions in densely populated island countries such as Indonesia and Japan.

In the Kuril Islands 68 surface volcanoes are identified; among them 36 are active and potentially dangerous.

During recent decades higher volcanic activity has been characteristic of the northern part of the Kuril Islands (Chikurachki and Ebeko volcanoes). In the southern and central Kuril Islands there has not been an eruption for more than 18 years.

At the present time in the Kuril Islands three seismic stations exist (Kuril'sk, Yuzhno-Kuril'sk, Severo-Kuril'sk) with analogue registration (SF GS RAS) function. Because the equipment is old and underpowered, it cannot be used for local monitoring of volcanic activity even where it is located close to a restless volcano. For more detailed observation and prediction of eruptions it is necessary to re-equip the base stations with new generation devices with digital registration and to build on this base to create telemetric systems of observation; first in importance for monitoring are volcanoes Tyatya, Mendeleev, Ivan Groznyy, Baranskii, Chirip – Bogdan Khmel'nitskii, Ebeko, Chikurachki, and Alaid because these are the most dangerous for the population of the Kuril Islands. The development of seismic methods requires rather large expenditures, and improved monitoring has been economically possible in recent years only for the above-mentioned volcanoes which constitute only about 20% of the total number of active Kuril Islands volcanoes. Most of the active volcanoes are located a considerable distance from settlements or sea transport lanes and they will probably not be covered by a network of constant surface observations in the near future.

In 2003 the Sakhalin Volcanic Eruptions Response Team (SVERT) was created to organize the monitoring of the active volcanoes of the Kuril island arc under the auspices of the Institute of Marine Geology and Geophysics (IMGG) FEB RAS and with the active support of the Alaska Volcano Observatory (AVO) and KVERT (IVS FEB RAS).

SVERT's zone of responsibility first included all active volcanoes of the Kuril Islands. At the international meeting "Monitoring of the volcanic activity of the Kuril-Kamchatka region: The past, the present and the future" in Petropavlovsk-Kamchatskii it was decided to delegate the responsibility for assuring the security of the airplane flights in the area of the Northern Kuril Islands (Paramushir and Atlasov islands) to the KVERT group because the region is almost

inaccessible for Sakhalin volcanologists. At present SVERT conducts the monitoring of active volcanoes located on sites from Kunashir Island to Onekotan Island.

For six years we have conducted the receiving, primary processing, and operative analysis of data from the territory of the Kuril Islands. Daily, TERRA satellite data (MODIS radiometer, 36 channels) with spatial resolution of 250, 500, and 1000 m sent by Far East Branch FGUNPP «ROSGEOLFOND» (Russian Ministry of Natural Resources) are received and analyzed. Data from NOAA satellites are used only when detailed observations are required to analyze the dynamics of spreading ash clouds.

Visual monitoring is conducted only for volcanoes of the Southern Kuril Islands (Golovnin, Mendeleev, Tyatya, Ivan Groznyy, Chirip, Bogdan Khmel'nitskii, and Baranskii). Observers on the Kuril'sk and Yuzhno-Kuril'sk seismic stations provide data about all changes in the state of active volcanoes.

During the period of SVERT existence there were no great eruptions on the territory of the Southern and Central Kurils. The materials received during this period show that with the help of the MODIS radiometer it is possible to detect even insignificant changes in the state of the Kuril Islands volcanoes. All events connected with intensification of volcanic activity (steam-gas outbursts from Sinarka and Severgin volcanoes, ash-gas outburst from Chirinkotan Volcano, gas-ash ejection from Severgin Volcano, mud flows from the flank vent of Tyatya Volcano) were observed during this period.

A daily report about the volcanic activity in the Kuril Islands is created on the basis of the data received and sent by e-mail to KVERT, AVO, meteorological centers of airports (AMC) of Elizovo and Yuzhno-Sakhalinsk, Tokyo VACC, Washington VACC, and other interested organizations.

SVERT personnel took part in studies of this almost inaccessible region and the little-studied active volcanoes within the bounds of the NSF project "The Kuril Biocomplexity Project: Human Vulnerability and Resilience to Subarctic Change". The data obtained during the 3-year period of the expeditions make it more possible to interpret the data received from satellites.

SVERT's financial support during last three years is from the budget of IMGG FEB RAS.

OVSICORI-UNA: 25 YEARS OF VOLCANO AND SEISMIC MONITORING IN COSTA RICA

E. Duarte, E. Fernández

Volcanological and Seismological Observatory of Costa Rica (OVSICORI), Universidad Nacional, P.O. Box 2346-3000, Heredia, Costa Rica. Email: eduarte@una.ac.cr, fax (506)2610303

The Volcanological and Seismological Observatory of Costa Rica (OVSICORI-UNA) is the institution in-charge of volcano and seismic monitoring in this Central American country. For more than 25 years it has supported Costarrican development by studying, documenting, publishing and sensitizing mass public, mass media and decision makers. (www.ovsicori.una.ac.cr).

Two main groups: volcano and seismic monitoring carry out work in the entire Costarrican territory and beyond: in the Pacific islands and along the ocean floor.

The volcano monitoring group comprises professionals from different disciplines and is divided up in four small teams: Volcano seismology, deformation, geochemistry and observation of physical changes. Each of these groups apply different methods and techniques to gather all the necessary information from volcanoes to reduce impact on small communities around volcanoes and the keep all those audiences rapidly informed.

The seismic group operates a seismographic telemetric network consisting of 25 stations (analogical and digital) covering the entire country. Instruments transmit and collect data 24 hrs a day in their headquarters at Universidad Nacional. Some of the main purposes of this group are; to assess the current seismotectonic setting and daily monitoring of seismic activity associated to the various active volcanoes.

Moreover, OVSICORI is committed to give a significant contribution to the Costarrican society by reducing, translating and disseminating valuable information to reduce human and material losses. Education about volcano and seismic hazards has been included in the national education curricula at the levels of primary and secondary school. Thanks to sustained media coverage of OVSICORI's achievements and messages, the general public has built a wide vocabulary related to our daily research.

WAVE DISTURBANCES IN THE ATMOSPHERE CAUSED BY STRONG EXPLOSIVE ACTIVITY AND FORMATION OF PYROCLASTIC FLOWS FROM BEZYMIANNY VOLCANO (KAMCHATKA)

Pavel P. Firstov, Alexander B. Tristanov

Kamchatkan Experimental and Methodical Seismological Department, Geophysical Service, RAS, Petropavlovsk-Kamchatskiy, Russia.

Intense volcanic explosions produce wave disturbances in the atmosphere in the infrasonic frequency range of 0.003-1.0 Hz and long-wave disturbances with frequency less than 0.003 Hz. Disturbances in the infrasonic range are generated as a result of strong convective processes in the atmosphere during formation of an eruptive cloud. The eruptive cloud forms when eruptive products are ejected into the atmosphere and when hot and gassy volcanic material covers a large area. Turbulent pulsations emerging in the ascending convective column produce infrasonic signals.

Wave disturbances in the infrasonic range at $f = 0.3$ Hz were registered for the first time during the 1983-1986 eruptions of Bezymianny during the formation of pyroclastic flows. The correlations between acoustic and seismic emissions accompanying the eruptions are believed to be criteria for understanding the origin of the former.

Long-wave disturbances arise in a strong eruptive column that reaches the substratosphere (tropopause). This phenomenon can be observed during paroxysmal eruptions ("the directed-blast type of eruption" according to G.S. Gorshkov's classification), accompanied by ejection of a significant amount of highly dispersed volcanic materials and gases. The specific feature of the long-wave disturbances indicates the existence of the deep exhaustion phase. On March 30, 1956 a directed-blast Bezymianny eruption produced a long-wave disturbance that circled the globe without distortion of the wave form.

On May 9, 2006 a paroxysmal Bezymianny eruption generated a wave disturbance with a 1 minute exhaustion phase along with air waves believed to be related to the processes occurring in the crater. Generation of the negative phase is likely related to air inflow during continuous emission of the heated ash-and-gas mixture and condensation of the water; more than 90% of the volume of volcanic gases is made up of water.

TSUNAMI SOURCE OF THE 1963 KURILE EARTHQUAKE

Kei Ioki¹, Yuichiro Tanioka¹

¹*Institute of Seismology and Volcanology, Hokkaido University, Japan.*

On 13 October 1963, a great earthquake (M_w 8.5) occurred off Etorofu Island. This event was an underthrust earthquake due to the subduction of the Pacific Plate beneath the Kurile Islands. The Pacific Plate subducts about 8cm per year under the Kurile Islands, and many great underthrust earthquakes have occurred in the Kurile-Kamchatka subduction zone. The location of the epicenter of the 1963 earthquake is 44.8°N, 149.5°E. A large tsunami was generated by that earthquake and propagated through the Pacific Ocean and Okhotsk Sea. The most recent great underthrust earthquake was the 2006 Kurile Islands earthquake (M_w 8.3) which occurred about 350 km northeast of the epicenter of the 1963 Kurile Islands earthquake.

We estimated slip distribution by tsunami waveform inversion using observed and synthetic waveforms at 14 tide gauges along the Pacific Ocean and Okhotsk Sea coast. The location of the earthquake's epicenter and locations of tide gauge stations are shown in Fig. 1. Parameters of the fault model of the earthquake obtained from previous seismological study [Kanamori, 1970] were length=250km, width=150km, shallowest depth=4km, strike=223°, dip=22°, rake=90°. In order to compute the tsunami wave passing between the Kurile Islands, nonlinear long-wave equations were solved in the shallow sea where the depth is shallower than 100m, and linear long-wave equations were solved in the deep sea where the depth is greater than 100m. The finite-difference scheme with a staggered grid system was used to solve those equations. First we divided the fault into 15 subfaults, each with a size of 50km×50km. Next, tsunami waveforms were calculated for each subfault and each observed point. Then the slip amount on each subfault of the 1963 event was estimated by the inversion of tsunami waveforms.

The estimated slip distribution shows that the largest slip amount of 4.5m was found in the southeast part of the fault (Fig. 2). The seismic moment was calculated to be 4.2×10^{21} Nm (M_w 8.3) by assuming a rigidity of 7×10^{10} N/m². This result is smaller than the seismic moment of 7.5×10^{21} Nm (M_w 8.5) estimated from surface waves by Kanamori [1970] and larger than the seismic moment of 2.7×10^{21} Nm (M_w 8.2) estimated from teleseismic body waves by Beck and Ruff [1987].

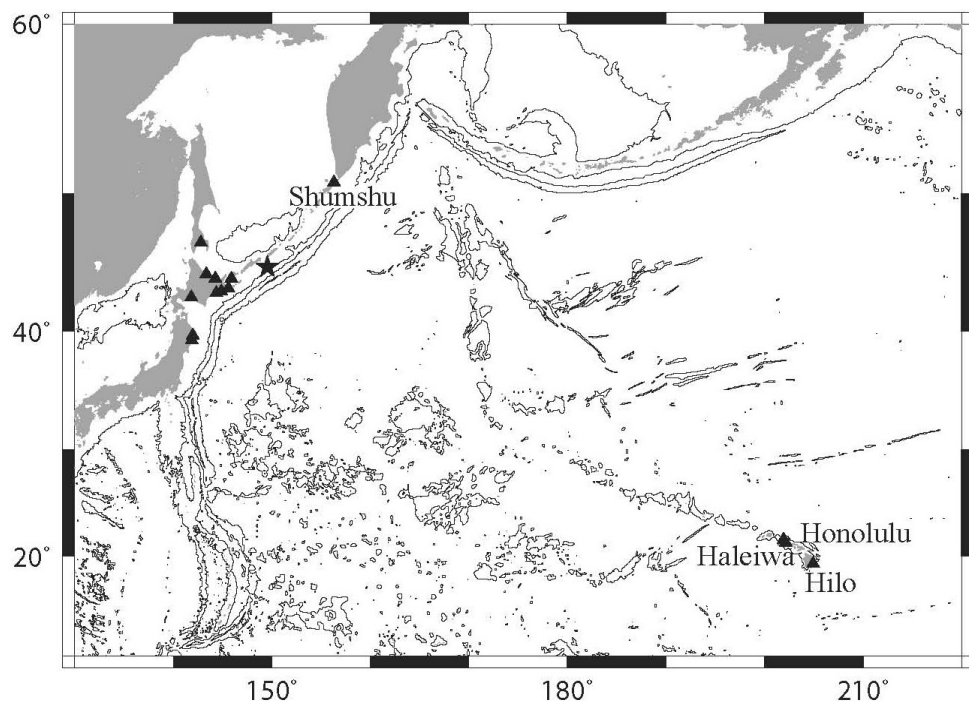


Figure 1. Epicenter of the 1963 earthquake (star). Triangles indicate locations of tide gauges used for tsunami waveform analyses.

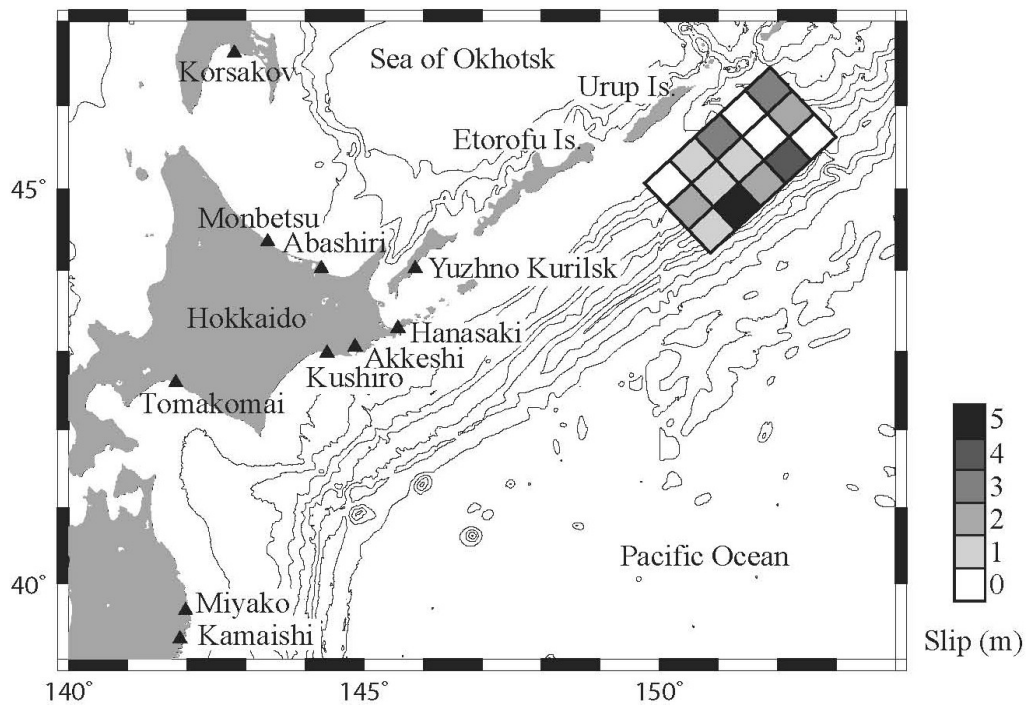


Figure 2. Slip distribution of the 1963 earthquake derived from tsunami waveform inversion. Size of the subfault is 50km×50km. Triangles indicate locations of tide gauges used for tsunami waveform analyses.

CURRENT DATA DESCRIBING THE CONDITION OF THE INTRACALDERA LAKE BIRYUZOVOE (KURIL ISLANDS)

D.N. Kozlov, R.V. Zharkov

Institute of Marine Geology and Geophysics FEB RAS, Yuzhno-Sakhalinsk, Russia.

From July 1 until August 14, 2007, two international complex expeditions "Kuriles-2007" were conducted in the area of the Central Kuril Islands. The tasks were to study the developmental history of the volcanoes and their current state. The group leader was Dr. Rybin, Chief of the Laboratory of Volcanology and Volcanic Hazards. One object of research was the Zavaritskii Volcano caldera.

Zavaritskii Volcano is in the southern part of Simushir Island (The Central Kuril Islands) and is made up of three nested; the diameter of the youngest is about 2.5 km. The walls of this caldera are very abrupt, and Biryuzovoe Lake fills the crater. In the northern part of the crater there are two domes: Northern and Eastern.

The formation of the Eastern effusive dome occurred between 1916 and 1931. The history of Northern dome formation is more complex. On the Japanese maps made in 1916 it is shown as a scoria cone with a diameter of about 500 m and a completely closed crater. After an eruption in 1920 the southern part of the cone collapsed, and in the center of the crater a small extrusive dome formed. An eruption began in the area of the scoria cone on November 12, 1957; this eruption ended on December 1, 1957. As a result of this eruption the northern part of the caldera was covered with tephra, a new extrusive dome with a diameter of 350 m and height of 40 m was formed in the place of the cone, and a short lava flow extended down the dome's southeastern slope. Large solfataras were active for a long time on the border between the dome and the lava stream (Markhinin, 1960; Pots, 1967). Now there are no solfataras on the dome or lava stream, and the surface of the dome is overgrown by lichen.

For the first time we have conducted a bathymetrical echo sounding of the intracaldera Biryuzovoe Lake using Eagle Sea Charter 320DF sounder. Echo sounding while deploying a GPS receiver has allowed increased mapping accuracy. The echo sounding of Biryuzovoe Lake generated 30 echo profiles, and a detailed bathymetrical map was created on the basis of those profiles.

The level of the lake during last 50 years has risen by 10 meters; the current maximum depth of the lake is 87 m. The echo sounding has confirmed the presence of a wide longitudinal fissure stretching across the bottom of the lake, discovered during the earlier measurements by Zelenov (1962). Detailed echo sounding allowed two funnels more than 80 m deep to be mapped on the bottom of the fissure, and a 42 m deep funnel was found in the northwestern part of the lake. Similar funnels have been found in the intracaldera lakes of Golovnin Volcano on Kunashir Island (Belousov and Goats, 2006). The Lake Biryuzovoe funnels may be explosive, but in contrast to Kipyashchee and Goryachee lakes of Golovnin Volcano, there are no gas emissions from the Biryozovoe funnels. With the help of echo sounding, we detected a site with intensive gas emissions in the southwestern part of the lake. Here a group of thermal springs, which were described in 1940-50, has been flooded by the waters of the lake (Korsunskaya 1958, Markhinin 1960, Zelenov 1962, etc.). The gas bubbles and steam on the surface of the lake suggest the presence of a submerged hydrothermally heated area in the southwestern part of the lake. The area extends to the lake shore, where the sand is heated from 20 up to 91.2°C. The pH of the lake water is 7.5.

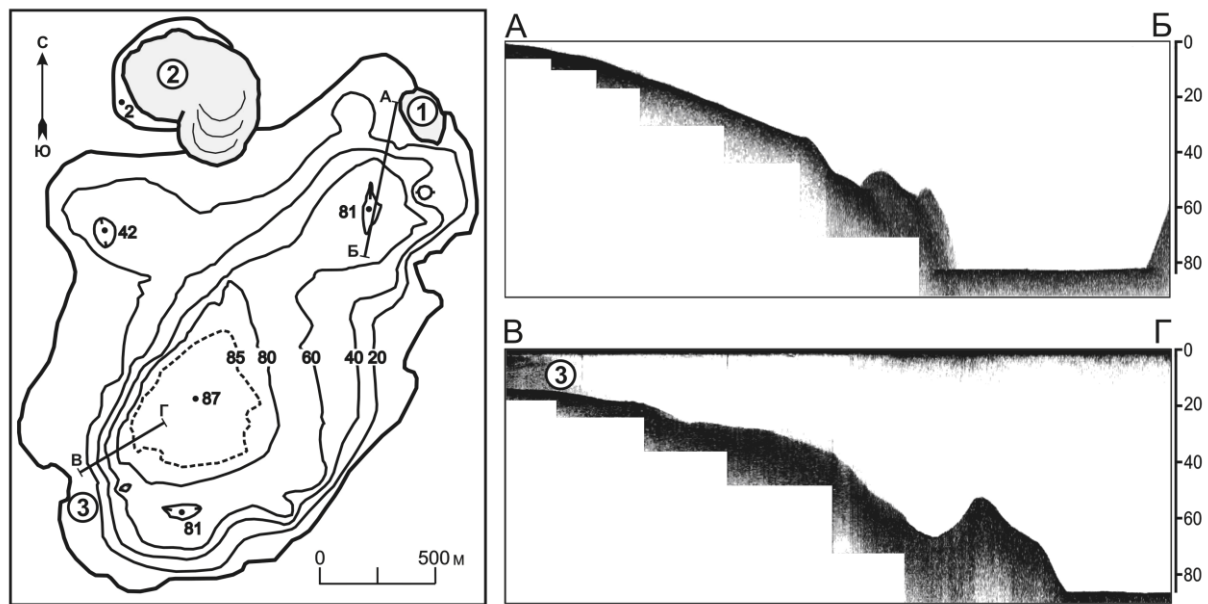


Figure 1. Bathymetric map of Birusovoe Lake.

Financial support for these expeditions came from the ARC-0508109 project of the US National Science Foundation. Field and analytical work of the volcanological group were supported by the 06-II-CO-08-031, 06-III-B-08-371 and 07-III-D-08-097FEB grants from the Russian Academy of Sciences.

ELECTROMAGNETIC SOUNDING AND 2D DC TOMOGRAPHY OF THE SHALLOW STRUCTURES OF KAMCHATKA VOLCANOES, FAR-EASTERN RUSSIA

Yuri Manstein

Trofimuk Institute of Petroleum Geology and Geophysics, SB RAS, Novosibirsk, Russia.

The results of 2007 and 2008 field work on Mutnovsky, Severo-Mutnovsky, Uzon, and Akademii Nauk volcanoes will be presented in this work. The shallow structures of the volcanoes were studied, including mud pots, mud volcanoes and their subsurface “roots”, ore-forming sites, geysers, thermal lakes, fumaroles, maars, and underwater craters.

These studies were accomplished using two techniques: near-surface electromagnetic frequency induction sounding (NEMFIS) and DC tomography. NEMFIS (figure.1) was developed by IPGG SB RAS. The soundings were performed at 14 frequencies in the range between 2.5 and 250 kHz. The data obtained were processed by the ISystem software that is part of NEMFIS. Geoelectrical cross-sections were created along observation lines. Apparent specific resistance (ρ_a) 2D distribution maps, and cross-sections were plotted. The 3D visualization was performed using commercial software.



Figure 1. NEMFIS in operation, Uzon Volcano.

The NEMFIS sounding allows us to describe the ρ_a distribution down to 6 m depth. Because the sounding spot is quite small in size it is possible to study the geoelectrical anomalies caused by vertical spring water paths and different mineralization of solutions.

The DC tomography was used with a 48-electrode resistivity meter. The spacing between electrodes was 1-5 m. For work on lakes the multicore cable was equipped with floats (figure 2). Results of 2D and 3D tomography in water up to 93 m deep will be shown in my presentation.



Figure 2. DC tomography of underwater crater, Karymskoe Lake, Academii Nauk Volcano

ALOS PALSAR INTERFEROMETRY OF THE KLYUCHEVSKAYA GROUP OF VOLCANOES, KAMCHATKA

Dmitry Melnikov

Institute of Volcanology & Seismology, Petropavlovsk-Kamchatskiy, Russia.

Here we report the first preliminary ALOS PALSAR radar data describing the Kluchevaskaya group of volcanoes (Kamchatka). This region has complicated topography with a relative elevation of about 4 km, volcanic deposits (lava flows, cinder fields, pyroclastic deposits), and thick glaciers. Two volcanoes from this group (Kluchevskoy and Bezymianny) are the most active. Bezymianny Volcano is the most interesting with respect to radar data use and relief deformation studies because here a gradual growth of the lava dome is currently in progress, usually accompanied by 1-2 explosive eruptions per year.

ALOS PALSAR is radar with L-band = 23.5 cm; the satellite repeats its orbit every 46 days. Three interferometric pairs of FBD data with ascending orbit were used for this research: 09.06.2007-25.07.2007, 25.07.2007-09.09.2007, and 09.09.2007-25.10.2007. Each of these pairs exhibits a different coherence. Pair 25.07.2007-09.09.2007 has the best coherency; 09.09.2007-25.10.2007 has the worst. For all three pairs the best coherency is represented by the lava flows of the New Tolbachik cinder cones (1975-1976), the worst by the mountain glaciers and cinder deposits. Two interferometric pairs (09.06.2007-25.07.2007, 25.07.2007-09.09.2007) show deformations of several centimeters in the area of the Bezymianny Volcano lava dome. More detailed estimations of the degree of deformation are hampered at present because some parts of the lava dome are non-coherent. We cannot see deformations in the volcano area in the 09.09.2007-25.10.2007 interferometric pair; the data are non-coherent. Most likely this is due to the fact that on 14-15 October 2007 an explosive eruption of Bezymianny Volcano took place, and part of the lava dome underwent rapid and extensive changes, resulting in non-coherency of the data. Use of the interferometric pairs with higher temporal intervals (for example, 09.06.2007-25.10.2007) has shown that these pairs have very low coherency.

Therefore, we conclude that using radar data for analysis of deformations at the Kluchevskoy group of volcanoes is possible if due attention is paid to a set of conditions. Nevertheless, we encountered a problem with data coherence caused by the local topography features and the different types of underlying surface (snow, glaciers, cinder deposits, intensive denudation).

This work was supported by Russian Foundation for Basic Research grants 06-05-72008 and 08-05-00453.

THE KVERT PROJECT: ASH DANGER FOR AVIATION IN KAMCHATKA AND NORTHERN KURILES IN 2005-2008

Anton A. Nuzhdayev and Olga A. Girina

Institute of Volcanology and Seismology FED RAS, 683006, Petropavlovsk-Kamchatsky, Russia

The Kamchatkan Volcanic Eruption Response Team (KVERT) is a collaborative project of scientists from the Institute of Volcanology and Seismology, the Kamchatka Branch of Geophysical Surveys, and the Alaska Volcano Observatory.

KVERT staff has monitored the active volcanoes of Kamchatka (30) and the Northern Kuriles (6) constantly from 1993 and 2003, respectively. The main purpose of KVERT is to issue timely notification about eruptions and ash plume warnings.

KVERT interprets MODIS and MTSAT images, and processes AVHRR data to look for evidence of volcanic ash. Between 2005 and 2008, Sheveluch, Kluchevskoy, Bezymianny, Karymsky, Koryaksky, Mutnovsky, and Chikurachki volcanoes erupted explosively, and their ash plumes presented a hazard to airlines. More than 1500 ash plumes from these volcanoes were detected in 2005-2008.

The eruptions of Klyuchevskoy posed the greatest danger for aircraft: the average length of the ash plumes exceeded 200 km with the maximum length of 5000 km. Ash plumes extended evenly in all directions from the volcano. Most ash plumes from Sheveluch (> 60% of all ash plumes) moved to the northeast and east, and spread for more than 500 km from the volcano. The average length of ash plumes from Bezymianny was 180 km with the maximum distance of 1500 km. These plumes primarily moved to the east and southeast (up to 30% in each direction). The maximum length of Karymsky's ash plumes was 450 km; the plumes primarily moved to the east and southeast (about 32 % in each direction). Koryaksky's ash plumes extended for about 200 km, mainly (~65 %) to the northeast of the volcano.

INITIAL SOURCE EVALUATION OF ARCHAEOLOGICAL OBSIDIAN FROM THE KURIL ISLANDS, FAR EASTERN RUSSIA, USING PORTABLE XRF

S. Colby Phillips

Department of Anthropology, Univ. of Washington. Seattle, WA, USA.

Over the last decade, a number of studies have detailed the obsidian sources and prehistoric obsidian use in Northeast Asia including Japan, Kamchatka, Sakhalin Island and Primorye (Far Eastern Russia) (Doelman et al. 2008; Glascock et al., 2006; Kuzmin 2006a, 2006b; Kuzmin and Popov, 2000; Kuzmin et al. 1999, 2002, 2008; Speakman et al. 2005). During recent Kuril Biocomplexity Project (KBP) field expeditions, obsidian artifacts were recovered from 18 archaeological sites on eight islands across the little-studied Kuril Island archipelago in the North Pacific Ocean. These samples suggest a wide-ranging distribution of obsidian throughout the island chain over the last 2,500 years. Although there are no identified geologic sources of obsidian native to the Kurils known to have been used prehistorically, known sources exist in Hokkaido, Japan, and Kamchatka, Russia--the southern and northern geographic regions respectively from which obsidian may have entered the Kuril Islands.

I analyzed a sample of 131 obsidian artifacts with a portable X-ray fluorescence (pXRF) instrument to determine their trace-element composition and to compare artifact data with data from previously characterized obsidian sources in NE Asia. Obsidian from nine different sources--four located on Hokkaido and five on Kamchatka--were identified in the artifact sample (Fig. 1; Phillips and Speakman 2009). Dividing at Chirpoi, the obsidian shows affinity with Kamchatka sources in the northern Kurils and with Hokkaido sources in the southern Kurils. These data provide a foundation for addressing research questions concerning the movement of people and materials throughout the Kuril Islands and the prehistoric use of non-local geological resources.

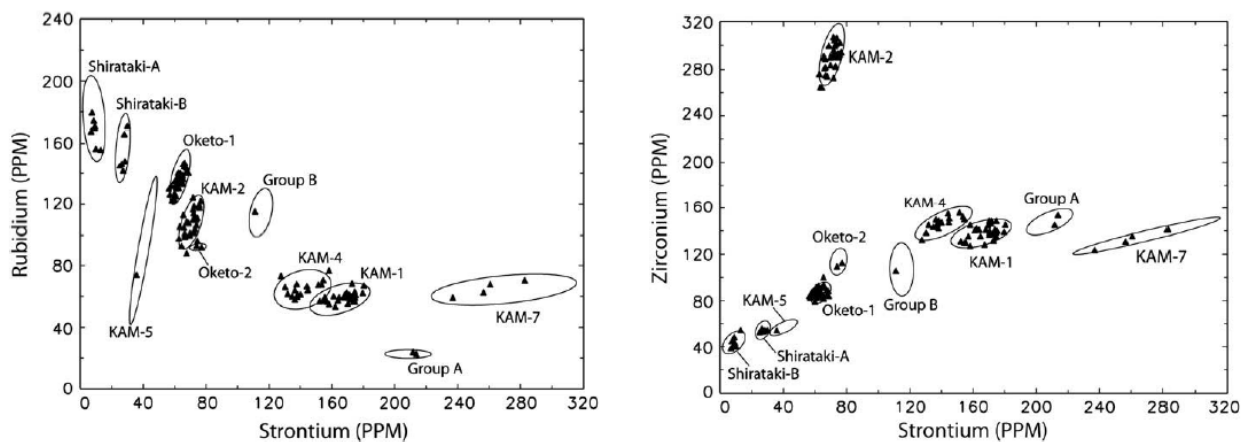


Figure 1. Strontium–rubidium and strontium-zirconium plots of obsidian-artifact compositions from the Kuril Islands (from Phillips and Speakman, 2009). Ellipses surrounding each group are drawn at the 95% confidence level. Confidence ellipses were drawn using a minimum of four data points from a larger group of obsidian artifacts, but only Kurils analyses are shown as points.

References

- Doelman, T., R. Torrence, V. Popov, I. Ionescu, N. Kluyev, I. Sleptsov, I. Pantyukhina, P. White, and M. Clements (2008). Source Selectivity: An Assessment of Volcanic Glass Sources in the Southern Primorye Region, Far East Russia. *Geoarchaeology* 23(2):243–273.
- Glascock, M.D., V.K. Popov, Y.V. Kuzmin, R.J. Speakman, A.V. Ptashinsky, and A.V. Grebennikov (2006). Obsidian Sources and Prehistoric Obsidian Use on the Kamchatka Peninsula: Initial Results of Research. In *Archaeology in northeast Asia: on the pathway to the Bering Strait*. D.E. Dumond and R.L. Bland (eds.): 73–88. Eugene, Oregon: University of Oregon Museum of Natural and Cultural History.
- Kuzmin, Y.V. (2006a). Palaeoenvironment and Chronology. In *Archaeology of the Russian Far East: Essays in Stone Age Prehistory*. S.M. Nelson, A.P. Drevianko, Y.V. Kuzmin, and R.L. Bland (eds): 13–40. BAR International Series 1540. Oxford: Archaeopress.
- Kuzmin, Y.V. (2006b). Recent Studies of Obsidian Exchange Networks in Prehistoric Northeast Asia. In *Archaeology in northeast Asia: on the pathway to the Bering Strait*. D.E. Dumond and R.L. Bland (eds.) pp. 61–71. Eugene, Oregon: University of Oregon Museum of Natural and Cultural History.
- Kuzmin, Y.V. and Popov, V.K., eds., 2000. *Volcanic Glasses of the Russian Far East: Geological and Archaeological Aspects*. Vladivostok: Russian Academy of Sciences, Far Eastern Branch, Far Eastern Geological Institute. In Russian with English abstracts.
- Kuzmin, Y.V., A.V. Tabarev, V.K. Popov, M.D. Glascock, and M.S. Shackley (1999). Geochemical source analysis of archaeological obsidian in Primorye (Russian Far East). *Current Research in the Pleistocene* 16: 97–99.
- Kuzmin, Y.V., M.D. Glascock, and H. Sato (2002). Sources of Archaeological Obsidian on Sakhalin Island (Russian Far East). *Journal of Archaeological Science* 29: 741–749.
- Kuzmin, Y.V., R.J. Speakman, M.D. Glascock, V.K. Popov, A.V. Grebennikov, M.A. Dikova, and A.V. Ptashinsky (2008). Obsidian use at the Ushki Lake complex, Kamchatka Peninsula (Northeastern Siberia): implications for terminal Pleistocene and early Holocene human migrations in Beringia. *Journal of Archaeological Science* 35(8): 2179–2187.
- Phillips, S.C. and R.J. Speakman (2009). Initial source evaluation of archaeological obsidian from the Kuril Islands of the Russian Far East using portable XRF. *Journal of Archaeological Science* 36(6): 1256–1263.
- Speakman, R.J., M.D. Glascock, V.K. Popov, Y.V. Kuzmin, A.V. Ptashinsky, and A.V. Grebennikov (2005). Geochemistry of Volcanic Glasses and Sources of Archaeological Obsidian on the Kamchatka Peninsula (Russian Far East): First Results. *Current Research in the Pleistocene* 22: 11–13.

Participation in the Kuril Biocomplexity Project was made possible in part by a grant from the US National Science Foundation (ARC-0508109; Ben Fitzhugh, PI) and various logistical and financial support from: the University of Washington, Seattle, WA, USA; the Hokkaido University Museum (Sapporo, Japan); the Historical Museum of Hokkaido (Sapporo, Japan); the Sakhalin Regional Museum (Yuzhno-Sakhalinsk, Russia); and the Far East Branch of the Russian Academy of Sciences (IMGG: Yuzhno-Sakhalinsk, IVGG: Petropavlovsk-Kamchatsky, NEISRI:Magadan). Olga Shubina supplied obsidian samples from Kunashir Island.

GRAIN SIZE COMPOSITION AND MICROFISSILS FROM DEPOSITS OF THE 15 NOVEMBER 2006 TSUNAMI IN THE CENTRAL KURILE ISLANDS

N.G. Razzhigaeva¹, L.A. Ganzey¹, T.A. Grebennikova¹, E.D. Ivanova¹, V.M. Kaistrenko², A.A. Kharlamov³

¹Pacific Institute of Geography FEB RAS, Vladivostok, Russia.

²Institute of Marine Geology and Geophysics FEB RAS, Yuzhno-Sakhalinsk, Russia.

³Institute of Oceanology RAS, Moscow, Russia.

We studied the grain size and composition of tsunami deposits collected in summer 2007 on Simushir and Matua islands, which we interpret to have been deposited by the 15 Nov 2006 central Kuril Islands tsunami. We performed granulometric analysis by sieving and weighing and compared our results to samples collected from possible source material such as the beach. We also identified diatoms, foraminifers and the remains of other sea organisms present in the deposits. The tsunami deposited highly variable sand and gravel on these islands, even on one island, greatly depending on source material. As a whole, grains size and diatom assemblages indicate that the on-land tsunami deposits were mainly eroded and transported from the nearshore, beach and ancient storm ridges. Sublittoral diatoms predominate among marine diatoms. At the same time, presence of deeper-water benthic foraminifera in tsunami deposits shows that tsunami wave seized small amount material from deep-water zones.

Dushnaya Bay, Simushir Island.

For Dushnaya Bay, the grain size and marine-diatom assemblage of the tsunami deposits shows that main source of the material brought by tsunami was eroded sediment from coast accumulative forms [e.g., dunes, beach ridges] and from the nearshore zone. In the north part of bay, there was erosion of the narrow shoreline terrace consisting of coarse boulder-pebble material, and of lower parts of slopes (also see MacInnes et al., 2009). Moderately sorted gravelly patches of tsunami deposits contain sand with polymodal size distribution (modes 1.6-2; 3-4; 5-7 mm). Diatom valves in these samples are broken. In the central part of the bay tsunami deposits most closely match material from former storm ridges. The deposit here is sheet-like, up to 7 cm thick, and fining away from the shoreline. The upper part of the deposit contains a finer fraction. Tsunami deposits in the south part of the bay are moderately well sorted medium sand. Their composition is practically identical to sampled dune sands. Diatoms are best preserved in this part of bay, except large *Cocconeis pellucida*; however, many valves of *Synedra kamtschatica*, in spite of their size, are preserved in colony [adhered to one another]. Fragments of neritic and open-ocean diatoms are also present including *Coscinodiscus* sp., three species of *Thalassiosira*, and *Porosira glacialis* (Grun.) Jorg.

In all samples remains of littoral organisms dominate: *Cocconeis stauroneiformis* (Rabenh.) Okuno, *C costata* Greg., *C scutellum* var *morrissii* W. Sm., *C californica* Grun., *C pellucida* Grun., *C verrucosa* Brun., *C interrupta* Grun., *Synedra kamtschatica* Grun., *Grammatophora angulosa* Ehr., *Navicula entoleia* Cl., *N. directa* W. Sm. All species are benthic and inhabit shallow depths. Some deep-water (neritic and open-ocean) diatoms are also present in deposits. Valve content is high in some samples. The tsunami deposits also contain small, rounded shell debris, remains of marine algae, single fragments of crustaceans, and in some samples multiple fragments of byssal threads from mussels byssus. Freshwater diatoms are also present in the tsunami deposits, but in small amount and with poor species composition.

Matua Island

Dvoynaya Bay. In one case, we studied tsunami deposits trapped in an old pump-house, where they were protected from reworking by wind and rain. The deposits are poorly sorted pebble gravel with a polymodal sandy matrix, and contain thirty-four species of sublittoral, neritic and oceanic diatoms. Many diatom valves are broken, especially thin-walled, deep-water species. Sublittoral benthic species dominate: *Cocconeis costata* (28.8-40%), *Amphora costata* W. Sm.(8%), *Grammatophora hamulifera* Kütz. (9-9.6%), *Cocconeis scutellum* Ehr.(6.3%), *Cocconeis californica* (up to 2.6%), *Navicula directa* (up to 3.6%). Brackish-water, neritic and oceanic diatoms are also present, as well as some freshwater forms from boggy environments. The deposits also contain broken and rounded, thin-shelled tests of neritic-bathyal benthic foraminifera *Cibicides lobatulus* (Walker et Jacob), *Quinqueloculina longa* Gudina, *Trifarina kozurraensis* Asano. We found one thick-shelled, deep-water species *Stainforthia loeblichii* (Feuling-Hansen) possibly from O(500 m), one ostracod shell, multiple small-mollusk shell fragments, and pieces of bryozoans, sponge spicula, sea-urchin tests.

Ainu Bay. In southern Ainu Bay, the tsunami deposits are moderately well sorted medium sand. The grain size distribution of the tsunami deposits along profiles does not change much, but can include a coarse-sand mode, and fines slightly inland. The deposits are similar to sands from the central to backbeach and probably were derived from eroded storm ridges. As a whole, diatom assemblages from tsunami sands indicates that the tsunami wave basically, moved the material from shallow bay bottom. Twenty forms of marine diatoms are present in tsunami deposits 100 m from coast line – 15 sublittoral, 5 neritic and ocean. The dominant benthic diatoms are sublittoral – *Cocconeis costata*, *C. stauroneiformis*, *Navicula directa*, *N. entoleia*, *Cocconeis californica*, some *Cocconeis scutellum*, *Navicula dithmarsica*, *Amphora costata* and others typical of shallow bays. Additional sublittoral benthic diatoms in other tsunami deposits include *Cocconeis verrucosa*, *Grammatophora hamulifera*, *Hyalodiscus odsoletus*. Sublittoral planktonic diatoms are represented by *Achnanthes groenlandica* and *Coscinodiscus nitidus*; ocean and neritic diatoms include *Thalassionema nitzschiooides*, *Actinocyclus divisis* (Grun.) Hust, *Neodenticula seminae*, *Thalassiosira eccentrica*, and warm-water *T. oestrupii* (Ostenfeld) Pr.-Lavr. The sublittoral benthic *Cocconeis costata*, *C. stauroneiformis*, brackish-water *Nitzschia sigma* (Kütz.) W. Sm. and neritic *Thalassionema nitzschiooides* are found in tsunami deposits near maximal tsunami penetration, where there are rich freshwater microflora as well.

MacInnes, B.T., Pinegina, T.K., Bourgeois, J., Razhegaeva, N.G., Kaistrenko, V.M., and Kravchunovskaya, E.A., 2009, Field survey and geological effects of the 15 November 2006 Kuril tsunami in the middle Kuril Islands, in Cummins, P.R., Kong, L.S.L., and Satake, K., ed., Tsunami Science Four Years After the 2004 Indian Ocean Tsunami; Part II Observation and Data Analysis: *Pure and Applied Geophysics* Topical Volume, 166, DOI 10.1007/s00024-008-0428-3

Field work for this project was funded by the Kuril Biocomplexity Project (NSF grant #0508109, PI-Ben Fitzhugh), by a grant to the Institute of Marine Geology & Geophysics, FED RAS, Yuzhno-Sakhalinsk and by RFBR grant 08-05-00066.

MICROMETER-SCALE VOLCANIC ASH COLLECTION AND CHARACTERIZATION STUDIES IN ALASKA AND KAMCHATKA

Peter Rinkleff, Catherine Cahill

Alaska Volcano Observatory, Univ. Of Alaska, Fairbanks, Fairbanks, AK, USA.

Volcanic ash poses a significant threat to aircraft safety, public health, and human activities. Little is known about chemical reactions which occur on ash surfaces in volcanic plumes and chemical ageing during long-range tropospheric transport. Satellite ash detection methods are based on models and have not been verified or calibrated by direct observations of concentration, size distribution, and composition of ash contained in volcanic plumes.

Volcanic ash from the eruptions of Augustine, 2006, Pavlof, 2007, Okmok, Cleveland, and Kasatochi, 2008, and possibly Kliuchevskoi, Bezymianny, and Sheveluch during 2008 and 2009, have been collected with DRUM cascade impactors. Ash samples have been analyzed for mass by β -gauge and elemental composition by synchrotron x-ray fluorescence. Results from the Augustine and Pavlof eruptions will be presented along with those from other eruptions if available. Further analysis of aerosol morphology and composition by scanning electron microscopy is being conducted to determine formation processes for volcanic ash, degree of surface alteration ash particles experience, and types of coatings formed on ash surfaces.

Aerosols collected during the explosive and continuous eruptive phases of the 2006 eruption Augustine Volcano show distinct size and compositional differences. Silicon-bearing aerosols collected during the explosive eruption phase are mainly coarse mode ($35\text{--}2.5 \mu\text{m}$ diameter) while those collected during the continuous eruption phase are much smaller ($<2.5 \mu\text{m}$). The measurements show that the shift in size and composition is due to different aerosol formation processes. Short duration explosive eruptions produce ash by mechanical fragmentation while continuous phase eruptions may produce ash from either mechanical disintegration of magma from brittle fracture of a foamy, viscous liquid, vigorous disintegration of pyroclasts in a pyroclastic flow, or by gas-to-particle conversion of magmatic volatiles.

Aerosols collected during the waning phase of the Pavlof eruption from 27 August through 2 September 2007, show a strong diurnal cycle that brought ash to the sampling site. Ash concentrations are highest in the morning (~07:15 AKDT) and lowest in the early afternoon (~15:15 AKDT). Unusually calm wind conditions allowed for this pattern. Although no ash fallout was observed at the sampling site, these results demonstrate volcanic ash can be present in respirable size fractions downwind of an erupting volcano even during periods of low eruptive activity.

PRELIMINARY RESULTS FROM A STUDY OF ACTIVE CENTRAL KURIL ISLANDS VOLCANOES UNDER THE AUSPICES OF THE "KBP 2006-2008" PROJECT

Rybin A.V., Zharkov R.V., Kozlov D.N., Chibisova M.V., Degtereov A.V.

Institute of Marine Geology and Geophysics FEB RAS, Yuzhno-Sakhalinsk, Russia

In this report we present preliminary data about geological structure and active volcanoes of the central and part of the northern sector of the Kuril Islands (Simushir, Keto, Yankicha, and Ryponicha [islands of the Ushishir group], Rasshua, Matua, Shiashkotan, Chirinkotan, Onekotan, and Ekarma). These data were collected during a three-year expedition supported by the US National Science Foundation (NSF) project "The Kuril Biocomplexity Project: Human Vulnerability and Resilience to Subarctic Change" ARC-0508109, 2006-2010 (Lead scientist B. Fitzhugh).

Scientists from the University of Washington (Seattle, USA) and Hokkaido University (Japan) took part in the expedition. Most of the Russian scientists were from the Institutes of FEB RAS: the Institute of Marine Geology and Geophysics, the Institute of Volcanology and Seismology, the Pacific Institute of Geography, the Northeastern Complex Scientific-Research Institute, and the Sakhalin Local Museum. In total the expedition staff numbered 39 persons working on various projects.

This project was the logical continuation of research conducted under the auspices of the International Kuril Island Project (IKIP); IKIP research was conducted in the islands in 1994-1999. The main target of the IKIP project was the study of Kuril Islands biodiversity.

The 2005-2010 Kuril Biodiversity Project (KBP) project has a wider scope of work. The Kuril Islands are considered to be a natural laboratory for the study of biogeographical processes. The broad range of questions to be addressed in the project required the participation of specialists from different disciplines: archeology, volcanology, geology, tsunami, geophysics, seismology, biology, and ecology.

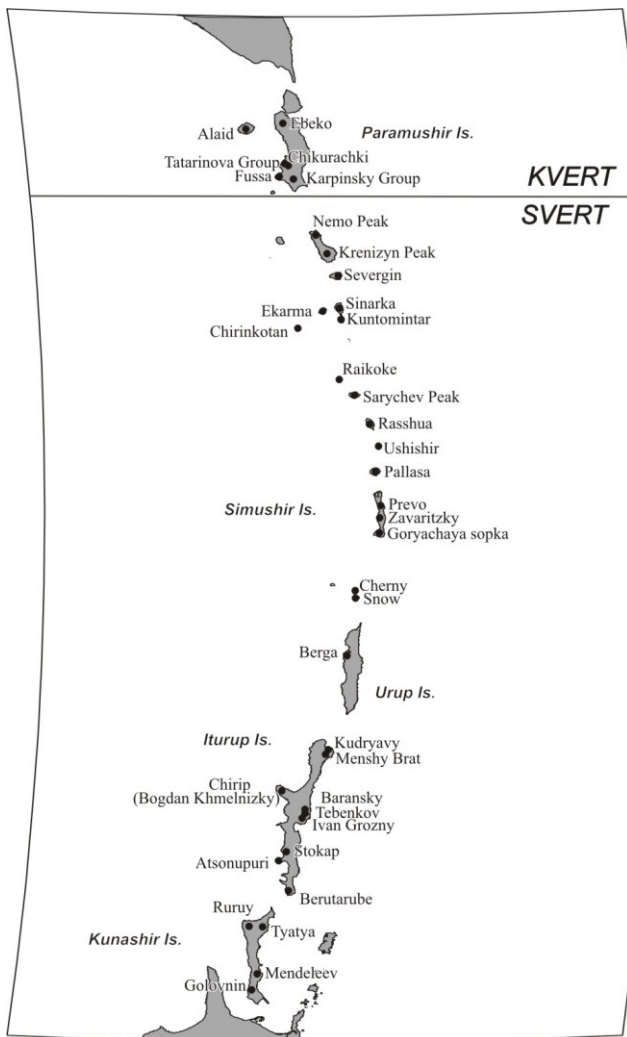
Groups of expedition staff work independently: two archeological groups, led by B. Fitzhugh and V. Shubin; two paleotsunami groups, led by D. Bourgu and T. Pinegina; one volcanological group, led by A. Rybin and N. Razzhigaeva; one palinological group, led by A. Lozhkin and P. Anderson; and a geodetical group, led by N. Vasilenko.

The main task of the volcanological group was to evaluate the influence of such natural processes as volcanic eruptions, earthquakes, and tsunami on peoples living in the Kuril Islands during the last seven thousand years. Additional questions to be addressed include the geological structure and paleogeography of the islands and the modern state of active volcanoes.

At present, Gorshkov's (1967) work and several publications by Kamchatka and Sakhalin volcanologists are the only sources of information about the islands' geological structure. The last field work on these volcanoes was conducted more than 25 years ago.

Thirteen active volcanoes are located in the central part of the Kuril arc, and eight of them erupted in the twentieth century; in addition, there have been at least ten giant caldera-forming eruptions during last several tens of thousands of years in the Kuril Islands. In spite of the absence of a constant population here, the volcanoes pose a threat to international airways from Asia to North America.

The only operative source of information about volcanic activity in the Central Kuril Islands is satellite surveillance; satellite data are received by SVERT (Sakhalin Volcanic



regime of constant fumarolic activity and have shown no signs of eruptive activity during last decades.

Similarly, visual observations of Prevo, Rasshua, Kuntomintar, and Nemo volcanoes suggest their constant fumarolic activity.

Interesting data were received for the Sinarka Volcano, located on Shishkotan Island. The very large area of fumarolic outflow thermal fields is characteristic of this volcano. Temperature measurements conducted at fixed points in 2007 and 2008 showed an average temperature increase of 2-5 °C in the thermal fields on the slopes of the volcano, while the near-mouth part of one fumarole on top of the volcano increased by 62 °C; in August 2007 the measured temperature was 387 °C, and in August 2008 it had increased to 449 °C.

Eruptions Response Team), but they are insufficient for accurately evaluating the degree of volcanic danger to this territory.

The data that have been collected allow us to conduct detailed comparisons of the isotopic-geochemical characteristics of the volcanic activity products from Southern and Central Kuril Islands calderas to reveal details about the origin and evolution of magmatic melts in these structural zones, and to evaluate the differences in their deep geological structure.

The study of peat bog sections, soil-pyroclastic covers, and aeolian covers including buried soils and volcanic ash from active volcanoes offers a possibility of reconstructing the sequence of catastrophic Holocene events in the central part of the Kuril Islands. Part of these sections are located near the archeological camp sites where the archeological excavations were conducted, allowing us to reconstruct local landscape changes that occurred near ancient human habitations caused by climate changes and the effect of volcanic eruptions.

A detailed investigation into the modern state of the active volcanoes Chirpoi, Snow, Pallas, Goryashchaya Sopka, Zavaritskii, Ushishir, Sarychev, Chirinkotan, and Harimkotan showed that they are in a

NEW ADVANCES IN THE COLLABORATIVE USGS/SMITHSONIAN WEEKLY VOLCANIC ACTIVITY REPORTS: DOCUMENTING CURRENT ACTIVITY FOR SCIENTISTS AND NON-SCIENTISTS

Sally Kuhn Sennert^{1,2}, Edward Venzke², Lee Siebert², Paul Kimberly²

¹*US Geological Survey, 12201 Sunrise Valley Dr, Reston, VA, USA.*

²*Smithsonian Institution, Global Volcanism Program, NMNH MRC-119, Washington DC, USA.*

Since late 2000, the Smithsonian's Global Volcanism Program (GVP) and the US Geological Survey's Volcano Hazard Program have collaborated to create the Weekly Volcanic Activity Report (WVAR), an online summary of global volcanic activity on a weekly basis that can be accessed via the Global Volcanism Program's website. The WVAR provides reliable reports for scientists and non-scientists alike to learn about current unrest and eruptive activity at the world's volcanoes. In addition to the brief summaries of current activity, several features that add context include links to the information sources and to definitions for technical terms in the USGS photoglossary, background information about the reported volcanoes compiled by GVP staff, a world map showing the locations of the reported volcanoes, maps highlighting regional geography, a list of commonly used acronyms and abbreviations, and links to more comprehensive reports that are published monthly in the *Bulletin of the Global Volcanism Network*. The compilation of the WVAR has become a frequently utilized resource that reaches an average of 5,000 daily visitors to the WVAR pages on the GVP site alone.

Advancements in communication technologies have provided new mechanisms to more rapidly disseminate information about volcanic activity to the public, scientists, and to those responsible for hazard identification and mitigation. One of the primary new features of the WVAR is the generation of database programming that allows output of RSS (Really Simple Syndication) and CAP (Common Alerting Protocol) news feeds that have been available since March 2008. Each volcano report includes a link from the volcano's name back to the more complete information on the GVP website. The increasingly popular social networking sites and the ever-expanding capabilities of Google programs have provided additional outreach capabilities. The WVAR reaches new readers through automatically imbedded weekly RSS feeds on the GVP Facebook page, providing a mechanism for "fans" of the WVAR and GVP sites to access reports of volcanic activity. Since June 2006 GVP has provided a regularly updated built-in volcano layer used by Google Earth; one future initiative for the WVAR is to provide a Google Earth fly-through of the volcanoes covered each week. The Google Map interface also promises to improve the maps provided on the WVAR website. With the support of the volcanological community, we continue to explore new ways to inform scientists and educate the public about volcanoes and their eruptions.

METHANE ESCAPE, GAS HYDRATES, AND MUD VOLCANOES IN THE SEA OF OKHOTSK AND ON SAKHALIN ISLAND

Renat Shakirov, Anatoly Obzhirov

V.I. Il'ichev Pacific Oceanological Institute, FEB RAS. Vladivostok, Russia.

Methane emissions induced by different geological conditions in the second largest marginal sea of the Pacific Ocean, the Okhotsk Sea, and on Sakhalin Island were explored from 1989-2008. Active methane vents within the thick (≤ 10 km) Cenozoic sediment basins are linked to multiple hydrocarbon accumulations, mainly oil-gas deposits and gas (methane) hydrates. According to our data, in most cases methane is the most prevalent gas in sediments ($\leq 90\%$ vol.), while in the volcanic Hokkaido-Kurile-Kamchatka area carbon dioxide is most abundant.

All methane emission sites discovered are located within zones of the highest density of hydrocarbon generation in sediments (PHG); they are related genetically to hydrocarbon accumulations and spatially to local and fault structures, and are controlled particularly by recent faulting, especially along the plate boundaries and in the Kurile Basin that is influenced by subduction processes along the Kurile Islands.

Eastern Sakhalin Island and the Sakhalin offshore region are related to the transform plate boundary. Modern high seismic activity and active faults that break through the sea floor create a favorable gas-permeable state along this border. Evidently, those anomalously high ambient methane concentrations in the water column (up to 30.000 nano-liters/liter above gas hydrates deposits) reflect that situation geochemically. It is highly likely that the intersections of the NE-striking transverse faults on land with the Central Sakhalin and Hokkaido-Sakhalin Shear Zones determines the sites of mud volcanoes, and that this pattern continues offshore where intersections with the East Sakhalin and West Derugin Shear Zones determine gas vents sites.

We observed that when gas-saturated fluids migrate through the upper sediments and penetrate the sea floor, particularly via fault systems, deformations of the Bottom Simulating

Reflector (BSR), mud volcanoes, gas-hydrothermal springs, and pockmark-like structures can occur. Submarine gas vents are usually accompanied by contrast acoustic anomalies in the water column (up to 250 methane vents prior to 2008 above methane hydrates off NE Sakhalin, see photo of methane hydrate sample from 2005).



On Sakhalin Island (2001, 2005-2007), gas geochemical parameters if the Yuzhno-Sakhalinsky Mud Volcano (YSMV) and the Pugachevsky Mud Volcano vary with seismic activity. In the YSMV the methane content ranged from 2-32 vol%. A main gas component of this volcano was CO₂, which

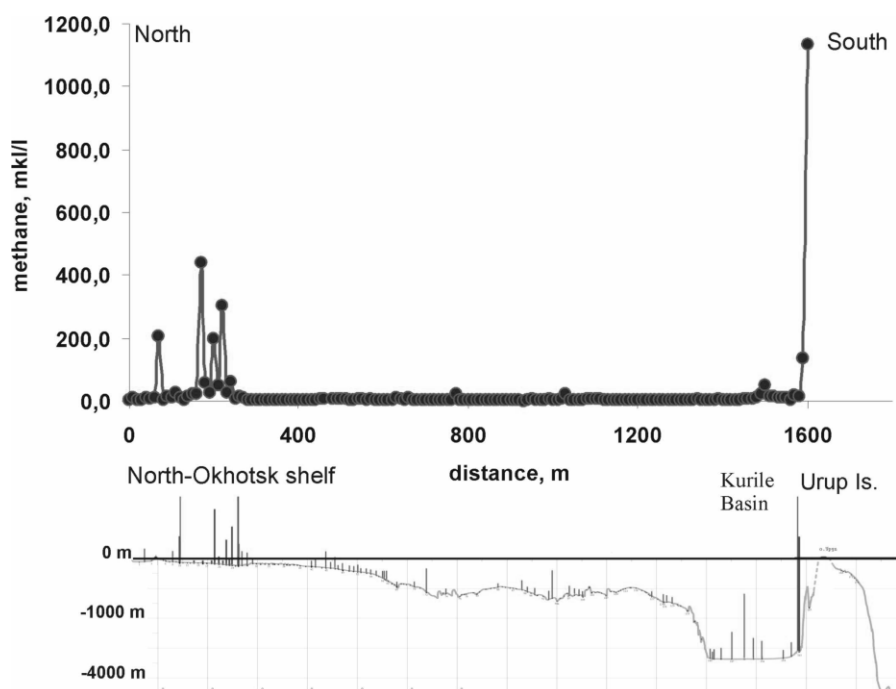
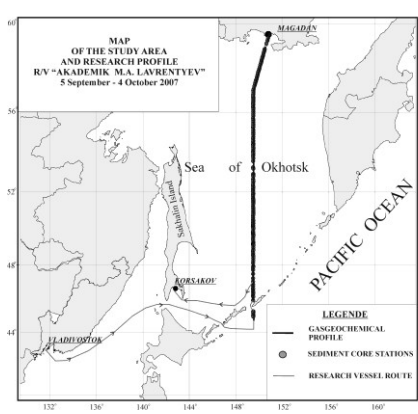


Fig. 2. Diagram of methane distribution on a bathymetric profile across the Sea of Okhotsk from north to south and methane anomalies in the upper sediments measured in the sediment core bottoms. The profile location is plotted on the map. The greatest methane anomaly was found on the north slope of Kurile Island.

The available representative expedition and analytical data on distribution and variability of CH₄, CO, CO₂, N₂, He, ³He/⁴He, ¹⁸O, temperature, and pH in the hydrothermal and magmatic gas emission structures allow us to discern the basic geological types of methane emission structures in the Okhotsk region: cold vents, mud volcanoes, wide seepage areas above oil-gas deposits and abrasion zones, gas-hydrothermal springs, submarine methane-barium saturated fluid vents, and others. Their distribution and origins characteristically depend on regional and local variability of geological conditions, which are partially dictated by subduction processes.

These marine expeditions were carried out as part of the KOMEX I-II Projects (Russia-Germany, 1998-2004, grant 03G0535), the CHAOS Project (Russia-Japan-Korea, 2003, 2005-2006), and the SSGH Project (Russia-Japan-Korea, 2007-2008).

ranged from 66–94 vol%. An increase in spontaneous gas emission and gas chemical variations as well as a temperature rise under the mud field surface of the YSMV during an earthquake in August 2007 (the catastrophic Nevelsk Earthquake, 6.7 Richter magnitude, 2 August 2007) were observed on south Sakhalin Island (Fig. 2). This and other changes are probably indicators of tectonic stress increase before an earthquake. No gas or fluid discharges were registered in the central deep-sea area because these areas have the thinnest sediment strata, lowest PHG ($<5 \times 10^6$ t/km²), and low seismic activity. The background methane field is located there.

THERMAL ANOMALY TEMPERATURE RESEARCH ON ACTIVE KAMCHATKAN VOLCANOES WITH THE PURPOSE OF DETERMINING THEIR SHORT-TERM ERUPTION PRECURSORS

Sobolevskaya O.V., Senyukov S.L.

Kamchatka Branch of Geophysical Survey RAS, Petropavlovsk-Kamchatsky, Russia.

There are 29 active volcanoes on Kamchatka Peninsula. The Kamchatka Branch of the Geophysical Survey of RAS (KF GS RAS) monitors active volcanoes with the purpose of estimating volcanic danger. One observation method is satellite monitoring of thermal anomalies and ash plumes based on AVHRR data from NOAA 16 and 17 weather satellites.

Information is received by the Kamchatkan center of connection and monitoring. The Research Laboratory of Seismic and Volcanic Activity of KF GS RAS began processing AVHRR sensor data in September 2002. We used the HRPT Reader program, and published the results on the Internet (<http://www.emsd.ru/~ssl/monitoring/main.htm>). Thanks to the help of the Institute of Space Research (XV_HRPT reformat program) and the Alaskan Volcano Observatory (ENVI 4.0 program) we began to measure thermal anomaly temperatures in October 2006.

The quantity of pixels, their orientation in relation to the tops of volcanoes, and their maximal temperature are determined for each thermal anomaly. Anomaly parameters are measured for volcanoes and pyroclastic flows, and background temperature is estimated from nearby surfaces.

The results of all this work is used as an additional seismic monitoring parameter for forecasting Kamchatka volcano eruptions. The satellite information is compared with seismic, visual, and video data, allowing us to more accurately trace the process by which a volcano prepares to erupt.

As a result of this research, it was determined that before eruptions of the Sheveluch, Klyuchevskoy, and Bezymianny volcanoes, an increase in temperature and growth of thermal anomaly is observed for one to a few weeks before eruption. The thermal anomaly of Karymsky Volcano is observed only during periods of active eruptions.

GREAT INTERPLATE EARTHQUAKES ALONG THE CENTRAL KURILE SUBDUCTION ZONE

Yuichiro Tanioka, Kei Ioki

Institute of Seismology and Volcanology, Hokkaido University, Japan.

Several great interplate earthquakes occurred along the Kurile trench due to subduction of the Pacific plate beneath the Kurile Islands, and large tsunamis have been generated by those earthquakes (Figure 1). Recently, a great Kurile interplate earthquake (Mw8.3) occurred off Simushir Island along the central Kurile subduction zone on November 15, 2006. The previous great interplate earthquake along the central Kurile region was the 1963 Kurile earthquake (Mw 8.3) which occurred off Urum Island (Figure 1). The tsunami waveform analysis of the 1963 earthquake (Ioki and Tanioka, in this JKASP meeting) indicates that the fault length is 200km and a large slip was found in the shallow part of the source area. The 1918 great Kurile earthquake (Mw 8.2) also occurred in this central Kurile region, and generated large tsunami. Previous study indicated that the source area of the 1918 earthquake should be located northward of the source area of the 1963 Kurile earthquake. However, the distance between the rupture areas of the 2006 and 1963 Kurile earthquake is less than 70 km which may be too short to allow another great earthquake to occur between the two great earthquakes. A key question remains: Where is the source area of the 1918 Kurile earthquake (Figure 1)? In this paper, we attempt to discover the source area of the 1918 great Kurile earthquake using the tsunami waveforms recorded by tide gauges along the Pacific coast.

The tsunami waveforms for the 1918 earthquake were detected at tide gauges in Japan, including Choshi and Chichijima (Nakamura, 1919, in Japanese). The tsunami was also detected at tide gauges in Honolulu and San Francisco. Figure 2 shows the locations of these tide gauges. The tsunami waveform data recorded in the USA were collected at NOAA-NGDC to analyze the source process of the earthquake. At first, all of the observed tsunami waveforms showed positive first waves, meaning that the earthquake was not a normal fault event along the outer rise such as the 2007 Kurile earthquake; instead, it was an interplate earthquake. We numerically computed tsunami using various fault models located at different plate interfaces along the central Kurile subduction zone. The observed tsunami waveforms at four tide gauges were compared with computed ones to find the best fault model. There may have been large errors in the tide gauge record time scales in 1918. It was difficult to decide the best fault model with such large errors in timing. If we assumed that time scale error is less than 20 minutes, we found that the source area of the 1918 Kurile earthquake was closer to the source area of the 2006 Kurile earthquake than to that of the 1963 Kurile earthquake, suggesting that the 2006 Kurile earthquake was a recurrence of the 1918 Kurile earthquake. The total seismic moment of the 1918 Kurile earthquake was $4.0 \times 10^{21} \text{ Nm}$ (Mw8.4) if we assume a rigidity of $4 \times 10^{10} \text{ N/m}^2$.

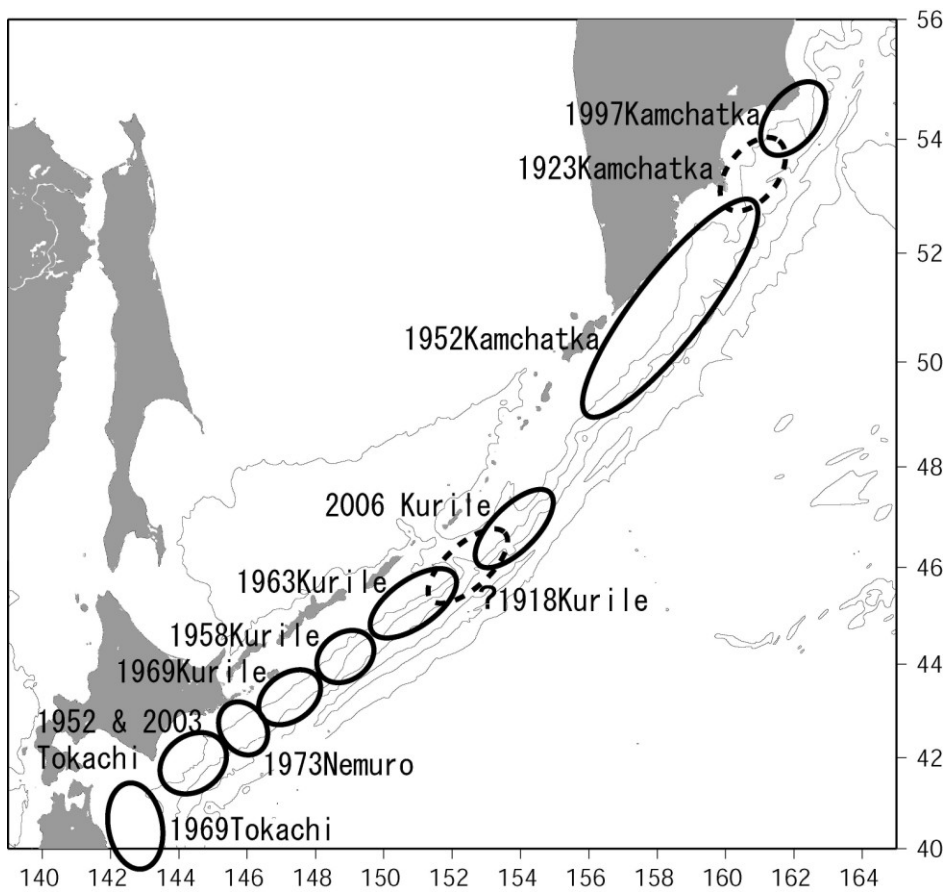


Fig.1 Great interplate earthquakes occurred along the Kurile subduction zone

a) The 1918 great Kurile earthquake

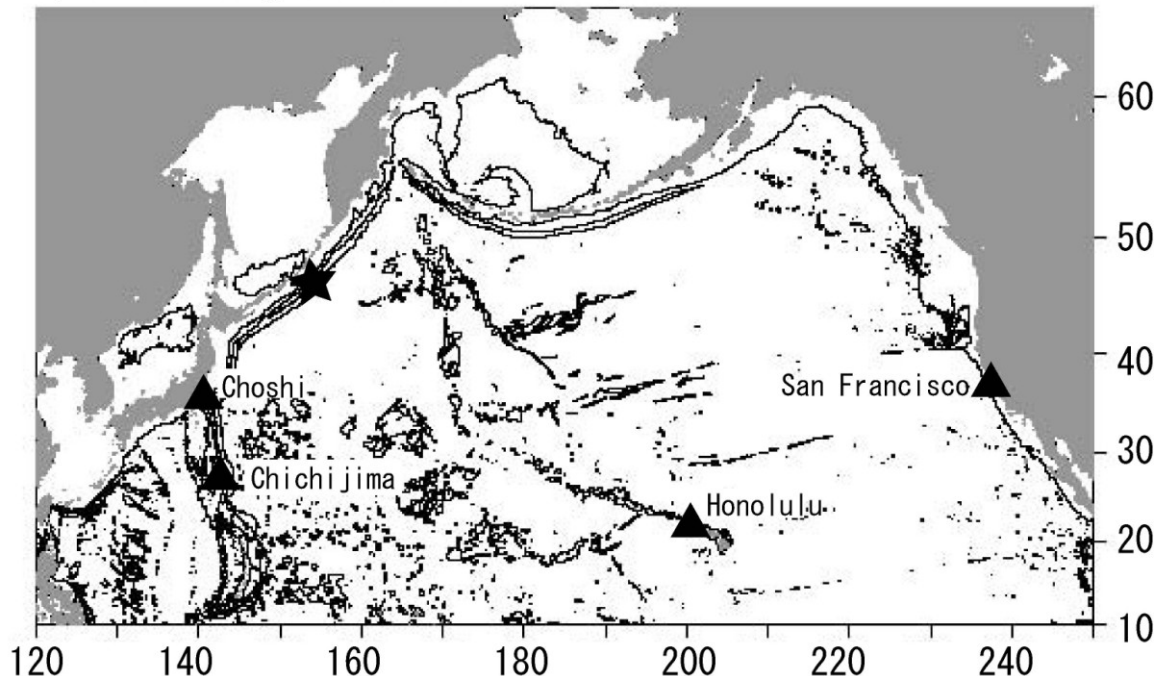


Fig.2 The location of the tide gauges that recorded the 1918 Kurile tsunami

OKHOTSK MIGRATION AND ANIMAL PROCUREMENT IN NORTHERN JAPAN AND THE RUSSIAN FAR EAST: ISOTOPIC ANALYSIS OF HUMANS, PIGS, DOGS, AND BEARS

James W. Taylor

Department of Anthropology, University of Washington, Seattle, WA, USA.

The Okhotsk people were a highly maritime group of hunter-gatherers who occupied the southern Sea of Okhotsk between the 5th and 13th centuries A.D. This group of marine foragers spread rapidly from Sakhalin Island, Russia, around the coastal margins of Hokkaido, Japan, and throughout the entire Kuril Island chain in less than five hundred years. They brought with them an unusual suite of animal familiars, including pigs and dogs, and a bear sacrifice ceremony similar to the historic Ainu Iyomante or ‘bear sending’ ritual. Despite their rapid expansion throughout a vast expanse of coastline, the Okhotsk people all but disappeared from the region or were assimilated by neighboring Satsumon people within 200-300 years. By investigating the rapid movement of these mariners and their unusually strong relationship with a few terrestrial animals we may contribute to a broader understanding of colonization events, especially in island settings, in other parts of the world.

I have utilized Sr, Pb, O, and C isotopic analysis of human and animal tooth enamel to investigate the timing and rate of movement of humans throughout the Okhotsk range, as well as the paleophylogenetic distribution of bears and pigs in the past. Furthermore, I provide data on the feeding practices of humans and of culturally significant terrestrial animals to better understand the strategic adaptations of the Okhotsk people, with a specific focus on pig domestication and ritual bear treatment. By comparing these data with regional information on resource availability, climatic events, and large-scale natural disasters such as volcanic eruptions, earthquakes and tsunamis, we can understand key factors that contribute to human migration and colonization of island settings on a broader scale.

Participation in the Kuril Biocomplexity Project was made possible in part by a grant from the US National Science Foundation (ARC-0508109; Ben Fitzhugh, PI), the Japanese Society for the Promotion of Science, the University of Washington NSF IGERT-MCCE, and various logistical and financial support from: the University of Washington, Seattle, WA, USA; the Hokkaido University Museum (Sapporo, Japan); the University of Tokyo’s Tokoro Archaeological Laboratory (Tokoro Town, Japan); the Sapporo Medical College (Sapporo, Japan); the Sakhalin Regional Museum (Yuzhno-Sakhalinsk, Russia); and the Far East Branch of the Russian Academy of Sciences (IMGG: Yuzhno-Sakhalinsk, IVGG: Petropavlovsk-Kamchatsky, NEISRI:Magadan).

THE MODERN SOLFATARIC-HYDROTHERMAL ACTIVITY OF THE VOLCANOES OF THE CENTRAL AND NORTHERN KURILS

R. Zharkov, D. Kozlov

Institute of Marine Geology and Geophysics, Yuzhno-Sakhalinsk, Russia.

From 2006-2008 international expeditions were conducted in the area of the Central and Northern Kuril Islands under the auspices of the "Kuril Biocomplexity Project: Human Vulnerability and Resilience to Subarctic Change" (Ben Fitzhugh, Principle Investigator). The task of the volcanological group was to study the development history of the Kuril Islands volcanoes and their modern solfataric-hydrothermal activity. In the course of the field work the authors studied Zavaritskii, Goryashchaya Sopka, and Ikanmikot volcanoes on Simushir Island, Sinarka Volcano on Shiashkotan Island, Ushishir Volcano on Yankicha Island, Sevvergin Volcano on Harimkotan Island, and Ekarma, Chyornyi, and Snow volcanoes on Chirpoi Island.

The last eruption of Zavaritskii Volcano caused the formation of the northern extrusive dome in 1957 (Markhinin, 1958), but modern activity in the caldera has considerably decreased. Solfataras and hydro-solfataras observed as recently as 1970 in the area of the northern dome have completely disappeared. The intra-calderal Biryuzovoe Lake rose nearly 10 m and flooded the thermal springs in the southwestern part of the caldera. Intensive gas emissions from the bottom of the lake, fixed by echo-sounding, and the temperature of the shore sand, which reaches 91.2 °C, testify to the presence of flooded thermal springs.

At present, Goryashchaya Sopka Volcano exhibits very low fumarolic activity in the area of the explosive crater on top of the dome (Gorshkov, 1967). The temperature of small outputs of steam is about 43-54 °C.

Ikanmikot Volcano is a dead volcano of the composite type. Outputs of low-temperature thermes were found on the Pacific shore at the basement of the volcano (Korsunskaya, 1958). We succeeded in finding two small thermal springs with temperatures of 32-34 °C.

On Sinarka Volcano we measured the temperature of the steam-gas outputs in the central extrusive dome, and studied the northeastern and western solfataric fields. The temperature of most solfataric outputs on the extrusive dome was 100-150 °C. The temperature of one of the great solfataras was about 450 °C. The high temperature of the gases testifies to the high level of volcanic activity. On the northeastern solfataric field we found considerable changes from the descriptions of E. Markhinin and D. Stratula (1977), although, as before, solfataras with temperatures up to 100 °C are active on the solfataric field. Recently a new geyser-type spring ("Chyornyi Drakon") appeared in the northern part of the field. This spring is heated to 93 °C, with water pH = 7.1. According to the chemical composition the spring is a sulphate-chloride calcium-magnesium-natrium type of hydrotherm (Tabl. 1). The western solfataric field exhibits little change. Springs with small discharge rates of sulphate-chloride calcium-magnesium composition with temperature = 28-42 °C and pH = 2.8 occur here.

Ushishir Volcano caldera is a circle ridge with Craternaya Bay in the center. The solfataric field is located on the southeastern shore of the bay. Both solfataras with temperatures of 100-103 °C and "boiling" thermal springs of chloride-natrium composition with mineralization 23-27 g/l (Tabl. 1) are found here. The temperature of the springs is ≤101 °C, and pH=2.8-3.7. Considerable changes in the solfataric-hydrothermal activity of this volcano were not observed.

On Harimkotan Island we studied the modern state of Severgin Volcano. The last Severgin eruption was in 1933 (Gorshkov, 1967). In the upper part of the dome the temperatures of the weak-steam solfataric sites were measured to be 90-97.4 °C.

The thermal springs located near the northern foot of Ekarma Volcano have changed little during the last 45 years. The hydrocarbon-sulfur sodium-calcium-magnesium hydrotherms (Tabl. 1) with temperature ≤ 40 °C and pH=6.1 issue from shore cliffs for a distance of several tens of meters. We also studied the new thermal Chirkov Springs which were found in 2008 in a small bay in the northwestern part of the island. The temperature of these thermal spring waters does not exceed 40° C, and the chemical composition differs from that of the northern springs (Tabl. 1).

On Rasshua Island the famous group of "Snow Baths" thermal springs was studied. Sulfur calcium-magnesium therms (Tabl. 1) with temperatures of 33-43 °C discharge on the shore of the Pacific Ocean. On the shore of the Okhotsk Sea a new thermal field was found 3 km north of Malen'kaya Bay. These springs, named "Koroteev Baths" are located on a 35x15 m site in the tidal zone. The temperature of the spring water is 22-36.2 °C, and the chemical composition differs greatly from that of the "Snow Baths" springs (Tabl. 1).

On Chirpoi Island the modern activity of Chornyi and Snow volcanoes was studied in detail. In the Chornyi Volcano crater the temperatures of different groups of fumarolic outlets range from 100-371 °C. On the western slope of the volcano are found the largest solfataric outlets with temperatures ≤ 230 °C. No substantial changes from data collected in 1992 were found for either Chornyi or Snow volcanoes. Steam outlets on the northern slope of Snow Volcano and on the ridge of the crater measure 60-70 °C. In the crater only a small site with solfataric outlets was found, with temperature ≤ 91 °C.

Among all the volcanoes studied, Sinarka Volcano on northern Shiashkotan Island displayed the greatest solfataric-hydrothermal activity. The highest-temperature solfataras were found on this volcano's dome, and new thermal springs have appeared in the solfataric fields. Substantial changes from data collected by previous researchers were not observed on other volcanoes.

This work was funded by a US National Science Foundation grant № ARC-0508109, an RFBR grant № 07-05-10070K, and FEB RAS grants № 06-II-CO-08-031, № 06-III-B-08-371, and № 07-III-Д-08-097.

Table 1. Temperature, pH, and chemical composition (mg/l) of volcanic thermal springs

	Sinarka Volcano			Ushishir Volcano	Ekarma Volcano		Rasshua Volcano	
	1	2	3	4	5	6	7	8
T, °C	93.1	38.1	67.0	100.0	37.0	40.0	43.0	36.2
pH	7.1	2.8	6.9	3.4	6.1	6.5	3.1	7.5
Na ⁺	84.0	175.0	2030.0	7050.0	94.0	222.0	62.0	833.0
K ⁺	12.2	11.2	122.0	760.0	10.0	33.0	9.7	46.0
NH ₄ ⁺	1.1	0.1	1.1	0.7	0.5	0.7	0.4	0.1
Ca ²⁺	217.0	536.0	261.0	1077.0	93.2	115.0	167.0	215.0
Mg ²⁺	47.4	304.0	109.0	42.5	92.4	43.8	68.7	35.2
Fe ²⁺	0.76	0.05	<0.05	0.48	0.12	<0.05	<0.05	<0.05
Fe ³⁺	0.08	89.60	0.3	<0.05	0.36	0.2	0.2	0.2
H ⁺	-	5.0	-	0.4	-	-	1.1	-
Σ cations	362.5	1120.9	2523.4	8931.1	290.6	414.7	309.1	1129.5
Cl ⁻	206.0	1028.0	3758.0	13756.0	127.0	355.0	121.0	1560.0
SO ₄ ²⁻	580.0	1960.0	335.4	206.0	335.0	290.1	745.0	278.6
HCO ₃ ⁻	91.5	-	168.0	-	415.0	256.0	-	85.4
Σ anions	877.5	2988.0	4261.4	13962.0	877.0	901.1	866.0	1924.0
SiO ₂	104.0	179.0	182.0	102.0	127.0	178.0	144.0	41.5
TDS	1344.0	4287.9	6966.8	22995.1	1294.6	1493.8	1319.1	3095.0

Notes: 1: The "Chornyi Drakon" spring, northeastern solfataric field; 2: Western solfataric field; 3: Springs near the foot of the volcano; 4: Southeastern solfataric field; 5: Springs near the northern foot of the volcano; 6: Chirkova Springs; 7: "Snow Baths" springs; 8: "Koroteev Baths" springs.245

Author Index

A

Abers, 125
Almberg, 229

B

Bakhtiarov, 189
Begét, 178
Bellesiles, 143
Belousov, 97, 217, 273
Belousova, 113
Benowitz, 190
Blokh, 115
Bourgeois, 37, 255
Briggs, 35
Bronicki, 213
Browne, 61
Bull, 51
Bulochnikova, 274
Buurman, 65

C

Cameron, 66
Chebrov, 192
Chibisova, 275
Christensen, 144
Chubarova, 145
Churikova, 117

D

Dean, 53
Dirksen, 67, 69
Droznin, 194
Duarte, 119, 277

E

Eichelberger, 99
Elliott, 196

F

Fedotov, 71, 126
Firstov, 278
Fitzhugh, 257

Freymueller, 43

G

Gardine, 147
Gavrilenko, 73
George, 148
Girina, 54, 75, 265
Gorbach, 230
Gordeychik, 76
Grapenthin, 197

H

Haney, 128
Hasegawa, 102
Honda, 198

I

Ioki, 279
Izbekov, 218

J

Jicha, 103

K

Kayzar, 104, 219
Keranen, 39
Khleborodova, 78
Kimata, 130
Kohno, 171
Konovalova, 131, 149
Kozhevnikova, 151
Kozlov, 281
Krasheninnikov, 80
Krivomazova, 232
Kugaenko, 152
Kuvikas, 233
Kyle, 105

L

Larsen, 55
Lopez, 235
Lu, 266
Lundgren, 267

M

MacInnes, 200, 259
Maeda, 132
Manstein, 283
Matsushima, 172
Melnik, 221
Melnikov, 285

N

Nakagawa, 261
Neal, 44
Neill, 236
Nelson, 202
Nicolsky, 204
Nishimoto, 82
Nuzhdayev, 286
Nuzhdina, 154
Nye, 46

P

Pavlov, 155
Payne, 120
Phillips, 287
Pinegina, 205
Plechov, 106, 223
Power, 173

R

Rader, 121
Ramsey, 57
Razzhigaeva, 289
Rinkleff, 291
Ruppert, 60, 134
Ryan, 179
Rybin, 292

S

Saltykov, 157, 159
Samoilenko, 160
Sanderson, 121
Scholl, 135
Sennert, 294
Senyukov, 226, 238
Serovetnikov, 239

Shakirov, 295
Shanina, 240
Shcherbakov, 242
Shestakov, 207
Shipman, 244
Shuler, 161
Sobolevskaya, 297
Steblov, 181
Steiner, 61
Sterling, 183
Storcheus, 84, 163
Stovall, 86, 246
Suleimani, 185

T

Takahashi, 136, 165
Tanioka, 298
Taylor, 300
Thelen, 247
Tsvetkova, 249

U

Uesawa, 87

V

van Manen, 251
Vaughan, 268
Volynets, 89

W

Watts, 91
Webley, 269
West, 175

Y

Yamaguchi, 138
Yamashita, 166
Yogodzinski, 92
Yoshimoto, 122
Yun, 209

Z

Zharkov, 301